Dissertation zur Erlangung des Doktorgrades
der Fakultät für Chemie und Pharmazie
der Ludwig-Maximilians-Universität München

Proteomic exploration of molecular mechanisms of HIV-1 infection in the host cell

Lin Chen
aus
München, Deutschland

2020

Erklärung

Diese Dissertation wurde im Sinne von § 7 der Promotionsordnung vom 28. November 2011 von Herrn Prof. Dr. Oliver T. Keppler betreut und von Herrn Prof. Dr. Stingele von der Fakultät für Chemie und Pharmazie vertreten.

Eidesstattliche Versicherung

Diese Dissertation wurde eigenständig und ohne unerlaubte Hilfe erarbeitet.

München, den 09.11.2020 Lin Chen

Dissertation eingereicht am	11.11.2020
1. Gutachter	Prof. Dr. Julian Stingele
2. Gutachter	Prof. Dr. Oliver T. Keppler
Mündliche Prüfung am	22.02.2021

Acknowledgments

After three and a half years of up and downs, working for more than 350 hours in the BSL3 laboratory, producing more than 40 ml concentrated infectious HIV, harvesting more than 520 mg protein, using around 400 compounds and 350 hours of coding time, the doctoral thesis has been completed. This whole project would have been impossible without the energetic support of certain persons.

I want to thank Prof. Dr. Julian Stingele and Prof. Dr. Oliver T. Keppler for the doctoral supervision, the access to first-class virology laboratories and, in particular, their feedback and suggestions during this project.

A very special word of thanks goes to my extraordinary principipal investigator, Dr. Christian Schölz. There are no words which are able to describe how grateful I am for being a member in his research group, for the professional and personal guidance he provided. Christian's door was always open for me and he was willing to lend me an ear in any situation. I feel blessed to be led and strongly supported by him. I thank him for everything he has done for me.

I also would like to thank the former members of the group, Ari and Franzi, for the great teamwork and for the nice time we had together. Moreover, I would like to express my gratitude to all the interns, Tobi, Corinna, Jonathan, Erik, Pedro and Alishan for their help.

I also want to thank our collaboration partners, Dr. Helmut Blum for the RNAseq, Prof. Dr. Matthias Mann and Dr. Igor Paron as well as Dr. Thomas Fröhlich and Bachuki Shashikadze for the LC-MS/MS analysis.

When times were tough, two amazing individuals always know how to make me smile: They are two inspiring scientists with the most incredible dancing skills I have ever seen and the best food buddies one can meet. I am very happy for having Rebecca and Ramya not only as colleagues but also as good friends. I am very grateful for the fun time with them during my doctorate journey.

It is the atmosphere that makes the "201 lab" very special. Therefore, I also want to express my gratitude to other members of the Sewald or Baldauf group, Hanna-Mari, Xaver, Patricia, Fabian, Luca, Alejandro and Lisa. In addition, I also want to thank my other colleagues in the "Virology gang", Manuel, Marcel, Ernesto, Hong-Ru, Madeleine, Qianhao, Stephi, Robin, Kathi, Johanna, Linda, Jeli, Jenni, Adrian, Niklas, Burak, Augusto and Ina - people who shaped the positive working atmosphere I enjoyed.

Finally, I would like to thank Philipp and my family for ensuring that I am fed well, even in very busy times, and their endless support during my studies and work.

Abstract

Human immunodeficiency virus 1 (HIV-1) relies heavily on the host cell for its replication, where it reprograms the cellular environment for production of viral progeny as well as to escape antiviral immune defenses. In the last years, alteration of host signaling pathways by HIV-1 have been described to be heavily dependent on post-translational modifications (PTMs). Therefore, the global analysis of HIV-1-host interactions including PTM enzymes, respective interactors and substrates as well as their PTM status is crucial to improve the understanding of HIV-1 pathogenesis. Additionally and apart from the identification and PTM status of HIV host targets, studies disclosing and quantifying those HIV-1 host interactions with temporal resolution are still lacking.

Within this study, the first hand-curated database summarizing current knowledge of phosphorylation-, acetylation- and ubiquitination-regulated processes during HIV-1 infection was created to serve as solid base for further research. Moreover, an optimized set-up for *in vitro* infection-studies with a full-length and replication competent HIV-1 strain was established, which enabled (i) the monitoring of HIV-1 infection progress over time as well as (ii) the quantitative and time-resolved global proteomic and PTMomic analysis of HIV-1 infection in $CD4^+$ T-cells. Thereby, a comprehensive data resource of host protein dynamics, including changes of the two different PTM types, phosphorylation and acetylation, in response to HIV-1 infection was generated. For high-throughput exploratory analysis and visualization of affected signaling pathways, an bioinformatic workflow was designed for automated processing of (prote)omics data and graphical visualization.

In addition, functional analysis of two acetylation sites of the viral Tat protein, K28 and K50/51, revealed their important role in regulating Tat's transactivation ability by controlling binding to the viral LTR promoter as well as to host interactors. Moreover, further knowledge about the function of the second exon of Tat was determined, suggesting an active role in the regulation of transcription factor interaction.

Based on the putative role of lysine acetylation, not only for HIV-1 replication but also for latency, a screening for novel latency reversing agents (LRAs) was conducted and resulted in the identification of two novel compounds of the HDAC inhibitor type, HBOB and SR-4370, with favorable limited cytotoxic and T-cell activating side effects. Additionally, two other HDAC inhibitors with latency reversing properties, sodium-butyrate and bufexamac, could be identified, which impaired *de novo* HIV-1 infection.

In conclusion, this study provides novel insights into the molecular mechanisms during HIV-1 infection in the host and resembles a valuable resource for the identification of vulnerable nodes during acute HIV-1 infection. It is strongly believed, that the data determined within this project will help to initiate several new scientific projects and will provide substantial information for researchers, clinicians and the pharmaceutical industry.

Contents

1. Introduction

1.1. The human immunodeficiency virus HIV-1

1.1.1. HIV-1 infection as a global health threat

At the beginning of the 1980s, unusually high rates of rare types of lung infection and cancer in young homosexual men and Injection Drug Users were reported in the US and soon after, increasing cases of severe immunodeficiency were registered worldwide [1]. The disease was termed Acquired Immunodeficiency Syndrome (AIDS) and it was found to be sexually or blood transfusion-transmitted. Two years later, Dr. Françoise Barré-Sinoussi and her colleagues from the Pasteur Institute in France identified a retrovirus - which later was termed human immunodeficiency virus (HIV) - as cause of AIDS [2, 3]. Infections with HIV have become one of the most devastating pandemics in the recorded history and are still the leading cause of death in Africa. HIV type 1 (HIV-1) is the virus causing the vast majority of today's pandemic, indicated by approximately 38 million people living with the virus worldwide and 1.7 million reported new infections at the end of 2019 [4]. For HIV infected people, no cure exist so far. Untreated HIV infection causes progressive decay in $CD4^+$ T-cells, resulting in severe immunological abnormalities as well as in an increased risk of infectious and oncological complications [5]. Viral suppression can be achieved in HIV-infected people receiving anti-retroviral therapy (ART) and further transmission can be prevented. As a consequence of joint international effort to respond to the global health threat by HIV infections, access to HIV testing and medication has been steadily improved in the last decades. However, gaps in HIV services are still existing especially in low-income regions. Moreover, despite possible adverse side effects, ART requires a patient's lifelong commitment and strong adherence to the treatment schedule. Treatment interruptions lead to rapid viral rebound within few weeks, since HIV pharmacotherapy allows only control of the HIV load to undetectable levels, but does not eradicate the so-called latent viral reservoir, an ART-surviving source of infected immune cells, competent of being activated to produce new infectious HIV [5, 6]. To target this difficulty, new promising treatment strategies such as gene therapy [7], immunotherapy by utilizing broadly neutralizing antibodies [8] or the development of the first candidate of HIV vaccine [9] have been approached. Moreover, studies on compounds with latency reversing properties have moved the so-called "shock-and-kill" approach forward [10]. The idea behind this treatment approach involves the drug-induced reversal of latency and increase of viral gene expression ("shock"), rendering the HIV-1 reservoir sensitive to elimination by the immune system or by effective ART. However, despite the diversity of current HIV-1 eradication approaches, these strategies have not been clinically successful so far. Therefore, further research on HIV remains essential and of high

priority in order to improve our current understanding of HIV pathogenesis and to develop more potent and conceptionally novel treatment strategies for the cure of HIV/AIDS.

1.1.2. Organization of the HIV-1 genome and its encoded viral proteins

In the last decade, many scientific advances in the field of HIV research have been accomplished by protein-focused research on HIV-1. The foundation of all these advances is based on a comprehensive understanding of the HIV-1 encoded proteins. The compact HIV genome comprises two identical copies of single-stranded RNA [11]. As for many RNA viruses, the genome coding capacity of HIV-1 ($<$ 10 kB) is limited because of the instability of RNA [12]. As a consequence, HIV-1 utilizes a complexly intertwined repertoire of host biological processes to enable an efficient and parsimonious expression of viral proteins: By exploiting processes like overlapping open reading frames (ORFs), frameshifting, differential RNA splicing, alternative translation initiation and protease processing, HIV-1 is able to produce three essential polyproteins (coded by *gag*, *pol* and *env*) for infectivity and six further proteins supporting the course of viral replication [11]. After protease processing, HIV-1 provides a set of 15 functional proteins (fig. 1.1). Structural proteins expressed by *gag* comprise *matrix* (MA), *capsid* (CA or p24) *nucleocapsid* (NC) and p6 and are the most abundant proteins in the virion. Proteins encoded by *pol* comprise the viral *protease* (PR), *reverse transcriptase* (RT) and *integrase* (IN). Expression of *env* results in the envelope *glycoproteins 120* (gp120) and *41* (gp41). The other HIV-1 genes encode for the regulatory proteins, *transactivator of transcription* (Tat) and *regulator of expression of viral proteins* (Rev), as well as the accessory proteins *virion infectivity factor* (Vif), *viral protein R* (Vpr), *viral protein U* (Vpu) and *negative factor* (Nef). Tat and Rev are critical for HIV-1 replication, whereas Vif, Vpr, Vpu and Nef are not crucial for replication *in vitro*, but play a role in efficient disease progression in vivo [13–15]. This small set of proteins is sufficient to takeover the host cellular processes in order to fulfill HIV-1's requirements to establish its replication within the host cell.

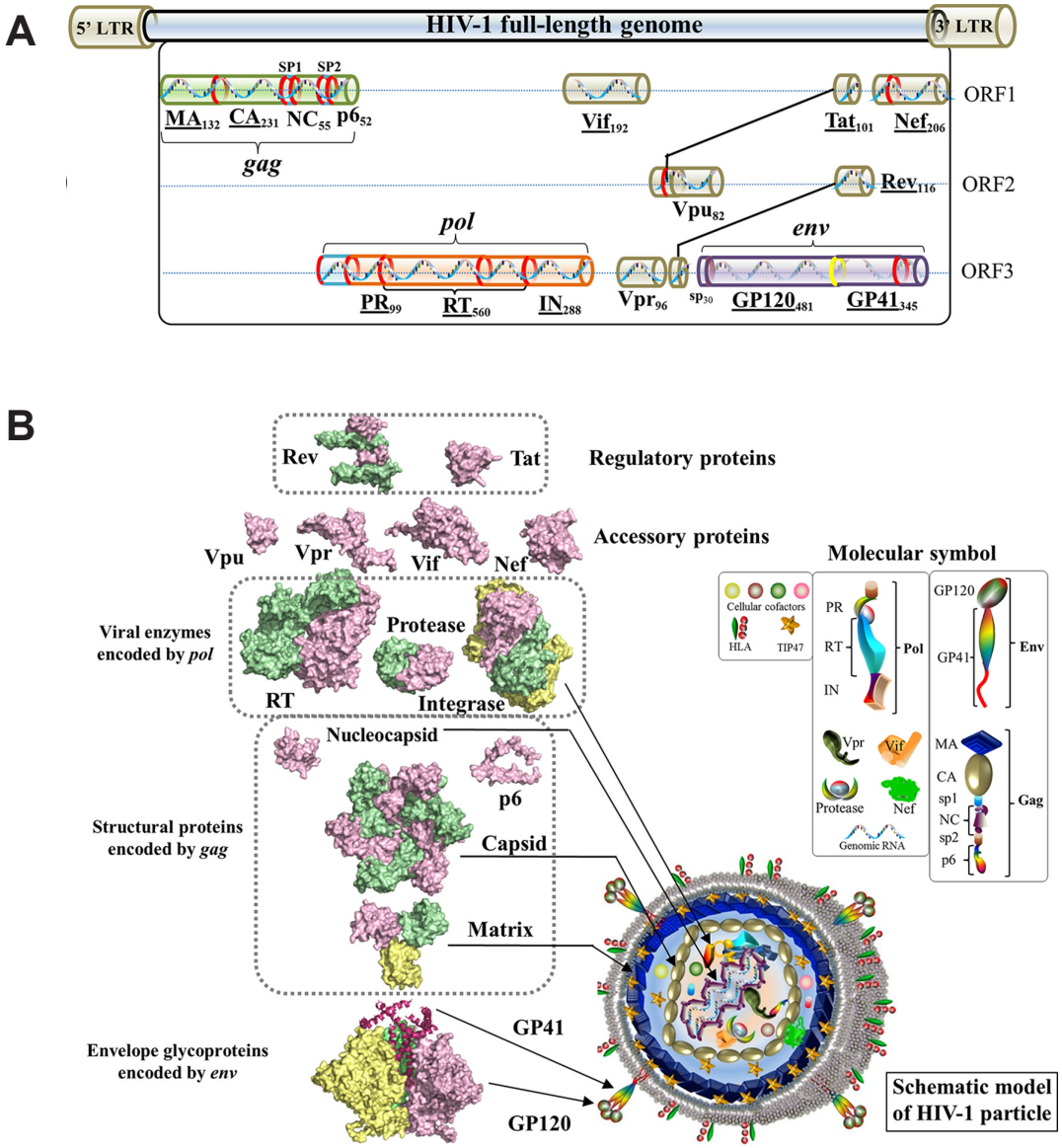

Figure 1.1. Gene maps and protein structures of HIV-1.
(A) Model of the HIV-1 full-length genome (reference strain HXB2). HIV-1 protein names and amino acid lengths are indicated beneath the protein coding regions in the three open reading frames (ORFs). Names of multimeric proteins are underlined. Within the gene map, red rings mark viral protease cleavage sites during viral maturation. Within the env gene, a yellow ring marks the cleavage site of human proteases (e.g. furin). The HIV-1 genome is flanked by 5' and 3' long terminal regions (LTRs).
(B) Surface representations of HIV-1 protein structures and schematic view of the HIV-1 particle. Representation of the HIV-1 proteins are clustered according to their functional roles: Monomeric proteins are shown in pink, different subunitis of multimeric proteins are distinguished with green, yellow or red. HIV-1 protein structures are scaled precisely for a direct and intuitive comparison. At the bottom right, a schematic model of a mature viral particle is illustrated and the key shows protein annotations.
Figure is adapted from [14].

1.2. CD4+ T-cells as target cell of HIV-1

HIV-1 infects *T-cell surface glycoprotein CD4* (CD4) expressing cells, which comprise T-lymphocytes, monocytes, macrophages and dendritic cells - cells that normally coordinate the adaptive immune response to defend the host against pathogens. Following, the focus will be on CD4+ T-cells (T-helper cells) as host as they have been identified as the primary target of HIV-1 [16–18]. In general, CD4 on T-cells contributes to T-cell recognition by antigen presenting cells (APC), resulting in T-cell activation. The activation of T-cells leads to their proliferation and differentiation into effector T-cells, which is dependent on the production of cytokines, in particular *interleukin 2* (IL2) [19, 20]. Antigen-stimulated, proliferating CD4+ T-cells help to regulate the immune response by stimulating other components of the adaptive immune system such as macrophages, B lymphoytes, CD8 cytotoxic T-cells and other immune cells to fight infection by pathogens [21].

Activated CD4+ T-cells are the preferred target of HIV-1, since productive infection is dependent on the metabolic and proliferating state of the infected cell [22, 23]. In activated CD4+ T-cells, host factors such as the *nuclear factor κB* (NF-κB), *nuclear factor of activated T-cells* (NFAT) and *transcription factor Sp1* (SP1), that positively regulate HIV-1 transcription, are more abundant [24–27]. Since these factors are largely triggered by T-cell activation, their availability is limited in resting CD4+ T-cells, thereby, suppressing the transcription of HIV-1 genes. Consequently, resting CD4+ T-cells are largely non-permissive to productive HIV-1 infection [28]. Beside the blockage of HIV-1 transcription, other antiviral barriers exist in resting cells. These barriers include rigid layers of cortical actin or an impaired reverse transcription, being triggered by the host factor *deoxynucleoside triphosphate triphosphohydrolase SAMHD1* (SAMHD1) [23, 29–32]. Notably, infection of "permissive resting CD4+ T-cells" is believed to result more likely in a latent infection [29, 33].

HIV-1 infection causes a disturbed cellular homeostasis, resulting in deregulation of size and composition of the CD4+ T-cell population and, if untreated, leads to the depletion of CD4+ T-cells, which consequently leads finally to a severely damaged immune system [34]. Therefore, investigation of HIV-1 associated changes in the T-cell environment is indispensable for improving general understanding of HIV-1 pathogenesis. In the recent years, global proteomic screens enabled identification of new regulatory mechanisms of HIV-1 hijacked TCR activation and also other pathways, that are reprogrammed in the presence of HIV-1 proteins. Consequently, elucidation of respective interactions between viral and host proteins are essential to decipher HIV-1 pathogenesis.

1.3. HIV-1 replication and virus-host-interactions

HIV-1 consists of a small genome and thus relies heavily on the host cellular machinery for production of viral progeny or for evasion of anti-viral host response. Therefore, understanding of the interplay between viral proteins and host cellular factors during the course of infection is fundamental for the search of novel therapeutic targets. Interactions between HIV-1 and host proteins regulate all stages of the HIV-1 replication cycle, from (i) the adhesion of the virion to the target host cell, (ii) the fusion of viral and host cell membranes, (iii) the uncoating to release the conical capsid core into the cytoplasm, (iv) the start of reverse transcription of viral RNA into double-stranded cDNA, (v) the nuclear import of the newly synthesized viral cDNA as well as its integration into the host genome, (vi) the establishment of HIV-1 latency or the expression of the HIV-1 provirus to synthesize new viral RNA and proteins to (vii) the assembly of viral particles and (viii) the release of viruses (fig. 1.2) [35].
In the last decade, substantial progress has been achieved towards the understanding of biomolecular mechanisms underlying the interaction of the HIV-1 with the host cell. According to the HIV-1 Human Interaction Database (HHID), available through the National Library of Medicine, a total of 3142 human genes are involved in 12,786 described virus-host-protein interactions [36]. To note, those data are partly derived from next generation sequencing approaches and from systems-wide mass spectrometry. For example, 497 physical interactions between individual human proteins and HIV-1 proteins have been identified by affinity-tagged purification mass spectrometry and thus, require further validation [37]. Studies of HIV-1-host interactions on protein level have assisted to identify several cellular pathways that are hijacked by the virus to modulate critical steps during its replication cycle.

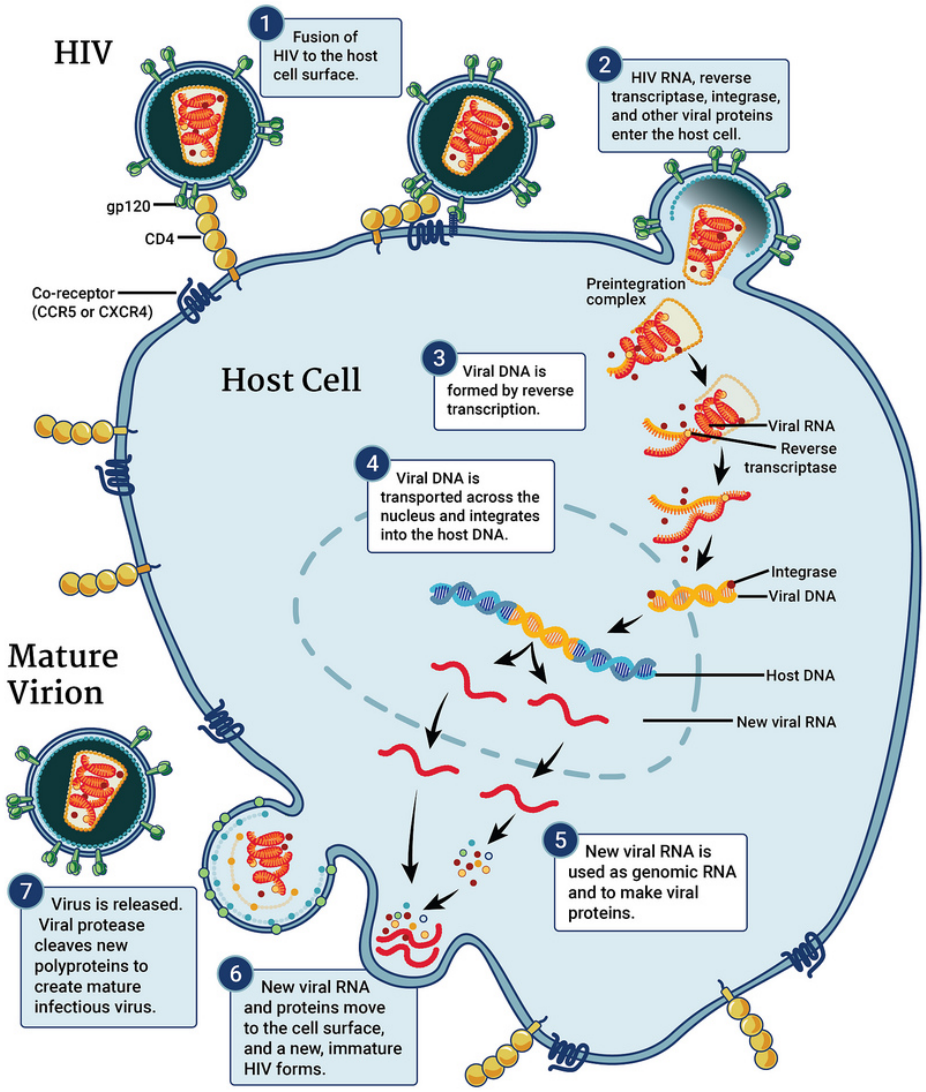

Figure 1.2. HIV replication cycle.
The HIV replication cycle begins with the fusion of HIV with the surface of its host cell, which requires binding of the viral envelope with the CD4 receptor and respective co-receptors (1, 2). The shell of the capsid disintegrates and the HIV reverse transcriptase transcribes the viral RNA into DNA (3). The viral DNA is transported across the nucleus, where the HIV protein integrase integrates the HIV DNA into the host's DNA (4). The host's normal transcription machinery transcribes HIV DNA into multiple copies of new HIV RNA. Some of this RNA becomes the genome of a new virus, while the cell uses other copies of the RNA to make new HIV proteins (5). The new viral RNA and HIV proteins move to the cell membrane, where a new, immature HIV forms (6). Finally, the virus is released from the cell, and the HIV protease cleaves newly synthesized polyproteins to create a mature infectious virus (7). Figure from [35]

1.4. Post-translational modification-based regulation of HIV replication

1.4.1. Post-translational modification of proteins

In addition to the identification of relevant HIV-1 host interactions, new technologies have enabled the discovery of novel mechanisms, by which invading viruses are able to reprogram a hostile host environment. This includes newest insights of post-translational modifications (PTMs) of proteins contributing to viral hijacking of the host and cellular responses to infection. PTMs provide cells with the plasticity for dynamic and reversible control of a protein's function, localization and interaction without involvement of genomic, transcriptomic or translational regulation. Therefore, PTMs enhance the already multifunctional nature of viral proteins and offer another level of functional diversity within the limited genetic space of the viral genome. So far, over 200 different PTM types have been reported [38, 39]. Among the most frequently analyzed PTMs are protein phosphorylation, acetylation and ubiquitination [38] (fig. 1.3).

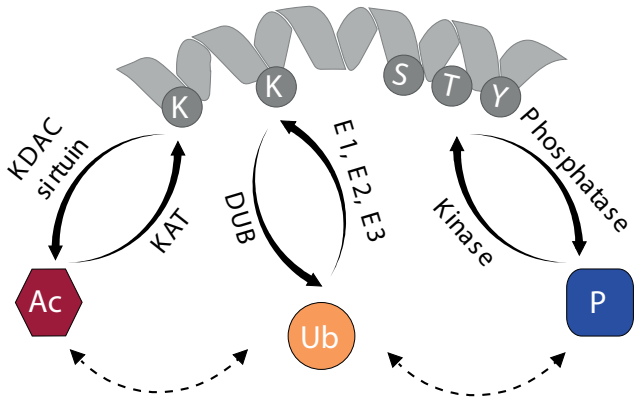

Figure 1.3. Protein phosphorylation, acetylation and ubiquitination.
Proteins can be modified by different enzymes, which either introduce a functional group ("writers") or remove it ("erasers"). Thereby, lysine acetylation is achieved by lysine-acetyltransferases (KATs) and the backward reaction is fulfilled by lysine deacetylases (KDACs, also known as histone deacetylases (HDACs)) or sirtuins. Lysines can be also modified by ubiquitin in presence of E1 ubiquitin-activating-, E2 ubiquitin-conjugating-enzymes, and E3 ubiquitin ligases. Reversal of ubiquitin linkages is achieved by deubiquinating enzymes (DUBs). Another frequent modification occurs at serine-/threonine- and/or tyrosine-residues, where phosphate groups are transferred to by kinases. Removal of phosphorylation is carried out by phosphatases. All three modifications can influence each other and might occur at the same protein. Figure from [40].

Phosphorylation

Protein phosphorylation was one of the first described PTMs by E. H. Fischer and E. G. Krebs [41]. In 1992, these two researchers were awarded with the Nobel Prize on Physiology or Medicine for their discovery concerning protein phosphorylation as a biological regulatory mechanism. To date, protein phosphorylation is one of the most intensively studied and best understood PTM on proteins. Reversible phosphorylation defines the enzymatic transfer of a negatively charged phosphate group to serine, threonine and tyrosine residues. The presence of the charged, hydrophilic group results in changes of protein conformation regulating protein activity, stability, localization and interaction with other factors. In particular, series of phosphorylation events are commonly used for amplification of cell signaling in order to regulate cellular growth control, differentiation and other biological processes. Enzymes responsible for phosphorylation are protein kinases whereas phosphatases conduct the reverse dephosphorylation processes. Protein kinases and phosphatases are estimated to constitute 1.5 to 2% of the entire protein-coding genes of eukaryotes [42]. Typically, phosphorylated proteins constitute only a small fraction of the proteome. As a consequence, analysis of phosphoproteins usually requires efficient enrichment strategies such as immobilized metal ion affinity chromatography (IMAC) and metal oxide affinity chromatography (MOAC) [43, 44].

Acetylation

Protein acetylation is considered as "rival" of phosphorylation in terms of regulatory modifications [45]. Protein acetylation occurs on the ε-amino group on lysines and is a reversible PTM, which neutralizes the positive charge of lysines, thereby, changing protein function in diverse ways [46]. Recent studies revealed that 5-10% of mammalian and bacterial proteins undergo lysine acetylation [47]. Originally, this PTM was identified as nuclear event on histone proteins only and was long known for its role in epigenetic and DNA-dependent processes [46, 48]. With growing numbers of large-scale acetylation studies, it has become evident, that lysine acetylation is ubiquitous and also occurs on cytoplasmic and mitochrondial proteins. As a consequence, the role of reversible protein acetylation emphasizes its function in regulation of gene expression, but also in other processes such as cell-cycle control, DNA damage response, cytoskeletal organization, metabolism and immune signaling [48–50]. On the analogy of protein kinases and phosphatases, lysine acetylation is mediated by the opposing activities of lysine acetyltransferases (KATs) and deacetylases (KDACs)/sirtuins. Apart from KATs and KDACs/sirtuin, proteins with so-called bromodomains specifically recognize and bind acetylated lysines, thereby, regulating chromatin organization, transcription and cell homeostasis [51, 52]. Notably, some KATs are also bromodomain-containing proteins [51]. In human cells, 22 different KATs and 18 KDACs/sirtuins have been identified so far [53]. In contrast to protein phosphorylation, technological limitations have complicated a global analysis of lysine acetylation so far. Nevertheless, the introduction of antibodies specific for

acetylated lysine residues to enrich modified protein/peptides has significantly improved the detection of endogenous acetylation sites by mass spectrometry [48].

Ubiquitination

In contrast to protein phosphorylation and acetylation, which represent small chemical modifcations of amino acids, ubiquitination is a protein-based modification [54]. Ubiquitin is attached to lysine residues by a three-step enzymatic cascade [55] involving E1 ubiquitin activating [56], E2 ubiquitin conjugating [57] and E3 ubiquitin ligating enzymes [58–60]. Ubiquitinated proteins are recognized by proteins with ubiquitin-binding domains [61] and the modification is removed by so-called deubiquitinases (DUBs) [62, 63]. Whole proteome studies found several thousands of proteins in almost every signaling pathway to be modified by ubiquitination [64, 65]. The concerted action of ubiquitinating, deubiquitinating and ubiquitin-binding proteins determines a modified proteins's fate [66]. Ubiquitin chains can target proteins to the 26S proteasome and, thereby, regulate proteosomal degradation [67]. Ubiquitination at the cell membrane can also induce endocytosis and lysosomal degradation [68, 69]. Apart from the proteolytic functions, ubiquitination can also influence a protein's localization, activity and protein interactions in distinct signaling pathways [66]. Similar to acetylation, antibodies, that recognize diglycine-containing peptides following trypsin digest, are utilized for ubiquitinome studies [70].

1.4.2. Post-translational modifications during the HIV-1 replication cycle

Pathogens utilize different mechanisms to hijack the host cellular machineries to promote infection. In the recent years, PTMs have been increasingly recognized as key strategies used by pathogenes to manipulate and regulate host proteins [71–73]. The importance of PTMs during HIV-1 infection has been emphasized by several studies, that used inhibitors of PTM enzymes to reduce viral load or to reactivate latent HIV-1 successfully. This was exemplified by the use of SRC-family kinase inhibitors, which resulted in inhibited HIV-1 infection [74] and the use of lysine-deacetylase inhibitors in order to reactivate latent HIV-1 in different cell systems [75]. In the following sections, several phosphorylation-, acetylation- and ubiquitination-regulated virus-host interactions will be highlighted for different stages of the HIV-1 replication cycle starting from the viral entry to the release of newly produced and maturated viral particles to illustrate the diversity of PTM-controlled mechanism during HIV-1 infection.

1.4.3. Virus fusion and entry

The HIV-1 replication cycle starts with the fusion of the virus with the surface of the host cell. Binding of the viral envelope consisting of gp41/gp120 trimers with the CD4 receptor and co-receptors CCR5 for R5-tropic or CXCR4 for X4-tropic HIV induces membrane fusion [76, 77]. In the course of this process, several intracellular signaling processes are triggered by the virus to gain access to cellular components in order to overcome intracellular barriers [78]. Many of these early HIV-1-hijacked aberrant phospho-signaling cascades lead to highly dynamic rearrangement of the cytoskeleton e.g. as a result of activated G-protein coupled receptor signaling involving several kinase activations such as *phosphatidylinositol 4,5-bisphosphate 3-kinase* (PI3K), *dual specificity mitogen-activated protein kinase kinase 1 (MAP2K1)* or *protein-tyrosine kinase 2* (PYK2) [79, 80] (fig. 1.4).

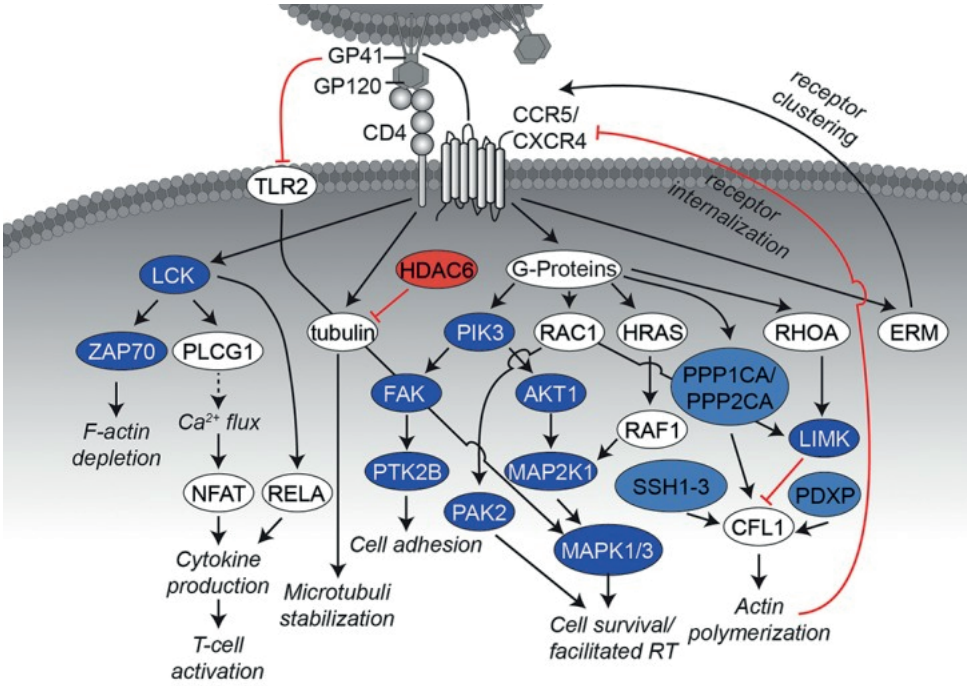

Figure 1.4. Interaction networks of HIV-1 and host protein during virus entry
Binding of the viral envelope gp160 complex, consisting of gp120 and gp41, to CD4 as well as the co-receptors CXCR4 or CCR5 induces activation of several protein kinases. Thereby, the cytoskeleton becomes rearranged, which promotes entry and subsequent nuclear import of HIV-1. The interaction network displays an overview of relevant interactions. Black pointy arrows indicate activating effects and red "inhibitory"-arrows indicate inhibitory effects. Kinases are shown in dark blue, phosphatases in light blue and KDACs in light red Other host proteins are colored white. Figure modified from [40].

In addition to processes related to cytoskeleton modulation, phosphorylation regulated signaling triggered upon virus binding via phosphorylation of *tyrosine-protein kinase Lck* (LCK) induces also activation of specific transcription factors e.g. *transcription factor p65* (RELA; also known as NF-κB) [81] or NFAT [79]. Activation of NF-κB or NFAT results in the production of cytokines e.g. IL2 promoting T-cell activation and, thereby, the cell becomes conditionized towards viral replication [82]. In addition to the several phosphorylation events modulating the organization of the cytoskeleton or T-cell activation, regulation by lysine (de-)acetylation was also reported for *histone deacetylase 6* (HDAC6). HDAC6 has been found to de-acetylate α-tubulin. Thereby, HDAC6 counteracts the formation of the acetylated form of α-tubulin, which is required for microtubule stabilization and supports HIV-1 envelope-dependent cell fusion and infection.

1.4.4. Uncoating and reverse transcription

After fusion of virus and host cell, the viral conical capsid core is released into the cytoplasm and a process called uncoating is initiated. Thereby, the viral RNA as part of the reverse transcription complex (RTC) is released and the RT becomes active starting the reverse transcription of the viral RNA into double-stranded cDNA. In brief, there are three models suggesting the potential mechanism of uncoating (reviewed by [83]): (i) "immediate uncoating", describing rapid disassembly of the viral core capsid after fusion [84, 85], (ii) gradual uncoating, supporting the model of partial core disassembly in the cytoplasm, while RTC associated viral CA mediates critical interactions with host vectors and nuclear import [86, 87], (iii) nuclear core complex (NPC) uncoating, by which the core stays intact and prevents detection of the viral double stranded cDNA by host cytosolic DNA sensors until its arrival at the nuclear core, complex while dynamic capsid pores enables import of nucleotides to fuel reverse transcription [88–90]. Independently from the respective models, experimental evidences have been reported that the capsid core structure as well as CA mediate important functions for reverse transcription and nuclear import during the uncoating processes. Several of these functions have been described to be regulated by PTMs (fig. 1.5). For example, three phosphorylation sites within CA (S109, S149, S178) were described to have a major impact on reverse transcription [91]. One of the three sites (S149) was identified as target of *maternal embryonic zipper kinase* (MELK) and its phosphorylation seems to be crucial for optimal uncoating and reverse transcription of viral RNA into cDNA [92]. Another phosphorylation site within CA (S16) is targeted by *mitogen-activated protein kinase 1* (MAPK1; also known as ERK2) which is required for *peptidyl-prolyl cis-trans isomerase NIMA-interacting-1* (PIN1)-dependent disassembly of the HIV-1 core. [93, 94]. Interestingly, MAPK1 was reported to be incorporated into HI virions. As virion associated protein kinase, MAPK1 activity might be already enhanced during virus

binding and fusion, leaving the spatiotemporal interaction between MAPK1 and CA under debate [91].

Simultaneously to the uncoating process, reverse transcription is initiated. Thereby, PTMs seem to be pivotal for the optimal viral cDNA synthesis. For example, the interaction between the HIV envelope with the CD4 receptor and co-receptors CCR5/CXCR4 activates the Gαi-dependent MAPK pathway (involving MAPK1 and MAPK3) via phosphorylation, which enables reverse transcription already during the virus binding process [95]. After fusion, PTM based modulation of reverse transcription has been also reported e.g. for the interaction with *cyclin-dependent kinases* (CDK) such as CDK2. CDK2 was identified as direct interactor of HIV-1's RT and phosphorylates the RT on T216, resulting in enhanced RT efficacy and stability. Furthermore, *cyclin-dependent kinase inhibitor 1A* (CDKN1A, also known as P21), which functions as a cell-intrinsic CDK2 inhibitor was able to block HIV-1 reverse transcription by inhibition of CDK2-mediated phosphorylation of the viral RT [96]. Interestingly, higher levels of P21 expression have been reported in $CD4^+$ T-cells from "HIV elite controllers", supporting the data of reduced RT activity by inhibition of CDK2 [96–98].

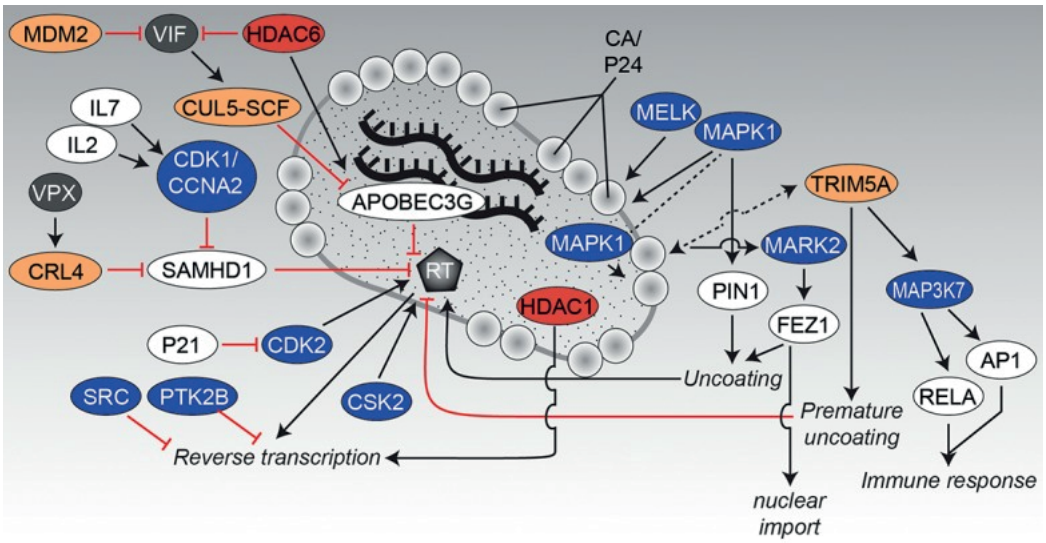

Figure 1.5. Interaction networks of HIV-1 and host protein during uncoating and reverse transcription. The figure shows an overview of protein-protein interactions, that have been described during uncoating and reverse transcription. Please note, that Vpx is only expressed in HIV-2 and SIV but not in HIV-1. CRL4 complex consists of *cullin 4A* (CUL4A), *DNA damage binding protein 1* (DDB1), *RING H2 finger protein* (RBX1) and the *DDB1 and CUL4-associated Factor 1* (DCAF1). Black arrows indicate activating effects and red "inhibitory"-arrows indicate inhibitory effects. Kinases are shown in dark blue, KDACs in light red and E3 ligases in orange. Other host proteins are colored white, whereas viral proteins are indicated in gray. Figure modified from [40].

Parallel to the enhancing effects of the RT by specific kinases, phosphorylation and dephosphorylation also affect host antiviral factors. For example, *interleukin 7* (IL7) induces phosphorylation of *deoxynucleoside triphosphate triphosphohydrolase SAMHD1* (SAMHD1) by the *cyclin A2* (CCNA2)/*cyclin dependent kinase 1* (CDK1) complex [99]. The phosphorylation of SAMHD1 by CDK1/CCNA2 results into its decreased activity to reduce the intracellular dNTP pool and to counteract reverse transcription [99–101].
Apart from SAMHD1, HIV-1 developed also mechanism to counteract *DNA dC→dU-editing enzyme APOBEC-3G* (APOBEC3G), which is also a host restriction factor. APOBEC3G is able to inhibit reverse transcription and to introduce virus-inactivating hypermutations into the newly synthesized viral DNA based on its DNA deamination function [102–104]. This process is counteracted by HIV-1 Vif. Vif induces polyubiquitination of APOBEC3G by recruiting the *cullin-5* (CUL5)-SCF complex resulting in the proteosomal degradation of APOBEC3G [105, 106]. Simultaneously, *E3 ubiquitin-protein ligase Mdm2* (MDM2) is able to target Vif for proteosomal degradation and, thereby, increases APOBEC3G-levels [107].
Apart from MDM2, also HDAC6 exhibits antiviral activity by promoting autophagic degradation of Vif. HDAC6 has been described to stabilize APOBEC3G and, thereby, the APOBEC3G/HDAC6 complex is able to impair reverse transcription [108]. Different from HDAC6, HDAC1 was found to be incorporated in a complex with *histone deacetylase complex subunit SAP18* (SAP18) and *paired amphipathic helix protein Sin3a* (SIN3A) in newly generated HIV-1 virions. Virion-associated HDAC1 has been described to be required specifically during reverse transcription and influences infectivity of the produced virions, which was demonstrated by enzymatically inactive HDAC1 mutants leading to an early block of reverse transcription [109].

1.4.5. Nuclear import and integration

The process of uncoating and reverse transcription results in newly synthesized viral cDNA, which interacts with several viral (IN, RT, Vpr and MA) and an incompleteley characterized group of host proteins forming the preintegration complex (PIC) [85, 110–114]. HIV-1 hijacks the cellular nuclear import machinery to actively transport the PIC into the nucleus, where integration of viral cDNA into the host genome takes place. On the way to the nucleus, the PIC encounters several interactions regulated by PTMs (fig. 1.6). One example is represented by kinesin adaptor *fasciculation and elongation protein zeta-1* (FEZ1), which is a capsid-associated host regulator of early HIV-1 transport towards the nucleus [115]. Within the course of this process, the capsid also binds *serine/threonine-protein kinase MARK2* (MARK2), which induces FEZ1 phosphorylation on viral cores to modulate HIV-1 uncoating and motility [116].

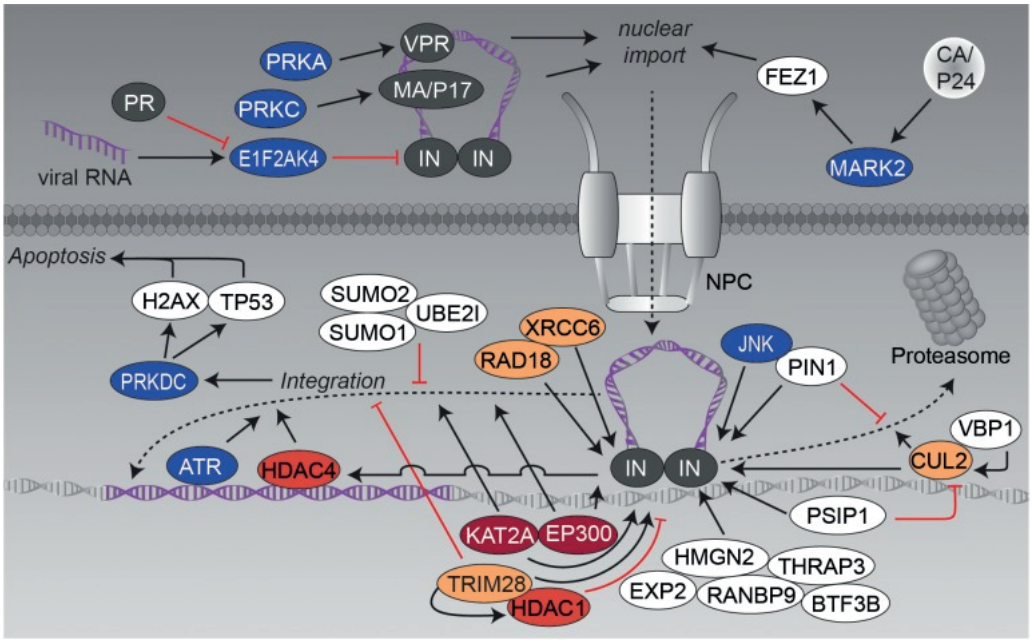

Figure 1.6. Interaction networks of HIV-1 and host protein during nuclear import and integration. The graphic shows the participation of post-translational modifying enzymes during the nuclear transport of the PIC and integration of the viral cDNA into the host genome. Black arrows indicate activating effects and red "inhibitory"-arrows indicate inhibitory effects. Kinases are shown in dark blue, KDACs in light red and E3 ligases in orange. Other host proteins are colored white, whereas viral proteins are indicated in gray. Figure modified from [40].

Not only the traffic towards the nucleus is regulated by PTMs, the viral enzyme IN itself is also subject to PTM-based interactions. Another example for phosphorylation controlled processes is demonstrated by IN's interaction with *eukaryotic translation initiation factor-2-alpha kinase 4* (EIF2AK4, also known as GCN2), which was identified as antiviral host factor restricting DNA integration [117]. Upon HIV-1 infection induced cellular stress response mediated decrease in protein translation, GCN2 is activated in the presence of viral RNA and phosphorylates IN at S255, thereby, decreasing its efficiency in its integration activity. This antiviral response is counteracted by HIV-1 PR, which triggers proteolytic inactivation of GCN2 [117–119].

Apart from phosphorylation, IN has been shown to be modified by lysine-acetylation as well. This is exemplified by acetylation of IN by *histone acetyltransferase p300* (EP300) at three lysine residues within the DNA binding domain (K264, K266 and K273), which enhances IN's integration capacity by increasing its affinity to DNA [120]. The importance of acetylation was also demonstrated by IN's interaction with *histone acetyltransferase KAT2A* (KAT2A, also known as GCN5). Similar to EP300, GCN5 dependent acetylation of IN enhances viral integration [121]. Notably, GCN5 acetylates the same lysine residues as EP300, while K258 is acetylated by GCN5 exclusively. However, an obligate role for acetylation at the respective lysines within IN could not be confirmed so far, since arginine substitution mutagenesis of the respective sites did not inhibit the production of competent viruses [122]. Acetylated

IN has been shown to be targeted by several cellular proteins e.g. by antiviral protein *transcription intermediary factor 1-beta* (TRIM28, also known as TIF1B or KAP1). Binding of IN by TRIM28 also recruits HDAC1 and results in deacetylation of IN leading to inhibited HIV-1 integration [123]. Interestingly, not all lysine deacetylases exhibit integration inhibitory activity: HDAC4 was found to be associated with HIV-1 DNA in an IN dependent manner and was described to be important for efficient transduction of HIV-1-based vectors within the course of post-integration DNA repair [124, 125].
Studies utilizing the translation inhibitor cycloheximide and the proteosomal inhibitor MG-132 have shown, that IN is a relatively short-lived protein and polyubiquitinated IN is targeted for proteosomal degradation [126]. Here, *prefoldin subunit 3* (VBP1) has been identified as interacting protein, that mediates ubiquitination of IN by *cullin-2* (CUL2) for degradation [127]. However, IN degradation has been described to be important for later HIV-1 replication, since mutated degradation-associated lysines (K211, K215 and K219) resulted in reduced release of infectious viral particles [127]. Different host proteins have been reported to inhibit IN degradation: For example, complexing of *PC4 and SFRS1-interacting protein* (PSIP1, also known as LEDGF) with IN [111, 128] seems to prevent IN degradation. IN stabilizing properties have also been identified for *E3-ubiquitin protein ligase RAD18* (RAD18) and *X-ray repair cross-complementing protein 6* (XRCC6), however, their role during HIV-1 replication remains elusive [129, 130].

1.4.6. Transcription and latency

After successful nuclear import and integration of the viral cDNA into the host genome, the HIV-1 provirus functions like a cellular gene, in which the 5'-LTR acts as a promotor and the 3'-LTR as polyadenylation- and termination-site. Upon transcription from the 5'-LTR, one primary transcript is produced, which is subjected to alternative splicing resulting in at least 109 different mRNAs [131]. After integration, a provirus either is actively expressed or transcription from the provirus is suppressed resulting in a latent HIV provirus. HIV-1 transcription and latency activation depend on many factors such as cell cycle, activation state of the infected host or integration site (reviewed in [132]). Both processes are tightly interconnected and regulated by PTM dependent mechanisms. Examples for phosphorylation and acetylation involving processes are highlighted in the following sections for HIV-1 transcription (fig. 1.7) and latency (fig. 1.8) respectively.

Transcription

HIV-1 transcription is regulated by some viral proteins, host proteins or transcription factors forming the transcription pre-initiation complex (PIC). The PIC involves RNA polymerase II (RNAPII) and binds to the 5'-LTR, thereby, recruiting several essential transcription factors like NF-κB [133], NFAT [134] and SP1 [24]. Early transcription results in a few fully spliced mRNAs, which encode for the viral proteins Tat and Rev. Both proteins are active in the nucleus and are essential for the regulation of HIV-1 gene expression. Since Rev's function is mainly assigned to the escort of late viral transcripts from the nucleus into the cytoplasm, the following section is focused on Tat's function as nuclear transcriptional activator of viral gene expression. In the absence of Tat, HIV-1 transcription is still initiated at the 5'-LTR, however the RNA Pol II generates only short or non-processive transcripts [135]. Moreover, elongation of transcription is also stalled by *negative elongation factor* (NELF) and *DRB sensitivity-inducing factor* (DSIF, also known as SUPT5H). Tat stimulates the elongation properties of the transcription machinery by binding to the HIV-related RNA stem loop structure encoded by the trans-activation responsive region (TAR) (fig. 1.7) [136, 137]. As a consequence, positive transcription elongation factor b (P-TEFb), consisting of the *cyclin-dependent kinase 9* (CDK9) and *cyclin-T1* (CCNT1), is recruited for phosphorylation of RNAPII, resulting in enhanced transcription elongation [138–140] (fig. 1.7). Apart from CDK9, *cyclin-dependent kinase 7* (CDK7) was also reported to phosphorylate RNAPII [141].

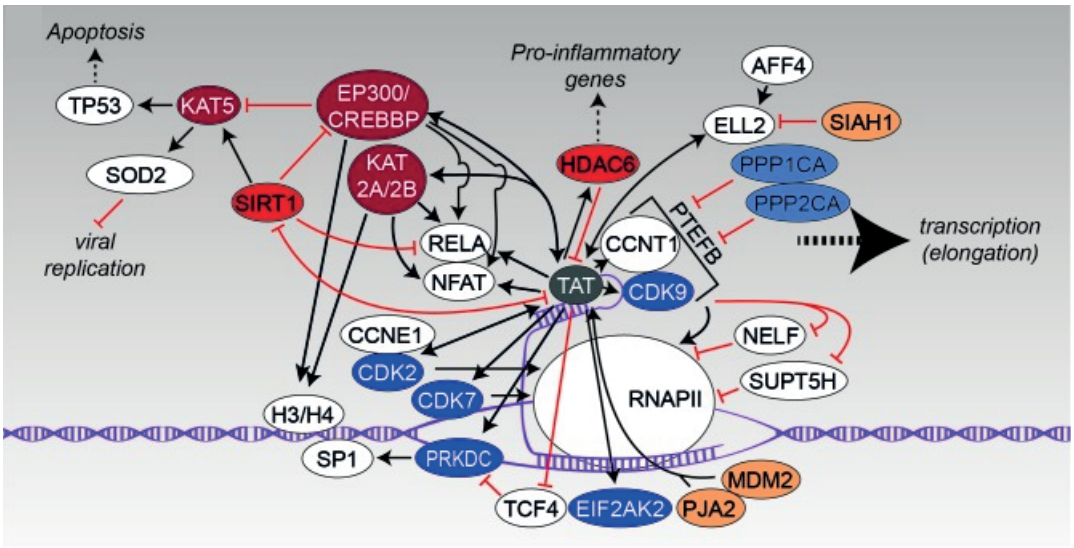

Figure 1.7. Interaction networks of HIV-1 and host protein during transcription.
The graphic shows protein-protein interactions, that have been described to promote HIV-1 transcription. Black pointy arrows indicate activating effects and red "inhibitory"-arrows indicate inhibitory effects. Kinases are shown in dark blue, phosphatases in light blue, KATs in dark red, KDACs/sirtuins in light red and E3 ligases in orange. Other host proteins are colored white, whereas viral proteins are indicated in gray. Figure modified from [40].

In addition to the phosphorylation of RNAPII, Tat also induces phosphorylation of NELF and DSIF by P-TEFb leading to activation of transcription elongation [142, 143]. As counteracting factors of Tat and P-TEFb, *serine/threonine-protein phosphatase PP1* (PP1) and *serine/threonine-protein phosphatase 2A* (PP2A) have been identified, which target and destabilize the Tat-P-TEFb complex [144, 145].

The interaction of Tat with P-TEFb exemplifies one of the >100 phosphorylation-associated virus-host interactions [40]. However, the interactome of Tat is not limited to protein kinases and phosphatases. The extensive repertoire of cellular proteins interacting with Tat includes >180 different nuclear proteins identified in a proteomic screen [146] and also involves several lysine acetyltransferases and deacetylases. For example, Tat recruits GCN5 and *P300/CBP-associated factor* (PCAF, also known as KAT2B) to the 5'-LTR to promote transcription [147, 148]. Additionally, NF-κB was found to be acetylated in a Tat-dependent manner leading to a higher DNA binding properties of NF-κB and increased transcription rates [149]. Moreover, Tat itself serves as acetylation substrate. For example, K28 of Tat is acetylated by PCAF and enhances Tat's binding to P-TEFb [150–152] while HDAC6 deacetylates Tat at K28 resulting in suppressed Tat mediated transactivation of the 5'-LTR [153]. Another acetylation target site was found at K50 which is acetylated by EP300 and induces dissociation of Tat from the TAR [151, 152]. Different from Tat's interaction with EP300, acetylation at K50/51 by GCN5 results in increased Tat's transcriptional activity [154]. *NAD-dependent protein deacetylase sirtuin-1* (SIRT1) was identified to bind and deacetylate Tat at K50. Thereby, SIRT1 recycles non-acetylated Tat for binding to TAR and P-TEFb [155]. These examples of reversible Tat (de-)acetylation demonstrate the importance of controlled cycles between Tat acetylation and deacetylation to regulate HIV-1 transcription. However, the mechanism, by which Tat switches its acetylation state for transcriptional fine-tuning needs to be further characterized. Apart from the transcription-associated processes, the interaction between Tat and SIRT1 also induces proteosomal degradation of *histone acetyltransferase KAT5* (KAT5, also known as TIP60) resulting in decreased TP53 mediated apoptosis [156–158]. Moreover, Tat/SIRT1 caused KAT5 degradation also decreases expression of *manganese-dependent superoxide dismutase* (Mn-SOD), which exhibits antiviral activity [159].

Similar to HIV-1 IN (section 1.4.5), K48-linked ubiquitination targets Tat for proteosomal degradation [160]. Moreover, Tat has been shown to interact with several E3 ubiquitin-protein ligases in a non-proteolytic manner. For example, MDM2- or *E3 ubiquitin-protein ligase Praja-2* (PJA2)-mediated ubiquitination of Tat has been described to stimulate the transcriptional properties of Tat [161, 162].

Latency

Apart from PTM-regulated processes contributing to active transcription as described above, integrated HIV-1 proviruses can also remain transcriptionally inactive and, thereby, establish latent HIV-1 reservoirs. These long-living reservoirs contribute to viral rebound after the interruption of ART treatment. Since latently infected cells are neither detected nor eliminated by the immune system or current therapeutics, stable reservoirs remain a major obstacle to HIV-1 eradication [6, 163–165]. Latency itself is established during early acute infection in $CD4^+$ T-cells albeit with low frequency *in vivo* (approximately 1 in $1x10^6$ resting $CD4^+$ T-cells in patients under ART) [166, 167]. Viral proteins in latently infected cells are expressed at very low levels facilitating immune evasion [168, 169]. The molecular mechanisms for the establishment of latency and its maintenance are still elusive. It is anticipated, that the inactive viral state mainly underlies the resting nature of $CD4^+$ T-cells, whereas activated $CD4^+$ T-cells are more prone for productive infection [170]. Nonetheless, it is out of question, that chromatin reorganization within the region of the integrated provirus, epigenetic modifications, regulation of transcription factors and several other processes of gene silencing are required to promote HIV-1 latency [171–173]. In this context, (de-)acetylation of the chromatin environment close to the viral integration site was demonstrated to affect reactivation of latent HIV [174, 175].
For example, inhibition of KDACs regulating histone acetylation and accessibility of DNA to transcription factors showed the potential to reactivate HIV from the latent state [75]. The relevance of KDACs during latency establishment is also emphasized in studies disclosing the recruitment of KDACs to the HIV-1 5'-LTR by transcriptional repressors such as *alpha-globin transcription factor CP2* (TFCP2, also known as LSF) or *transcriptional repressor protein YY1* (YY1) (fig. 1.8). One of these recruited KDACs is exemplified by HDAC1, which augments repression of the LTR by YY1 and LSF, resulting in inhibited HIV-1 expression [176, 177]. Another link between transcription factors and HDAC1 in the context of latency maintenance is represented by the interaction between the subunits (p50, p65) of NF-κB and HDAC1. Interestingly, the p50/p65 heterodimer of NF-κB serves as activator of HIV-1 transcription (as described in the section before) whereas the p50 homodimer recruits HDAC1 to the 5'-LTR, inducing chromatin condensation and reduced binding of RNAPII to the 5'-LTR [178, 179].

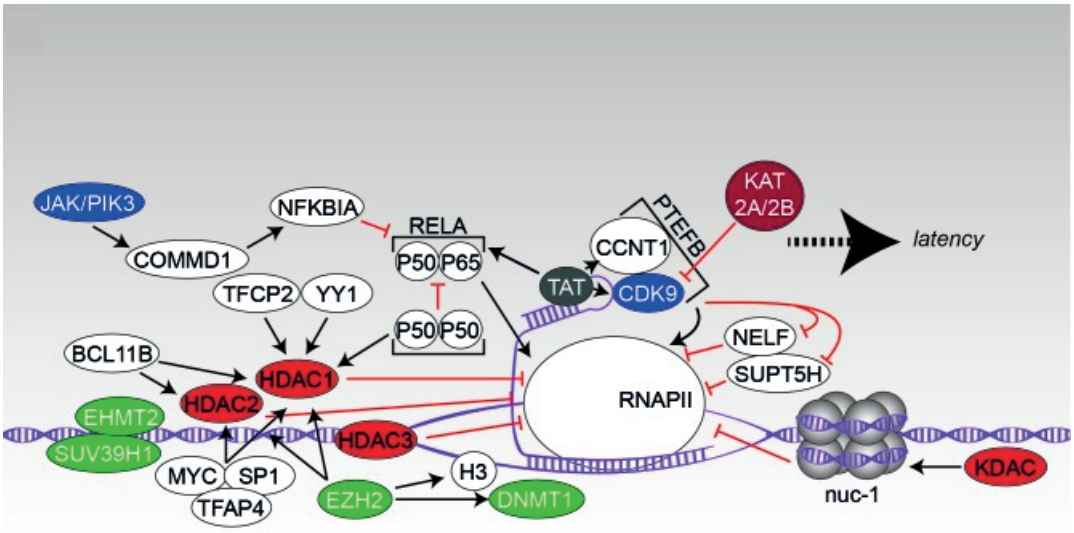

Figure 1.8. Interaction networks of HIV-1 and host protein during latency establishment.
The interaction network indicates the influence of modifying enzymes onto HIV-1 latency. Black arrows indicate activating effects and red "inhibitory"-arrows indicate inhibitory effects. Kinases are shown in dark blue, KATs in dark red and KDACs in light red. In addition, methyltransferases are shown in green (not discussed here). Other host proteins are colored white, whereas viral proteins are indicated in gray. Figure modified from [40].

Similar relationships were also reported for the recruitment of HDAC1 by transcriptional factors/repressors *recombination binding protein suppressor of hairless* (RBPJ, also known as CBF1), *transcriptional factor AP-4* (TFAP4, also known as AP4), *Myc proto-oncogene protein* (MYC) or SP1 promoting decreased binding of RNAPII to the HIV-1 promotor region and transcriptional silencing [180–183]. Apart of HDAC1, other KDACs associated with the establishment of HIV-1 latency were HDAC2 and HDAC3. Inhibition of these KDACs by respective KDAC inhibitors increased histone acetylation at the 5'-LTR and induced viral outgrowth [184, 185]. Apart from the mechanisms involving deacetylation of histones by KDACs for latency maintenance, acetylation of non-histone proteins was also reported, which silences transcription of the provirus. For example, acetylation of CDK9 by GCN5 and PCAF prevents phosphorylation of CD99 and, thereby, reduces P-TEFb mediated viral transcript elongation by RNAPII [186, 187].

Apart from acetylation, there are also regulatory mechanisms of HIV-1 latency, which are based on phosphorylation. The expression of an endogeneous inhibitor of RELA (NF-κB), *NF-kappa-B inhibitor alpha* (NFKBIA, also known as IκBα) is increased by *tyrosine-protein kinase JAK* (JAK)/*phosphatidylinositol 4,5-bisphosphate 3-kinase* (PIK3)-mediated activation of *COMM domain-containing protein 1* (COMM1), which stabilizes NFKBIA and, thereby, attenuates NF-κB signaling, which leads to enhanced HIV-1 latency [188]. The role of phosphorylation during HIV-1 latency is also emphasized by the chemical compound, small molecule activator of protein phosphatase 1 (SMAPP1), which increases phosphorylation of CDK9 and induces up-regulation of P-TEFb, thereby, inducing reactivation from HIV-1 latency and HIV-1 replication [145].

As an example for the involvement of ubiquitination in the regulation of HIV-1 latency, *E3 ubiquitin-protein ligase SIAH1* (SIAH1) (fig. 1.7) has been described to be required for HIV-1 transcription through its interaction with *elongation factor for RNA polymerase II 2* (ELL2). ELL2 forms together with other proteins such as the *elongation factor for RNA polymerase II 1* (ELL1), HIV-1 Tat, CCNT1, CDK9 and *AF4/FMR2 Family Members 1 and 4* (AFF1/4) the super elongation complex (SEC), promoting transcriptional elongation. SIAH1-induced proteosomal degradation of ELL2 has been reported to inhibit Tat-dependent HIV-1 gene expression [189, 190]. Mentioned examples and other PTM related processes (including methyltransferases associated interactions, which are not discussed here) in the context of HIV latency are illustrated in fig. 1.7 and fig. 1.8.

1.4.7. Virus assembly, budding and release

In the late stages of HIV-1 replication, virus production relies on the host protein synthesis machinery involving ribosomes, tRNAs, factors for translation initiation, elongation and termination. The cellular resources such as amino acids have to be re-distributed in favor of viral protein synthesis. Additionally, intracellular transport systems and other cofactors are used for virus assembly and maturation. Moreover, infection induced stress responses and antiviral restriction factors have to be overcome for successful viral replication. All these processes require a coordinated interplay of the virus with components of hijacked cellular pathways, where PTMs play an important regulatory role (fig. 1.9).
One example for phosphorylation regulated cellular localization of *gag* encoded viral proteins during virus particle assemby is represented by their interaction with *protein kinase C* (PKC). PKC mediated phosphorylation of *gag* encoded p6 is required for the incorporation of Vpr into newly synthesized virions supporting infectivity [191]. Similar to PKC, MAPK1 also phosphorylates MA, thereby, increasing viral release. As mentioned in the section of uncoating and reverse transcription (section 1.4.4), host proteins such as MAPK1 were also incorporated into new viral particles [192, 193]. Other virion-incorporated kinases were *nuclear Dbf2-related kinase 1* (NDR1, also known as STK38) and *nuclear Dbf2-related kinase 2* (NDR2, also known as STK38L), which are proteolytically cleaved by viral PR within the producer cell or within virions and regulate the subcellular localization as well as the enzymatic activity of NDR1/NDR2. NDR1/NDR2 are involved in cytokine induced inflammation and innate immune response against bacteria and viruses [194]. However, how these enzymes contribute to viral replication is still under debate. Similar to the mentioned kinases, catalytic active HDAC1 complexed with SAP18 was also found to be virion-associated in an IN-dependent manner (as discussed in the section 1.4.5) with positive effects on HIV-1 infectivity [109].

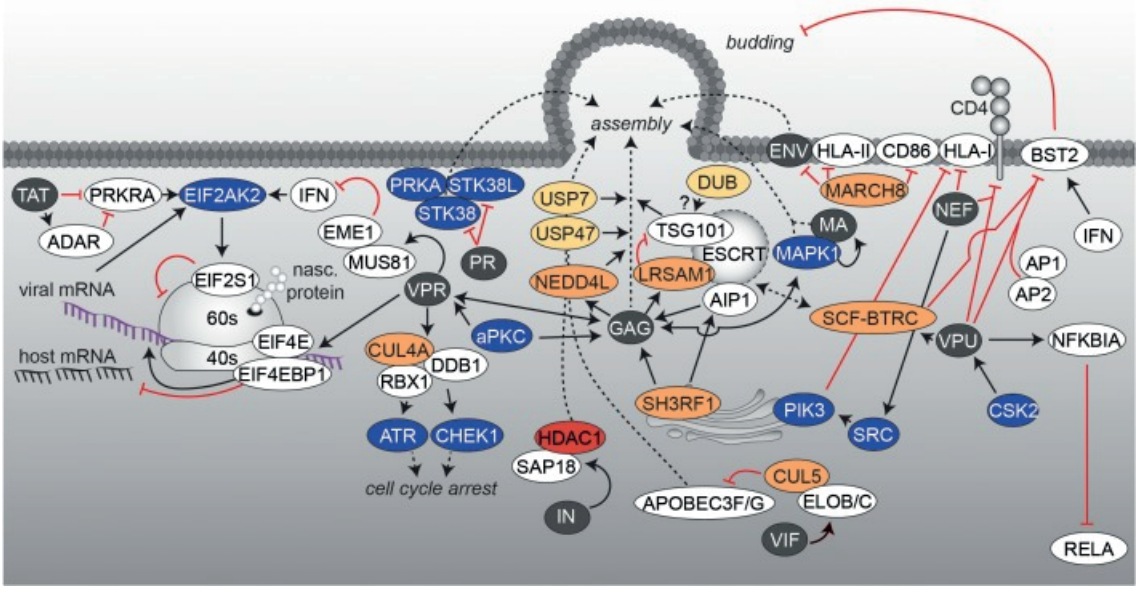

Figure 1.9. Interaction networks of HIV-1 and host protein during virus assembly, budding and release. The interaction network illustrates processes during the late stages of HIV-1 infection and the formation of newly synthesized virus particles. Black arrows indicate activating effects and red "inhibitory"-arrows indicate inhibitory effects. Kinases are shown in dark blue, KDACs in light red, E3 ligases in orange and DUBs in yellow. Other host proteins are colored white, whereas viral proteins are indicated in gray. Figure modified from [40].

Apart from processes facilitating virion assembly and co-incorporation of host factors into new viral particles, several host defense mechanisms are also PTM-regulated. One of these host counteractions is induced by the expression of interferons (IFN) in the presence of viruses. Upon host's detection of viral RNA, IFN production induces activation of *interferon-induced, double-stranded RNA-activated protein kinase* (EIF2AK2, also known as PKR) leading to the subsequent phosphorylation of *eukaryotic translation initiation factor 2* (EIF2A). EIF2A functions in the early step of protein synthesis and its phosphorylation downregulate overall protein synthesis to block the production of viral proteins (host shut-off mechanism). PKR activation is mediated by *interferon-inducible double-stranded RNA-dependent protein kinase activator A* (PRKRA, also known as PACT) - a process, which is diminished by Tat in concert with *double-stranded RNA-specific adenosine deaminase 1* (ADAR1) [195–197].

In parallel, HIV-1 Vpr assembles with a complex comprising E3 ubiquitin-protein ligase *cullin-4A* (CUL4A), *E3 ubiquitin-protein ligase RBX1* (RBX1) and *DNA damage-binding protein 1* (DDB1) [198]. This Vpr-CUL4A/RBX1/DDB1 complex induces the activation of *serine/threonine-protein kinase ATR* (ATR)/*serine/threonine-protein kinase Chk1* (CHK1) mediated G2/M arrest, which is thought to be beneficial for virus production [140, 199, 200].

During virus assembly, HIV-1 exploits the host protein sorting and trafficking machinery. In this context, ubiquitination has been shown to play an important role for HIV-1 Gag's transport to the cell surface. As first example, the trans-Golgi network (TGN)-associated *E3 ubiquitin-protein ligase SH3RF1* (SH3RF1) has been identified to be important for

HIV-1 Gag's targeting to the plasma membrane [201], thereby, augmenting HIV-1 egress. Further studies identified *programmed cell death 6-interacting protein* (PDCD6IP, also known as AIP1), a substrate of SH3RF1 and member of the endosomal sorting complex required for transport (ESCRT) machinery, as obligatory factor for HIV-1 release [202]. In contrast, *E3 ubiquitin-protein ligase LRSAM1* (LRSAM1) has been reported to ubiquitinate *susceptibility gene 101 protein TSG101* (TSG101), a member of the ESCRT complex, thereby, inactivating TSG101-mediated sorting of Gag and preventing efficient HIV-1 budding [203]. The relevance of DUBs during virus release has been described by experiments with inhibitors of *ubiquitin carboxyl-terminal hydrolases 7* (USP7) and *ubiquitin carboxyl-terminal hydrolases 47* (USP47), P22077 and PR-619 respectively, which were able to impair Gag processing and reduce virus infectivity [204]. Apart from its role during Gag processing, the ubiquitination system also involves cellular anti-HIV-1 countermeasures, exemplified by *E3 ubiquitin-protein ligase MARCH8* (MARCH8). Cell membrane-associated MARCH8 has been identified as restriction factor, which blocks the incorporation of HIV-1 envelope glycoproteins into new synthesized viral particles [205].
As an important note, the before mentioned HIV-1 host interactions during virus entry, uncoating/reverse transcription, nuclear import/integration, transcription/latency and virus assembly/budding/release were arbitrarily selected and did not mirror the entirety of known PTM-regulated and HIV-1-associated interactions. Nevertheless, taken together, all these exemplified findings demonstrate the close interrelationship between protein phosphorylation, acetylation and ubiquitination and reflect the importance of PTMs at the different stages during HIV-1 replication.

1.5. Objective of this study

Starting from HIV-1 entry to viral release, PTM-regulated cellular processes are found in every stage of HIV-1 replication cycle. The examples in the last sections demonstrate the wide-ranging role of PTMs in the control or fine-regulation of cellular pathways during HIV-1 infection. Due to recent technological advances for identification and quantification of changes in the global PTM landscape mainly by proteome-wide screens using mass spectrometry, many additional PTM-driven interactions are expected to be uncovered in the future. However, studies disclosing HIV-1 host interactions with spatial as well as temporal resolution are still lacking. Filling these information gaps might support the discovery of vulnerable nodes of virus-host interaction facilitating new approaches to treat HIV-1-infected patients or to protect individuals of higher infection risks.
Following up on this, the study presented here aims to provide a broad-range and unbiased investigation of HIV-1 induced interactions and reconfigurations in the host T-cell environment at full proteomic level as well as at PTM level. For this purpose, state-of-the-art

mass spectrometry (MS) has been combined with advanced virological, cell biological, biochemical techniques as well as bioinformatic methods to identify and quantify novel HIV-1 infection-related changes in the host proteome/PTMome with temporal resolution. In terms of the HIV-1 associated PTM landscape, the focus has lain on phosphoproteome and - more particulary - the largely unexplored acetylome.

As first step, a database of PTM-based HIV-1-host-interactions, with focus on protein phosphorylation, acetylation and ubiquitination, has been established to provide a comprehensive overview of known PTM-associated mechanisms during HIV-1 infection and to facilitate comparison with upcoming experimental data. Next, changes in the cellular full proteome, phosphoproteome and acetylome have been elucidated during different stages of the HIV-1 replication cycle aiming for temporal resolution of HIV-1 associated interactions. For this purpose, a wildtype, full length and replication competent HIV-1 lab strain has been used for infection to be closer to genuine HIV-1 infection scenarios. Since large quantities of HIV-1-infected cells are required for high coverage MS analysis of PTMs due to their low-abundant and substochiometric nature, HIV-1 infection set-ups as well as methods to monitor ongoing infection in host cells have been established and optimized. Simultaneously, with respect to the challenge of analyzing increasingly growing MS data in an efficient, comprehensive and reproducible manner, a robust and accessible MS data analysis workflow has been established, which enabled faster data processing/visualization and easier interpretation.

In this study, a special focus has been on the HIV-1 protein Tat. Considering the close interrelationship between Tat and the host acetylation machinery (fig. 1.7 and fig. 1.8), the role of acetylation sites within Tat for its transactivation ability and its interactions with host proteins has been studied. In addition to Tat's acetylation sites which are located within the region encoded by the first exon, the largely unknown role of the second exon on Tat's transactivation ability and the Tat-dependent interactome has been investigated.

Apart from the investigation of the molecular mechanisms in a host T-cell upon HIV-1 infection, employment of novel strategies for the treatment of HIV-1 are still of high interest. Since epigenetic modifications (such as histone deacetylation) have been described to contribute to HIV-1 gene silencing [206], an epigenetic compound library has been screened for latency reversing agents in order to identify new potential drugs as HIV-1 treatment. In parallel, the impact of KDAC/sirtuin inhibitors on *de novo* infection has been evaluated to assess their associated risk to reseed HIV-1 reservoirs.

Overall, results from these study are anticipated (i) to disclose fundamental mechanisms involved during the interaction between HIV-1 and its host cell, (ii) to assess the dependency of HIV-1 on PTM-regulated cellular pathways and (iii) to provide an important resource for scientists, physicians and pharmaceutical industries to improve current combination antiretroviral treatment.

2. Material and methods

2.1. General reagents, chemical compounds and overview of key resources

Standard reagents and chemicals were supplied by Carl Roth (Germany), Sigma Aldrich (Germany), TH. Geyer (Germany) and Thermo Fisher Scientific (USA), if not otherwise stated. An overview of key resources with additional information is also provided in the following tables.

Table 2.1.Overview of cells

Designation	Source	Identifiers	Add. information
STBLII	Thermo Fisher Scientific	10268019	Chemically competent *E. coli*
HEK293T	DSMZ	ACC 635	Highly transfectable derivative of primary embryonal kidney cell line 293
HeLa	DSMZ	ACC 57	Cell line established from epitheloid cervix carcinoma of a 31-year-old woman in 1951
HCT-116	DMSZ	ACC 581	Cell line with human near-diploid karyotype
TZM-bl	NIH AIDS Reagent Program	8129	HIV reporter cell line derived from HeLa, stably expresses large amounts of CD4 and CCR5 and constitutively expresses CXCR4
SupT1.CCR5	Max von Pettenkofer Institute		T-cell line expressing CD4, CXCR4 and CCR5
Jurkat-E6	ATCC	TIB-152	T-cell line
J-Lat, clone 8.4	NIH AIDS Reagent Program	9847	HIV-1 latent T-cell line
$CD4^+$ T-cells	Isolation from healthy donors		Confirmed by ethics committee of the LMU; Germany

Table 2.2.Overview of recombinant DNA reagents

Designation	Source or reference	Identifers	Add. information
pNL4-3	NIH AIDS Reagent program	114	Full length HIV-1 expression vector (replication and infection competent)
pNL4-3-IRES-eGFP	Max von Pettenkofer Institute/LMU, Dept. Virology		Full length HIV-1 expression vector with GFP reporter
pNL4-3-dNef-GFP	Max von Pettenkofer Institute/LMU, Dept. Virology		HIV-1 expression vector with GFP reporter cloned into the Nef coding region
pCH058.c/2960	NIH AIDS Reagent program	11856	HIV-1 Transmitted/Founder expression vector
pMTAT(-)	NIH AIDS Reagent program	2085	Full length, non-infectious HIV-1 subtype B HXB2 expression vector, that is unable to synthesize Tat (termination codon TGA in place of the initiator codon ATG in the Tat coding region)
pMTAT30	NIH AIDS Reagent program	2087	Full length, non-infectious HIV-1 subtype B HXB2 expression vector, that produces defective Tat (Cys to Gly substitution within the Tat cysteine cluster)
pcDNA3.TAT-HA	Addgene	14654	Expression vector for HIV-1 Tat with C-terminal HA-tag
pCDH.EF1-luc2-T2A-BFP	Gift from Dr. Manuel Albanese (Max von Pettenkofer Institute/LMU, Dept. Virology		Lentiviral vector expressing firefly luciferase and BFP driven by EF1 alpha promoter
pCMV-dR8.91	Life Science Market	PVT2323	Packaging plasmid used for lentivirus production expressing GAG-POL driven by CMV promotor
pMD2.G	Addgene	12259	VSV-G envelope expression vector for production of lentiviral particles
pEV731	[168]		Vector containing LTR-Tat-IRES-GFP sequence

Table 2.3.Overview of primers

Designation	Sequence	Application
pcDNA3-ColE-for	5'-CGAACTGAGATACCTACAGCGTGAG-3'	Cloning
pcDNA-ColE-rev	5'-CTCACGCTGTAGGTATCTCAGTTCG-3'	Cloning
TAT K28A for	5'-AACAATTGCTATTGTGCAAAGTGTTGCTTTCAT-3'	Mutagenesis
TAT K28A rev	5'-ATGAAAGCAACACTTTGCACAATAGCAATTGTT-3'	Mutagenesis
TAT K28R for	5'-CAATTGCTATTGTCGAAAGTGTTGCTTTCAT-3'	Mutagenesis
TAT K28R rev	5'-ATGAAAGCAACACTTTCGACAATAGCAATTG-3'	Mutagenesis
TAT K28Q for	5'-CAATTGCTATTGTCAAAAGTGTTGCTTTCAT-3'	Mutagenesis
TAT K28Q rev	5'-ATGAAAGCAACACTTTTGACAATAGCAATTG-3'	Mutagenesis
TAT K50A for	5'-ATCTCCTATGGCAGGGCGAAGCGGAGACA-3'	Mutagenesis
TAT K50A rev	5'-TGTCTCCGCTTCGCCCTGCCATAGGAGAT-3'	Mutagenesis
TAT K50R for	5'-TCCTATGGCAGGAGGAAGCGGAGACAG-3'	Mutagenesis
TAT K50R rev	5'-CTGTCTCCGCTTCCTCCTGCCATAGGA-3'	Mutagenesis
TAT K50Q for	5'-TCCTATGGCAGGCAGAAGCGGAGACA-3'	Mutagenesis
TAT K50Q rev	5'-TGTCTCCGCTTCTGCCTGCCATAGGA-3'	Mutagenesis
TAT K51A for	5'-ATGGCAGGAAGGCGCGGAGACAG-3'	Mutagenesis
TAT K51A rev	5'-CTGTCTCCGCGCCTTCCTGCCAT-3'	Mutagenesis
TAT K51R for	5'-ATGGCAGGAAGCGGCGGAGACAG-3'	Mutagenesis
TAT K51R rev	5'-CTGTCTCCGCCGCTTCCTGCCAT-3'	Mutagenesis
TAT K51Q for	5'-TATGGCAGGAAGCAGCGGAGACAG-3'	Mutagenesis
TAT K51Q rev	5'-CTGTCTCCGCTGCTTCCTGCCATA-3'	Mutagenesis
TAT K50/51A for	5'-CTATGGCAGGGCAGCTCGGAGACAGCG-3'	Mutagenesis
TAT K50/51A rev	5'-CTATGGCAGGGCAGCTCGGAGACAGCG-3'	Mutagenesis
TAT K50/51R for	5'-CTATGGCAGGAGGAGGCGGAGACAGC-3'	Mutagenesis
TAT K50/51R rev	5'-GCTGTCTCCGCCTCCTCCTGCCATAG-3'	Mutagenesis
TAT K50/51Q for	5'-TCCTATGGCAGGCAGCAGCGGAGACAGC-3'	Mutagenesis
TAT K50/51Q rev	5'-GCTGTCTCCGCTGCTGCCTGCCATAGGA-3'	Mutagenesis
TAT Δexon2 for	5'-GCTTCTCTATCAAAGCAATACCCATACGATGTTCCAGA-3'	Deletion
TAT Δexon2 rev	5'-TCTGGAACATCGTATGGGTATTGCTTTGATAGAGAAGC-3'	Deletion
RT assay for	5'-TCCTGCTCAACTTCCTGTCGAG-3'	SG-PERT
RT assay rev	5'-CACAGGTCAAACCTCCTAGGAATG-3'	SG-PERT
luc2-HA-for	5'-GAGGGGCCCCATGATCATGAG-3'	Insertion
luc2-HA-rev	5'-CCGCGGATCCGGCAGCGTAATCTGGAACATCGTATGGGTACTTGCCGCCCTTCTTGGCC-3'	Insertion
TatLenti-for	5'-GCCTACTCTAGAGCTAGCGAATTCGCCACCATGGAGCCAG-3'	Cloning
TatLenti-rev	5'-ACTTCCTCTGCCCTCGGATCCGGCAGCGTAATCTGGAACATCG-3'	Cloning

Table 2.4.Overview of antibodies

Designation	Source or reference	Identifiers	Application
RosetteSep™ Human CD4+ T-cell enrichment cocktail	Stemcell Technologies	15022	$CD4^+$ T-cell isolation
Tritest™ CD4/CD8/CD3	BD Biosciences	340298	Flow cytometry
Dynabeads Human T-Activator CD3/CD28	Thermo Fisher Scientific	111.61D	T-cell activation
APC Mouse Anti-Human CD25	BD Biosciences	555434	Flow cytometry
Anti-Human CD4 FITC/CD69 PE/CD3 PerCP	BD Biosciences	340365	Flow cytometry
Human 8-Color Immunophenotyping kit	Miltenyi Biotec	130-120-640	Flow cytometry
Anti-human CD4 antibody clone SK3	BioLegend	344602	HIV fusion inhibitor
KC57-FITC	Beckman Coulter	6604665	Flow cytometry
Anti-Vinculin antibody, mouse monoclonal	Sigma-Aldrich	V9264	Immunoblot
Anti-HA.11 Epitope Tag, clone 16B12	BioLegend	901513	Immunoblot
Peroxidase AffiniPure Goat Anti-Mouse IgG (H+L)	Jackson ImmunoResearch	115-035-003	Immunoblot
PTMScan® Acetyl-Lysine Motif [Ac-K]	Cell Signaling Technology	13416	Enrichment of acetylated peptides
Pierce® Anti-HA Magnetic Beads	Thermo Fisher Scientific	88837	Pull-down of HA-tagged proteins

Table 2.5.Overview of drugs and compounds

Designation	Source or reference	Identifiers	Add. information
Enfurvirtide (Fuzeon®, T-20)	Roche	14879573	HIV fusion inhibitor
Efavirenz	Bristol-Myers Squibb	NA	HIV reverse transcription inhibitor
MG-132	Sigma-Aldrich	474790	Proteasome inhibitor
Epigenetics Compound Library	TargetMol	L1200	380 compounds related to epigenetic regulation
Apicidin	Sigma-Aldrich	183506-66-3	HDAC inhibitor
Bufexamac	Sigma-Aldrich	2438-72-4	HDAC inhibitor
Cl-994	Sigma-Aldrich	112522-64-2	HDAC inhibitor
LBH589	Sigma-Aldrich	404950-80-7	HDAC inhibitor
M344	Sigma-Aldrich	251456-60-7	HDAC inhibitor
Nicotinamide	Sigma-Aldrich	98-92-0	HDAC inhibitor
Romidepsin	Sigma-Aldrich	128517-07-7	HDAC inhibitor
SAHA	Sigma-Aldrich	149647-78-9	HDAC inhibitor
SBHA	Sigma-Aldrich	38937-66-5	HDAC inhibitor
Scriptaid	Sigma-Aldrich	287383-59-9	HDAC inhibitor
Sodium butyrate	Sigma-Aldrich	156-54-7	HDAC inhibitor
Splitomicin	Sigma-Aldrich	5690-03-9	HDAC inhibitor
Trichostatin A (TSA)	Sigma-Aldrich	58880-19-6	HDAC inhibitor
Tubacin	Sigma-Aldrich	537049-40-4	HDAC inhibitor
Valproic acid	Sigma-Aldrich	599-66-1	HDAC inhibitor

Table 2.6.Overview of commercial products and kits

Designation	Source or reference	Identifiers	Add. information
GeneJET Plasmid Miniprep Kit	Thermo Fisher Scientific	K0503	Purification of plasmid DNA up to 20 µg
Nucleobond® Xtra Midi Kit	Macherey Nagel	740410.50	Purification of plasmid DNA up to 500 µg
Phusion™ Site-Directed Mutagenesis	Thermo Fisher Scientific	F541	Introduction of insertions, deletions or point mutations into plasmid DNA
PCR clean up/gel extraction	Macherey Nagel	740609.50	Purification of DNA fragments
SE Cell Line 4D-Nucleofector Kit	Lonza	V4XC-1032	Electroporation
QuickTiter™ Lentivirus Titer Kit	Cell Biolabs	VPK-107	Detection and quantitation of the lentivirus associated HIV-1 p24 core protein
Pierce® Firefly Luciferase Glow Assay Kit	Thermo Fisher Scientific	16176	Detection of intracellular luciferase activity
SILAC Protein Quantitation Kit (Trypsin)	Thermo Fisher Scientific	A33973	Stable isotope labeling for protein/peptide quantification
Reversed-phase Sep-Pak C18 cartridges	Waters	WAT051910	Peptide purification
High-Select™ TiO_2 Phosphopeptide Enrichment Kit	Thermo Fisher Scientific	A32993	Enrichment of phosphorylated peptides
High-Select™ Fe-NTA Phosphopeptide Enrichment Kit	Thermo Fisher Scientific	A32992	Enrichment of phosphorylated peptides
TMT6plex Mass Tag Labeling	Thermo Fisher Scientific	90066	Isobaric labels for protein/peptide quantification
High pH Reversed-Phase Peptide Fractionation Kit	Thermo Fisher Scientific	84868	Fractionation of peptides prior to MS measurement
iST Sampe Preparation Kit	Preomics	P.O.00001	Sample preparaton for mass spectrometry
CellTiter-Glo® Luminescent Cell Viability	Promega	G7570	Viability testing
7-AAD	Invitrogen	A1310	Viability testing

2.2. Plasmid preparation

2.2.1. Preparation of competent bacteria

For preparation of competent *E.coli* (STBLII; Thermo Fisher Scientific), 50 µl of bacterial cell suspension were used to inoculate 10 ml LB medium and cells were cultured at 37°C shaking at 175 rpm overnight. The next day, the pre-culture was transferred into 100 ml LB medium. Growth was continued and the absorbance at 600 nm (A_{600}) was monitored every 30 to 60 min. At A_{600} of 0.4 to 0.5, the culture was cooled on ice for 5 to 10 min. Cells were pelleted (3,000 x g, 4°C, 10 min). The cell pellet was re-suspended in 40 ml transformation buffer A (30 mM potassium acetate, 100 mM $RbCl_2$, 10 mM $CaCl_2$, 50 mM $MnCl_2$, 15% (v/v) glycerol, pH 5.8) and incubated for 15 min. Cells were harvested (2,000 x g, 4°C, 10 min) and the pellet was re-suspended in 2 ml transformation buffer B (10 mM MOPS, 75 mM $CaCl_2$, 10 mM $RbCl_2$, 15% (v/v) glycerol, pH 6.5) on ice. Competent cells were aliquoted, flash frozen in liquid nitrogen and stored at -80°C.

2.2.2. Amplification and purification of plasmid DNA

Plasmid DNA was propagated in competent *E.coli* (STBLII) cells (see section 2.2.1). 0.5 µg plasmid DNA was added to 50 µl competent cells and incubated on ice for 20 min. Next, cells were heat-shocked at 42°C for 30 s and, thereafter, cooled on ice for 1 min. Then, 300 µl LB medium was added to the bacterial suspension. After 30 min of incubation (37°C shaking at 700 rpm), transformed bacteria were spun down (20,000 x g, RT, 10 s), volume was reduced to 100 µl, cells were re-suspended and plated on a LB agar plate supplemented with the respective antibiotic for selection (50 µg/ml ampicillin or 50 µg/ml kanamycin). Plated bacteria were cultured at 37°C overnight or at RT for 48 to 72 h. Thereafter, single colonies were picked and used for inoculation of 5 ml TB medium supplemented with the respective antibiotics. Pre-cultures were grown at 37°C shaking at 200 rpm for at least 8 h or overnight. For plasmid purification up to 20 µg, plasmid DNA were isolated from 2 ml pre-culture using the GeneJET Plasmid Miniprep Kit (Thermo Fisher Scientific) according to the manufacturer's instructions. Purified DNA was eluted in 50 µl nuclease-free water and stored at -20°C.

For plasmid production of up to 500 µg, pre-cultures were used to inoculate 400 ml of TB medium supplemented with the respective antibiotics and incubated at 37°C overnight. Cells were pelleted (3,400 x g, 4°C, 10 min) and the supernatant was discarded. Plasmid DNA was purified using the Nucleobond® Xtra Midi kit (Macherey Nagel) according to the manufacturer's instructions. Purified DNA was reconstituted in 200 to 300 µl nuclease-free water and stored at -20°C. Plasmid DNA concentration was determined on the NanoDrop One photospectrometer (Thermo Fisher Scientific) adjusted to 1 µg/µl.

2.2.3. Qualitative and quantitative restriction digest and gel electrophoresis

Restriction digest of plasmid DNA was performed for DNA analysis or processing. For this purpose, the FastDigest restriction enzyme system (Thermo Fisher Scientific) or the High Fidelity (HF®) restriction endonuclease system (New England Biolabs) was used according to the manufacturer's instructions. 1 µl of each restriction enzyme were used to digest 0.5 to 1 µg of plasmid DNA at 37°C for 30 min. Digested samples were loaded onto an analytical agarose gel (1% agarose in TAE) supplemented with SYBR Safe DNA Gel Stain (1/20,000, Invitrogen). Gel electrophoresis (Biometra Compact XS/S, Analytik Jena) was conducted at constant 100 V for 45 to 60 min (PowerPac™ HC High-Current Power Supply, Bio-Rad). Stained DNA bands were imaged using the UVP UVsolo touch gel documentation system (Analytik Jena). Cutting out of DNA bands were performed using the transilluminator ETX-F20.L (Vilber).

2.2.4. Site-directed mutagenesis

To study gene or protein functions, the Phusion™ Site-Directed Mutagenesis kit (Thermo Fisher Scientific) was used to introduce point mutations at specific sites within the gene sequence by designing a mismatch in the mutagenic primer. PCR and ligation were performed according to the manufacturer's instructions. Transformation was performed as described in section 2.2.2. Plasmid DNA was isolated and purified from selected clones. Respective gene sequences were further verified by Supreme Sanger sequencing provided by GATC services (Eurofins Genomics) and obtained sequencing results were analyzed in Serial Cloner vers. 2.6.

2.2.5. Ligation-based cloning

Ligation-dependent cloning was performed to transfer genes of interest into a different vector. Inserts containing the genes of interest were amplified by PCR according to the instructions of the Phusion™ Site-Directed Mutagenesis kit (Thermo Fisher Scientific). To generate "sticky ends", the PCR product of the insert as well as the target vector were digested with the same pair of restriction enzymes as described in section 2.2.3. Gel electrophoresis was performed to verify correct lengths of the PCR product and the fragments from the digested vector. Next, the PCR product as well as the desired fragment of the digested vector extracted from the gel were purified using the PCR clean up/gel extraction kit (Macherey Nagel) according to the manufacturer's instructions. Purified insert and target backbone were eluted from the silica membrane using 30 µl nuclease-free water. Plasmid DNA concentration was determined to conduct ligation of insert and backbone in an 1:3 molar ratio at RT for 60 min using the T4 DNA ligase (Thermo Fisher Scientific). To reduce false positive clones during transformation

by self-ligated vectors, the ligation product was digested with AgeI (New England Biolabs) at 37°C for 20 min. Afterwards, the ligation product was subjected to transformation and propagation in *E.coli* (STBLII) as described in section 2.2.2. Isolated and purified plasmid DNA from single clones was analyzed by qualitative restriction digest (see section 2.2.3) to check for correct fragment lengths and, subsequently, verified by Supreme Sanger sequencing provided by GATC services (Eurofins Genomics). Obtained sequencing results were analyzed in Serial Cloner vers. 2.6.

2.3. Cell culture

2.3.1. Cultivation of cell lines

Suspension as well as adherent cell lines were cultured at 37°C and 5% CO_2. Suspension cell lines were grown in RPMI Medium 1640 (Gibco) supplemented with 10% heat-inactivated FCS and antibiotics (100 U/ml Penicillin, 0.1 mg/ml Streptomycin; Merck) and maintained at cell concentrations between $1x10^6$ and $2x10^6$ viable cells per ml. Medium was changed every two to three days depending on the cell density.
Adherent cell lines were cultured in DMEM (Gibco) supplemented with 10% heat-inactivated FCS and antibiotics (100 U/ml Penicillin, 0.1 mg/ml Streptomycin; Merck). At 90% confluency, cells were washed with PBS and incubated with trypsin/EDTA (0.05%/0.02% in PBS; Biochrom) at 37°C for 5 to 10 min. For inactivation of trypsin, detached cells were re-suspended in DMEM supplemented with 10% heat-inactivated FCS and antibiotics. For passaging, an appropriate aliquot of the cell suspension was transferred into a new culture vessel.
All used cell lines were confirmed to be mycoplasma negative using the MycoAlert™ Mycoplasma Detection kit (Lonza).

2.3.2. Freezing and thawing of cell lines

For long-term storage in liquid nitrogen, cell lines were frozen at a density of $10x10^6$ to $20x10^6$ viable cells per ml. For this purpose, cells were pelleted (500 x g, RT, 5 min) and re-suspended in freezing medium (90% FCS, 10% DMSO). Cells were stored in CellCamper boxes (neoLab) at -80°C overnight and, thereafter, transferred into liquid nitrogen.
To start culture from stocks stored in liquid nitrogen, frozen cells were thawed quickly in a 37°C water bath and then transferred into 10 ml PBS to dilute residual DMSO. Cells were pelleted (500 x g, RT, 5 min), re-suspended in culture medium and plated/seeded into an appropriate culture vessel.

2.3.3. Isolation, activation and cultivation of primary CD4$^+$ T-cells

Blood cones (Terumo BCT leukocyte reduction system) containing erythrocytes and enriched leukocytes of anonymized and healthy donors provided by the Hospital of the University of Munich, Dept. of Immunohematology, infection screening and blood bank (ATMZH) were used to isolate CD4$^+$ T-cells (approval by the ethics committee of the LMU München, Munich, Germany with the project No. 17-202-UE).
Blood cones were rinsed with PBS (Gibco) and T-cell isolation was performed using the RosetteSep™ Human CD4+ T cell enrichment cocktail (Stemcell Technologies) according to the manufacturer's instructions. In brief, 1 ml of enrichment cocktail was added per 20 ml blood sample, mixed and incubated at RT for 20 min. Sample was diluted with PBS and the resulting suspension was overlayed onto 15 ml Biocoll (1.077 g/L; Biochrom) as separating medium. After centrifugation (700 x g, RT, 35 min) with slow acceleration and deceleration, enriched lymphocytes were collected from the interphase between plasma and Biocoll layer. To remove excess plasma, isolated cells were pelleted (500 x g, RT, 5 min). washed with PBS, re-suspended in RPMI Medium 1640 (Gibco) supplemented with 10% heat-inactivated FCS, antibiotics (100 U/ml Penicillin, 0.1 mg/ml Streptomycin; Merck) and IL-2 (100 U/ml; Biomol) to a final cell density of 2x10^6 cells per ml. To activate purified cells, phytohemagglutinin-P (PHA-P) (5 µg/ml; Sigma Aldrich) was added (fig. 2.1C). Purity of isolated cells was monitored on the flow cytometer BD FACSLyric™ (BD Biosciences) after staining for flow cytometry using BD Tritest™ CD4/CD8/CD3 antibody stain (BD Biosciences) according to the manufacturer's instructions (fig. 2.1A and B). After four days of activation at 37°C and 5% CO_2, medium was replaced by PHA-P-free medium and culture was continued for one to four more days. Activation of isolated cells was verified by flow cytometry (fig. 2.1D) using anti-human CD4/CD69/CD3 antibody staining solution (BD Biosciences) according to the manufacturer's instructions.

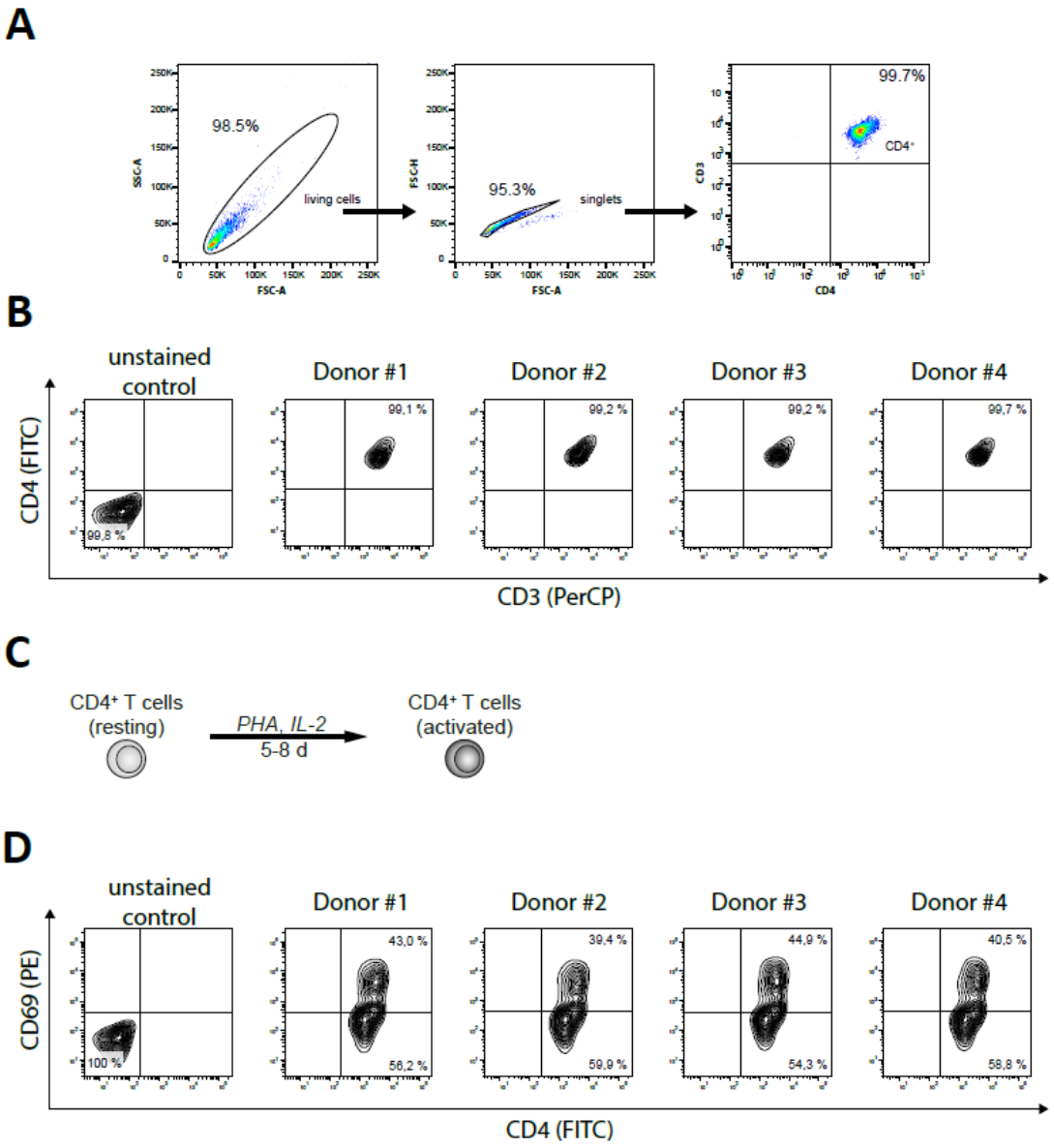

Figure 2.1. Isolation and activation of CD4$^+$ T-cells. **(A)** CD4$^+$ T-cells were isolated from blood of healthy donors using RosetteSep^{TM} technology. Subsequently, purity of isolated cells was analyzed by fluorescence-based flow cytometry using anti-CD3 /-CD4 staining. Flow cytometry plots display the gating strategy for living cells (lymphocytes; left), single cells (middle) and enriched CD4$^+$ T-cells (right). Numbers display the percentage of cells within the respective gate. **(B)** Representative flow cytometry plots of CD4$^+$ T-cell isolation based on the gating strategy in A from four different donors, which were used later in four-donor-pools. **(C)** Schematic illustration of T-cell activation. Isolated CD4$^+$ T-cells (resting) were cultivated in the presence of PHA and IL-2 for 5-8 days to gain activated CD4$^+$ T-cells. **(D)** Representative flow cytometry plots of the isolated cells from B after activation. CD69 was used as activation marker.

2.3.4. T-cell activation assay

$CD4^+$ T-cells were isolated and purity was controlled as described in section 2.3.3. For activation testing, $2x10^6$ cells were cultured in presence of either 10 µM phorbol-12-myristate 13-acetate (PMA) or Human T-Activator CD3/CD28 dynabeads (Thermo Fisher Scientific) according to the manufacturer's instruction, or the test compounds. Subsequently, activation of T-cells was determined by flow cytometry using the anti-human anti-human CD4/CD69/CD3 antibody staining solution (BD Biosciences) in combination with anti-human CD25 (BD Biosciences). Resting T-cells which were vehicle-treated served as control.

2.3.5. Immunophenotyping

$CD4^+$ T-cells were isolated and purity was controlled as described in section 2.3.3. Subsequently, cells were treated with test compounds or vehicle control and cultured for 24 h. After washing twice with cold PBS (Gibco), cells were stained with the human 8-Color Immunophenotyping kit (Miltenyi Biotec) according to the manufacturer's instructions. Stained cells were analyzed by flow cytometry using a FACSLyric™ flow cytometer (BD Biosciences). First, doublets were excluded by gating for single cells in forward scatter area (FSC-A) versus forward scatter height (FSC-H). Viable cells were identified by 7-Aminoactinomycin (7-AAD) staining (Invitrogen) according to the manufacturer's instructions. After exclusion of residual cell debris by classical FSC/SSC analysis, the population of CD45+ leucocytes was identified and further separated into CD14+ and CD19+ cells. Remaining cells were distinguished between SSC high (neutrophils, eosinophils) and SSC low cells by the side scatter. SSC low cells were further divided into CD3+, CD16/56+, and CD16/56+/CD3+ cells. Finally, CD3+ cells were separated into CD4+ and CD8+ cells.

2.3.6. Resazurin cytotoxicity assay

As measure for cytotoxicity, reduction of non-fluorescent resazurin to fluorescent resafurin by living, metabolically active cells was utilized. For this assay, resazurin (Sigma-Aldrich) was added to the cells in black 96-microwell format as well as to blank wells (filled with culture medium) to a final concentration of 25 µg/ml and incubated at 37°C and 5% CO_2 for 4 h. The resafurin output was measured at a the CLARIOstar Plus microplate reader (BMG Labtech) using a wavelength of 560 nm for excitation and 590 nm for emission. Data was blank corrected and normalized to the sample of highest viability e.g. untreated cells.

2.3.7. Preparation of SILAC spike-in standard

To enable quantitative analysis of proteins or peptides relative to a SILAC standard [207] Jurkat-E6 cells were metabolically labeled with heavy amino acids (L-arginine-$^{13}C_6$-$^{15}N_4$ and L-lysine-$^{13}C_6$-$^{15}N_2$) using the SILAC Protein Quantitation kit (Thermo Fisher Scientific) according to the manufacturer's instruction. After ten cycles of proliferation, labeled cells were tested for incorporation of heavy amino acids by mass spectrometry using the iST Sample Preparation kit (Preomics) according to the manufacturer's instructions for preparatiion of mass spectrometry ready samples. Thereafter, successfully labeled cells were expanded in SILAC culture medium, until required cell number was reached.
To harvest labeled cells, cells were pelleted (500 x g, 4°C, 5 min), washed twice with cold PBS (Gibco) and lysed in modified RIPA buffer (50 mM Tris-HCl pH 7.5, 150 mM NaCl, 1 mM EDTA, 1% NP-40, 0.1% sodium deoxycholate) supplemented with cOmplete™ protease inhibitor cocktail (Roche). To free chromatin-bound proteins, cell extracts were mixed with 1/10 volume of 5 M NaCl and incubated on ice for 15 min. For lysate homogenization, samples were sonicated (12 x 5 s pulses with 5 s pause between cycles, 15 W). Last, eight volumes of ice-cold acetone were added to the lysate to precipitate proteins at -20°C overnight. Acetone precipitates were pelleted (2300 x g, 10 min, 4°C), dried at RT for 15 to 30 min and re-constituted in urea lysis buffer (6 M urea, 2 M thiourea in 80 mM Tris-HCl pH 7.6) supplemented with 1 mM DTT to reduce disulfide bonds. Protein concentration was determined by Quick Start™ Bradford protein assay (Bio-Rad). Jurkat-E6 SILAC spike-in standard was stored at -20°C until further use.

2.4. Gene delivery techniques for human cell lines

2.4.1. Electroporation

The 4D-Nucleofector™ System (Lonza) combined with the SE Cell Line 4D-Nucleofector™ X Kit (Lonza) was used to introduce plasmid DNA into target cells by electroporation. For electroporation of Jurkat-E6 cells, cells were prepared according to the Amaxa™ 4D-Nucleofector™ Protocol for Jurkat clone E6.1 [ATCC®] in 16-well Nucleocuvette™ Strips (20 µl) format. As Nucleofector™ Program the one of following settings were selected according to the manufacturer's recommendation: CM-120, CM-137, DN-100, EH-100 and DF-120.

2.4.2. Lipofection

For small-scale transient transfection of up to 1.5x10^6 adherent cells, Lipofectamine® 2000 reagent (Invitrogen) was used to introduce plasmid DNA into target cells. In brief, adherent cells were plated in a way, that 70 to 90% confluency was reached at the day of transfection. 1 µg plasmid DNA was diluted in 125 µl plain DMEM (Gibco) and 3 µl of Lipofectamine® 2000 reagent was also mixed in 125 µl plain DMEM maintaining a total DNA to Lipofectamine® 2000 ratio of 1:3. To prepare DNA-lipid complexes, diluted plasmid DNA and transfection reagent were combined in an 1:1 ratio and incubated at RT for 15 min. Meanwhile, culture medium was replaced by plain DMEM after washing cells once with plain DMEM. Mixture containing formed DNA-lipid complexes were added to the cells in plain DMEM and incubated at 37°C and 5% CO_2 for 4 to 6 h. Thereafter, plain DMEM with the DNA-lipid complex was replaced by DMEM supplemented with 10% FCS and antibiotics (100 U/ml Penicillin, 0.1 mg/ml Streptomycin; Merck) and transfected cells were cultured at 37°C and 5% CO_2 for 48 to 72 h.

2.4.3. PEI transfection

For large-scale transient transfection of adherent cells, e.g. for virus stock production, PEI (MW 25,000; Polysciences) was used as transfection reagent [208, 209]. For this purpose, adherent cells were plated in a way, that 70 to 90% confluency was reached at the day of transfection. For transfection in ⌀15 cm culture plate format, 11 µg of total plasmid DNA and 33 µg PEI were diluted each in 1.25 ml plain DMEM (Gibco) maintaining a total DNA to PEI ratio of 1:3. After incubation at RT for 5 min, diluted plasmid DNA and PEI were combined in n 1:1 ratio and incubated at RT for 30 min to form DNA-PEI complexes. Mixture containing these DNA-PEI complexes was added to the plated cells and incubated at 37°C and 5% CO_2 for 48 to 72 h.

2.4.4. Lentiviral transductions

For establishment of stable expression of genes of interests, target cells were transduced with a lentiviral system. In order to produce lentiviral particles for transduction, HEK293T cells were co-transfected with a plasmid mix containing the gene of interest, envelope and packaging plasmid using PEI as transfection reagent (see section 2.4.3). In detail, for lentivirus production in ⌀15 cm culture plate format, the plasmid mix was prepared with 7 µg pCMV.d8.9 (packaging), 8 µg pMD2.G (envelope) and 11 µg of the vector carrying the gene of interest flanked by viral LTR sites. Plasmid mix as well as 80 µg PEI were diluted in plain DMEM and were processed as described in 2.4.3 while maintaining a total DNA to PEI ratio of 1:3. Supernatant containing lentiviral particles was harvested, filtered (0.45 µm, Millex-HV Filter; Millipore) and stored at -80°C until further use. Supernatant or

concentrated lentiviral particles were used to infect target cells (see also section 2.5.1 and 2.5.2). After 48 h, expression of genes was verified by immunoblotting or by flow cytometry (BD FACSLyric™; BD Biosciences). Optionally, positive cells were sorted using the cell sorter BD FACSAriaFusion™ (BD Biosciences)[a].

2.5. Virological methods

2.5.1. Virus preparation, purification and concentration

For the large-scale production of viruses, HEK293T producer cells were prepared and transfected as described in 2.4.3. Supernatant was filtered either with Millex-HV Filters (0.45 µm; Millipore) or with the Stericup Quick Release-HV Sterile Vacuum Filtration System (0.45 µm; Milllipore) to remove detached cells and residual cell debris. Next, open-top Polyallomer ultracentrifuge tubes (Seton Scientific) were filled with 6 ml 25% sucrose overlaid with 29 ml filtered supernatant. For concentration, virus particles from supernatant were purified by ultracentrifugation (Sorvall™ WX+ Ultra; Thermo Fisher Scientific) at 24,000 rpm (ca. 110,000 x g) and 4°C for 90 min (SW 32 Ti; Beckman Coulter or SureSpin™ 630/36; Thermo Fisher Scientific). After ultracentrifugation, supernatant was discarded and pelleted viral particles were re-suspended in 100 µl PBS. Virus suspensions from the same batch were pooled before aliquoting and storage at -80°C.

2.5.2. Spin-infection

For enhanced viral infection of suspension cells, spin-inoculation [31, 210] was applied (1,200 x g, 37°C, 90 min) after combining virus with target cells ($2x10^5$ or $4x10^5$ cells in 200 µl) in Costar® V-bottom 96-well format (Corning®). After spinning, infected cells were re-suspended and culture was continued for defined time period.

2.5.3. Inhibition of HIV infection by anti-retroviral drugs or antibodies

HIV infection inhibition experiments were conducted by treating cells with anti-retroviral compounds or with anti-human CD4 antibodies. Compounds or antibodies were added to cells 1 h prior to infection. As HIV fusion inhibitor, enfuvirtide (also known as Fuzeon® or T-20; Roche) was used at a final concentration of 100 µM. Alternatively, cells were incubated with anti-human CD4 antibody clone SK3 (BioLegend) at a final concentration of 100 µg/ml. As inhibitor of reverse transcription, efavirenz (EFN, also known as Sustiva® or Stocrin®; Bristol-Myers Squibb) at a final concentration of 20 mM was used to treat cells. Infection and fixation/inactivation for analysis were performed as described in section 2.5.2 and 2.5.4.

[a] Cell sorting was performed by Dr. Lisa Richter, technical manager of the core facility Flow Cytometry Biomedical Center Munich, Ludwig Maximilians University of Munich

2.5.4. PFA fixation

For fixation or inactivation of infected adherent cells, cells were detached either with a cell scraper or using trypsin/EDTA (0.05%/0.02% in PBS; Biochrom) as described in section 2.3.1. Detached cells were washed with PBS (Gibco), then pelleted (500 x g, RT, 5 min) and re-suspended in 4% PFA in PBS. After incubation at RT for 90 min, cells were pelleted (1212 x g, 4°C, 10 min) and re-suspended in PBS. Samples were stored in PBS at 4°C for short term until further processing.
For suspension cells, cells were trypsinated prior to fixation, if enhanced sensitivity of intracellular staining of target antigens for flow cytometric analysis was desired (see section 2.5.5). For this procedure, cells were spun down (500x g, RT, 5 min) and washed with 2 mM EDTA in PBS. Cell debris were removed by low-speed centrifugation (90x g, RT, 10 min). Pelleted viable cells were treated with trypsin/EDTA (0.25%/0.10% in PBS; Biochrom) at 37°C for 10 min. Trypsination was stopped by adding RPMI Medium 1640 (Gibco) supplemented with 30% FCS and at 37°C incubation for 5 min. Afterwards, cells were pelleted and washed in RPMI Medium 1640 (Gibco) supplemented with 30% FCS one more time (500x g, RT, 10 min). As last step before fixation, cells were washed with PBS (500 x g, RT, 5 min). After the PBS wash, cell pellets were re-suspended in 4% PFA in PBS and incubated at RT for 90 min. Thereafter, cells were spun down (1212 x g, 4°C, 10 min) and stored in PBS at 4°C for short term until further processing.

2.5.5. Intracellular staining of HIV-1 core protein (p24) for flow cytometry

To analyze infection levels by staining HIV-1 core protein for flow cytometry, PFA-fixed and in PBS re-suspended samples of infected cells (see section 2.5.4) were pelleted (1212 x g, 4°C, 10 min) and re-suspended in Perm/Wash™ buffer (BD Biosciences) for permeabilization at 4°C for 15 min. After incubation, cells were spun down (1212 x g, 4°C, 10 min) and washed with Perm/Wash™. For staining of HIV-1 core antigens including the 55 kDa precursor protein, the 39 and 33 kDa intermediates and the 24 kDa core protein, KC57-FITC (Beckman Coulter) was diluted 1/100 in Perm/Wash™ to prepare the staining diluent (p24 staining). Samples were incubated in the staining diluent protected from light at 4°C for 30 min. Thereafter, stained samples were washed twice with Perm/Wash™ (1212 x g, 4°C, 10 min) and stored in PBS at 4°C prior to flow cytometric analysis (see section 2.5.6).

2.5.6. Flow cytometry and virus quantification

Flow cytometric data was acquired on a FACSLyric™ flow cytometer (laser configuration: violet (405 nm), blue (488 nm), red (635 nm); BD Biosciences). Cell events were pre-selected based on forward scatter (FSC) and side scatter (SSC) to filter for living single-cell events to exclude aggregates, debris and doublets. (Stained) negative controls and "dump" channels

were used to define gates for the population of interest and to distinguish signals from "noise" (e.g. due to autofluorescence of dead cells). An example of gating strategy is demonstrated in fig. 2.2. Acquired data was analyzed in FlowJo™ vers. 10 (TreeStar), Excel 2016 (Microsoft) and GraphPad Prism vers. 7.04 (GraphPad Software).

For virus quantification, infection-associated output, e.g. GFP-expression or KC57-FITC signal, was used to determine the multiplicity of infection (MOI)-based on the inversed Poisson distribution [211,212].The percentage of infected events served as estimate for the probability P of a cell that will be infected by at least one virus particle (n>0) as result of infection with a given MOI. The MOI was calculated using the following estimation and formula:

$$P\{n > 0\} \approx \frac{\#\text{ infected cells}}{\#\text{ total cells}} \tag{2.1a}$$

$$MOI = -\ln\{(1 - P\{n > 0\})\} \tag{2.1b}$$

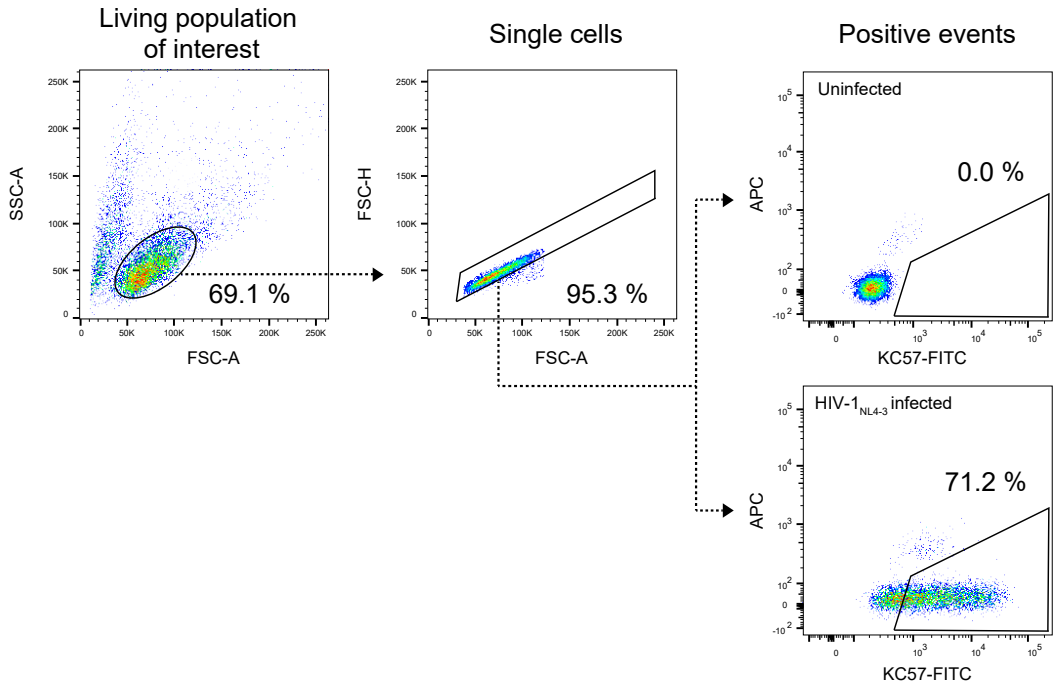

Figure 2.2. Gating strategy demonstrated for HIV-1_{NL4-3} infected Jurkat-E6 cells. Infected Jurkat-E6 cells stained against HIV-1 core antigens (KC57-FITC) were first gated for living cell population, second for single cells and finally for HIV-1 positive events. The APC channel served as "dump" (exclusion) channel.

2.5.7. Quantification of virus-associated HIV-1 p24 core protein by ELISA

QuickTiter™ Lentivirus Titer Kit (Cell Biolabs) was used to specifically detect and quantify viral particles based on virus-associated HIV-1 p24 core proteins in viral supernatant (or in concentrated virus stocks) with an enzyme-linked immunosorbent assay (ELISA). In brief, viral supernatant was diluted (1:1 or 1:2 ratio) in culture medium. 1 ml sample was treated with ViralBind™ reagent to pull down viral particles and processed according to the manufacturer's instructions. The absorbance was detected on the CLARIOstar Plus microplate reader (BMG Labtech) using 450 nm as the primary wavelength.

2.5.8. Luciferase-based transactivation assay in HIV reporter cell line TZM-bl

HIV-1 Tat-dependent firefly luciferase gene assays conducted in TZM-bl cells [213] were used to measure effect on transactivation of different Tat variants. TZM-bl cells were either transfected with Tat expression plasmids (see section 2.4.2 or 2.4.3) or infected with lentiviral particles. To perform the transactivation assay, Pierce® Firefly Luciferase Glow Assay kit (Thermo Fisher Scientific) was applied according to the manufacturer's instructions. Luciferase output was measured on the CLARIOstar Plus microplate reader (BMG Labtech).

2.5.9. Latency reversal assay

J-Lat cells (clone 8.4) were cultivated in the presence of increasing concentrations of different compounds (see table 2.5). The respective highest concentration of solvent (either DMSO or H_2O) was used as control. 24 h post treatment, J-Lat cells were pelleted (500 x g, RT, 5 min) and washed with PBS, fixated and inactivated (see section 2.5.4). Subsequently, GFP positive cells were determined by flow cytometry and data were normalized to the control.

2.5.10. Visualization of reactivated HIV-1 by fluorescence microscopy

Using GFP reporter systems, fluorescent microscopy was performed to visualize reactivation of HIV-1 latency in J-Lat cells. For sample preparation, cells were separated from cell debris by low speed centrifugation (23 x g, RT, 5 min). Thereafter, cells were re-suspended in culture medium supplemented with 4 % PFA (Electron Microscopy Sciences) and inactivated at RT for 90 min. Subsequently, cells were spun down (1212 x g, 4°C, 10 min), washed with culture medium, and embedded in Prolong™ Diamond Antifade Mountant (Invitrogen) on microscopy glass slides sealed by a glass cover slip. After 16 to 24 h of incubation at RT protected from light, samples were imaged (brightfield exposure time: 200 ms, GFP exposure time: 100 ms) using the Eclipse Ti2 microscope (Nikon) in combination with a DS-Qi2 camera (Nikon) under control of NIS Element AR software vers. 5.0 (Nikon). Acquired images with 0.365 µm/pixel

resolution were overlaid and analyzed using ImageJ vers. 1.52a (https://imagej.nih.gov/ij/) and the ND2 Reader plug-in (Nikon Instruments Inc).

2.6. Biochemical methods

2.6.1. Transcriptome analysis

RNA was isolated from trizol lysates of cells using Direct-zol RNA Miniprep Kit (Zymo Research) following manufacturer's instructions. In addition, RNA was purified using Agencourt RNAClean XP beads (Beckman Coulter) following the manufacturer's instructions. After quantification (NanoDrop One photospectrometer (Thermo Fisher Scientific), the RNA quality was assessed using a Bioanalyzer (Agilent Technologies). RNA of sufficient quality (RIN $>$ 7) was used to generate sequencing libraries by using 500 ng total RNA in a Sense mRNA Seq Library Prep Kit V2 for Illumina platforms (Lexogen) following the manufacturer's instructions. Libraries were quantified and subsequently sequenced on an Illumina HiSeq 1500 (sequencing mode: 100 nt, single-end). The sequencing data was pre-processed on a Galaxy server[b]. After demultiplexing, the data was trimmed according to Lexogen. The output was mapped to the human genome (hg19) using STAR (vers. 2.5.2b-0). Abundant reads were further analyzed using HTSeq-count (vers. 1.0.0) and a differential gene expression analysis was performed using DESeq (v. 1.0.19) setting the FDR $<$ 0.01. Adjacent data analysis was performed using Perseus (vers. 1.6.5.0) [214,215], R software environment (vers. 3.6.2) [216] in combination with the bioconductor package (vers. 3.10), g:Profiler [217] and GraphPad prism software (vers. 7.05).

2.6.2. Inhibition of the proteasome

To study dependency of cellular effects on the proteolytic activity of the 26S proteasome complex, target cells were cultured in proteasome inhibitor supplemented media for 4 h. MG-132 (Sigma-Aldrich) as inhibitor was diluted with culture medium to a final concentration ranging from 1 to 50 µM. Changes in the abundance of proteins of interest were monitored by immunoblotting (described in section 2.6.4).

2.6.3. Magnetic pull down of HA-tagged proteins from supernatant

Supernatant was produced from cell lines expressing HA-tagged proteins of interest. For this purpose, cells were seeded at a density of 0.75×10^6 in 15 ml total volume of fresh media. Supernatant was harvested after 72 hours and freed from cells and debris by centrifugation

[b] RNAseq was performed in collaboration with Dr. Helmut Blum, group leader at Gene Center Munich, Ludwig-Maximilians-Universität München

(500 x g, 4°C, 5 min). For pull down, 50 µl Anti-HA Magnetic Beads (Thermo Fisher Scientific) were washed in PBS (Gibco) and then added to the supernatant. After 4 h of incubation on a rotator at 4°C, magnetic forces were applied to collect beads with bound proteins and to remove the "flow through". Magnetic beads were washed with PBS three times before eluting HA-tagged proteins from the beads by incubating two times in 50 µl urea lysis buffer (8M urea in 80 mM Tris-HCl pH 7.6) supplemented with NuPAGE™ LDS sample buffer (Invitrogen) and NuPAGE™ sample reducing agent (Invitrogen) (final concentration of 1X) at 65°C for 5 min. Residual magnetic particles were removed by applying magnetic forces again. Eluted protein samples were pooled and stored at -20°C before analysis by SDS-PAGE and immunoblotting (described in section 2.6.4).

2.6.4. SDS-PAGE and immunoblotting

Immunoblotting was used to separate and identify specific proteins from complex cell extracts or cell supernatants. Pull down of HA-tagged proteins from supernatant is described in section 2.6.3. To extract proteins from cells, cells were washed in PBS (Gibco), pelleted (500 x g, 4°C, 5 min) and re-suspended in urea lysis buffer (8M urea in 80 mM Tris-HCl pH 7.6) or in modified RIPA buffer (50 mM Tris-HCl pH 7.5, 150 mM NaCl, 1 mM EDTA, 1% NP-40, 0.1% sodium deoxycholate). After 10 min of incubation on ice, lysate was cleared by centriguation at 20,000 x g at 4°C for 30 min. The supernatant was collected and protein concentration was determined on a NanoDrop One photospectrometer (Thermo Fisher Scientific) or by performing the Quick Start™ Bradford protein assay (Bio-Rad) according to the manufacturer's instructions. Cell lysates were stored at -20°C until further use.
For protein gel electrophoresis, lysates were mixed with 4X NuPAGE™ LDS sample buffer (Invitrogen) as well as 10X NuPAGE™ sample reducing agent (Invitrogen) and incubated at 65°C for 10 min. Samples and PageRuler™ Plus prestained protein ladder (10 to 250 kDa; Thermo Fisher Scientific) were loaded onto NuPAGE™ 4-12% Bis-Tris or Bolt™ 12% Bis-Tris protein gels. Protein gel electrophoresis was performed at constant voltage of 120 V (PowerPac™ HC High-Current Power Supply, Bio-Rad) for 90 min in Mini Gel Tanks (Thermo Fisher Scientific) filled with 1X NuPAGE™ MOPS SDS running buffer (Invitrogen). 45 min of protein transfer onto Amersham™ nitrocellulose membranes (0.45 µm; GE Healthcare) was performed at constant voltage of 20 V using the Mini Blot Module (Thermo Fisher Scientific) and 1X NuPAGE™ transfer buffer (Invitrogen) supplemented with 20% MeOH.
After transfer, nitrocellulose membranes were blocked with 5% milk in TBS at RT for 30 min. Blocking solution was removed by washing the membrane twice with TBS. Primary antibody solution was prepared by diluting primary antibodies in 3% albumine in TBS/0.05% sodium-azide as recommended by the manufacturer. The membrane was submerged in primary antibody solution and incubated at 4°C overnight. Thereafter, primary antibody solution was removed and the membrane were washed three times. Secondary antibody

solution was prepared by diluting HRP secondary antibodies in 3% albumine in TBS as recommended by the manufacturer. After incubation of the membrane in secondary antibody solution at RT for 1 h, the membrane was washed in TBS three times. WesternBright Sirius HRP substrate (Advansta) was used according to manufacturer's instructions and chemiluminescence was detected on the Fusion FX7 (Vilber). Quantification of signals was performed using ImageJ vers. 1.52a (https://imagej.nih.gov/ij/).

2.6.5. Co-immunopreciptation for HIV-1 Tat interactomics studies

For identification of protein-protein interactions by using anti-HA antibodies to capture proteins that are bound to HA-tagged HIV-1 Tat, cells were washed in PBS (Gibco), pelleted (500 x g, 4°C, 5 min) and re-suspended in modified RIPA buffer (50 mM Tris-HCl pH 7.5, 150 mM NaCl, 1 mM EDTA, 1% NP-40, 0.1% sodium deoxycholate) supplemented with cOmplete™ protease inhibitor cocktail (Roche), 2 mM $MgCl_2$ and 5 U/ml DNAse. After incubation at 4°C for 1 h, cell extract was cleared by centrifugation (20,000 x g, 4°C, 35 min) and the supernatant was collected. Pierce™ Anti-HA Magnetic Beads (Thermo Fisher Scientific) were washed in modified RIPA buffer and then added to the lysate. After 4 h of incubation on a rotator at 4°C, magnetic forces were applied to collect beads with bound proteins and to remove the supernatant ("flow through"). Magnetic beads were washed three times with modified RIPA buffer before eluting proteins from the beads using the Lysis Solution provided in the EasyPep™ Mini MS Sample Prep kit (Thermo Fisher Scientific). Reduction, alkylation, trypsin digest and clean-up of peptides was performed according to the manufacturer's instructions. Purified and dried samples were re-constituted in MS buffer (0.5% acetic acid, 0.1% TFA) and peptide concentration was adjusted to 0.2 µg/µl prior to LC-MS/MS measurement.

2.6.6. Peptide preparation and purification

To prepare cell lysates for quantitative proteome analysis, cells were centrifuged (500 x g, 4°C, 5 min) and washed twice in cold PBS (Gibco). Cell pellets were re-suspended in modified RIPA buffer (50 mM Tris-HCl pH 7.5, 150 mM NaCl, 1 mM EDTA, 1% NP-40, 0.1% sodium deoxycholate) supplemented with cOmplete™ protease inhibitor cocktail (Roche). Cell lysates were mixed with 1/10 volume of 5 M NaCl and incubated on ice for 15 min to release chromatin-bound proteins. Subsequently, samples were sonicated (12 x 5 s pulses with 5 s pause between cycles, 15 W) for homogenization. Then, eight volumes of ice-cold acetone were added to the lysate to precipitate proteins at -20°C overnight. Acetone precipitates were pelleted (2300 x g, 10 min, 4°C), dried at RT for 15 to 30 min and re-constituted in urea lysis buffer (6 M urea, 2 M thiourea in 80 mM Tris-HCl pH 7.6) supplemented with 1 mM DTT to reduce disulfide bonds. Protein concentration was determined with the Quick Start™

Bradford protein assay (Bio-Rad). If samples were subjected for protein quantification by SILAC, cell lysate was mixed with SILAC standard (see section 2.3.7) in a 1:1 ratio at this point.
Subsequently, protein solution (with or without SILAC spike-in) was alkylated using chloracetamide at a final concentration of 5.5 mM at RT protected from light for 45 min. Thereafter, alkylated protein solution was diluted eight-fold in 50 mM Hepes buffer pH 7.5. Digestion of protein solution was conducted at 37°C overnight using Pierce™ Trypsin/Lys-C Protease Mix (Thermo Fisher Scientific) diluted 1:100 (w/w). Digestion was stopped by adding TFA to a final concentration of 1% (v/v) and pH was checked to be below 3 using indicator stripes.
For peptide purification, reversed-phase Sep-Pak C18 cartridges (Waters) were used pre-equilibrated first with 5 ml ACN and then twice with 0.1% TFA. Protein digest was cleared by centrifugation (2,500 x g, RT, 5 min) prior to loading on the cartridges. After loading by gravity flow, cartridges were washed twice with 5 ml 0.1% TFA and then with 5 ml ddH_2O. At this stage, peptides bound to the column material was stored at 4°C until processing for TMT labeling (see 2.6.7) or for PTM enrichment (see 2.6.8).

2.6.7. TMT labeling

For TMT labeling [218], purified peptides were eluted from reversed-phase Sep-Pak C18 cartridges (see section 2.6.6) using 3 ml of 50% ACN. Eluates were dried by vacuum concentration (Concentrator Plus; Eppendorf) and re-constituted in 100 mM Hepes buffer. Peptide concentration was determined by Quick Start™ Bradford protein assay (Bio-Rad). Using the TMT6plex Mass Tag Labeling Kit (Thermo Fisher Scientific) samples and controls were labeled according to manufacturer's instructions. TMT labeling reaction was terminated by adding 5% hydroxylamine. Equal amounts of labeled peptides of each condition were combined and dried by vacuum concentration. After re-constitution in 0.1% TFA, peptide concentration was measured using the NanoDrop One photospectrometer (Thermo Fisher Scientific) and the TMT-labeled peptide mix was fractionated using the Pierce™ High pH Reversed-Phase Peptide Fractionation kit (Thermo Fisher Scientific) according to the manufacturer's instructions. For elution, solutions of 12.5%, 17.5%, 22.5% and 50% ACN in 0.1% triethylamine were used and resulting fractions were dried by vaccum concentration. Each fraction was re-dissolved in MS buffer (0.5% acetic acid, 0.1% TFA) and adjusted to a final peptide concentration of 0.2 µg/µl for MS measurement.

2.6.8. Serial enrichment of acetylated and phosphorylated peptides

For enrichment of acetylated and phosphorlyated peptides from the same sample for MS-based PTM quantification, peptides purified in Sep-Pak C18 cartridges (see section 2.6.6) were eluted using 3 ml of 50% ACN and mixed directly with 100 µl 10X IAP buffer (500 mM MOPS pH 7.2, 100 mM sodium phosphate, 500 mM NaCl). ACN content was removed by vacuum cencentration and samples were filled up to 1 ml with ddH_2O.
For the enrichment of acetylated peptides by immunoprecipitation, PTMScan® Acetyl-Lysine Motif [Ac-K] kit (Cell Signaling Technology) was used. Antibody-beads were washed with PBS (Gibco) (1000 x g, 4°C, 5 min) and re-suspended in 1X IAP buffer. Additionally, 20 µl 5 M NaCl and 50 µl 10% NP-40 were added to the samples (final concentration of 100 mM NaCl and 0.5% NP-40) to reduce unspecific binding. Next, antibody-bead slurry was transferred to the samples and incubated at 4°C on a tube rotator overnight. Thereafter, antibody-beads were pelleted (1000 x g, 4°C, 3 min). Supernatant was collected as "flowthrough" and stored for the enrichment of phosphorylated peptides. Pelleted antibody-beads were washed twice with 1X IAP and once with ddH_2O (1000 x g, 4°C, 3 min). 100 µl 0.15 % TFA were added to the washed beads and incubated at RT for 5 min. After centrifugation (1000 x g, RT, 3 min), supernatant containing the eluted acetylated peptides was dried by vacuum concentration.
The "flow through" from the acetylation enrichment was used for the enrichment of phosphorylated peptides using the High-Select™ TiO_2 Phosphopeptide Enrichment kit (Thermo Fisher Scientific) according to manufacturer's instructions. During binding of the phosphorylated peptides to the TiO_2 resin, flow through was retained for a second phosphopeptide enrichment procedure using the High-Select™ Fe-NTA Phosphopeptide Enrichment kit (Thermo Fisher Scientific) according to the manufacturer's instructions. Eluates from both procedures were dried by vacuum concentration.

2.6.9. High pH reversed-phase peptide fractionation

Samples resulted from immunoprecipitation of acetylated peptides and from the enrichment of phosphorylated peptides were subjected to fractionation using the Pierce™ High pH Reversed-Phase Peptide Fractionation kit (Thermo Fisher Scientific). For this procedure, the dried peptides resulted from the phosphopeptide enrichment using TiO_2 and Fe-NTA resins were re-constituted in 0.1% TFA and combined, while the dried acetylated peptides were also re-solved in 0.1% TFA. Samples were processed according to the manufacturer's instructions. For elution, solutions of 7.5%, 12.5%, 17.5% and 50% ACN in 0.1% triethylamine were used and resulting fractions were dried by vaccum concentration. Each fraction was re-dissolved in MS buffer (0.5% acetic acid, 0.1% TFA) and adjusted to a final peptide concentration of 0.2 µg/µl for LC-MS/MS measurement.

2.6.10. Protein identification and quantification by LC-MS/MS

Measurements of prepared peptide fractions were realized using a Proxeon Easy-nLC system (Thermo Fisher Scientific) coupled to a Q Exactive HFX mass spectrometer (Thermo Fisher Scientific)[c]. Samples were loaded onto C18 reversed-phase chromatography columns (⌀75 µm x 15 cm) and a linear gradient from 6 to 40% ACN/H_2O in 0.5% acetic acid. Eluted peptides were subjected to electrospray ionization (2.0 kV) and measured in the mass spectrometer.The Q Exactive was controlled under Xcalibur vers. 2.2 with the LTC Orbitrap Tune Plus Developer kit vers. 2.6.0.1042 and was operated in data dependent acquisition mode enabling automatically switching between MS^1 and MS^2 spectra.
For peptide identification and quantification, MS raw files were analyzed with MaxQuant vers. 1.6.2.6a. [219]. Database search was performed against the human Uniprot database (Proteome ID: UP000005640, accessed: May 2019) or the HIV-1 group M subtype B (isolate HXB2) Uniprot database (Proteome ID: UP000002241, accessed: May 2019) to identify corresponding proteins. The false discovery rate (FDR) was set to 1% on peptide spectrum match (PSM) and protein level. The target-decoy search strategy [220] was used to estimate the FDR. Cysteine carbamindomethylation was enabled as fixed modification. N-acetyl protein and methionine oxidation were set as variable modifications. For fractions containing acetylated or phosphophorylated peptides, acetylation of lysine or phosphorylated serine/threonine/tyrosine served as additional variable modification respectively.
Downstream processing of Maxquant output was realized using the R software environment (http://www.r-project.org/) combined with the Proteus package [221], Perseus vers. 1.6.10.43 [214] and GraphPad Prism vers. 7.04 (GraphPad Software). Gene ontology (GO) term enrichment [222] was realized using the R package ClusterProfiler [223] and calculated using the Fisher's exact test. Pathway-based data integration and visualization was performed with the R package Pathview [224].

[c] LC-MS/MS measurement was performed by Dr. Igor Paron, research group of Prof. Dr. Matthias Mann, Max-Planck Institute Biochemistry, or Dr. Thomas Fröhlich, group leader at Gene Center Munich, Ludwig-Maximilians-Universität München

3. Results

3.1. Generation of a database for PTM regulated HIV-1-host interactions

For successful infection of the host cell, HIV-1 does manipulate several signaling pathways, which affects e.g. cell cycle, protein biosynthesis and degradation. Moreover, HIV-1 encodes and employs various strategies to disable host defense mechanisms of the innate immune system. Many of these HIV-1-dependent changes are controlled by rendering cellular PTM associated enzymes, such as protein kinases, acetyltransferases and E3 ubiquitin ligases. To gain a deeper overview of so far determined PTM-regulated HIV-1-host interactions and to construct an own state-of-the-art database for simplified bioinformatical analysis of raw data sets, a hand-curated data platform, that has not been existed so far, was created for protein acetylation, phosphorylation and ubiquitination using several sources. As foundation, the NCBI HIV Human Interaction Database (HHID) [36] was searched for HIV-1 protein interactions with PTM enzymes. Interactions were defined as direct, such as "Tat is acetylated by KAT2A" or "Nef binds to BST2", or as indirect events, such as "Vpr downregulates GSK3B" or "capsid induces IL2". According to the HHID, 138 acetyl-, 1899 phospho-, and 359 ubiquitin-associated HIV-1-host interactions were described. For acetylation, the HHID data set was further cross-analyzed with the HUGO Gene Nomenclature Commitee (HGNC) database [225] for the identification of human acetyltransferases and deacetylases revealing 11 lysine and N-terminal acetyltransferases out of 40 (28%) and 8 lysine deacetylases (KDACs/sirtuins) out of 18 (44%) in HIV-1-associated interactions. In the case of E3 ubiquitin ligases, the NHLBI ESBL human E3 ubiquitin ligases databank [226] served as data source and the correlation with the HHID showed interaction with 95 E3 ligases out of 377 (25%). In addition to the E3 ligases, the Ubiquitin and Ubiquitin-like Conjugation Database (UUCD) [227] determined overall 18 DUBs out of 103 (17%), which have been shown so far for HIV-1-related interactions. In comparison to protein acetylation and ubiquitination, protein phosphorylation has been studied more extensively and more comprehensive data were available. Here, data of the human kinome [228] as well as the human DEPhOsphorylation Database (DEPOD) [229] were included to determine 219 kinases out of 538 (41%) and 57 phosphatases (25%), which are regulated during HIV-1 infection (fig. 3.1A).

Further interaction analysis categorized by HIV-1 proteins showed the involvement of every single viral protein in the modulation of the host cell system at PTM level. Moreover, the analysis also indicated several viral interaction hubs, which extensively regulate the human PTM landscape during infection (fig. 3.1B). For example, 118 HIV-1 envelope glycoproteins

120 (gp120) involving interactions with enzymes of protein acetylation, ubiquitination and phosphorylation were identified. The viral protein R (Vpr) was also found to interact with 73 enzymes. Another outstanding hub was indicated for the HIV-1 trans-activator of transcription (Tat) interacting with 155 enzymes from all three considered PTM types. All interactions were sorted to different stages of the HIV-1 replication cycle to enable identification of potential important hubs, which can be utilized e.g. in posterior validation experiments.

The self-curated database of protein acetylation-, ubiquitination- or phosphorylation-regulated HIV-1-host interactions was used as standard repository for analysis of raw data sets. Updates are planned to be realized in a regular manner in order to include recently discovered interaction relationships. As the establishment of this data source revealed several new interaction networks, the presented data and results of the cross analysis are combined in a review [40] to allow easy access to other researchers in the field.

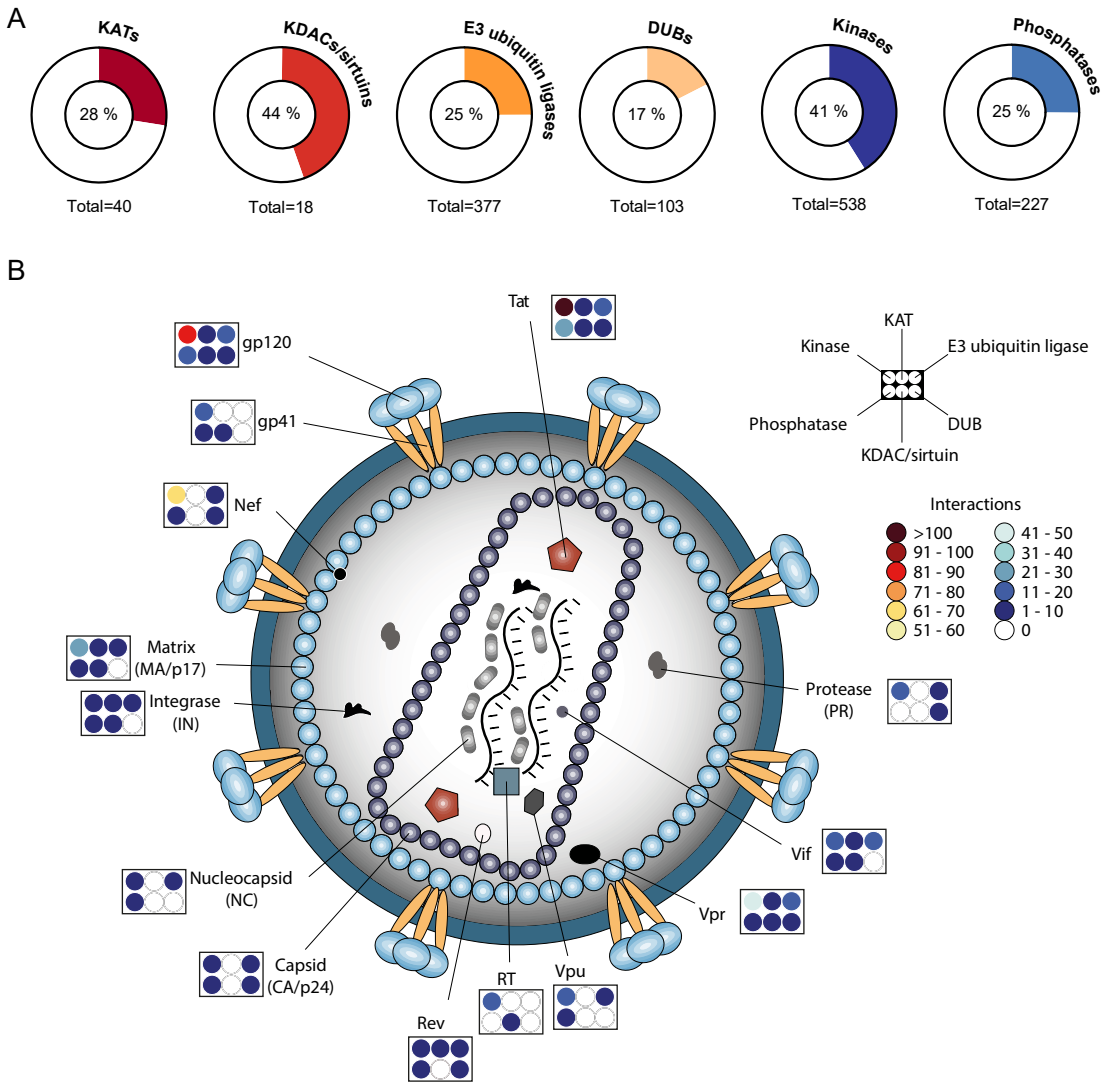

Figure 3.1. HIV-1-associated PTM enzymes.
(A) Analysis of interaction of viral proteins and PTM enzymes are based on the NCBI HHID. The pie charts illustrate percentages of interacting PTM enzymes of each classification based on the database of the HUGO Gene Nomenclature Committee [225], the National Heart Lung and Blood Institute ESBL human E3 ubiquitin ligases databank [226], the Ubiquitin and Ubiquitin-like Conjugation Database [227], databases for protein kinases [228] and the Human Dephosphorylation Database [229]. **(B)** Heatmap shows interactions between HIV-1 proteins and PTM enzymes of protein phopshorylation, acetylation and ubiquitination.

3.2. Virus production and optimization of infection

For elucidation of molecular mechanisms during acute HIV-1 infection using MS bottom-up approaches, large quantities of HIV-1-infected cells are required. To establish a protocol to generate cell lysates from HIV-1-infected T-cells for MS-based proteomic analysis, different infection conditions were evaluated for infection efficiency, consumption of virus stocks and feasibility to monitor the course of infection within a defined time frame.

As starting point, two commonly used HIV-1 lab strains, HIV-1_{NL4-3} and HIV-$1_{NL4-3-IRES-eGFP}$, were tested. As target cells for infection, primary $CD4^+$ T-cells were isolated from four healthy donors, activated and pooled. The two lab strains were compared by titration on the 4-donor pool (4DP) of primary activated $CD4^+$ T-cells using concentrated virus stocks. After 48 h, HIV-1_{NL4-3}-infected cells were stained for intracellular viral core protein p24 and the proportion of infected cells within the population was assessed by flow cytometry. In the case of the GFP reporter virus HIV-$1_{NL4-3-IRES-eGFP}$, the expression of GFP was determined by flow cytometry directly (fig. 3.2A). With both HIV-1 lab strains, the infection efficiency 48 h p.i. did not exceed 15% with the maximal used amount of 10 µl inoculum. Notably, the infection efficiency was on average 5% higher for the HIV-1_{NL4-3} at 10 µl incoculum (fig. 3.2B).

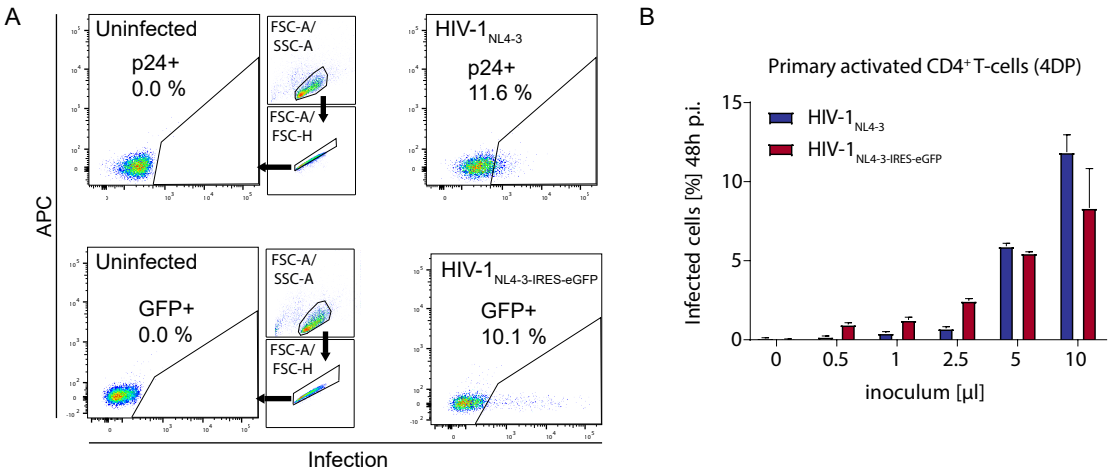

Figure 3.2. Initial HIV-1 infection in primary activated $CD4^+$ T-cells. (A) Flow cytometry plots of infected (p24- or GFP-positive) primary activated $CD4^+$ T-cells. Main plots shows uninfected (left) and infected (right) cell populations.Upper small plot displays cell distribution in FSC/SSC plot and the gated fraction of cells were used for further analysis. Lower small plot shows cell distribution in FSC-A/FSC-H plot and the gated single cell population was used for further analysis of the infected population. APC was used as a reference channel. **(B)** Titration of HIV-1_{NL4-3} and HIV-$1_{NL4-3-IRES-eGFP}$. A 4-donor pool (4DP) of primary $CD4^+$ T-cells was infected with increasing volumes of concentrated virus. The graph displays infected cells based on the gating strategy desribed in (A). Error bars show standard deviation of at least two independent measurements.

As an alternative for primary activated $CD4^+$ T-cells, two commonly used T-cell lines for HIV-1 infection, namely Jurkat-E6 and SupT1.CCR5 cells, were tested by infection with HIV-1_{NL4-3} for 48 h (fig. 3.3A). Moreover, spin-infection was evaluated in parallel to the standard inoculation in primary activated $CD4^+$ T-cells, Jurkat-E6 and SupT1.CCR5 cells (fig. 3.3B). In general, a higher infection efficiency could be achieved in the T-cell lines compared to the primary activated $CD4^+$ T-cells. Up to 56% of the Jurkat-E6 cells and up to 96% of the SupT1.CCR5 were p24-positive after 48 h using the maximal inoculum of 10 µl. With regard to spin-infection, infection efficiency could be improved up to 19.3-fold in the primary cells, up to 4.4-fold in Jurkat-E6 cells and up to 6.2-fold in SupT1.CCR5 cells using an even lower inoculum of 1 µl. In parallel with the infection efficiency, the number of events within the respective FSC/SSC gate was investigated as indicator for the number of living cells (fig. 3.3C). As expected, the increasing number of p24-positive cells was accompanied with higher rate of cell death (fig. 3.3C and D). Concerning this negative correlation, SupT1.CCR5 cells showed the most extreme outcome among the tested cell systems with almost 100% infection efficiency. However, the estimated number of living SupT1.CCR5 cells decreased down to 6% compared to the uninfected control. In the case of the primary cells, the decrease in living cells was more prominent when spin-infection was applied compared to standard inoculation. Jurkat-E6 cells also showed a decrease in living cells with increasing infection efficiency, however, to a much lower extent: 83.3% living cell were measured for the standard infection set-up and 79.1% for the spininfected condition using the maximal used inoculum of 10 µl. For Jurkat-E6 cells, the number of living cells in the spininfected condition seemed to be comparable with the standard conditions in contrast to primary activated $CD4^+$ T-cells and SupT1.CCR5 cells (fig. 3.3D).

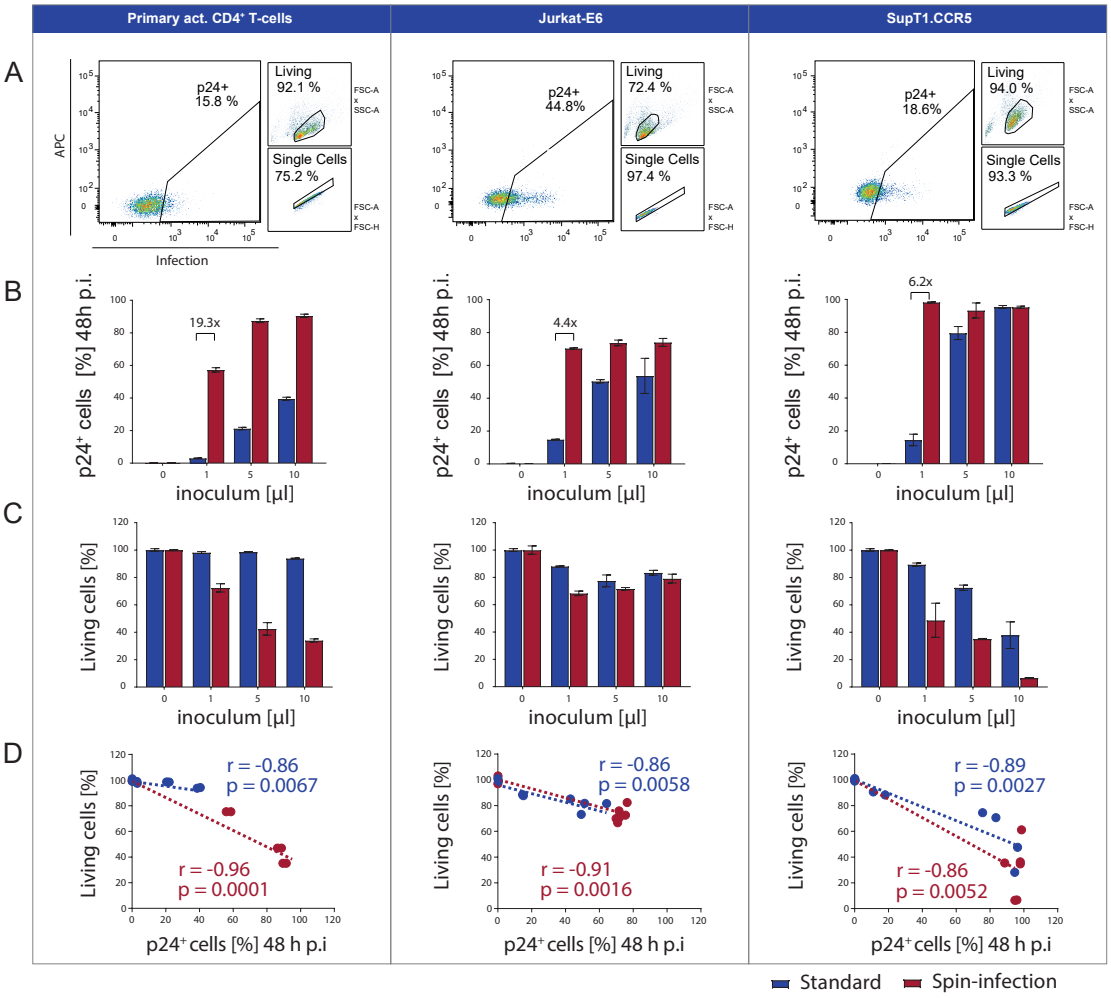

Figure 3.3. Comparison of HIV-1_{NL4-3} infection conditions in different cell systems. (A) Gating strategy for flow cytometry to assess percentage of infected (p24-positive) cells and the population of viable cells within the respective FSC/SSC gate. Representative plots are shown for primary activated $CD4^+$ T-cells, Jurkat-E6 and SupT1.CCR5 cells. Error bars show standard deviations. **(B)** Titration of HIV-1_{NL4-3} in primary activated $CD4^+$ T-cells, Jurkat-E6 and SupT1.CCR5 cells using standard or spin-infection mode. 48 p.i., cells were stained for p24. **(C)** Evaluation of the number of viable cells measured by the size of the respective population in the FSC/SSC gate after standard infection and spin-infection. Error bars (in B and C) show standard deviation of at least two independent measurements. **(D)** Correlation analysis of the number of events in the FSC/SSC gate and infection efficiency. Pearson correlation coefficient r and p value (slope significantly different from zero) are indicated.

3.3. Monitoring the course of HIV-1 replication within the first 24 hours

Routinely, infection assays were performed for 48 h. However, since one complete HIV-1 replication cycle is described to take approximately 24 h [230], an experimental set-up monitoring the increase of HIV-1 core protein in infected cells after the time points 0, 4, 8, 12 and 24 h p.i. was performed. For this purpose, primary activated $CD4^+$ T-cells or Jurkat-E6 cells were spin-inoculated with 5 µl concentrated HIV-1_{NL4-3} (saturating conditions, see also fig. 3.3B) and the fraction of p24-positive cells was measured by flow cytometry after specific time points (fig. 3.4A). At 4 h p.i., ca. 74% of the Jurkat-E6 cells and ca. 69% of the primary cells were already p24-positive indicating a fast increase within a few hours p.i.. At 24 h p.i., ca. 92% of the Jurkat-E6 cells and 88% of the primary cells were measured as p24-positive. For both cell types, an overall increase in p24-positive cells could be observed though all defined time points. Analogous to time course analysis of p24 using HIV-1_{NL4-3}, another time course using GFP reporter virus HIV-$1_{NL4-3-\Delta Nef-GFP}$ for spin-infection of Jurkat-E6 cells was performed. In the case of infection with HIV-$1_{NL4-3-\Delta Nef-GFP}$, GFP expressing Jurkat-E6 cells were measured by flow cytometry after defined time points (fig. 3.4D). In contrast to the early incease in p24-positive cells from 4 h p.i., the overall increase in GFP-positive Jurkat-E6 cells was observed only from 12 h p.i. onwards. Notably, the highest infection efficiency of 67%% on average was achieved in HIV-$1_{NL4-3-\Delta Nef-GFP}$-infected Jurkat-E6 cells at 48 h p.i..
As the next step, HIV-1_{NL4-3} spin-infection experiments in Jurkat-E6 cells treated with fusion inhibitors were performed to test, whether the observed increase in p24 (fig. 3.4A) was specific due to successful fusion of viral particles with the host cell. Therefore, the two fusion inhibitors, human anti-CD4 antibody and T-20 (also known as enfurvirtide or Fuzeon®) were tested (fig. 3.4B). Both compounds were able to reduce infection efficiency measured by p24-positive cells after 24 h by 651-fold (T-20) or 728-fold (anti-CD4) compared to the PBS control.
In addition to the fusion inhibition experiments, a series of trypsination experiments was conducted on HIV-1_{NL4-3}-spininfected Jurkat-E6 cells to test whether the observed increase in p24 within 4 h p.i (fig. 3.4A) was caused by extracellularly bound, but not fused, viral particles. For this purpose, spininfected Jurkat-E6 cells (4 h p.i.) were treated with 0.05% or 0.25% trypsin for 2, 5 or 10 min and subsequently stained for HIV-1 core protein (fig. 3.4C). Flow cytrometric analysis showed only a minor reduction ($< 5\%$) of positive cells compared to the PBS-treated cells, even when high trypsin concentration or prolonged incubation time was applied. At the same time, cells that were pre-treated with trypsin before addition of virus showed a decrease in p24-positive cells in an incubation time-dependent manner. Treating with 0.25% trypsin for 10 min led to an observed reduction of ca. 11% in reference to the PBS-treated condition.
In summary, spin-infection of Jurkat-E6 cells with HIV-1_{NL4-3} resulted in high infection

efficiency of up to 90%. The progress of HIV-1 replication within 24 h could be tracked by flow cytometric analysis of intracellularly stained p24, which increased with ongoing HIV-1 replication. Using this infection set-up, high yield of infected cell lysate for quantitative MS based proteomic analysis with reduced background to noise (from the uninfected cell population) can be produced.

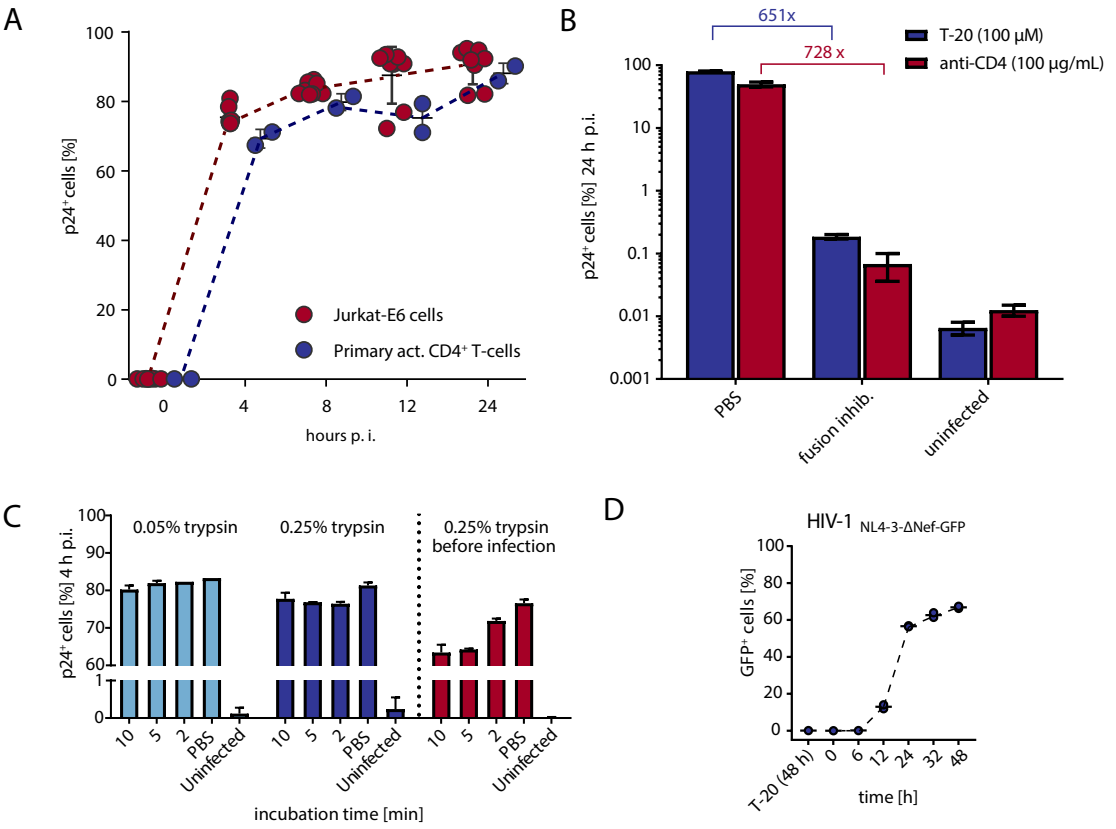

Figure 3.4. Intracellular staining of HIV-1 core protein (p24) to monitor progessing HIV-1 replication. **(A)** p24 time course of HIV-1_{NL4-3}-spininfected primary act. $CD4^+$ T-cells (4DP) or Jurkat-E6 cells. **(B)** Flow cytometric measurement of intracellular p24 in HIV-1_{NL4-3}-spininfected Jurkat-E6 cells treated with fusion inhibitors, T-20 or anti-CD4 antibody (24h p.i.). **(C)** Measurement of intracellular p24 of HIV-1_{NL4-3}-spininfected Jurkat-E6 cells (4 h p.i) after trypsination (light and darkblue bars). Trypsination before adding virus and spin-infection was also tested (red bars). **(D)** GFP time course of HIV-$1_{NL4-3-\Delta Nef-GFP}$-spininfected Jurkat-E6 cells. T-20 treated cells were used as control. Error bars (in A, B, C and D) show standard deviation of at least two independent measurements.

3.4. Time resolved proteomics in HIV-1-infected CD4$^+$ T-cells

3.4.1. HIV-1-regulated proteomic changes in infected Jurkat-E6 cells within 24 h

To investigate HIV-1-associated changes in the global proteome as well as at PTM level (here: phosphorylation and acetylation) within the first 24 h of viral replication, optimized parameters from section 3.2 and 3.3 were applied to design a time course experiment (overview illustrated in fig. 3.5A). In brief, Jurkat-E6 cells were spininfected with HIV-$1_{NL4\text{-}3}$ ($MOI_{24h} \approx 2.3$) and harvested after 4, 8, 12 and 24 h. Uninfected cells served as control (0h). During the harvest of infected cells, aliquots of each time point were subjected to flow cytometric analysis of infection by p24 staining. The median infection efficiency measured by p24-positive cells after 24 h was 93.3% (fig. 3.5B). Infected and control cells were harvested and lysed. For quantification of the global proteome of infected cells, tryptic digests of the cell lysates from each time point were subjected to TMT labeling. The larger portion of the lysates was used for PTM site quantification using the SILAC standard spike-in approach. After tryptic digest, acetylated and phosphorylated peptides were enriched by affinity-purification. Purified and fractionated TMT or SILAC samples were measured in duplicates by LC-MS/MS. Subsequently, MS data were processed and analyzed as described in the workflow of section 3.6.

The TMT experiment provided complete time courses of HIV-1 proteins encoded by *env*, *gag*, *pol* and *nef* (fig. 3.5E). All identified HIV-proteins showed increasing abundancy within the course of infection. Proteins encoded by *gag* showed the strongest increase in abundance ($\log_2$ fold change > 2) and the trend is consistent with the p24 time course measured by flow cytometry (fig. 3.5B). In contrast to other detected HIV-1 gene products, the abundance of *pol* gene products peaked in early stages of HIV-replication (4 h). In addition, Nef (encoded by *nef*) showed rather fluctuating abundance over time (increasing after 8 h, decreasing after 12 h and increasing after 24 h).

Apart from the time resolved data from HIV-1 proteins, complete time courses of over 4400 host proteins were acquired from the TMT experiment (fig. 3.5D). For analysis of differential expression, proteins with $\log_2$ fold changes ≥ 1 or $\log_2$ fold changes ≤ 1 relative to control were defined as up-regulated or down-regulated, respectively. Applying these criteria, 987 regulated proteins (616 up-regulated; 371 down-regulated) were found after 24 h of infection. Comparing the numbers of down- or up-regulated proteins through all time points, a drop in up-regulated and down-regulated proteins was noticed at the 8 h time point.

In contrast to the proteins from the TMT experiment, PTM sites were identified in only some time points. Consequently, many time courses of PTM sites contained missing data values leading to a reduced number of PTM sites within the complete time course (fig. 3.5C).

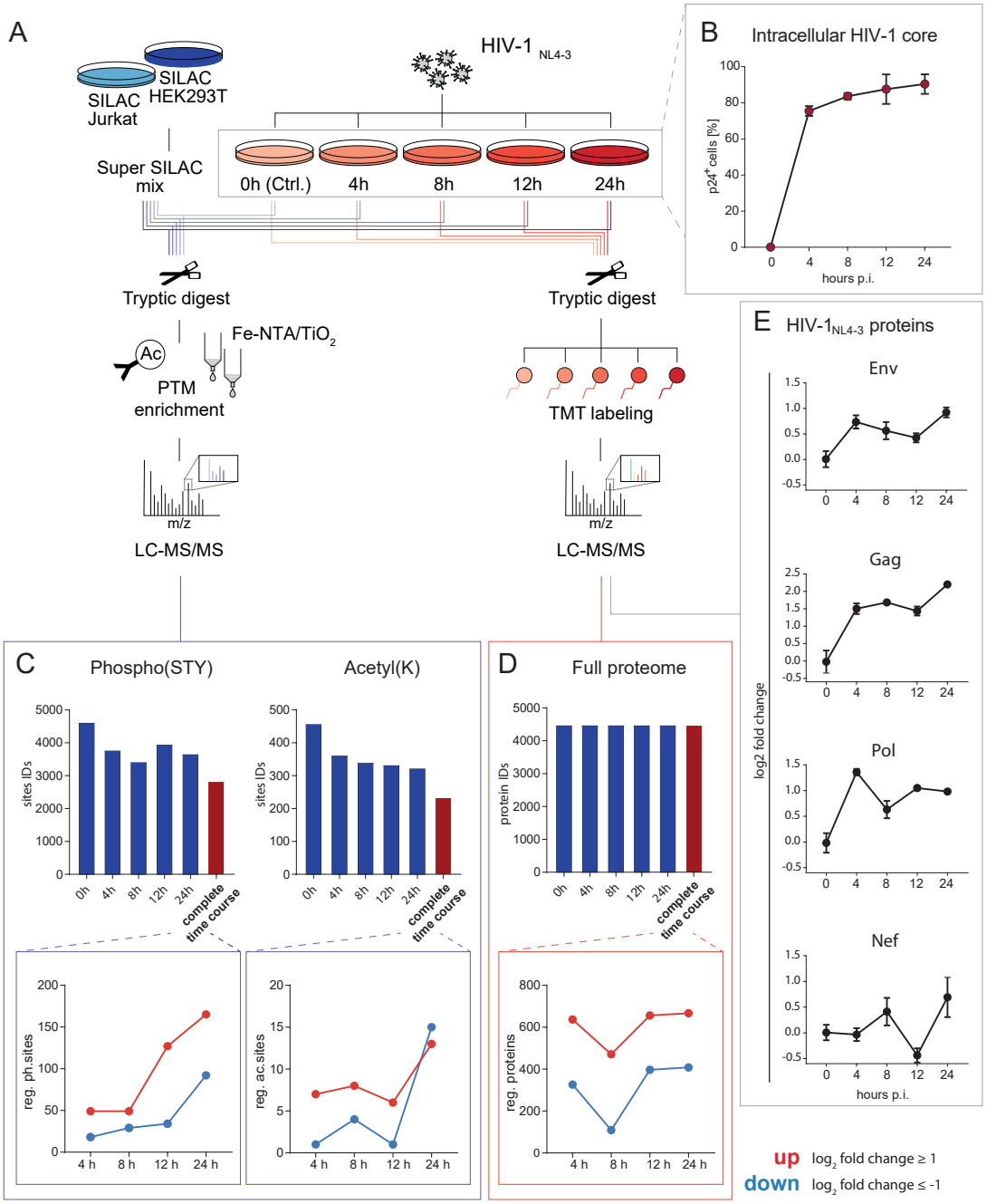

Figure 3.5. Time resolved proteomics of HIV-1_{NL4-3}-infected Jurkat-E6 cells. **(A)** Overview of the experimental design. Spin-infected Jurkat-E6 cells were harvested at defined time points. One part of the lysates was prepared for TMT labeling to quantify the full proteome by LC-MS/MS. For quantification of the phosphoproteome and acetylome, the other part of the lysates was mixed with a SILAC standard generated from labeled, untreated Jurkat-E6 and HEK293T cells. Acetylated peptides were enriched by immunoprecipitation and phosphorylated peptides were enriched using Fe-NTA/TiO_2 columns for LC-MS/MS analysis. **(B)** Time course of intracellular HIV-1 p24 determined by flow cytometry. **(C)** Numbers of identified PTM sites and regulated PTM sites per time point. **(D)** Numbers of identified proteins and regulated proteins per time point. **(E)** Abundancies of HIV-1 proteins (Uniprot gene names are indicated) over time. Fold changes are relative to the control (0 h). Error bars (B and E) show standard deviation of two independent measurements.

As a result, time courses of over 2800 phosphorylation sites and over 200 acetylation sites were determined. Applying the same criteria for definition of regulated sites as described for regulated proteins, 286 up- and 132 down-regulated phosphorylation sites were identified at 24 p.i. (total: 418). In the case of acetylation, 13 up- and 15 down-regulated sites were found (total: 28).

As expected, the majority of regulated proteins or PTM sites were observed at the 24 h time point. For the confirmation of identified proteins and modified sites, the NCBI HIV-1 Human Interaction Database (HHID) [36] was used to identify overlapping records (fig. 3.7A). 36.17% of the regulated proteins from the full proteome analysis were listed as host factors interacting with HIV-1. The regulated phosphorylation sites were assigned to 95 proteins. Of these, 54.74% were also reported as HIV-1 interacting proteins in the NCBI HHID. Regulated acetylation sites were assigned to 17 proteins. Of these, 64.71% were also found in the NCBI HHID. Additionally, a comparison with data of HIV-human protein complexes determined by affinity-tagged purification mass spectrometry [37] was conducted (supplemental fig. S2). This analysis showed, that 21.68% of the regulated proteome, 34.73% of the regulated phosphoproteome and 47.06% of the regulated acetylome was found on proteins or protein complexes with physical contact to HIV-1 proteins. In the case of the regulated phosphoproteome, the measured changes showed good correlation with a recent quantitative HIV-1-phosphoproteomics analysis by Johnson *et al.* [231] (fig. 3.6A and B). Examples of proteins with comparable phosphorylation changes in both data sets include the *thyroid hormone receptor-associated protein 3* (THRAP3), *stathmin* (STMN1), *leukosialin* (SPN) and *Bcl-2-associated transcription factor 1* (BCLAF1) (fig. 3.6B).

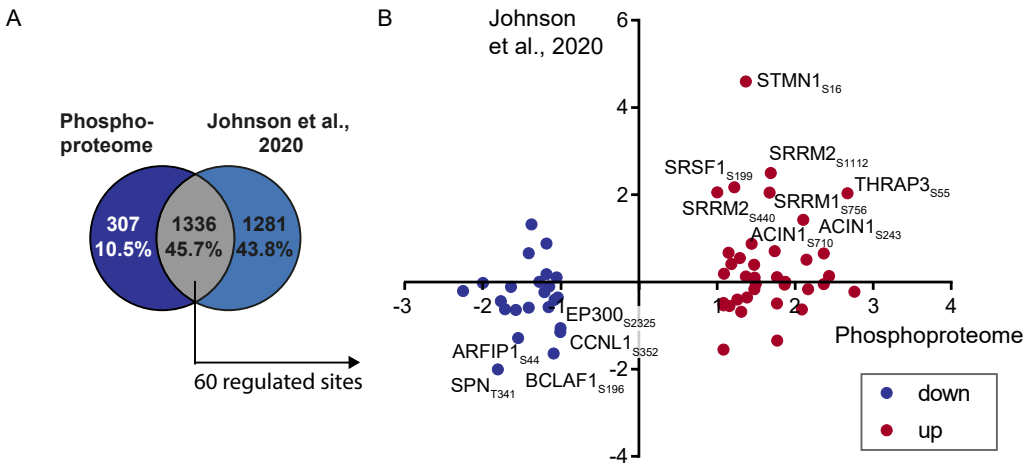

Figure 3.6. Comparison of HIV-1-associated phosphoproteome of this study with the data set of Johnson *et al.* [231]. **(A)** Venn diagram of total number of identified host phosphoproteins (24 h). **(B)** Correlation analysis of the regulated host phosphorylation sites. X- and y-axis indicate $\log_2$ fold changes (infected/uninfected) at the 24 h time point. Phosphorylation sites with $|\log_2 \text{ fold changes}| \geq 1$ were defined as regulated. Uniprot gene names and PTM site localization of example proteins are shown.

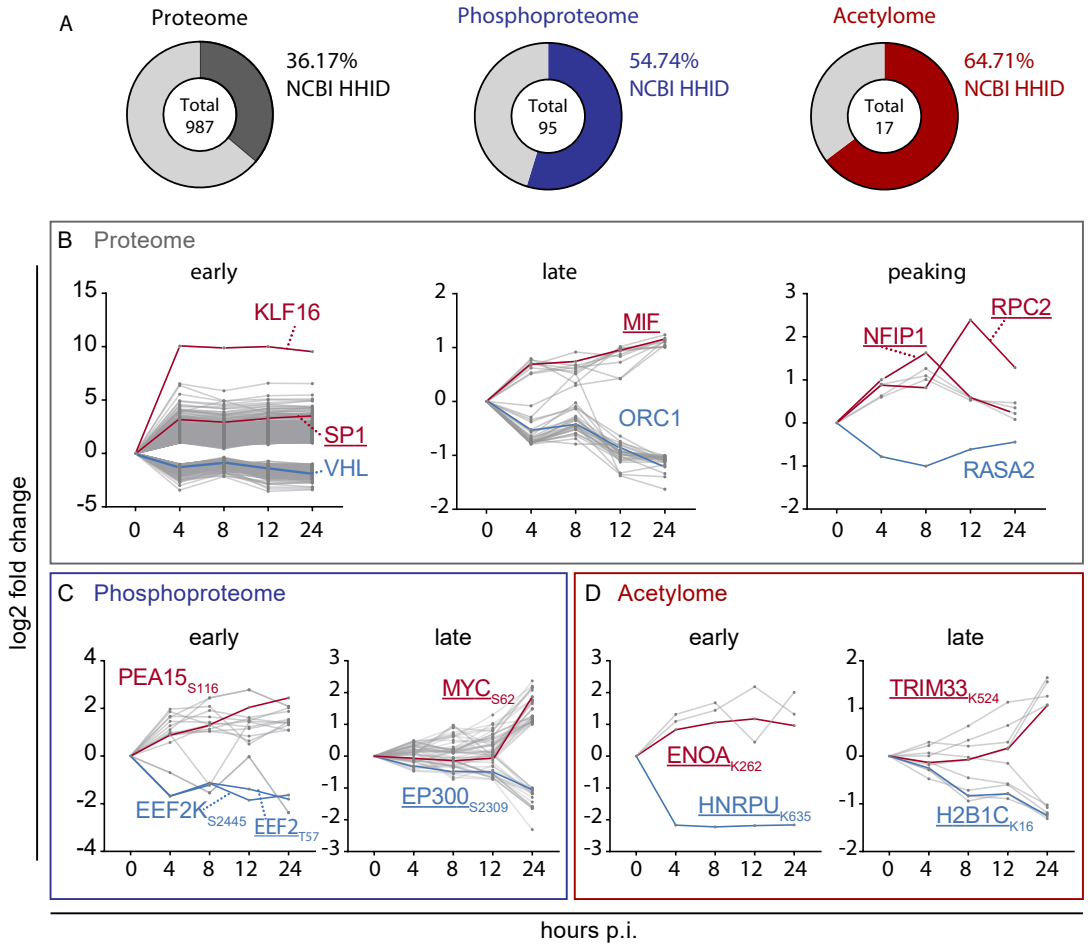

Figure 3.7. Time courses of regulated proteins or PTM sites associated with HIV-1 infection. (A) Number of regulated (phosphorylated/acetylated) proteins 24 h p.i. Percentage of proteins listed in the NCBI HIV-1 Human Interaction Database are highlighted. Clustered time courses are shown for the HIV-1-associated **(B)** full proteome, **(C)** phosphoproteome and **(D)** acetylome. Uniprot gene names and PTM site localization of example proteins are shown. Font color of exemplified proteins indicates up-regulation (red) or down-regulation (blue). Underlined proteins are also listed in the NCBI HHID [36]. Hierarchical clustering of time courses using Euclidian distance resulted in clusters for early (0-8 h) or late (12-24 h) regulation. Another cluster was defined by peaking responses.

Similar to the HIV-1 proteins (fig. 3.5E), host proteins also showed different time course patterns. Therefore, hierarchical clustering by similarity using Euclidian distance was performed resulting in the time course clusters "early", "late" and "peaking". Examples of regulated proteins with these time course profiles are illustrated in fig. 3.7B-D. Continuous up- and down-regulation within 4 to 8 h p.i. were defined as early, whereas up- and down-regulation starting from 12 h p.i. were considered as late. Most time courses of the full proteome (fig. 3.7B) were clustered as early, e.g. *Krueppel-like factor 16* (KLF16), *transcription factor Sp1* (SP1) and *Von Hippel-Lindau disease tumor suppressor* (VHL). Examples with a late profile were represented by *macrophage migration inhibitory factor* (MIF) and *origin recognition complex subunit 1* (ORC1). Interestingly, a few time courses showed a peak in the increase/decrease of protein abundance within the time course. Proteins

of this peaking cluster are exemplified by *NEDD4 family-interacting protein 1* (NFIP1), *DNA-directed RNA polymerase III subunit RPC2* (RPC2) and *Ras GTPase-activating protein 2* (RASA2) in fig. 3.7B.

For phosphorylated and acetylated proteins, most regulated PTM sites were identified at late time points, e.g the increase in *myc proto-oncogene protein* (MYC) phosphorylated at S62, decrease in *histone acetyltransferase p300* (EP300) phosphorylated at S2309 and increase in *E3 ubiquitin-protein ligase TRIM33* (TRIM33) acetylated at K524 at 24 h p.i. (fig. 3.7C and D). The increase of *astrocytic phosphoprotein PEA-15* (PEA15) phosphorylated at S116, *alpha-enolase* (ENOA) acetylated at K262 and the decrease of *heterogeneous nuclear ribonucleoprotein U* (HNRPU) acetylated at K635 served as examples for modified proteins in the cluster of early regulation.

In summary, time resolved data from viral and host (phosphorylated or acetylated) proteins were obtained from the TMT and SILAC experiments with HIV-$1_{NL4\text{-}3}$-infected Jurkat-E6 cells. More than one third of the up- or down-regulated proteins and more than half of the phosphorylated or acetylated proteins are described as interactors with HIV-1 proteins according to the NCBI HHID [36]. Time course analysis of regulated proteins or PTM sites revealed early, late or peaking responses to HIV-1 infection. Nevertheless, to gain more insights about the biological consequences of the HIV-1-associates changes in protein or site abundancies over time, further analysis in the context of cellular pathways was required.

3.4.2. Analysis of the HIV-1-regulated dynamics of protein abundancies

In order to gain more insights into the biological consequences of the HIV-1-regulated dynamics of protein abundance in infected Jurkat-E6 cells, acquired quantification data from the TMT and SILAC experiments were subjected to KEGG pathway enrichment analysis.
First, to differentiate between early and late events, top 20 enriched KEGG pathways including up- or down-regulated proteins or phosphorylation sites of 4 h (early) and 24 h (late) p.i. were compared (fig. 3.8). For both time points, 4 h and 24 h, infection disease-associated pathways (e.g. HIV-1, salmonella, hepatitis), cell metabolism related pathways (e.g. carbon metabolism, biosynthesis of amino acids) and pathways of neurodegenerative diseases (e.g. Alzheimer, Parkinson, Huntington disease) were determined. Moreover, structural constituents of spliceosome and ribosome were also enriched in early and in late stages of HIV-replication. Numerous elements of the spliceosome e.g. proteins of the U1 related small nuclear ribonucleoproteins (snRNPs) complex as well as several large and small subunits of the ribosome were up-regulated during the HIV-1 time course (supplemental fig. S3). Other subcomplexes of the spliceosomal machinery or ribosome showed mixed protein abundance patterns e.g. the U2 related snRNPs (supplemental fig. S3A) or the elongation factor Tu (EF-Tu) respectively (supplemental fig. S3B). In contrast to the 24 h time point, proteins of RIG-I-like receptor signaling pathway (supplemental fig. S5) and proteins involved in cell metabolism e.g. glycolysis/glyconeogenesis (suppplemental fig. S4) were over-represented at the 4 h time point. These pathways were absent in the top 20 at the 24 h time point, whereas differentially expressed proteins involved in ubiquitin mediated proteolysis, RNA degradation and cell cycle were enriched during the late phase of infection.

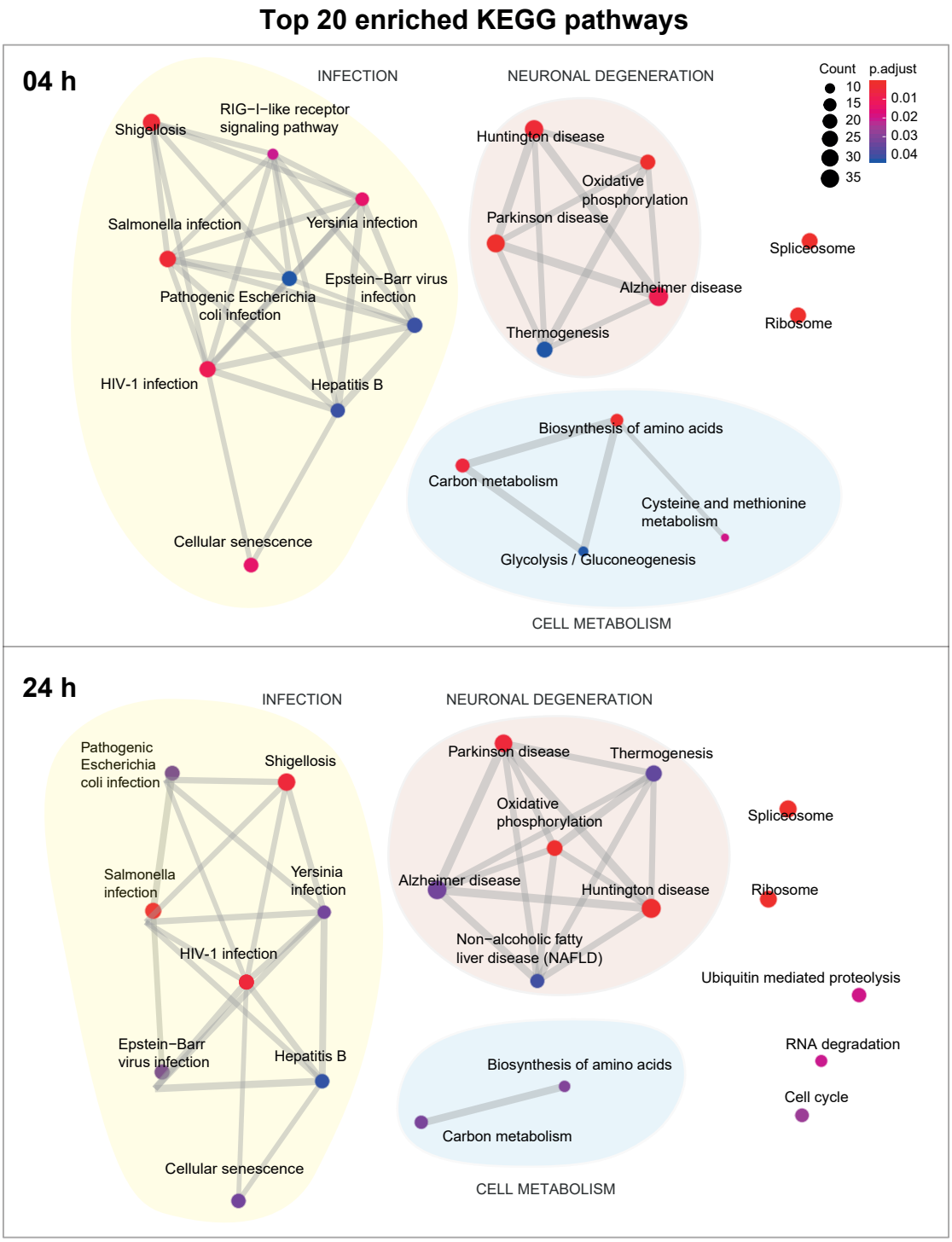

Figure 3.8. Enrichment maps of top 20 KEGG pathways overrepresented upon HIV-1 infection. Nodes represent enriched KEGG pathways 4 h or 24 h p.i and are color-coded according their respective adjusted (method: Benjamini Hochberg) p-value. Count of proteins assigned to a KEGG pathway is parsed to the node size. KEGG pathways with shared proteins are connected by edges. Cluster of related KEGG pathways are encircled.

3.4.3. Pathway mapping of temporal dynamics of HIV-1-regulated host proteins

Based on the results from the analysis of the HIV-1-regulated dynamics of protein abundancies and KEGG pathway enrichment analysis, different cellular pathways were found highly affected during early and late phases of HIV-1 infection, including the RIG-I-like receptor signaling (fig. 3.8, 4 h), glycolysis (fig. 3.8, 4 h) and cell cycle (fig. 3.8, 24 h). Cell cycle regulation has been shown to be critical for HIV-1 replication by various publications [232–234]. Therefore, the cell cycle was chosen to exemplify pathway-based data integration and visualization of quantified protein/PTM site abundancies upon HIV-1 infection (fig. 3.9). Time course data from the full proteome (fig. 3.9A) and phosphoproteome (fig. 3.9B) were used. Notably, because of the low counts of determined time courses of acetylated sites, KEGG pathway enrichment analysis could not be performed in a reasonable manner for the HIV-1-regulated acetylome. 62 proteins of the quantified proteome could be mapped to the KEGG cell cycle map resulting in a pathway coverage of 67.3%. Moreover, quantification of the phosphoproteome resulted in 19 phosphoproteins, which were additonally mapped into the cell cycle resulting in a coverage of 20.6%. Numerous proteins assigned to G1 or S phase of the cell cycle were found to be down-regulated e.g. *cyclin-dependent kinase 2* (CDK2), transcription factors E2F1, E2F2, or the origin recognition complex (ORC) (fig. 3.9A). Contrary to the proteins of early cell cycle phases, proteins of G2 or M phase were found highly up-regulated e.g. *cyclin-dependent kinase 1* (CDK1), *Wee-like protein kinase* (Wee) or proteins of the anaphase-promoting complex (APC/C). Mapping using phosphoproteomic data into the cell cycle showed more delayed response (up- or down-regulation at 12 or 24 h) compared to the time courses of the full proteome (fig. 3.9B). Examples are CDK1 and APC/C, which showed a strong increase in protein abundance from 4 h p.i., whereas the abundance of phosphorylated CDK1 or APC/C decreased at later phases (12-24 h p.i.).
Besides the cell cycle, pathway mapping was also performed for KEGG glycolysis (supplemental fig. S4) and KEGG RIG-I-like receptor signaling (supplemental fig. S5) and is shown in the supplement. In the case of glycolysis, strong up-regulation of key enzymes of the energy releasing phase, such as *glyceraldehyde-3-phosphate dehydrogenase* (GAPDH, EC: 1.2.1.12), *phosphoglycerate kinase 1* (PGK, EC: 2.7.2.3) and enolase (ENO3, EC: 4.2.1.11) was observed through the entire HIV-1 time course. In the case of the RIG-I-like receptor signaling pathway, which regulates pathogen sensing of RNA virus infection to initiate antiviral response [235] (supplemental fig. S5), up-regulation of *ubiquitin-like protein ATG12* (ATG12), a key regulator of the autophagy process [236], and regulators of the activation of NF-κB were shown. In parallel, *serine/threonine-protein kinase TBK1 (TBK1)* regulator of *interferon regulatory factor 3* (IRF3) and *interferon regulatory factor 7* (IRF7), which are part of the innate immune response against DNA and RNA viruses [237] were found to be down-regulated.

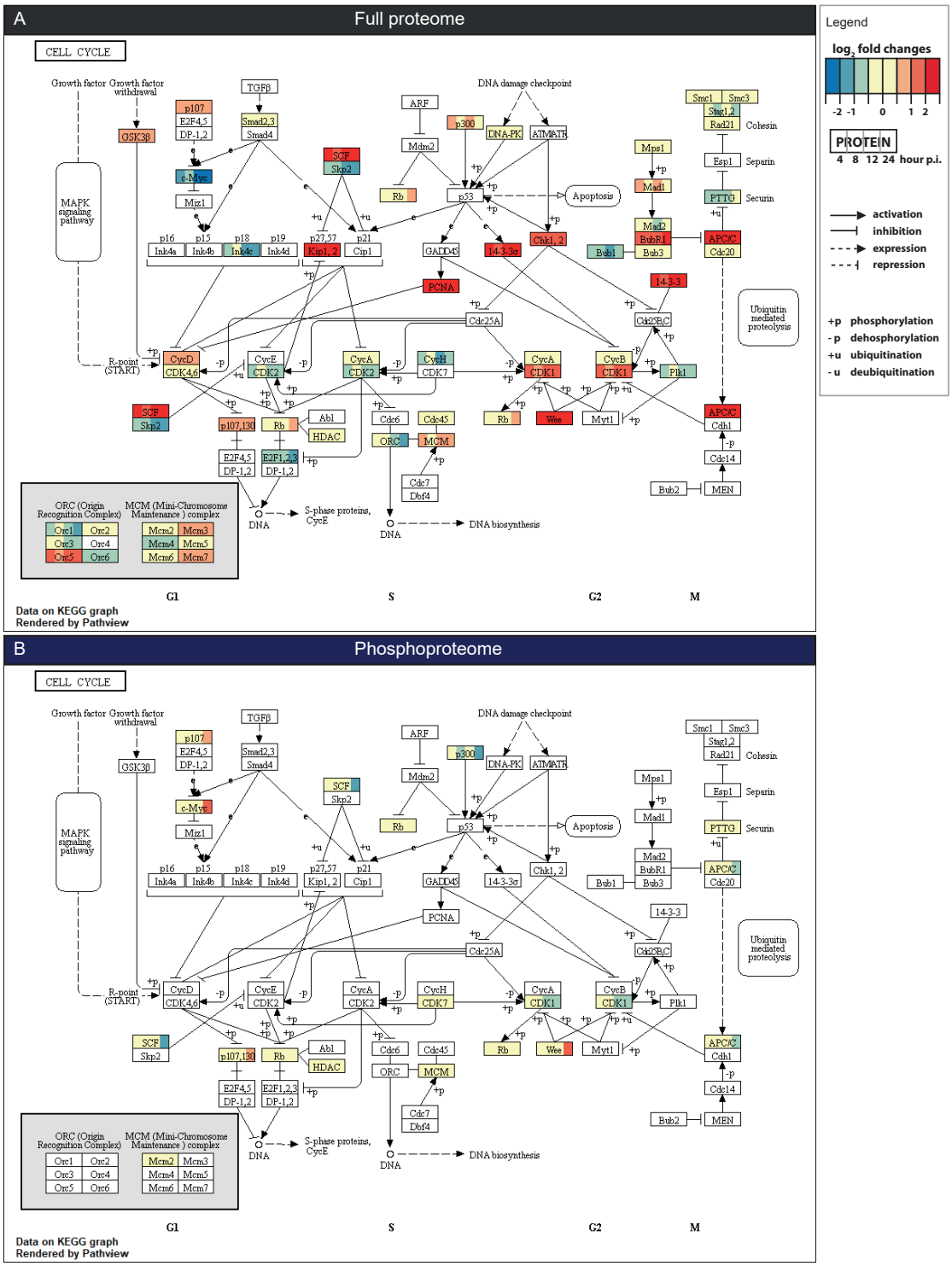

Figure 3.9. Temporal abundancies in the HIV-1-regulated full proteome/phosphoproteome in Jurkat-E6 cells mapped into KEGG pathway "Cell cycle". Proteins are shown as squared time bars ranging from 4 to 24 h color-coded according to the protein abundance relative to control as $\log_2$ fold changes. **(A)** Mapped protein and **(B)** phosphoprotein abundancies. Log_2 fold change of the respective phosphorylation site of highest intensity is represented in the case of multiple sites within the same protein.

The comprehensive KEGG pathway analysis of the cell cycle, glycolysis and RIG-I-like receptor signaling pathway exemplified, that many key proteins were (in-)activated by phosphorylation driven processes. Therefore, elucidation of HIV-1-associated kinase-substrate relationships would improve the understanding of these mechanisms.

3.4.4. Quantification of the HIV-1-associated kinase-substrate network

The time course analysis of the host full proteome exemplified by the cell cycle showed differentially increased or decreased expression of kinases and respective substrates. In order to identify further HIV-1-associated kinases, data from the time course analysis of the phosphoproteome was used in combination with the PhosphoSitePlus database (PSP) [238] to determine kinases, that target the differentially regulated sites. Site motif enrichment analysis (fig. 3.10A) identified early up-regulation (from 4 h) of substrates e.g. with casein kinase II, G protein-coupled receptor kinase 1 or 14-3-3 domain binding motifs. Substrates with e.g. PKA/PKC, GSK-3, ERK1, ERK2 and CDK5 motifs were found to be up-regulated from 12 h p.i. onwards. In the case of down-regulated sites, similar motifs to the up-regulated sites were found. However, the underlying proteins, to which the motifs belonged, were different from the proteins with up-regulated motifs.
Next, site-specific peptide sequences were used to identify respective kinases, that might not have been identified/quantified in the SILAC experiments, but are confirmed to phosphorylate respective sites according to the PSP database. 44 kinases were assigned to the quantified substrates (fig. 3.10B). 86.7% of them are described to to be linked with HIV-1 infection according to the NCBI HHID [36], while 13.3%, including *mitogen-activated protein kinase kinase kinase 8* (MAP3K8), *membrane-associated tyrosine- and threonine-specific cdc2-inhibitory kinase* (PKMYT1), *serine/threonine-protein kinase WNK2* (WNK2), *SRSF protein kinase 1* (SRPK1), *dual specificity protein kinase CLK1* (CLK1) and *dual specificity protein kinase CLK2*, have not been listed in the NCBI HHID yet. However, some substrates of the same kinase did not necessarily show similar differential regulation at the 4 h and 24 h time points. For example, sites of SRSF3 and PEA15 are targeted by AKT1 and both sites were up-regulated from 4 h p.i. onwards. However at 24 h p.i., SRSF3 was down-regulated, whereas PEA15 showed increased up-regulation. Different from the examples so far, there were also interactions, in which substrates targeted by a certain kinase, showed similar regulation patterns. This is exemplified by CDK2 substrates NPM1, NUP98, STMN1 and LIG1, which were found to be up-regulated at 24 h p.i.. Another example of similar regulation patterns is CDK1 and its substrates MPLKIP, RANBP2, GAPVD1, which were down-regulated.
Unfortunately, analyzing an HIV-1-associated lysine acetyltransferase-substrate network analagously was not possible because of the low number of quantified acetylation sites and because of scarce annotation of acetylation sites in databases in general.

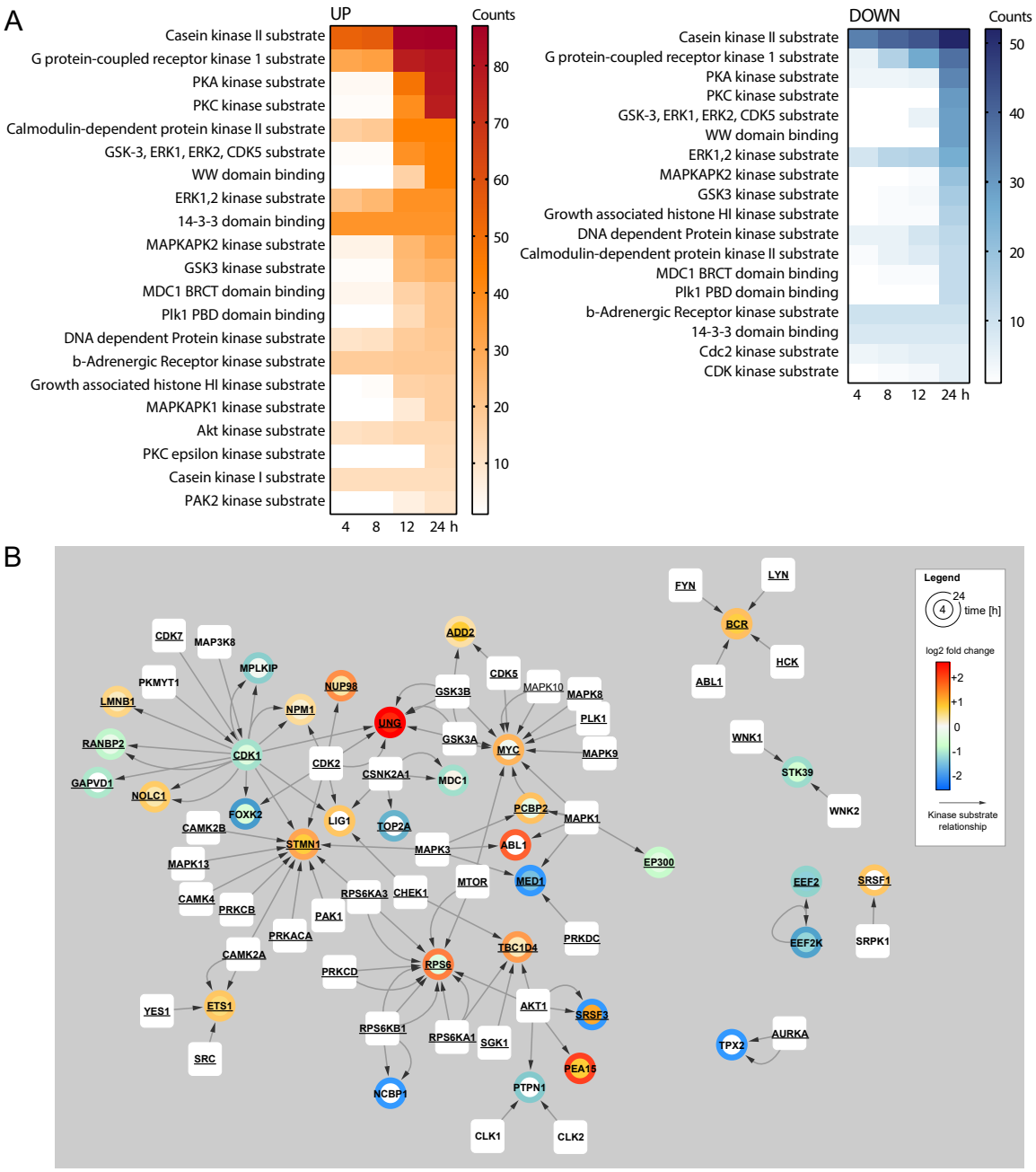

Figure 3.10. Analysis of differentially regulated phosphorylated proteins. **(A)** Heatmap of differentially regulated phosphorylation motifs **(B)** HIV-1-associated kinase-substrate network. Quantified phosphorylation sites of substrates (colored circles) were used to identify respective kinase (white squares) from the PhosphoSitePlus database. Names of proteins (HUGO gene nomenclature) already described in the HIV-1 context according the NCBI HHID [36] are underlined (see legend for node and edge definition).

3.4.5. Time resolved HIV-1 proteomics using different virus lab strains

For the HIV-1 time course analysis in HIV-1_{NL4-3}-infected Jurkat-E6 cells (see section 3.4.1), the percentage of p24-positive cells was used to monitor ongoing HIV-1 replication by flow cytometry (fig. 3.5B). However, it was not possible to distinguish cells, in which the infection resulted in productive HIV-1 replication by intracellular p24 staining. In contrast to HIV-1_{NL4-3}, GFP reporter viruses facilitates detection of productive HIV-1 replication, since GFP is expressed under the control of the LTR promoter together with the HIV-1 genes. Therefore, an additional time course experiment using HIV-$1_{NL4-3-\Delta Nef-GFP}$-infected Jurkat-E6 cells was performed analogous to the TMT-based time course experiment using HIV-1_{NL4-3}-infected cells for comparison (for the experimental design, please see section 3.4.1 and fig. 3.5A). Different from the HIV-1_{NL4-3}-time course, cells were infected for 48 h instead of 24 h to allow sufficient time for GFP expression and the cells were harvested after the time points 6, 12, 24 and 48 h p.i.. Using HIV-$1_{NL4-3-\Delta Nef-GFP}$ for spin-infection of Jurkat-E6 cells as described in section 3.2, 67% GFP-positive cells were determined by flow cytometry after 48 h (fig. 3.4D). The TMT-based LC-MS/MS analysis resulted in 3929 identified proteins, oh which 3833 proteins (97.6%) were quantified through all time points with a comparable range as for the prior HIV-1_{NL4-3}-time course experiment. Of these proteins, 2579 (48% overlap) were also identified in both time courses (fig. 3.11A).

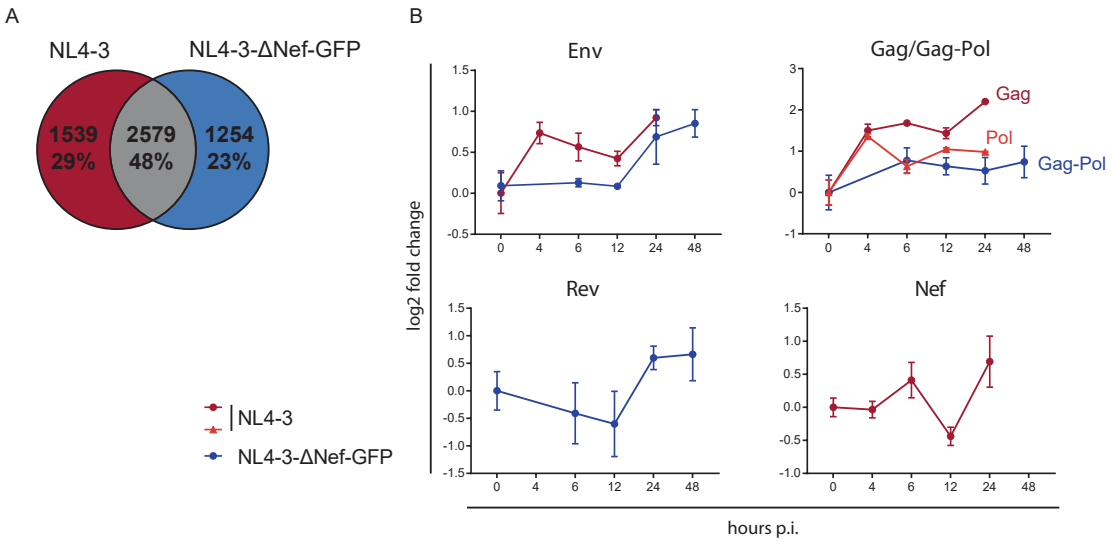

Figure 3.11. Time resolved proteomics using two different HIV-1 lab strains. (A) Comparison of the number of identified proteins of the two independent HIV-1 time course experiments by LC-MS/MS. In the first experiment, Jurkat-E6 cells were infected with HIV-1_{NL4-3} for 24 h. In the second experiment, Jurkat-E6 cells were infected with HIV-$1_{NL4-3-\Delta Nef-GFP}$ for 48 h. Number of proteins, that were identified in both data sets, are shown in the intersect (grey). **(B)** Abundancies of HIV-1 proteins (Uniprot gene names are indicated) over time. Fold changes are relative to the control (0 h). For the time course with HIV-1_{NL4-3}, Gag and Pol were identified independently, whereas the Gag-Pol precursor was identified in the time course with HIV-$1_{NL4-3-\Delta Nef-GFP}$ only. Error bars show standard deviation of two independent measurements.

In both time course experiments, HIV-1 proteins Env and Gag/Pol/Gag-Pol were quantified and showed comparable temporal progressions (fig. 3.11B). The analysis for enriched KEGG pathways (as described in section 3.4.2) also resulted in similar KEGG terms including "cell cycle" as illustrated in fig. 3.12). As exemplified for the KEGG pathway "cell cycle", the dynamic range in the HIV-$1_{NL4\text{-}3}$-time course (fig. 3.12A) was larger than in the HIV-$1_{NL4\text{-}3\text{-}\Delta Nef\text{-}GFP}$-time course (fig. 3.12B). However, the general trend of down- and up-regulated proteins, that are associated with "G1/S-" and "G2/M-transition" respectively, was consistent in both time-courses.

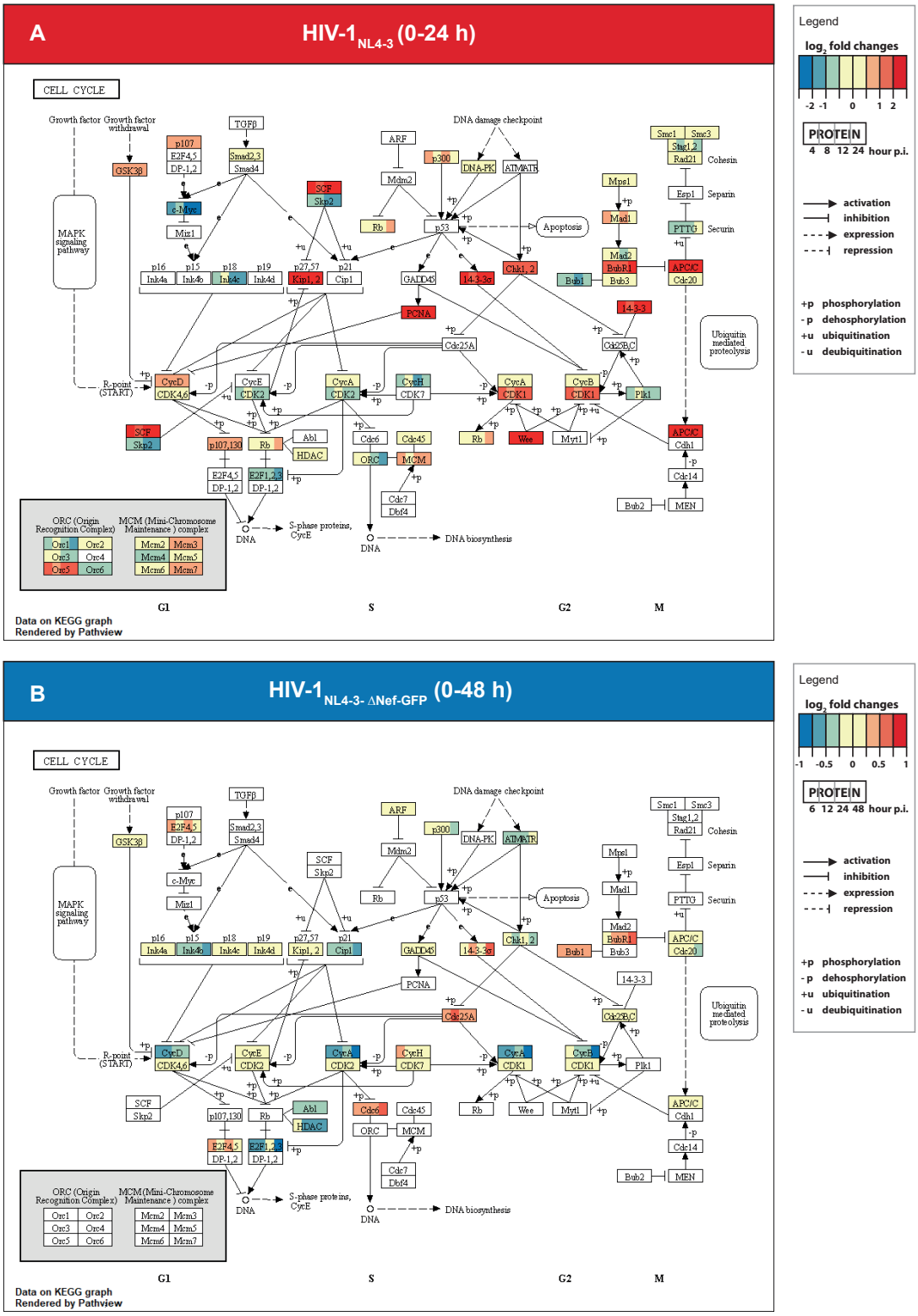

Figure 3.12. Temporal abundancies in the HIV-1-regulated full proteome in Jurkat-E6 cells mapped into KEGG pathway "Cell cycle". Proteins are shown as squared time bars color-coded according to the protein abundance relative to control as $\log_2$ fold change. **(A)** Time resolved data (4, 8, 12, 24 h p.i.) from the infection experiment with HIV-1_{NL4-3}. **(B)** Time resolved data (6, 12, 24, 48 h p.i.) from the infection experiment with HIV-$1_{NL4-3-\Delta Nef-GFP}$.

3.5. Quantification of the HIV-1-associated acetylome

The time resolved full proteome and phosphoproteome analysis of HIV-1_{NL4-3}-infected $CD4^+$ T-cells was used to investigate regulated signaling pathways, which could not be performed in a reasonable manner for the time resolved acetylome due to the unexpected low numbers of determined time courses of acetylated sites (fig.3.5C and fig. 3.7D). Based on the previous time resolved proteomic study in HIV-1_{NL4-3}-infected $CD4^+$ T-cells, it was assumed, that 24 h were not sufficient to observe large changes in the host acetylome, which might be related to a low amount of replication-active virus in these experiments. Therefore, SILAC-heavy-labeled Jurkat-E6 cells were spininfected with HIV-1HIV-$1_{NL4-3-\Delta Nef-GFP}$ (MOI≈1.1) and harvested after 48 h. SILAC-light-labeled and uninfected Jurkat-E6 cells served as control. Infected and control cells were harvested, lysed and combined in an 1:1 ratio for quantification. After tryptic digest, acetylated peptides were enriched by affinity-purification. Purified samples were measured in duplicates by LC-MS/MS. Subsequently. MS raw data were processed and analyzed as described in the workflow of section 3.6.

In total, 547 acetylated sites (belonging to 330 proteins) were quantified. Of these, 20 sites were found to be up-regulated ($\log_2$ fold change$\geq$SD, standard deviation SD=0.6) and 53 sites were found to be down-regulated ($\log_2$ fold change$\leq$-SD). Of the regulated proteins (total: 65), 48% have been associated with HIV-1 infection according to the NCBI HHID [36]. A large number of these regulated proteins/sites were clustered in functional protein-protein networks as identified by the STRING database [239] (fig. 3.13). GO and pathway enrichment analysis resulted in proteins, that were associated with "cytoskeleton dynamics" (GOBP, FDR: 0.0044), "glycolysis (KEGG, FDR: 0.0024), "ribosomes" (KEGG, FDR: 0.0024), "RNA processing" (KEGG, FDR: 0.0021), "viral genome integration into host DNA" (GOBP, FDR: 0.0044), "histones" (KEGG, FDR: 1.18e-9) as well as proteins with "positive regulation of transcription by RNA polymerase II" (GOBP, FDR: 0.0120). In the most clusters, down-regulation of respective lysine-acetylation was predominant, as exemplified for the cluster of "histones" or "glycolysis".

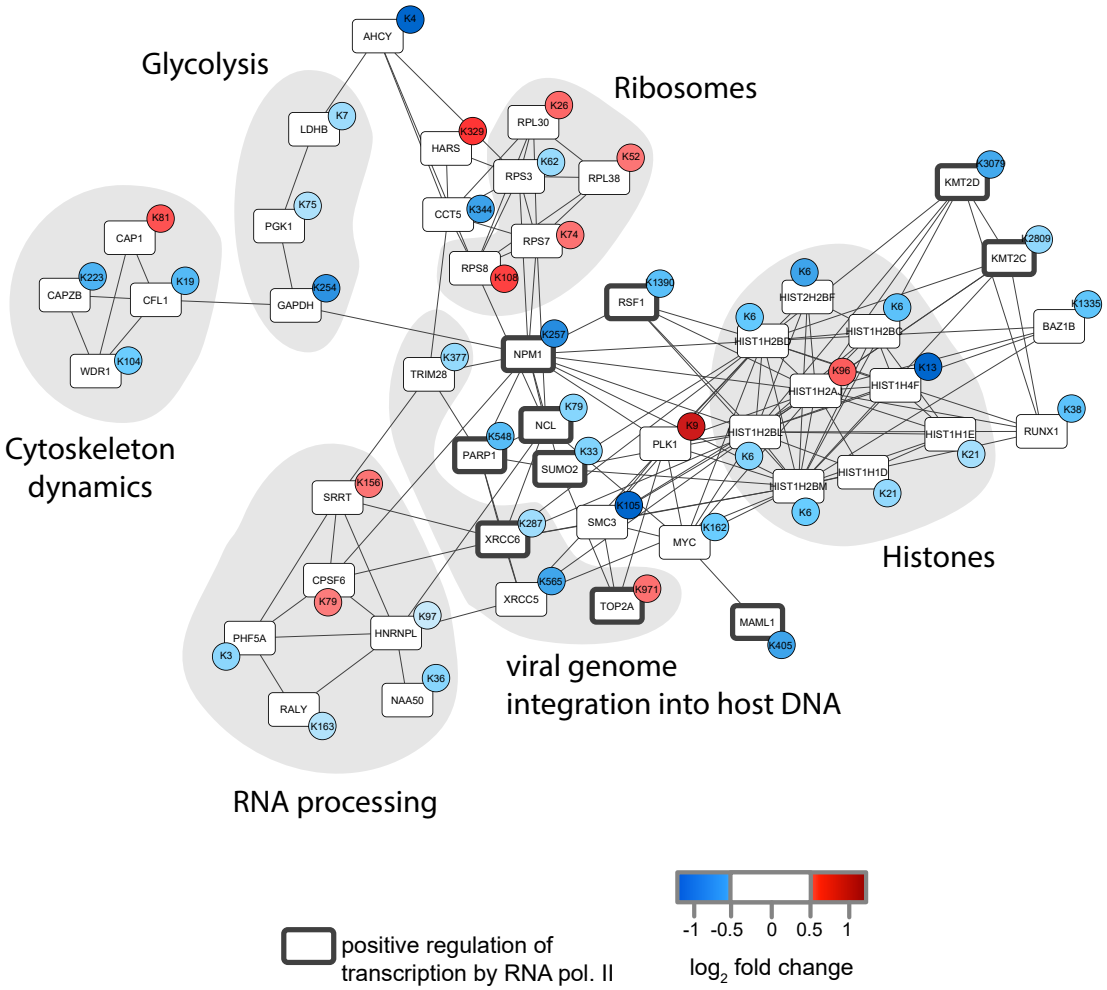

Figure 3.13. Quantification of the HIV-1-associated acetylome in Jurkat-E6 cells. Protein-protein interaction network analysis was performed using the STRING database [239] and network visualization was performed using Cytoscape [240]. Proteins with regulated acetylation sites upon HIV-1 infection (48 h) were displayed as white boxes. Acetylation sites were shown as circles. Log_2 fold changes were calculated from SILAC ratios (infected/uninfected), that were derived from two independent LC-MS/MS measurements. Clusters of certain KEGG pathways or GO biological processes are emphasized in grey areas. Proteins with positive regulation of transcription by RNA polymerase II are marked with thick borders. Orphan proteins were excluded.

3.6. MS data analysis workflow for quantitative studies of cellular signaling pathways

For the analysis/interpretation of quantitative MS data and to investigate infection-associated cellular signaling pathways, a downstream data analysis workflow was established. The open-source R environment was used to script the data analysis algorithm for processing MaxQuant output tables (evidence and PTM sites). An overview of the modular structure of the algorithm is illustrated in fig. 3.14.

The developed algorithm requires the evidence table, which combines the information of all identified/quantified peptides resulting from label-free, SILAC or TMT experiments. For the analysis of PTMs, the evidence table is complemented with respective site specific information from the PTM sites table (e.g. site position within the protein, localization probality), which results in the EvidSites table. Evidence table and EvidSites table, respectively, are subjected to downstream analysis using the Proteus R package [221]. Proteus provides functions to aggregate peptide intensities for identical peptide sequences and to aggegrate peptides to proteins. Moreover, Proteus includes tools for MS data quality control, differential expression analysis as well as interactive data exploration and visualization. Proteus output files were subsequently formatted and assigned with identifiers of different data base resources (e.g. Uniprot, Ensembl, KEGG, Entrez Gene) to fit the requirements for GO term or KEGG pathway enrichment analysis.

For the automated processing of biological term classification and enrichment analysis of protein clusters, the ClusterProfiler R package [223] was implemented. ClusterProfiler provides statistical analysis tools and annotation functions based on data and signaling maps from the Gene Ontology [241] and the KEGG resource [242]. Using the information from ClusterProfiler, signaling pathways of particular interest were selected for a more detailed analysis by mapping quantified proteins into signaling pathways. This was realized by implementing the Pathview R package [224] into the workflow, which provides tools for KEGG pathways-based data integration and rendering of experimental data on pathways graphs. In order to integrate quantified PTM site information into KEGG pathways, the "PTM status" of a protein needed to be defined. In the case of proteins aggregated from more than one modified peptide sequence (either multiple PTM sites on the same peptide or multiple modified peptides of the same protein), the "PTM status" of a protein was estimated either by the modified peptide with the highest intensity or by the median intensity of all assigned PTM sites. Alternatively, PTM sites with known biological function can be directly chosen for rendering into the pathway maps. The performance of MS data analysis using the developed workflow was tested in comparison with the analysis in Perseus, which is a commonly used computational platform for MS data [214,215]. Key performance indicators (e.g. number of identified unique peptides, number of differentially expressed proteins/PTM sites) could be exactly reproduced in Perseus (data not shown). The respective R script is

sourced and available on the servers of the Max von Pettenkofer Institute (Dept. of Virology).

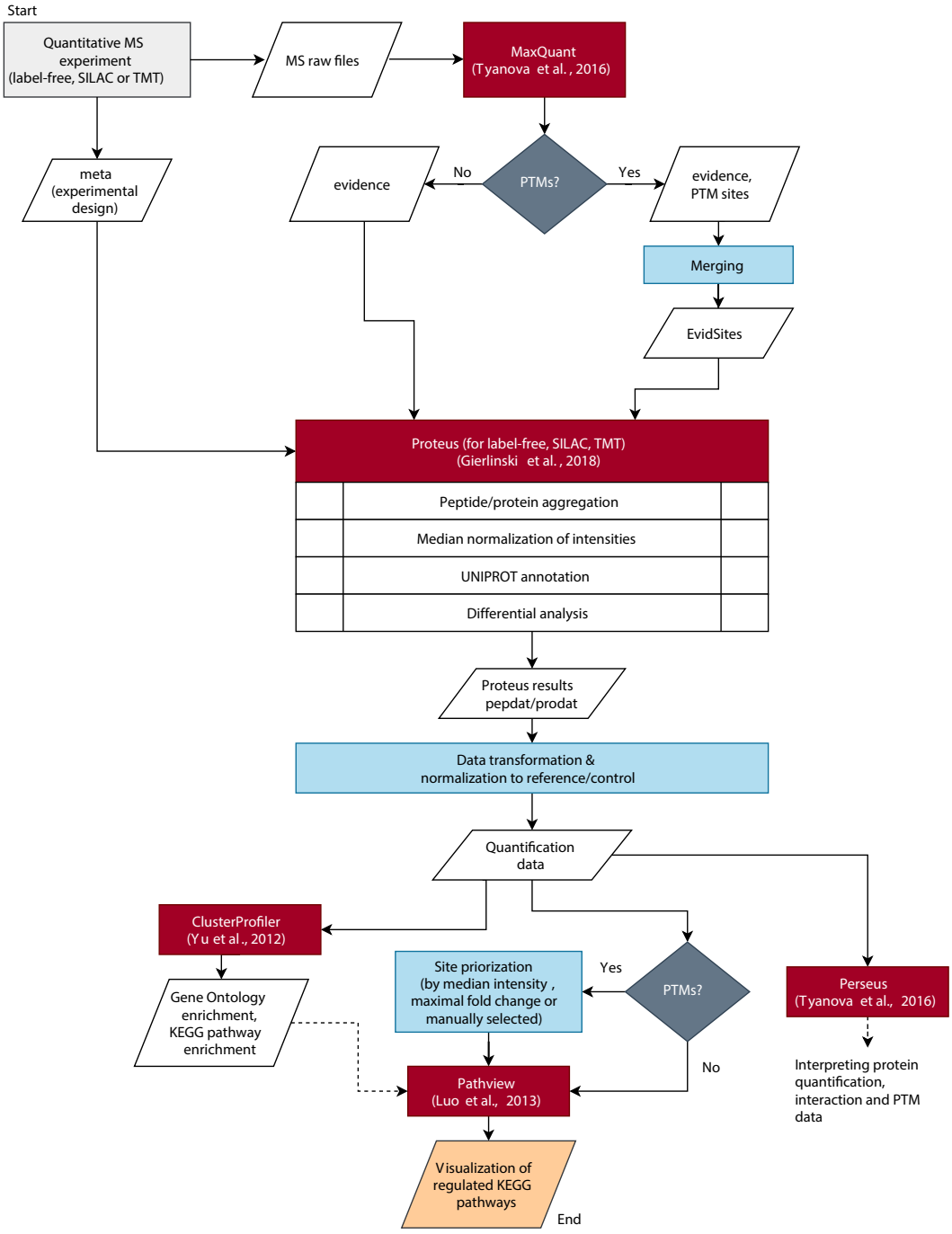

Figure 3.14. Flowchart of the data processing and analysis workflow for quantitative proteomic data. A data analysis workflow coded in the R environment was developed for efficient processing and interpreting of quantitative MS data from label-free, SILAC or TMT experiments. MaxQuant output files were used for downstream analysis using the Proteus R package. Resulting peptide/proteins data (pepdat/prodat) resulting from the Proteus analysis were normalized and transformed into a ClusterProfiler or Pathview compatible format for GO term enrichment analysis or for visualization of quantitative mapping of the data into KEGG pathways. Alternatively, pepdat/prodat were further processed in Perseus.

3.7. Study of the Tat regulated aspects of HIV-1 infection

3.7.1. Design of Tat expression plasmids and establishment of stable cell lines for interactome and acetylome studies

Design and cloning of HA-tagged Tat

As shown in the analysis of time resolved proteomics in HIV-1-infected Jurkat-E6 cells, numerous host proteins and PTM sites are regulated in a highly complex manner. Various cellular pathways are modulated upon the presence of HIV-1 proteins. Moreover, it has been shown, that the nuclear acetylome is subjected to large changes upon HIV-1 infection, which are facilitated by multiple interactions between HIV-1 proteins and host KATs, KDACs/sirtuins and bromodomain containing proteins [75, 243]. Notably, the viral encoded Tat, which is essential for the regulation of HIV-1 LTR transactivation, latency and apoptosis is involved with the majority of these interactions [40, 136, 137, 156–158]. In this context, Tat has been identified in HIV-1-host interactions with 42% of KATs, 22% of KDACs/sirtuins and 30% of bromodomain containing proteins in the human proteome [243, 244]. These interactions with the host acetylation machinery emphasizes the close connection of Tat's transactivation activity with lysine acetylation and Tat's role in shaping the host acetylome during HIV-1 replication. As an example, KATs that are recruited by Tat to the 5'-LTR to enhance transcription are PCAF, EP300 and GCN5 [147, 148, 154, 245, 246]. However, little is known about Tat regulated changes in the acetylome and the associated consequences for transcription and cellular signaling.

In order to identify potential proteins, that have not been linked to Tat function and HIV-1 infection so far, several Tat mutants were cloned simulating either an acetylated (K-to-Q) or non-acetylated state (K-to-R) by specific lysine substitutions [247] (fig. 3.15B).

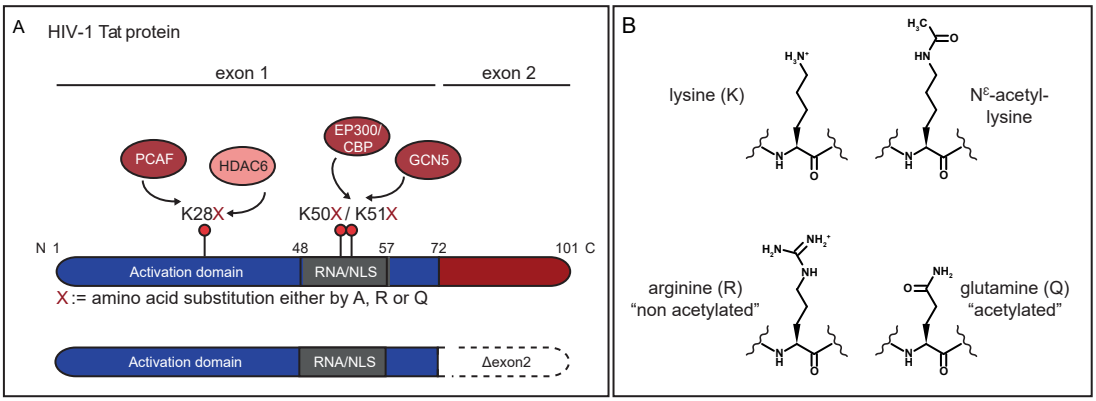

Figure 3.15. Lysine acetylation sites within HIV-1 Tat. (A) Schematic illustration of lysine acetylation sites within Tat targeted by several lysine acetyltransferases (dark red) and deacetylases (light red). **(B)** Mimicking lysine acetylation by substitution of lysine by arginine (R) or glutamine (Q) [247].

K-to-A substitution were also performed to simulate the absence of the entire lysine residue. Lysine acetylation sites (K28, K50, K51) were chosen based on known lysine acetyltransferases and deacetylases (PCAF [245], HDAC6 [153], EP300 [245, 246] or GCN5 [154]) targeting respective sites (fig. 3.15A).

Moreover, it has been shown, that the first exon of 72 amino acids is sufficient for transactivation of the HIV LTR [248]. The contribution of the second exon to HIV-1 replication is poorly understood. Therefore, an additional Tat mutant was cloned by deletion of the second exon (Δexon2) in order to study its interplay with host factors.

All Tat expression constructs were designed with a C-terminal HA-tag for simplified immunoprecipitation and immunoblotting (fig. 3.16A). In total, a set of 14 mutants was generated from pcDNA3.Tat-HA by site-directed mutagenesis (fig. 3.16B). The Neomycin-Geneticin expression cassette (NeoR) within the pTat-HA plasmid allowed generation of stable cell lines by culturing in selective media. Transient overexpression of Tat with lysine substitutions after chemical transfection was successful in different cell lines e.g. HEK293T (fig. 3.16B), HeLa, HCT116 or TZM-bl. Notably, the expression levels of Δexon2 mutant were remarkably lower than in the other variants expressing full length Tat (exemplified in fig. 3.16B).

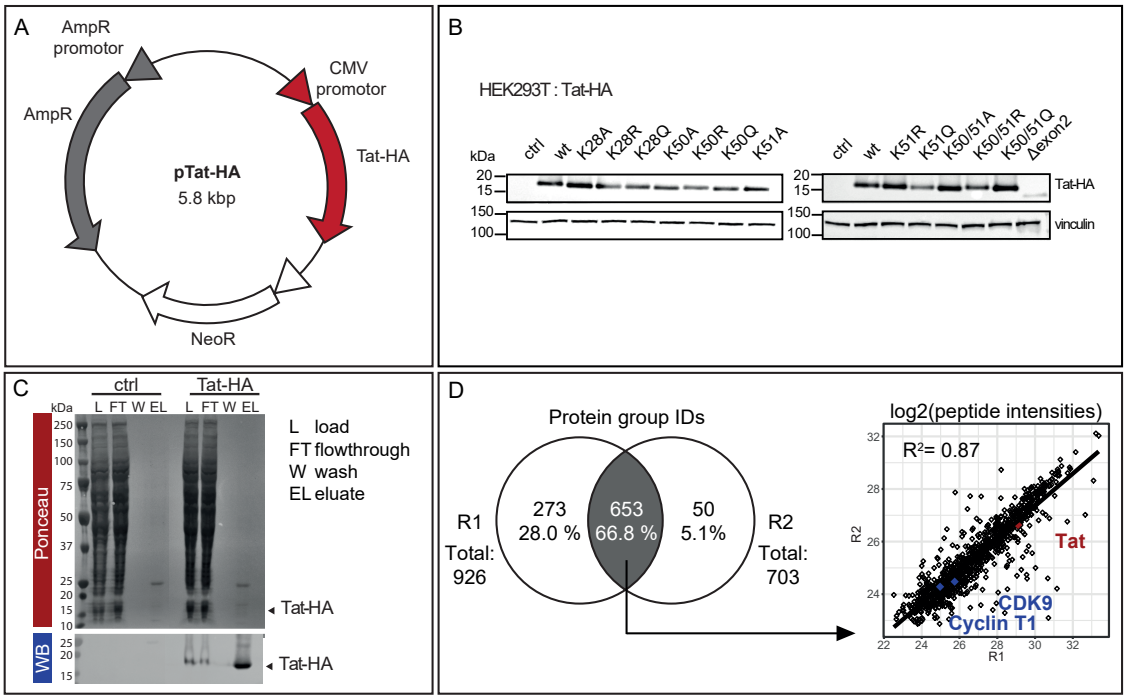

Figure 3.16. Cloning of HA-tagged Tat. (A) Schematic structure of the Tat-HA expression construct. **(B)** Immunoblots of transfected HEK293T cells (48 h p.t.) using the set of pTat-HA constructs. **(C)** Quality check of the co-immunoprecipitation (Co-IP) using magnetic anti-HA beads in HEK293T cell lysate by Ponceau staining and immunoblot. **(D)** Overlap of identified protein groups by LC-MS/MS after Co-IP for Tat-protein complexes in HEK293T cells and comparison of peptide intensities between two replicates (R1, R2).

Co-immunoprecipitation for Tat interacting proteins using anti-HA magnetic beads

Lysates from Tat-HA-transfected HEK293T cells (48 h post transfection) were used to test co-immunoprecipitation (Co-IP) of Tat-host protein complexes using anti-HA magnetic beads. To test for specificity, full lysate, Co-IP flowthrough, wash and eluate were processed for SDS-PAGE and immunoblotting. Ponceau staining showed efficient depletion of unbound proteins (fig. 3.16C, lane W and EL). Successful enrichment and elution of HA-tagged Tat protein were confirmed by immunoblotting using primary anti-HA antibodies (fig. 3.16C, lane EL). LC-MS/MS analysis of Co-IP eluates in two replicates resulted in 653 identified Tat interacting proteins with comparable MS intensities in each run (fig. 3.16D). Among the set of Tat interacting proteins, components of human transcription elongation factor P-TEFb such as Cyclin T1 and CDK9 (according to the CORUM database [249]) were also observed.

Establishment of stable T-cell line expressing Tat-HA by lentiviral transduction

In contrast to HEK293T, HeLa or TZM-bl cells, chemical transfection in T-cell lines such as Jurkat-E6 cells is less efficient making the establisment of a stable T-cell line more difficult. Chemical transfection of Tat-HA into Jurkat-E6 and SupT1 cells using Lipofectamine® 2000 or PEI was not successful (data not shown). Nucleofection (Lonza) showed also extremely low efficiency of transfection (data not shown). Therefore, the set of pTat-HA constructs was re-cloned into a vector flanked by 5'- and 3'-LTRs allowing lentiviral transduction (fig. 3.17A) into Jurkat-E6 cells. Additionally, another construct with Tat-HA replaced by a mock gene (luciferase 2; luc2) was generated to obtain a control for later Tat interaction studies. In the new set, Tat was flanked C-terminally by BFP being cleaved upon expression via an internal T2A site. Lentiviral particles were produced and used to transduce Jurkat-E6 cells under optimized conditions in terms of titer of concentrated virus and spin-inoculation (exemplified for Tat wt in fig. 3.18A). Flow cytometric measurement of BFP (72 h p.i.) was used to identify successfully transduced Jurkat-E6 cells (fig. 3.18B). The average transduction efficiency of 98.6% was achieved for all cloned constructs. Expression of Tat-HA in Jurkat-E6 cells was confirmed by immunoblotting (fig. 3.17B). Very similar to the transient Tat-HA expression in transfected cells, low expression levels of the Δexon2 mutant were observed in transduced Jurkat-E6 cells. Interestingly, the mean fluorescent intensity (MFI) of BFP, which is coded downstream of TAT(Δexon2)-HA showed comparable levels to the full length Tat variants (fig. 3.18B).

In order to prevent the outgrowth of the Tat-HA-T2A-BFP-negative population over time and to obtain a pure population, transduced Jurkat-E6 cells were sorted for BFP-positive cells[a]. After sorting, a population of 99.9% BFP-positive cells was obtained for every construct. BFP and Tat-HA expression was stable over time as confirmed by flow cytometry

[a] Cell sorting was performed on a BD FACSAriaFusion by Dr. Lisa Richter, technical manager of the core facility Flow Cytometry Biomedical Center Munich, Ludwig Maximilians University of Munich

or immunoblot analysis, respectively. 14 days after transduction, stable cell lines were tested for residual lentiviral particles in a p24 ELISA (supplemental fig. S6). The clearance measurement showed no residual virus-associated HIV-1 core protein p24. Consequently, generated Tat-HA-T2A-BFP expressing stable cells were transferred to biosafetly level 1 conditions.

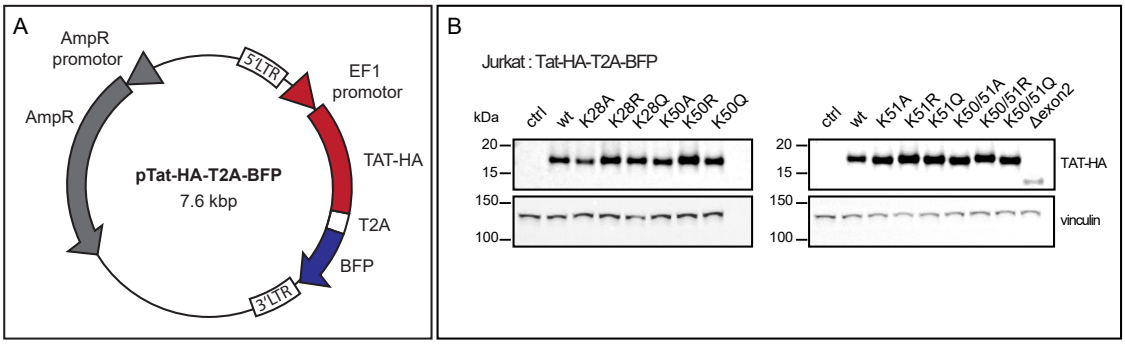

Figure 3.17. Cloning of HA-tagged Tat for lentiviral transduction. **(A)** Schematic structure of the Tat-HA-T2A-BFP expression construct. **(B)** Immunoblots of transduced Jurkat-E6 cells (72 h p.i.) using the set of pTat-HA-T2A-BFP constructs.

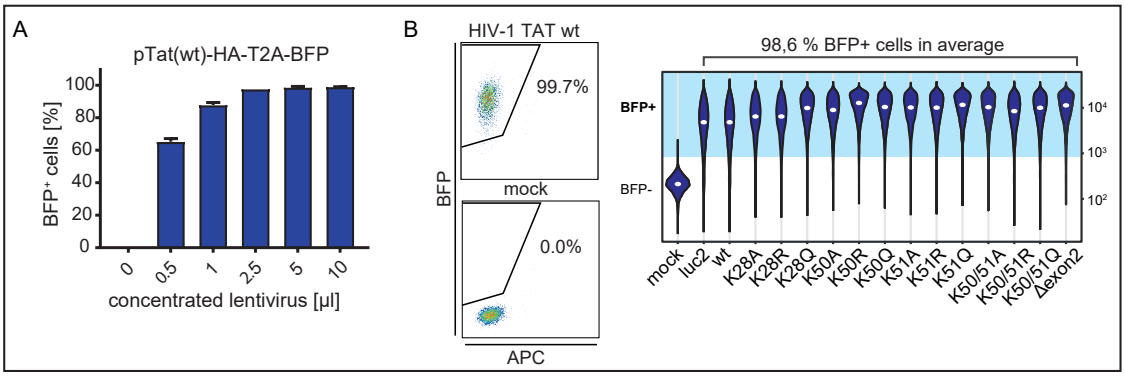

Figure 3.18. Establishment of stable Tat-HA-T2A-BFP expressing Jurkat-E6 cells by lentiviral transduction. **(A)** Titration of concentrated lentiviral particles for the transduction of Tat-HA-T2A-BFP into Jurkat-E6 cells. Flow cytometric measurement of BFP-positive cells was conducted 72 h p.i. Error bars show standard deviation of two independent measurements. **(B)** Flow cytometric measurement of BFP-positive Jurkats after transduction with the Tat-HA-T2A-BFP set (72 h p.i.).

3.7.2. Analysis of mutant function for HIV-1 LTR transactivation

Transactivation of HIV-1 LTR in TZM-bl and reactivation of J-Lats

As described in section 3.7.1, different Tat mutants were cloned simulating either an acetylated (K-to-Q) or non-acetylated state (K-to-R). Moreover, an additional mutant with exon 2 deletion was included. In the following, Tat wt and mutants were tested in different assays to investigate their efficiency in HIV-1 LTR transactivation. The HIV-1 reporter cell line TZM-bl expresses luciferase under the control of a HIV-1 LTR [250–254] and thus, was

used to analyze transactivation by Tat wt and mutants. For this purpose, two different experiments were performed: On the one hand, TZM-bls were transiently transfected with the pTat-HA set. Tat-HA expression was confirmed by immunoblot 48 h post transfection. On the other hand, TZM-bls were infected using lentiviral supernatant for transduction using the pTat-HA-T2A-BFP set. In this case, percentage of BFP-positive TZM-bls as measure for successful transduction was used for normalization of luciferase induction. Tat-HA-T2A-BFP expression was also confirmed by immunoblotting 48 h post transduction. Tat mutants showed similar luciferase fold induction tendencies in both experiments (fig. 3.19A). In contrast to the mock transfection or mock transduction, all Tat mutant were able to induce luciferase expression, however, to a varying extent. K50R, K51R, K50/51R showed comparable or even higher fold induction as the Tat wt. In the case of K28R, K50A, K50Q, K51A, and Δexon2, 53% of the transactivation efficiency was achieved in average in comparison to Tat wt. Mutants with almost lost transactivation ability were K28A (22%) and K28Q (9%) as well as the double mutants K50/51A (11%) and K50/51Q (13%). Noticeably, K-to-A substitutions showed similar low fold induction to their respective K-to-Q substitutions.

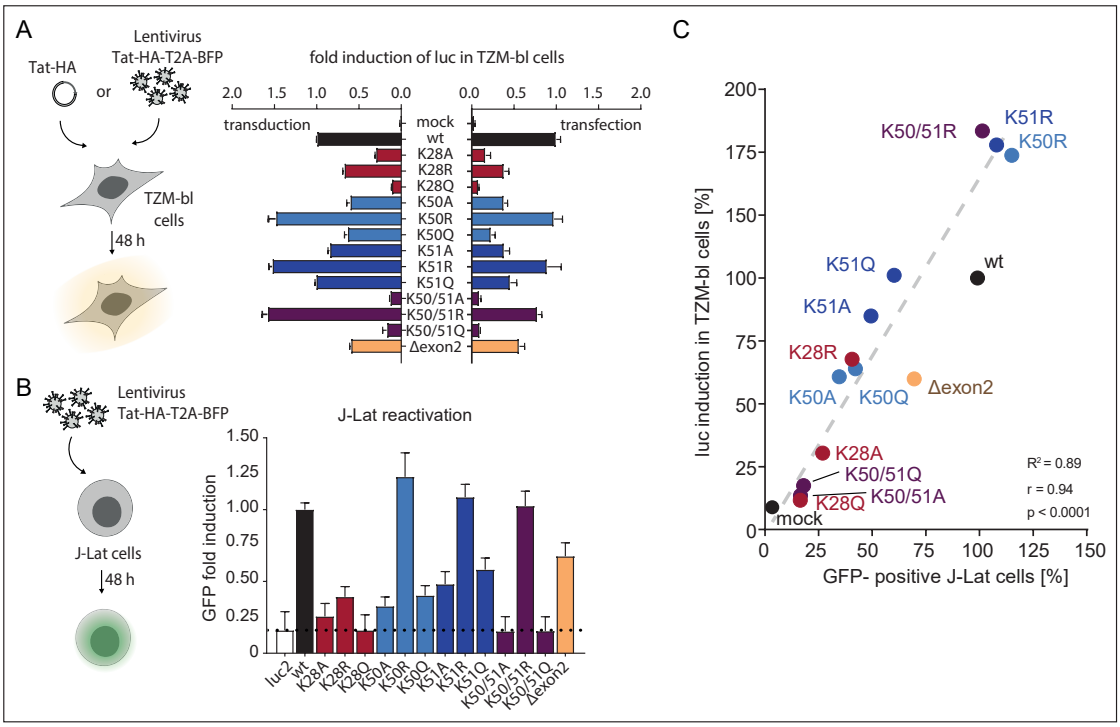

Figure 3.19. HIV-1 LTR transactivation in TZM-bl and J-Lat cells. **(A)** Luciferase transactivation assay in Tat-HA transfected or Tat-HA-T2A-BFP transduced TZM-bl cells. BFP expression was used for normalization in the transduction experiment. **(B)** Latency reversal in J-Lat cells by lentiviral transduction of pTat-HA-T2A-BFP quantified by GFP signal using flow cytometry. BFP expression was used for normalization. Error bars show standard deviation of two independent measurements. **(C)** Crosscorrelation analysis of luciferase transactivation assay in transduced TZM-bl cells with reactivation assay in transduced J-Lat cells. R^2 displays goodness of fit. Pearson correlation coefficient r and p value (slope significantly different from zero) are indicated.

To conduct an analogous transactivation experiment as in TZM-bl cells but in a system closer to the HIV-1 infection context, J-Lat cells were used. This T-cell line contains a near full length integrated HIV-1 genome (Δ*env* and *nef*-defective HIV R7), that expresses GFP upon LTR-activation and is commonly used for latency studies [168]. Here, J-Lat cells were transduced using the pTat-HA-T2A-BFP set (fig. 3.19B). 48 h later, BFP expression was used to normalize GFP signal to the number of successfully transduced cells. Lentiviral transduction of a mock protein (here: luciferase luc2) was used as control and to define the background signal, that is unspecific for Tat. In analogy to the transactivation assay in TZM-bl cells, Tat-dependent LTR activation and subsequent GFP expression were not or barely observed for K28A, K28Q, K50/51A and K50/51Q (fig. 3.19B) whereas K50R, K51R and K50/51R showed comparable or even higher transactivation efficiency as Tat wt. Overall, GFP fold induction in transduced J-Lat cells corresponded to the luciferase induction in transduced TZM-bl cells for Tat wt and the respective mutants (fig. 3.19C).

Effect on HIV-1 infection in Jurkat-E6 cells

Lentiviral transduction of Tat mutants into J-Lat cells showed differential ability to reverse latency (fig. 3.19B). In order to investigate the effect of Tat mutants on the course of HIV-1 infection, stable Tat overexpressing Jurkat-E6 cells were used for spin-infection with HIV-$1_{NL4\text{-}3\text{-}IRES\text{-}GFP}$ (MOI≈1). The experiment was designed under the assumption, that the copy number of Tat overexpressed in Jurkat-E6 cells overpowers the copy numbers of expressed Tat from the integrated HIV-$1_{NL4\text{-}3\text{-}IRES\text{-}GFP}$. After 24 h, GFP expression was measured by flow cytometry (fig. 3.20A).

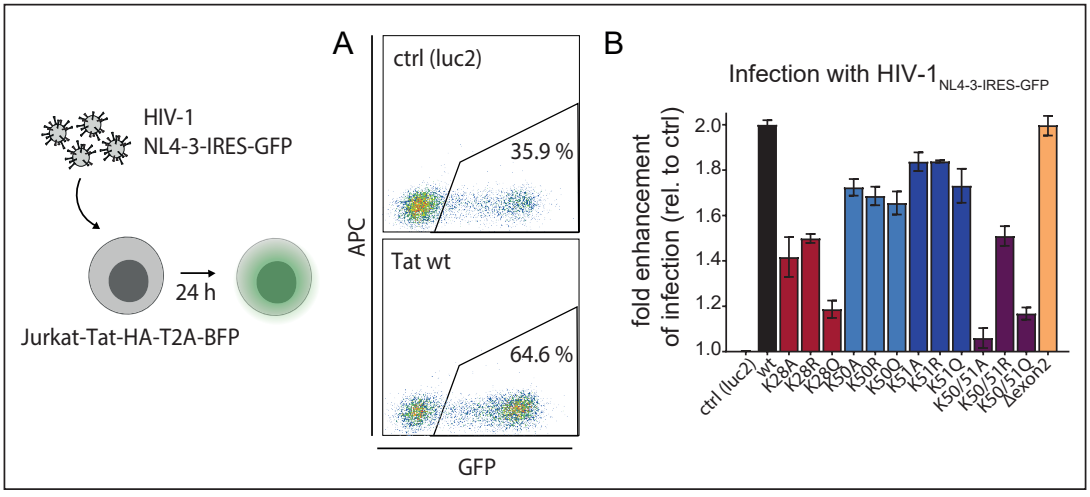

Figure 3.20. Effect of mutated Tat on the course of HIV-$1_{NL4\text{-}3\text{-}IRES\text{-}GFP}$ infection in Jurkat-E6 cells. **(A)** Flow cytometric analysis of infection measured by GFP expression (24 h p.i.) in control (luc2) or in Tat overexpressing Jurkat-E6 cells. **(B)** Fold enhancement of HIV-$1_{NL4\text{-}3\text{-}IRES\text{-}GFP}$ infection in stable Tat overexpressing Jurkat-E6 cells. Error bars show standard deviation of two independent measurements.

Thereby, luc2 overexpressing Jurkat-E6 cells served as control for effects caused by Tat expressed from HIV-$1_{NL4\text{-}3\text{-}IRES\text{-}GFP}$. Percentage of GFP-positive cells in the control condition (ca. 36% in average) was determined to define the signal caused by Tat expressed from HIV-$1_{NL4\text{-}3\text{-}IRES\text{-}GFP}$. Upon Tat wt overexpression, infection efficiency improved to 65% in average (1.9-fold compared to the control), which served as reference to compare with the mutants. For Δexon2, comparable infection levels as in the wt condition were achieved (fig. 3.20B). For most mutations including K28R, K50A, K50R, K50Q, K51A, K51R, K51Q and K50/51R, infection efficiency was improved to 54% in average (1.5-fold compared to control). On the other hand, enhancement of infection was marginal for K28Q, K50/51A and K50/51Q. Here, the infection levels (38% in average) were not considerably higher than in the control. Notably, K28Q, K50/51A and K50/51Q were also the mutants, which already showed strong impairment in transactivation analysis using TZM-bl and J-Lat cells as discussed in the section before (fig 3.19).

Influence of mutated HIV-1 Tat on virion production

The previous infection assay in Tat overexpressing Jurkat-E6 cells with HIV-$1_{NL4\text{-}3\text{-}IRES\text{-}GFP}$ showed differential influence on the course of infection for the Tat mutants. However, it was difficult to exclude the contribution by Tat proteins expressed from the integrated HIV-$1_{NL4\text{-}3\text{-}IRES\text{-}GFP}$ in this system. Consequently, Tat mutants (pTat-HA set) were tested in HEK293T cells co-transfected with pmTAT30 coding for a full length HIV-1 HXB2 ΔTat for their ability to induce virus production after 48 h. Virus containing supernatant was harvested to quantify virus-associated p24 by ELISA. A recombinant p24 standard (Cell Biolabs) was used to determine the amount of virus-associated p24 (fig. 3.21).

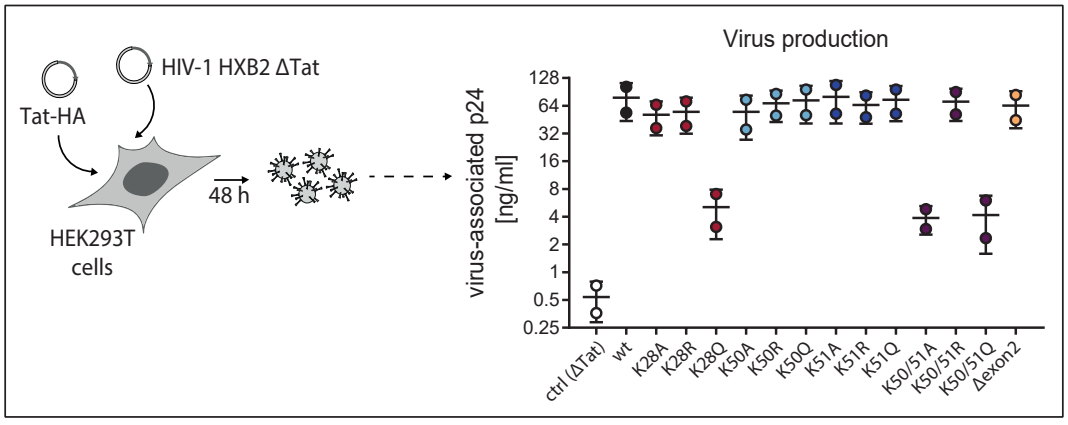

Figure 3.21. Influence of mutated HIV-1 Tat on virion production. Virus-associated p24 in supernatant after pTat-HA and HIV-1 HXB2 ΔTat co-transfection was quantified by ELISA.

Virus production in HEK293T cells co-transfected with pmTAT30 and pTat-HA wt was successful, since high amounts of virus-associated p24 (ca. 80 ng/mL) were measured. In the supernatant of control producer cells transfected with pmTAT30 only, the amount of virus-associated p24 was 160-fold lower. In the case of the mutants including K28A, K28R, K50R, K50A, K50R, K50Q, K51A, K51R, K51Q, K50/51R and Δexon2, 70 ng/mL of p24 was measured in average, which corresponds to 85% of the amount of the wt condition. In contrast, the determined p24 levels of 4 ng/mL in average for K28Q, K50/51A and K50/51Q were 20-fold lower than for the other Tat mutants.

Summary of Tat mutants and their effect on HIV-1 LTR transactivation

In order to test the functionality of the established Tat mutants in comparison with Tat wt, different experiments were conducted. Several aspects were investigated: (i) Binding of Tat to the LTR in transfected or transduced TZM-cells, (ii) ability to reverse latency in J-Lat cells, (iii) Tat's influence on the onset of infection in Jurkat-E6 cells, (iv) quality and quantity of virions produced in a rescued Tat deficient system (fig. 3.22). In total, striking differences from Tat wt were observed for single lysine substitutions at position 28 within the activation domain (fig. 3.22, red) and for double lysine substitutions at position 50 and 51 within the RNA binding domain/nuclear localization site (fig. 3.22, purple). For these position, severely impaired or loss of functionality were observed for K-to-Q substitutions. In contrary, K-to-R substitutions at these sites corresponded to the Tat wt conditions to a certain extend. Single lysine substitutions either at position 50 or 51 did not indicate an as strong impaired function as in the double lysine substitutions at position 50 and 51. Δexon2 was able to maintain at least 50% of its functionality. Based on these results, Tat Δexon2 as well as two pairs of acetylation mimickry (K28R and K28Q, K50/51R and K50/51Q) were selected for further analysis at interactome and acetylome level.

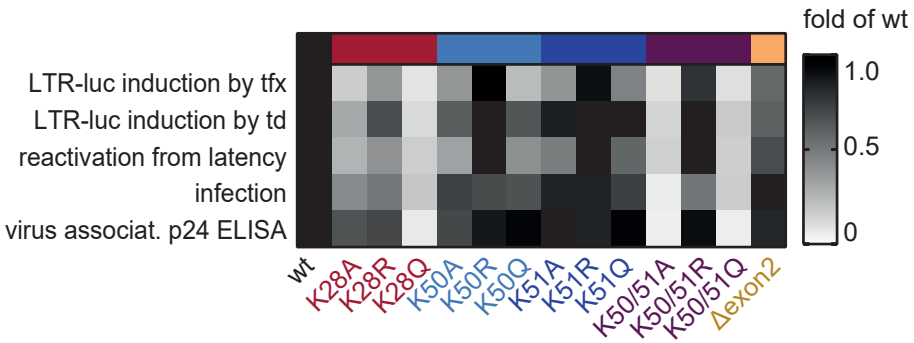

Figure 3.22. Heatmap summarizing differences of Tat wt from mutants in regard of LTR-luc induction, virus production, influence on the course of infection and latency reversal. Abbreviations: Transfection (tfx), transduction (td)

3.7.3. Analysis of the HIV-1 Tat interactome

The functionality analysis of HIV-1 Tat with mutations at K28 and K50/51 (fig. 3.22) showed, that K-to-Q substitution (mimicking an acetylated state) remarkely impaired Tat's transactivation ability in comparison to the respective K-to-R substitution (mimicking an non-acetylated state). To investigate the impact on Tat-host-interactions at protein level by the respective mutations, an MS-based interactome analysis was performed. Cell lysates were generated from Jurkat-Tat-HA-T2A-BFP cells, which stably express C-terminally HA-tagged Tat wt or the respective Tat mutant (see section 3.7.1). The HA-tagged Tat and magnetic anti-HA antibodies were utilized for co-immunoprecipiation (Co-IP) to enrich for Tat-interacting proteins. To identify unspecific binding, Co-IP was also performed on cell lysates from Jurkat cells, which stably express C-terminal HA-tagged luciferase (luc) as mock control. Enriched protein interactors were subjected to tryptic digest and peptide purification and were subsequently analyzed by LC-MS/MS. To obtain an dynamic view of the Tat interactome, label-free quantification of MS data derived from three independent measurements was performed (fig. 3.23A).
First, the specificity of the Co-IP was evaluated by identification of significantly enriched proteins in the control in comparison with the Tat expressing systems. For the evaluation of specificity, only proteins with at least two valid MS intensity values (in three independent measurements) were considered. As a result, 218 proteins were identified, of which 4 proteins (DIMT1, UBA52, RPL7A, RFX7) were significantly enriched in the control (two-sample t-test, FDR=0.05) defining the set of unspecific binders (fig.3.23B). These hits were not included for further analysis. In parallel, 17 proteins were found enriched in the the Tat expressing condition. The functional network analysis of these proteins identified a complex of ribosomal and RNA binding proteins and subunits of the P-TEFb complex or super elongation complex (SEC) (fig. 3.23C). Enriched proteins not assigned to certain complexes included histones (H3-5, H1-10), *splicing factor, proline- and glutamine-rich* (SFPQ), *FERM and PDZ domain-containing protein 4* (FRMPD4), *Fc receptor-like protein 3* (FCRL3) and *heterochromatin protein 1-binding protein 3* (HP1BP3). Approximately 65% of the proteins in this set have been linked to HIV-1 infection, while 29% have been associated with HIV-1 Tat according to the NCBI HHID [36]. For almost every mutant except for K50/51Q and Δexon2, enriched subunits of the P-TEFb complex or SEC were identified. Interestingly, P-TEFb or SEC subunits, which were identified but not enriched in the tested mutations comprised *protein ENL* (MLLT1), *protein AF-9* (MLLT3) and CDK9.

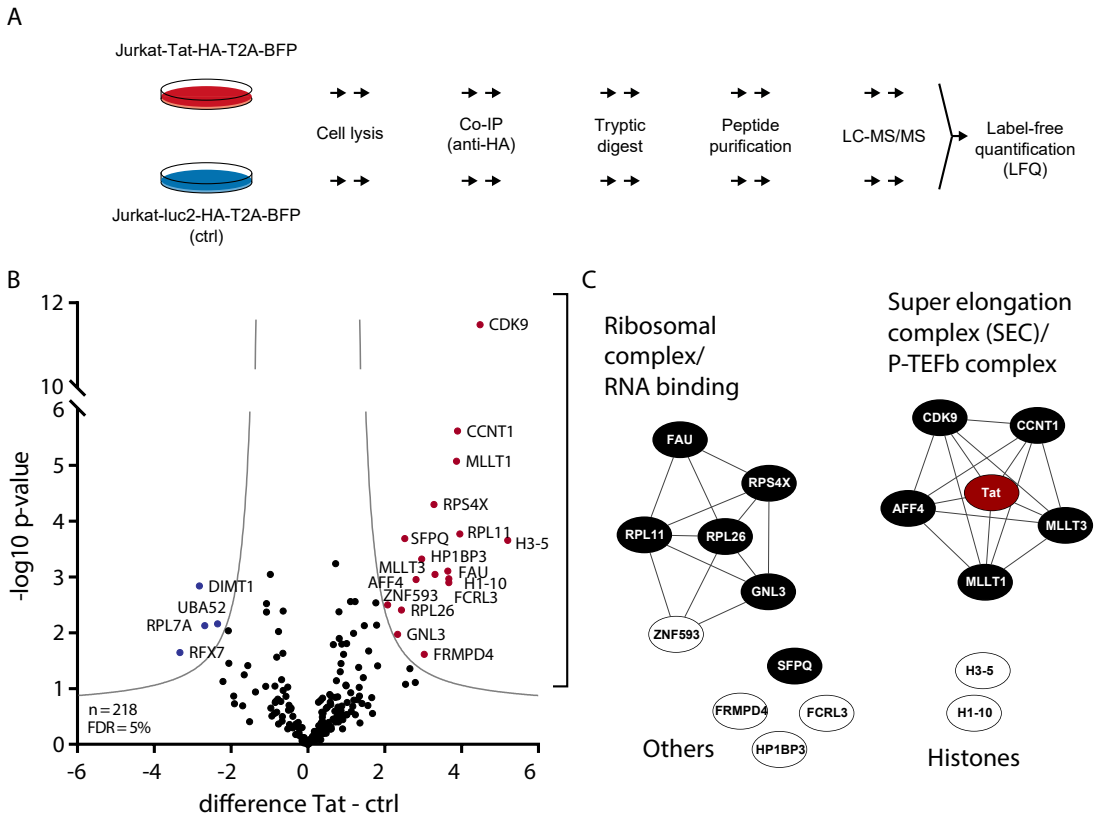

Figure 3.23. Interactome analysis of HIV-1 Tat. **(A)** Schematic illustration of the experimental design. Co-IP using anti-HA magnetic beads was performed using cell lysates of Jurkat-Tat-HA-T2A-BFP and Jurkat-luc2-HA-T2A-BFP (ctrl) cells. Enriched interactors were digested with trypsin, peptides were purified and analyzed by LC-MS/MS. **(B)** Volcano plot of enriched proteins in the HIV-1 Tat and control condition. Data was derived from three independent measurements. Red dots represent interacting proteins significantly enriched in Tat, blue dots indicate interactors significantly enriched in the control (two-sample t-test, FDR$\geq$0.05, slope $S_0 = 1$). **(C)** Functional interaction network of HIV-1 Tat interactors. Networks show significantly enriched Tat-interactors (see also A) after Co-IP (FDR$\geq$0.01, slope $S_0 = 1$). Network analysis was performed using the STRING database [239] and network visualization was performed using Cytoscape [240]. White nodes represent identified and enriched interactors. Interactors, which have been linked to HIV-1 infections according to the NCBI HHID [36] are marked as black nodes. Red node indicates HIV-1 Tat (not identified by LC-MS/MS, connecting edges to interactors according to the NCBI HHID).

Next, enriched proteins were identified for the mutant pairs K28Q versus K28R, K50/51Q versus K50/51R and Tat Δexon2 versus full length Tat. In the case of K28 (fig. 3.24A), abundancies of 117 proteins were compared, of which 12 were found enriched in K28R, e.g. *cyclin T1* (CCNT1) and *trans-acting T-cell-specific transcription factor GATA-3* (GATA3) while 9 proteins were found enriched in K28Q, e.g. *AF4/FMR2 family member 2* (AFF2), *RNA polymerase II elongation factor ELL* (ELL) and *E3 ubiquitin-protein ligase TRIM21* (TRIM21). In the case of K50/51 (fig. 3.24B), 123 proteins were compared. 12 proteins were enriched for K50/51R, e.g. FCRL3 and AFF2, and 8 proteins for K50/51Q, e.g. *pre-rRNA 2'-O-ribose RNA methyltransferase FTSJ3* (FTSJ3). For the analysis of Tat Δexon2, 100 proteins were compared, of which 11 proteins were enriched in Tat Δexon2, e.g. *probable ATP-dependent RNA helicase DDX5* (DDX5), *prothymosin alpha* and 10 protein in the full length Tat, e.g. CCNT1, ELL, *AF4/FMR2 family member 1* (AFF1) and AFF4 (fig. 3.24C).

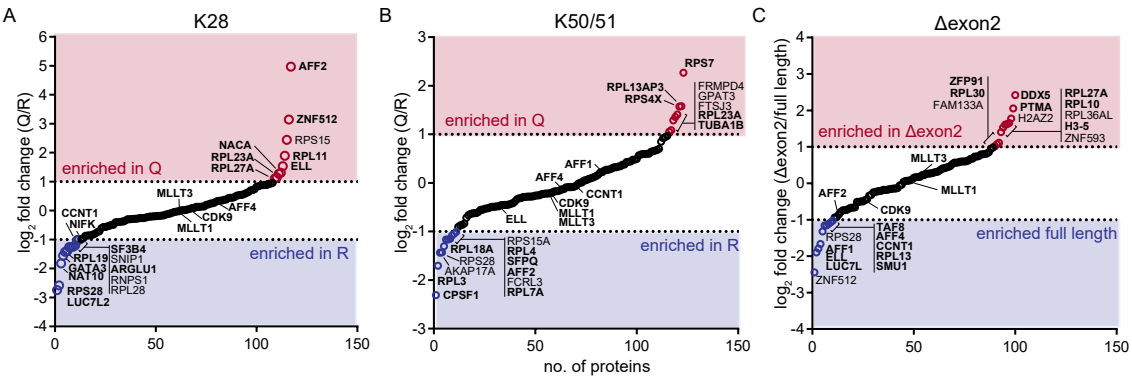

Figure 3.24. Interactome analysis of HIV-1 Tat mutants. (A) Dotplot of enriched protein interactors of K28R and K28Q. Colored areas represent cut-offs for enrichment in K28R (red, $\log_2$ fold change$\geq$1) and K28Q (blue, $\log_2$ fold change$\leq$-1). Bold gene names indicates proteins, which have been linked to HIV-1 infections according to the NCBI HHID [36]. For reasons of clarity, identified proteins, which were not classified as enriched or exclusively identified for K28R or K28Q, were not displayed in the network. **(B)** Dotplot of enriched protein interactors of K50/51R and K50/51Q. Cut-offs, annotations and color coding are analogous to A. **(C)** Dotplot of enriched protein interactors in Δexon2 and Tat wt. Cut-offs, annotations and color coding are analogous to A.

Moreover, interactors only identified in one of the mutants in each pair were also considered in the interactome analysis. The criteria of exclusively identified proteins was defined by at least two valid MS intensity values and three invalid (intensity of 0) values in the counter mutant (e.g. two valid values for K28Q and three invalid values in K28R in three independent measurements). In combination with the set of enriched proteins, interactome profiles were generated using the STRING database [239] and visualized as functional Tat-host-interacting networks for each R/Q pair and the Δexon2/full length pair (fig. 3.25A, B and C). HIV-1 Tat (not identified during LC-MS/MS analysis) was added to the networks and connected to confirmed, direct Tat-interactors according the NCBI HHID [36], e.g. constituents of the P-TEFb complex or SEC. Moreover, HDAC6 and KAT2B (PCAF) as well as EP300 and KAT2A (GCN5) (all not identified by LC-MS/MS analysis) were included in the respective networks of K28 and K50/51, since these PTM enzymes have been described to (de-)acetylates the respective acetylation sites [153, 154, 245, 246]. For reasons of clarity, identified proteins, which were not classified as enriched or only identified for one mutant in the pair, were not plotted in the network.

In general, subunits of the ribosomal protein complex were identified for every pair. For K28 and K50/51, enriched or exclusively identified proteins were also found as subunits of the spliceosome/pre-mRNA processing machinery. In the analysis of K28- (fig. 3.25A) and Δexon-associated network (fig. 3.25C), subunits of the P-TEFb complex or SEC could be assigned as direct Tat interactors. Elements of the P-TEFb complex or SEC were not found in the K50/51-associated network (fig. 3.25B), since they were not found enriched or exclusively identified in K50/51R or K50/51Q in contrast to other proteins such as *ATP-dependent RNA helicase DDX24* (DDX24). In every network, there were also several proteins, which have not been associated with HIV-1 Tat so far including AFF2 (fig. 3.25A and B), FCRL3 (fig. 3.25B) and *Smad nuclear-interacting protein 1* (SNIP1) (fig. 3.25C).

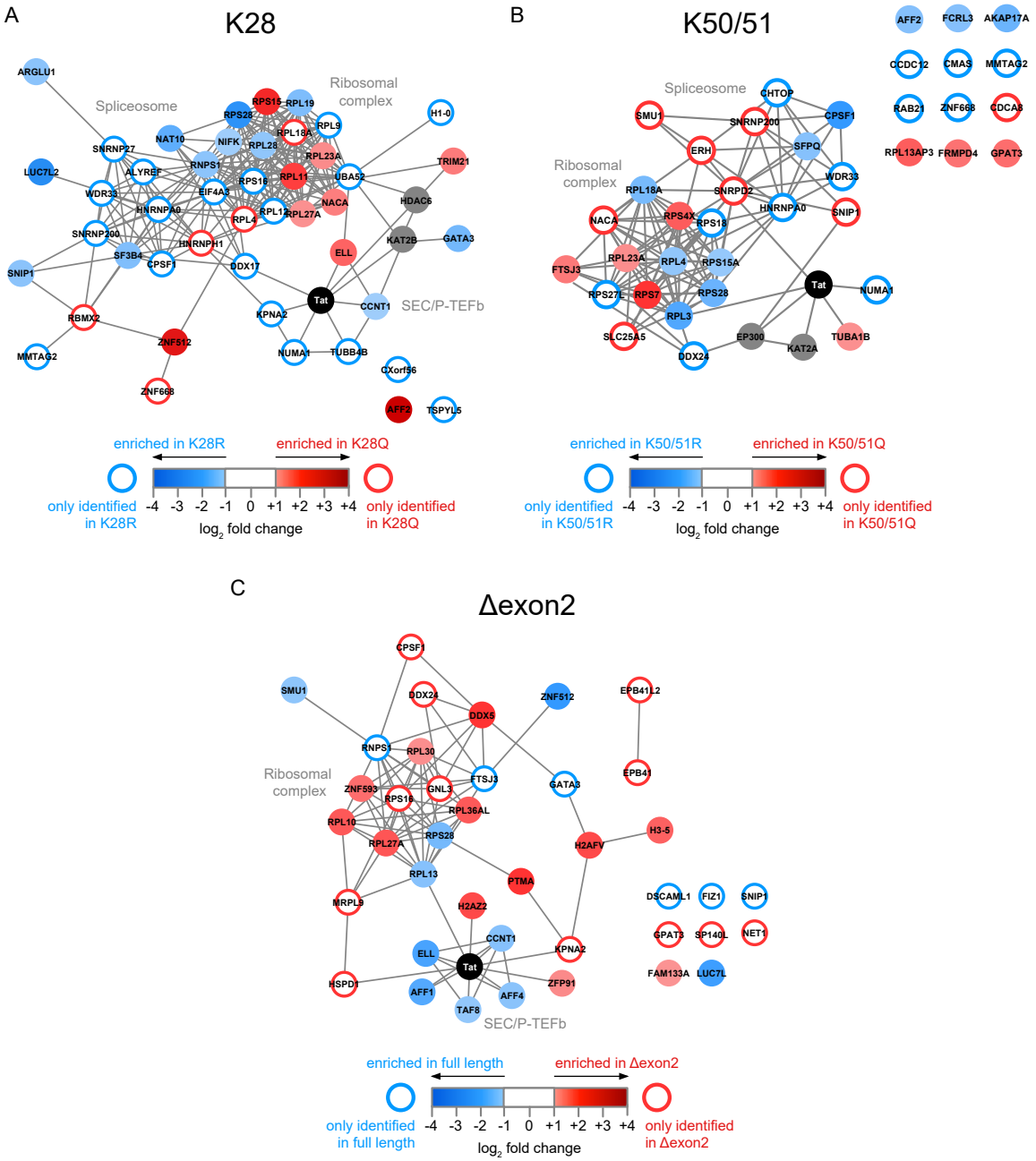

Figure 3.25. Functional interaction networks of enriched or exclusively identified Tat-interactors. (A) Network analysis of enriched or exclusively identified proteins in K28R and K28Q. Networks were generated using the STRING database [239] and visualized via Cytoscape [240]. HIV-Tat (black node) and host lysine acetyltransferases/deacetylates (grey nodes) were not identified during LC-MS/MS analysis, but included in the networks afterwards with connecting edges to interactors according to the NCBI HHID [36]. **(B)** Network analysis of enriched or exclusively identified proteins in K50/51R and K50/51Q in analogy to (A). **(C)** Network analysis of enriched or exclusively identified proteins in Δexon2 and full length Tat in analogy to (A).

3.7.4. Test for proteosomal degradation and extracellular secretion of HIV-1 Tat Δexon2

As shown previously by immunoblotting (fig. 3.16B and 3.17B), expression levels of the Tat Δexon2 in different cell systems was significantly lower compared to full length Tat wt and mutant constructs. However, experiments in pTat-T2A-BFP transduced Jurkat-E6 cells showed comparable mean fluorescent intensity of BFP (fig. 3.18B), which is expressed downstream of the Tat coding region. Therefore, it was assumed, that the copy number of transcribed Tat Δexon2 is as high as it is for full length Tat wt. On this basis, two different experiments were performed to investigate possible explanations for the low protein abundance of Tat Δexon2 as observed after immunoblot analysis.

To test if Tat Δexon2 is more prone to proteosomal degradation, Jurkat-E6 cells stably expressing either Tat wt or Tat Δexon2 were treated with proteosomal inhibitor MG-132 (concentration range of 5 to 50 µM) and cell lysates were analyzed by immunoblotting using a primary anti-HA antibody (fig. 3.26A). Contrary to the hypothesis, an increase in expression levels of Tat Δexon2 could not be detected upon MG-132 treatment.

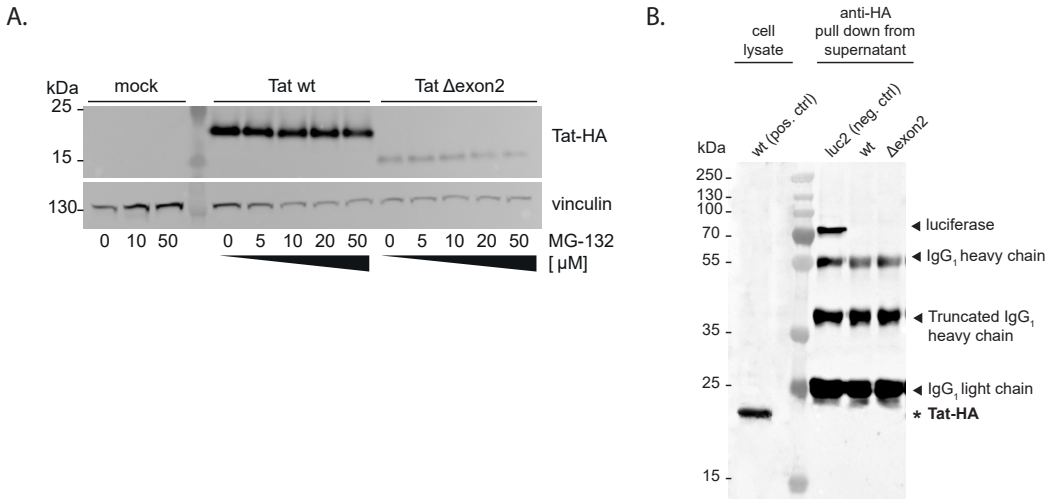

Figure 3.26. Analysis HIV-1 Tat Δexon2. (A) Analysis of proteosomal degradation of Tat exon2. Stable HIV-1 Tat Δexon2 expressing Jurkat-E6 cells were treated with different concentrations of MG-132 for 4 h and expression of Tat-HA was analyzed by immunoblotting using an anti-HA antibody in comparison with HIV-1 Tat wt. **(B)** Test for secretion of HIV-1 into the supernatant. 3 days old supernatant of stable Tat (wt and Δexon2) expressing Jurkat-E6 cells was subjected to magnetic enrichment of HA-tagged Tat and analysis by immunoblot.

Another hypothesis was, that Tat Δexon2 might be extracellulary secreted/transported into the supernatant resulting in lower levels in the intracellular space. In order to detect Tat proteins in the supernatant, HA-tagged proteins in three days old supernatant of Jurkat-E6 cells stably expressing HA-tagged Tat wt or Tat Δexon2 were enriched using magnetic anti-HA beads. The supernatant of cells expressing HA-tagged luciferase (luc2) served as control. Enriched proteins were harvested for immunoblot analysis (fig. 3.26B). Contrary to the hypothesis, tagged Tat protein could not be detected neither for Tat wt nor for Tat Δexon2. However, detection of HA-tagged luc2 verfied the experimental set-up. Therefore, secretion or transport into the supernatant of Tat due to the exon 2 deletion could not be shown here.

3.8. Epigenetic compound screening for reactivation of latent HIV-1

3.8.1. Establishment of a cell-based reporter system for high-throughpout compound screening

Besides the investigation of the molecular mechanisms in host cells upon HIV-1 infection, employment of novel strategies for the treatment of HIV-1 are still of high interest. In the last years, compounds targeting epigenetic modifications (such as histone deacetylation), which contributes to HIV-1 gene silencing and latency [206], have moved the "shock-and-kill" approach" forward [10]. However, trials of disrupting HIV-1 latency by pharmaceutical interventions trials have not been clinically successful so far [255, 256]. Consequently, there is still a strong demand to identify novel agents specifically targeting latent HIV-1 reservoirs. In order to identify new potentially effective drugs for the treatment of hidden viral reservoirs, an unique epigenetic compound library (TargetMol, No. L1200), harboring a collection of 380 compounds related to epigenetic regulation, was screened in this study. Compounds of this library include inhibitors of KDACs/sirtuin, KATs, lysine demethylases, DNA demethylases (DNMTs) and sirtuin activators (supplemental fig. S7). For a simplified screening of compounds with ability to reactivate HIV-1, a Jurkat-E6-based reporter system was established to enable the determination of the concentration-dependent efficacy and the cellular toxicity of the respective compounds under biosafety level 1 conditions (fig. 3.27A). For the construction of the latency reporter system, lentiviral particles were prepared for the transduction of Jurkat-E6 cells with HIV-1 LTR-Tat-IRES-GFP [168] to generate stable cell lines with a latent reporter HIV-1 provirus model[b]. 10 days after transduction, cells were tested for residual lentiviral particles in a p24 ELISA. The clearance measurement showed no residual virus-associated HIV-1 core protein p24, which enables sample handling under biosafety level 1 conditions. Subsequently, cells were sorted for viable, GFP-positive and GFP-negative cells[c].

Sorted and successfully transduced cells showed low basal GFP expression. As a positive control, the cells were treated with protein kinase C activator phorbol 12-myristate 13-acetate (PMA), which is known to reactivate HIV-1 by up-regulating NF-κB- and AP-1 signaling [257]. Here, GFP expression measured by the mean fluorescent intensity (MFI) was increased several fold (fig. 3.27B and C). To evaluate, whether single measurements from the PMA treatment were significantly different from the untreated (negative) control, the Z-factor was calculated for this system. Using the MFI values of the PMA treatment as positive control and untreated control cells as negative control, a Z-factor of 0.89 was

[b] Production of lentiviral particles and transduction was performed by Franziska Sippl, master student at Max von Pettenkofer Institute/Ludwig Maximilians University of Munich, Dept. Virology

[c] Cell sorting was performed on a BD FACSAriaFusion by Dr. Lisa Richter, technical manager of the core facility Flow Cytometry Biomedical Center Munich, Ludwig Maximilians University of Munich

determined verifying the robustness of this assay. Notably, the average Z-factor over all measurements in this cell system within this study was 0.77±0.17 (standard deviation). Simultaneously to reactivation assays, cell viability was evaluated using the resazurin cytotoxicity assay to identify toxic concentrations and to exclude false-positive results e.g. due to increased number of autofluorescent or dead cells. Since all compounds of the library were provided as DMSO stocks (10 mM), the background toxicity of DMSO was determined in the established Jurkat-Tat-IRES-GFP reporter cells. DMSO concentration $\leq$1% lead to a tolerable toxicity of $<$5% (data not shown). Therefore, 100 µM was set as the highest concentration ($\widehat{=}$ 1% DMSO) for the test compounds in this screen.

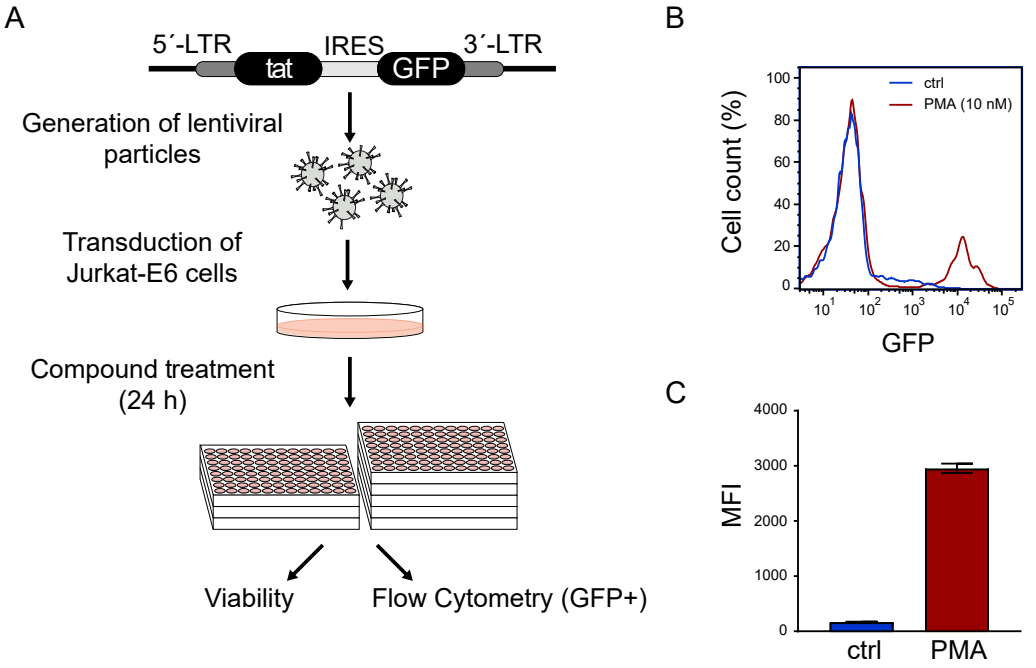

Figure 3.27. Cell-based reporter system for high-throughput screening of latency reversing agents (LRAs). **(A)** Schematic illustration of the LRA screening system. A stable Jurkat-E6 cell-line was established by lentiviral transduction carrying a Tat-IRES-GFP under the control of an HIV-1-derived LTR promoter site. Cells were treated with different compounds in a 96-well based format. Subsequently, successful reactivation and associated GFP expression was determined by flow cytometry. Simultaneously, cell viability was determined by resazurin assay to assess compound toxicity. **(B)** Flow cytometry analysis of vehicle-treated control cells (blue) and PMA-treated (reactivated) cells (red). **(C)** Corresponding bar chart of B, showing the mean fluorescence intensity (MFI) of PMA-treated (positive control) and vehicle-treated (negative control) cells. Error bars represent SD of at least three independent measurements.

3.8.2. Epigenetic compound screening

Using the Jurkat-Tat-IRES-GFP system, described in section 3.8.1, 380 compounds of the epigenetic compound library (TargetMol, No. L1200) were tested for their concentration-dependent efficacy in latency reversal and cellular toxicity. Throughout this screen, cells treated with 10 nM PMA served as positive control and were used to normalize all the results relative to the PMA-based activation. Test compounds were titrated on Jurkat-Tat-IRES-GFP cells in steps of factor 10, starting from 1 nM to to the highest concentration of 100 µM (fig. 3.28A, 3.29 and 3.30). For 139 compounds ($\widehat{=}$ 37%), the treatment resulted in reactivation of at least 10% (relative to PMA control), which defined the activation threshold. For eight compounds, the respective reactivation effectivities were more than 50%. One compound (histone methyltransferase inhibitor MI-136) achieved even higher reactivation than PMA. Two other compounds (bisdemethoxycurcumin and the HDAC II inhibitor MC1568) also resulted in higher reactivation effectivity than PMA, however, the treatment in parental Jurkat-E6 cells (lacking the GFP reporter) showed, that these compounds were intrinsically fluorescent (data not shown). Notably, with increasing concentrations, an associated toxicity, resulting in increased cell death and autofluorescent, was observed for the most tested compounds disqualifying them for further analysis. This was also the case for MI-136, where the high GFP signal was accompanied with increased cellular toxicity. To note, PMA treatment itself at a concentration of 10 nM was also associated with a profound reduction in cell viability down to 40%. A detailed overview of the measured reactivation efficacy and cell toxicity of every single compound is shown in fig. 3.29 and 3.30 (mentioned examples are marked with arrows). Overall, the primary screen in Jurkat-Tat-IRES-GFP resulted in 43 potential latency reversing agents (LRAs), which showed significant reactivation and a relatively low toxicity ($\geq$ 75% remaining cell viability). Among the candidate compounds were ca. 35% HDAC/sirtuin inhibitors, e.g. vorinostat, valproic acid and mocetinostat and a similar number of inhibitors of proteins with epigenetic reader domains, e.g. JQ1, I-BET151 and CPI-203.

3.8.3. Validation screen of selected candidate compounds

The high-throughput screening of the epigenetic compound library (TargetMol, No. L1200) in Jurkat-Tat-IRES-GFP reporter cells resulted in 43 LRA candidates (section 3.8.2). These selected compounds were further validated under biosafety level 3** using J-Lat cells, which contain a near full length integrated HIV-1 genome (Δ*env* and *nef*-defective HIV R7), that expresses GFP upon LTR-activation [168]. 13 further compounds, including SR-4370 (HDAC inhibitor) and AMI-1 (methyltransferase inhibitor), showed either reactivation very close to the 10% threshold or a strong reactivation accompanied with a toxicity closed to the 75% threshold for cell viability during the primary screen in Jurkat-Tat-IRES-GFP reporter cells (here, denoted as "threshold compounds"). These compounds were additionally included in

the secondary screen to define the respective thresholds in the J-Lat cells. Moreover, seven more compounds, which showed no or very weak reactivation in the primary screen were also tested in J-Lat cells as control conditions. In analogy to the screening in Jurkat-Tat-IRES-GFP cells, treatment with 10 nM PMA was used as positive control and for normalization. The screening of the selected compounds in J-Lat cells corresponded to the results from the primary screen (fig. 3.28B). While none of the control compounds was able to reactivate the HIV-1 promotor, most of the LRA candidates and also the "threshold compounds" showed a distinct reactivation effect in J-Lat cells. In comparison to the Jurkat-Tat-IRES-GFP system, the signal background in the J-Lat system was even lower. As a consequence, the threshold for reactivation was adapted to 5% GFP fluorescence (relative to the PMA treatment). Nevertheless, differences in cellular toxicity and signal intensity between both cell systems were observed. For example, the average cell viability at 100 µM (max. concentration) significantly shifted from 53.7% as determined in the primary screen to 70.5% in the J-Lat model. ($p=0.0002$, one-way ANOVA). In parallel, the required concentration for LTR activation in the J-Lat model was increased for most of the tested compounds in comparison with the Jurkat-Tat-IRES-GFP model.

The secondary screen resulted in six lead compounds leading to strong induction of the HIV-1 LTR promotor based on their reactivation efficacy and cell toxicity (fig. 3.28C). In addition, latency reactivation in lead compound treated J-Lat cells was visualized using fluorescence microscopy confirming the flow cytometry data (fig. 3.28D). The six lead compounds comprised four HDAC inhibitors vorinostat (SAHA), CI-994 (Tacedinaline), SR-4370 and HPOB as well as the two bromodomain inhibitors CPI-203 and bromosporine. While the effect of several HDAC inhibitors, including vorinostat and the two bromodomain inhibitors, on latency reactivation have been already described [257–259], the class I HDAC inhibitor SR-4370 and the HDAC6 inhibitor HPOB have not been reported as LRAs so far. Notably, HPOB treated cells resulted in a maximum reactivation of 137% compared to the PMA treatment (fig. 3.28C) while maintaining 82% cell viability. (fig. 3.31).

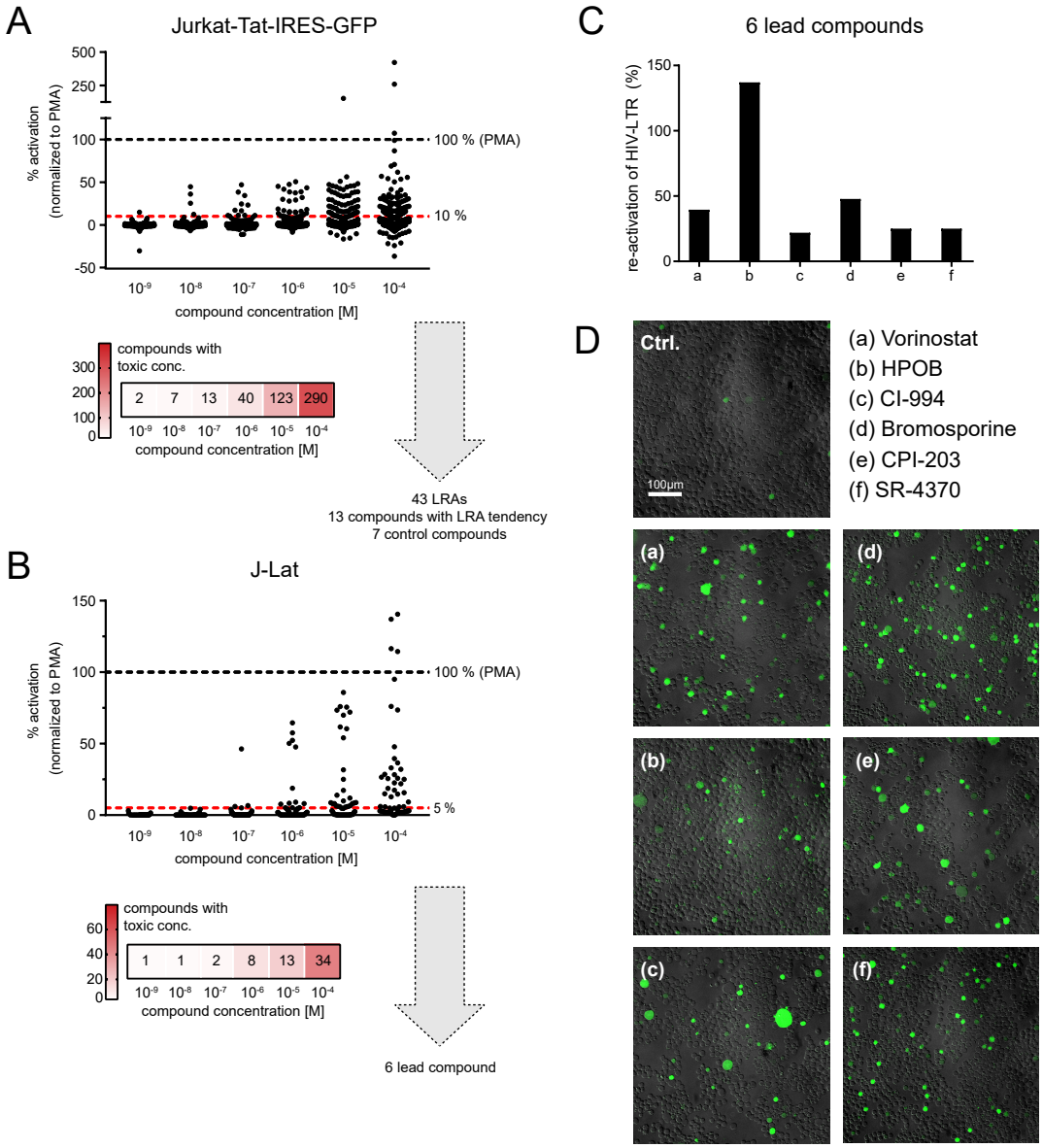

Figure 3.28. Compound screen latency reversing agents (LRAs). (A) Primary screen based on Jurkat-E6 reporter cells. Graph displays the average percentage of activated cells for each compound and concentration normalized to PMA-treated control cells. Activation threshold was set to 10% and only compounds causing $\geq$10% reactivation were defined as potential LRA. The corresponding small heatmap below displays the amount of compounds at the indicated concentration leading to non-tolerable cellular toxicity (viability threshold: 75%). **(B)** Secondary screen of dedicated compounds identified in A. **(C)** Bar chart displays percentage of reactivation in J-Lat cells caused by challenging the cells with the indicated six lead compounds. **(D)** Complementary analysis of latency reversing function of the six identified lead compounds in J-Lat cells by fluorescence microscopy. Representative pictures of J-Lat cells challenged for 24 h either with the indicated compound or with vehicle only (control).

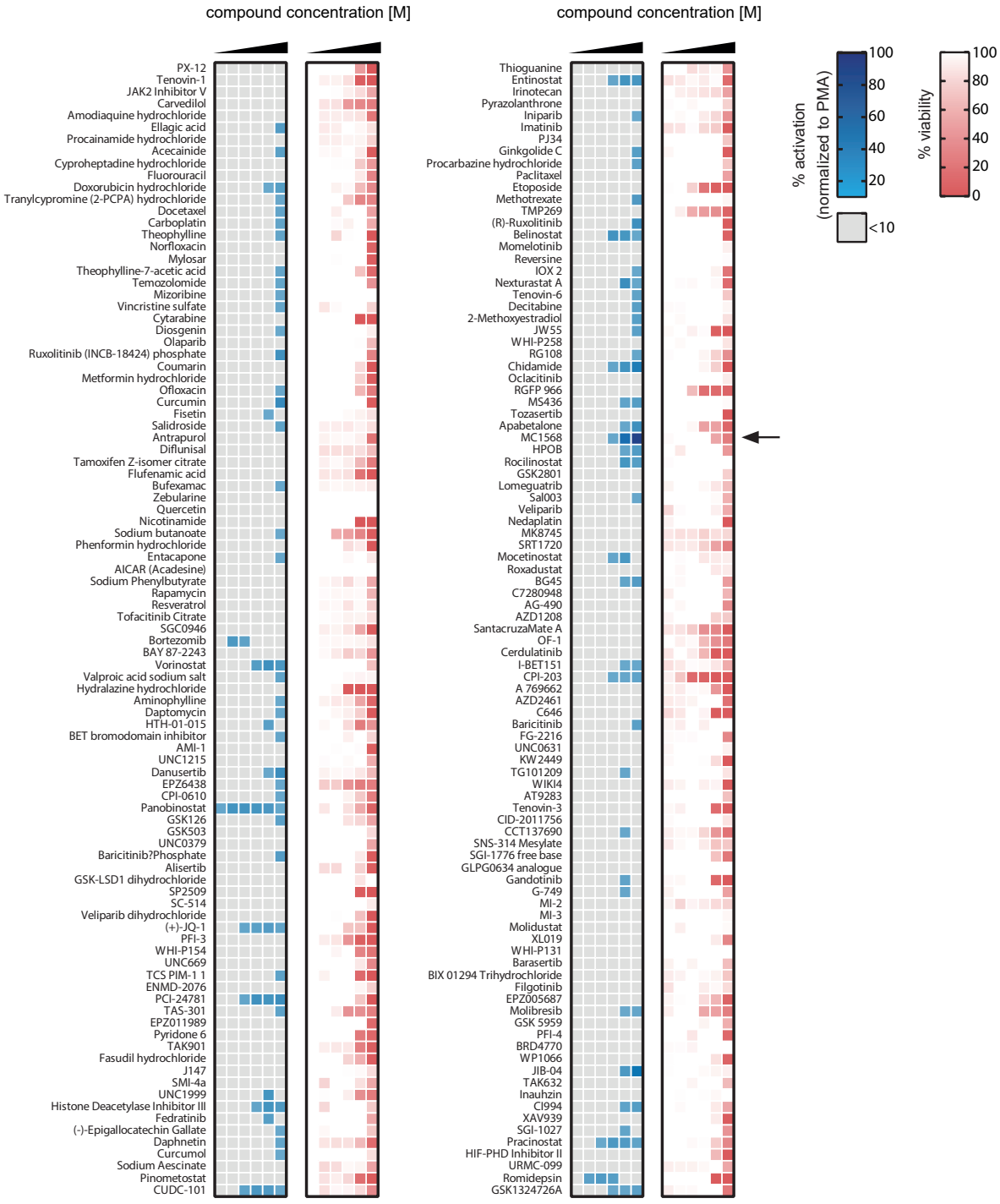

Figure 3.29. Treatment effects of tested compounds in Jurkat-Tat-IRES-GFP reporter cells (part 1). The heatmaps display the effects of treatment for the first set of 190 compounds of the epigenetics compound library. Compounds were titrated on reporter cells in steps of factor ten from 1 nM to 100 µM. The left panel shows the reactivation efficiency in percent normalized to PMA treatment. Color-code: Grey indicates reactivation up to 10%. Shades of green indicate reactivation equal or higher than 10%.The right panel shows the associated effect on cellular viability. Non toxic compounds (≙100% viability) are displayed in white color, increasing toxicity is visualized by red shades. Mentioned examples in section 3.8.2 are marked with black arrows.

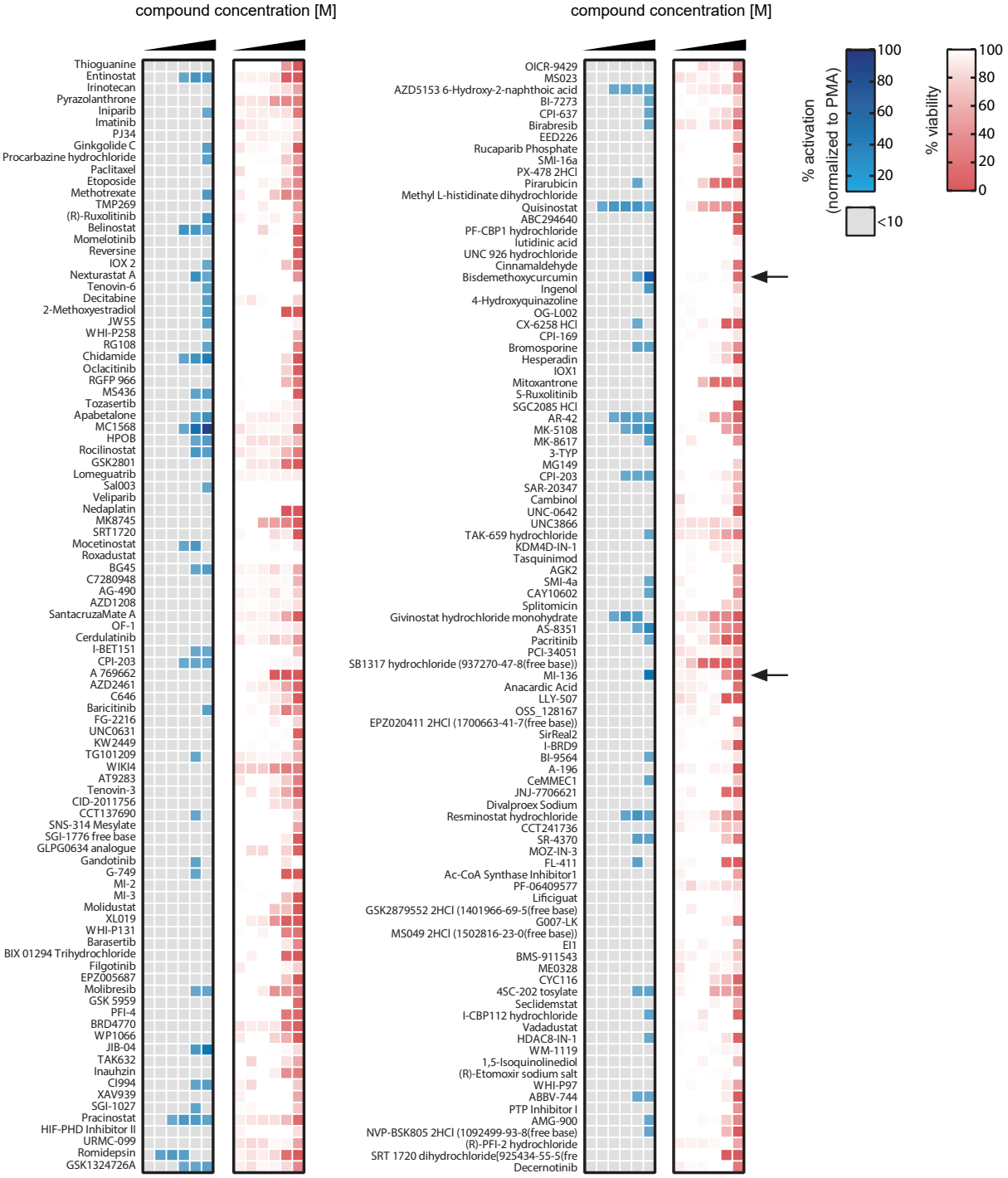

Figure 3.30. Treatment effects of tested compounds in Jurkat-Tat-IRES-GFP reporter cells (part 2). The heatmaps display the effects of treatment for the second set of 190 compounds of the epigenetics compound library. Compounds were titrated on reporter cells in steps of factor ten from 1 nM to 100 µM. The left panel shows the reactivation efficiency in percent normalized to PMA treatment. Color-code: As described in part 1. Mentioned examples in section 3.8.2 are marked with black arrows.

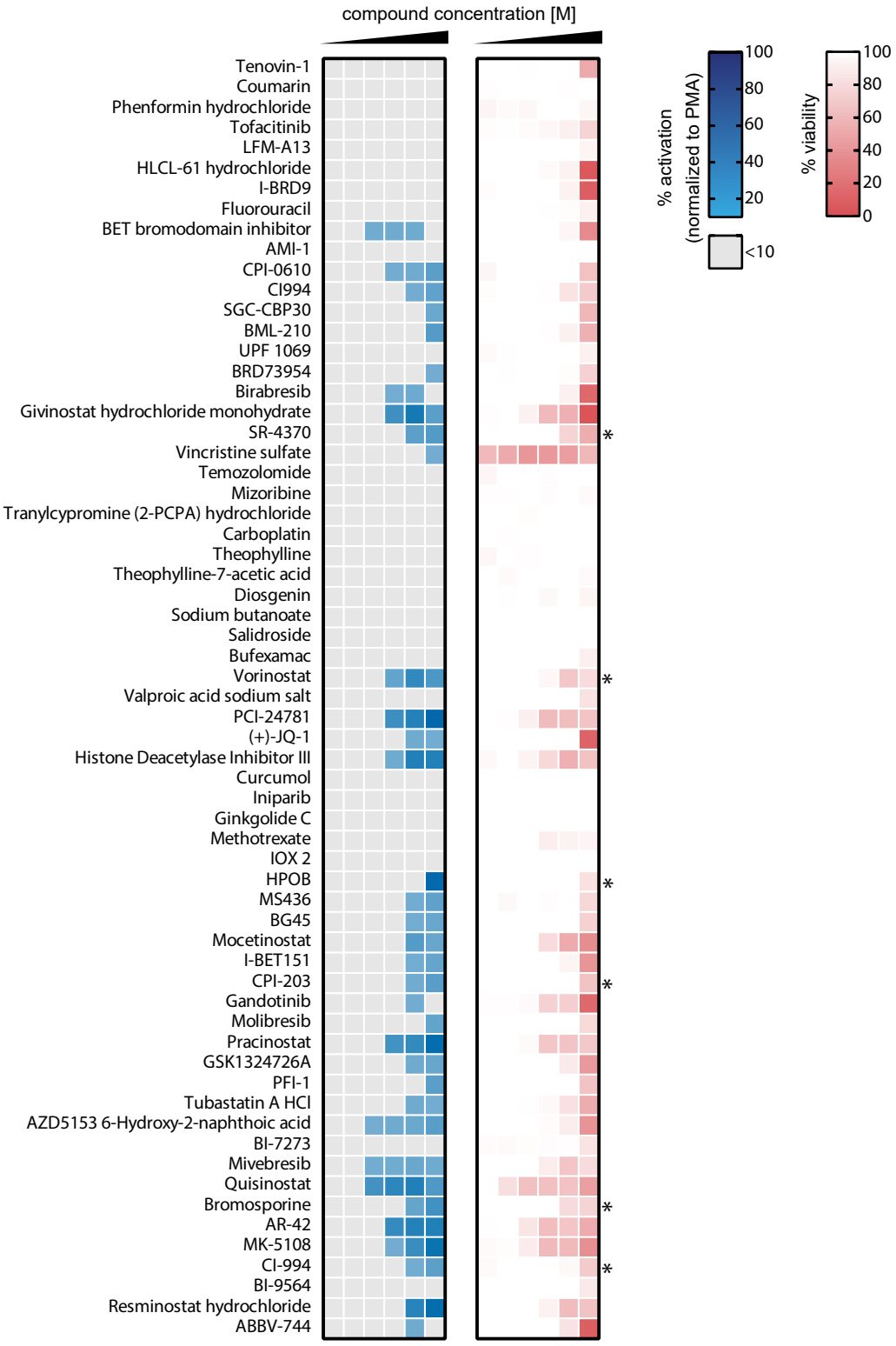

Figure 3.31. Treatment effects of candidate LRAs in J-Lat cells. The heatmaps display the effects of treatment for 43 candidate compounds (resulted from the primary screen) in J-Lat cells. Compounds were titrated in steps of factor ten from 1 nM to 100 µM. The left panel shows the reactivation efficiency in percent normalized to PMA treatment. Color-code: As described in fig. 3.29. Lead compounds were marked with *.

3.8.4. Determination of T-cell activation and side-effects on other leukocytes

Compound induced HIV-1 latency reactivation may not only activate viral gene transcription, it might also result in global T-cell activation, which may be accompanied by unfavorable cytokine production [260], which facilitates *de novo* infection of additional cells. Therefore, the identified lead compounds (section 3.8.3) were tested for possible T-cell activation properties. Here, resting $CD4^+$ T-cells were isolated from peripheral blood mononuclear cells (PBMCs) of healthy blood donors and treated with the respective lead compounds for 24 h. Thereafter, surface expression of early (CD69) and late activation antigens (CD25) was determined by fluorescence-based flow cytometry (fig. 3.32). Vehicle-treated cells were used as negative control whereas PHA or CD3/CD28-bead stimulated cells served as positive control. While the PHA or the CD3/CD28-bead treatment caused significant up-regulation of early and late activation markers, none of the six lead compounds showed an increase in CD25-, CD69- or CD25/CD69-positive cells.

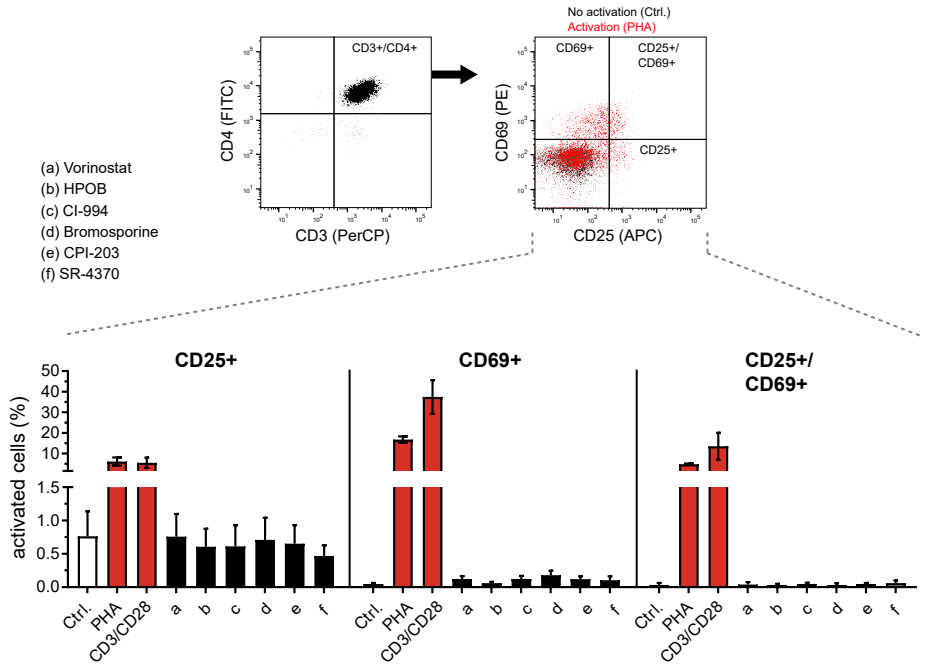

Figure 3.32. $CD4^+$ T-cell activation. Primary resting $CD4^+$ T-cells were treated with either PHA or CD3/CD28 beads (positive controls) or with the respective compound for 24 h. Vehicle-treated cells were used as negative control (Ctrl.). Subsequently, cells were stained for CD3, CD4, CD25 and CD69 and analyzed by flow cytometry for increased expression of activation markers CD25 and CD69. Left flow cytometry plots show gating for $CD3^+/CD4^+$ subset and right flow cytometry plot shows distribution of CD25/CD69 on control cells (black) and activated, PHA-treated cells (red). Bar charts indicate fractions of CD25, CD69, and CD25/CD69 positive cells. Error bars represent SD from three different donors.

Apart from unfavorable T-cell activation, compounds might also exert cytotoxic effects on leukocytes in general. To exclude potential cytotoxic effects to leukocytes, flow cytometric immunophenotyping of PBMCs 24 h post treatment was conducted and global cell viability was determined by 7-AAD staining. As a result, no difference in global cell viability nor significant changes in the cell fractions expressing $CD45^+$, $CD3^+$, $CD4^+$, $CD8^+$, $CD14^+$, $CD19^+$, $CD16/56^+$, $CD16/56^+/CD3^+$ surface antigens were observed (fig. 3.33). To note, a higher fluctuation was determined in the case of $CD14^+$ monocytes.

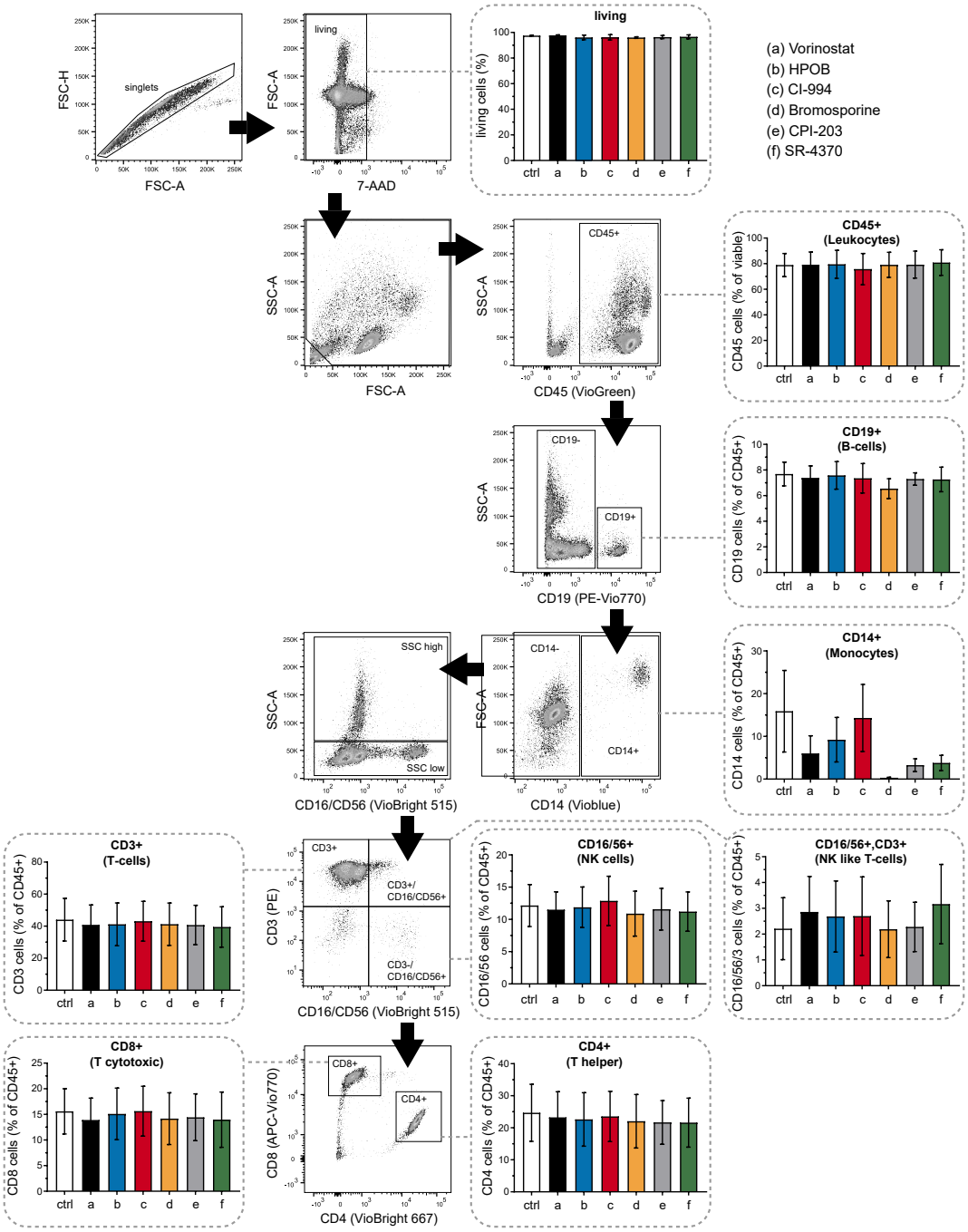

Figure 3.33. Immunophenotyping of PBMCs. PBMCs isolated from healthy donors were treated with the respective compounds for 24 h or with vehicle control and analyzed by flow cytometry for certain cellular markers. The flow cytometry plots show representatitve data of control cells and the underlying gating strategy. First, cells were gated for singlet and living cells (via 7-AAD stain). Cell debris were excluded by classical FSC/SSC analysis. The resulting population was analyzed for leukocytes (CD45). Leukocytes were distinguished in B-cells (CD19) and monocytes (CD14). CD19/CD14-negative cells were discriminated in eosinophils (SSC^{high}) and a $CD16^{dim}$ SSC^{low} population. The latter was analyzed for CD3 (T-cells), CD56 (NK cells) and CD3/CD56 (T-cell like NK cells) expressing populations. Finally, $CD4^+$ and $CD8^+$ T-cells were determined from the CD3 expressing fraction. Associated data from three different donors are shown as bar chart for each cell type. Error bars indicate SD.

3.9. Analysis of *de novo* HIV-1 infection in HDAC inhibitor treated CD4$^+$ T-cells

3.9.1. Reactivation of latent HIV-1 by HDAC inhibitors

The previous screening of epigenetic compounds for LRAs resulted in 43 candidate compounds with HIV-1 latency reversing properties where ca. 35% belong to the class of HDAC/sirtuin inhibitors. Even though, these HDAC/sirtuin inhibitors have been shown to be able to reactivate latently infected cells in a efficient way supporting the idea of the "shock-and-kill" approach, reactivation of latent HIV-1 might lead to *de novo* infections in tissues, where ART is not optimally effective and, thereby, re-establish new latent HIV-1 reservoirs. This clinical concern is also supported by a study showing, that high doses of HDAC inhibitor romidepsin are very effective in reactivation of latent HIV-1, but also enhance HIV-1 infection in CD4$^+$ T-cells at the same time [261]. So far, the "shock-and-kill" approach did not show a significant reduction of the size of latent HIV-reservoirs in patients [262], which might be associated with reseeded HIV-1 reservoirs. To analyze the possibility of HDAC inhibitor-dependent enhancement of *de novo* HIV-1 infection in target cells, a selection of 15 inhibitors covering the entire selectivity range for human HDACs/sirtuins was tested for their ability to reactivate latent HIV-1 from the latent state and for their effect on HIV-1 infection in primary activated CD4$^+$ T-cells (fig. 3.34).

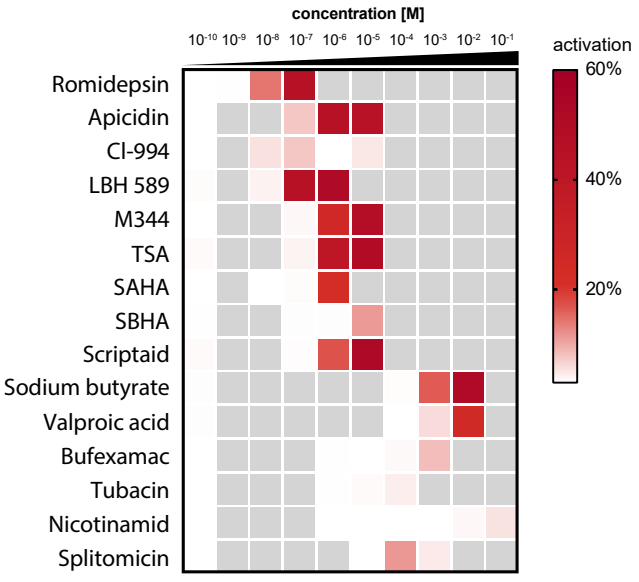

Figure 3.34. Reactivation of latent HIV-1 by HDAC inhibitors. The heatmaps display the titration of HDAC inhibitors on J-Lat cells. 24 h after treatment, percentage of reactivation was measured by GFP-based flow-cytometry. Data are derived from three independent experiments. Each tile represents the average induced reactivation for the respective concentration. Grey tiles indicates concentrations, that were not applied during titration of the respective HDAC inhibitor based on available literature and toxicity studies [75, 263–266].

First, J-Lat cells were treated with increasing concentrations of the respective compound of the panel to assess their latency reversing capability. The respective concentration range was defined based on other studies [75, 263–266]. GFP expression in J-Lat cells upon HIV-1 LTR activation by the inhibitor treatment was analyzed by flow cytometry, while solvent only treatment (DMSO or H_2O) served as control, which yielded 6-7% GFP-positive cells in average, defining the background signal in this experiment. Most HDAC inhibitors showed efficient reactivation of latent HIV-1 (fig. 3.34). Based on the potency, tested compounds were clustered into three groups: The first group comprised inhibitors, e.g. romidepsin, apicidin, TSA and LBH 589 (also known as panobinostat), in which HIV-1 reactivation was efficient within a low concentration range (10^{-5} to 10^{-7} M). The second group including valproate and sodium butyrate (Sb) induced reactivation at significantly higher concentrations (10^{-3} to 10^{-2} M). The third and last group comprised compounds, for which no significant HIV-1 reactivation was measured for the tested concentrations. This group comprises sirtuin inhibitors, splitomicin and nicotinamide, and HDAC6 inhibitors, bufexamax (Bu) and tubacin.

3.9.2. Effect of HDAC inhibitor treatment on HIV-1 *de novo* infection

Since all HDAC/sirtuin inhibitors in the panel were efficient in latency reversal, the compounds were tested for their impact on HIV-1 infection in primary activated CD4$^+$ T-cells. For this purpose, human primary activated CD4$^+$ T-cells were isolated from four healthy donors, activated, pooled and treated with the respective inhibitor for 24 h and, subsequently, infected with a full length, replication-competent HIV-1_{NL4-3} strain (fig. 3.35A). Applied drug doses were derived from physiological and scientifically used concentrations, e.g. 4 nM sodium butyrate [267], 0.5 µM SAHA [268], 30 nM LBH 589 [264]. A toxicity of 20% (determined by cytotoxicity assay) was tolerated for each compound, therefore, the lethal dose 20% (LC_{20}) was used as maximal concentration for the infection. An overview of LC_{20} of each HDAC inhibitor is provided in supplemental fig. S8). Infection of treated cells was analyzed by intracellular p24 staining and flow cytometry (48 h p.i.) (fig. 3.35B). Contrary to expectations, none of the compounds in the panel was able to enhance *de novo* infection in primary activated CD4$^+$ T-cells (fig. 3.35C). In most cases, HIV-1 infection levels were not or only moderately affected by the HDAC inhibitor treatment. Surprisingly, a significant decrease in p24-positive cells of ca. 70-75% (relative to the vehicle-treated control) was observed for sodium butyrate and bufexamac. An analogous infection experiment using a R5-tropic HIV-1 transmitter founder (T/F) strain CH058 [269] showed a very similar outcome (fig. 3.35D) as for the infection of treated cells with the X4-tropic HIV-1_{NL4-3} strain. Interestingly, despite of the common selectivity of bufexamac, tubacin and LBH 589 for HDAC6, a reduction in infection levels was not observed for tubacin or LBH 589 treated cells.

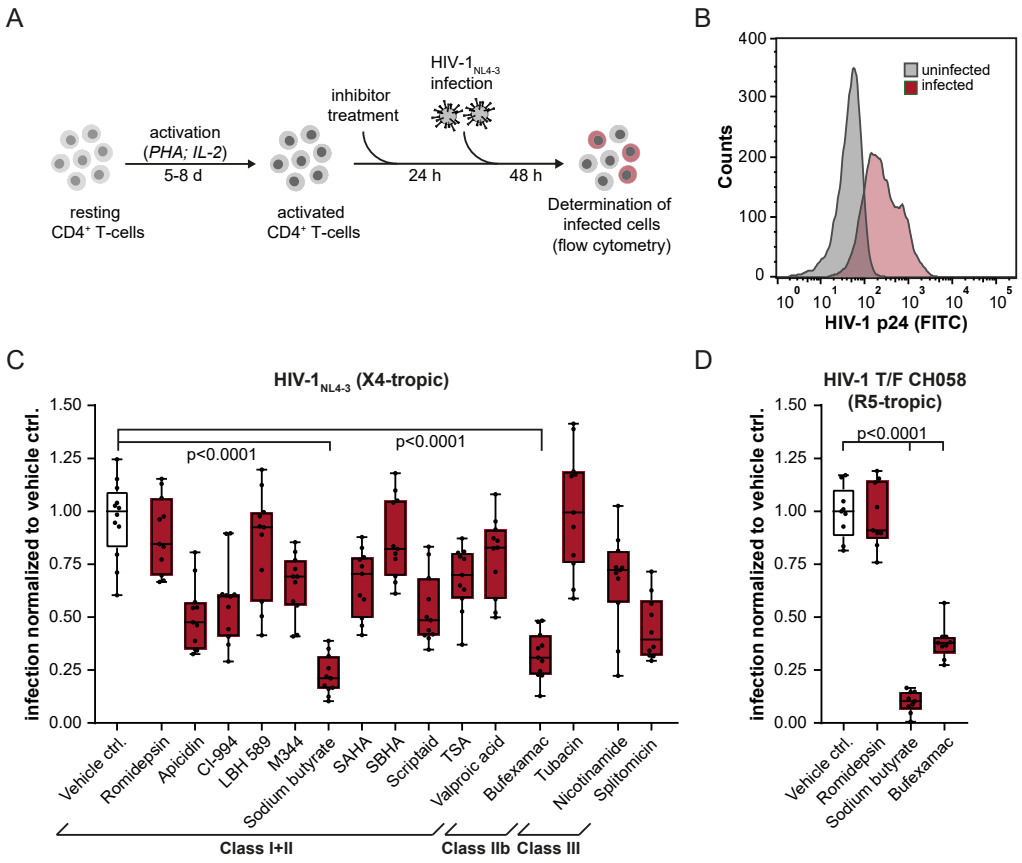

Figure 3.35. Effect of HDAC inhibitors on *de novo* HIV-1 infection. **(A)** Schematic overview of the experimental design. Isolated, primary CD4$^+$ T-cells were activated by PHA and IL-2 treatment for 5-8 days. Subsequently, cell were treated as 4DP with HDAC inhibitors for 24 h and, thereafter, infected with HIV-1_{NL4-3}. 48 h p.i., cells were stained for HIV-1 capsid protein p24 and analyzed by flow cytometry. **(B)** Representative flow cytometry histogram of the increase of p24 in infected CD4$^+$ T-cells (red). **(C)** Boxplots showing HIV-1_{NL4-3} infection levels in CD4$^+$ T-cells treated with the respective HDAC inhibitor. All data were normalized to the median of vehicle control. Boxes represent the lower and upper quartiles, whiskers indicate the minimum and maximal values, and the middleline inside the box shows the median. Individual data points are presented as dots. Sample size: n$\geq$10. Given p-values show statistically difference (ANOVA based Dunnetts' multiple comparison test) between vehicle control and sodium butyrate and bufexamac treated cells. **(D)** Graph analogous to C for infection with R5-tropic HIV-1 T/F CH058 virus. Sample size: n = 9.

3.9.3. Global analysis of transcriptome and proteome changes in CD4$^+$ T-cells upon sodium butyrate and bufexamac treatment

Transcriptome analysis of sodium butryate and bufexamac treated CD4$^+$ T-cells

Sodium butyrate and bufexamac have been shown to be potent LRAs, which impair *de novo* HIV-1 infection in human primary activated CD4$^+$ T-cells (section 3.9.2). In order to understand the underlying molecular mechanisms of both compounds, transcriptome and proteome analysis of sodium butyrate (Sb) and bufexamac (Bu) treated cells were performed (1.95 mM and 0.04 mM respectively, see also supplemental fig. S8). For transcriptomic analysis, human primary activated CD4$^+$ T-cells were treated with Sb or Bu for 48 h (number of independent experiments n =3 for each treatment including control). Comprehensive mRNA profiles were acquired by random-primed cDNA sequencing (RNAseq) with reduced representation of ribosomal RNA[d]. The average depth of mapped reads was around 22 million reads. In total, the RNAseq resulted in 15,396 transcripts for Sb-treated (fig. 3.36A) and 12,833 transcripts for Bu-treated cells (fig. 3.36B). Transcripts with failed statistical analysis (DESeg: no q-value) were excluded and not considered. More than 90% of the identified transcripts were assigned to ENSEMBL gene IDs. 3,585 differential expressed genes (DEGs) were found for Sb and 1,342 DEGs were found for Bu (DESeq; FDR=0.01). In Sb-treated samples, 1,342 genes were significantly up-regulated ($\log_2$ fold changes$\geq$1) and 814 genes were down-regulated ($\log_2$ fold changes$\leq$-1) (fig. 3.36A). In Bu-treated samples, 62 genes were found significantly up-regulated and 261 gene down-regulated (fig. 3.36B). The comparison with the NCBI HHID [36] showed, that ca. 25% of the DEGs in Sb and ca. 34% of the DEGs in Bu have been related to HIV-1 infection previously, e.g. *interleukin-8* (CXCL8) and *interleukin-4* (IL4). GO and pathway enrichment analysis using g:Profiler [217] resulted in genes related to "mitosis", "G1/S-" and "G2/M-transition" ot "DNA double strang break , which are affected by Sb- or Bu-treatment (fig. 3.36C). Additionally, KEGG pathway enrichment analysis showed regulation of "cell cycle" and "Fanconia anemia pathways". By mapping of the changes in protein abundance into the two KEGG pathways, significant de-regulation of the associated genes was observed in Sb- and Bu-treated samples (fig. 3.37).

[d]RNAseq was performed in collaboration with Dr. Helmut Blum, group leader at Gene Center Munich, Ludwig-Maximilians-Universität München

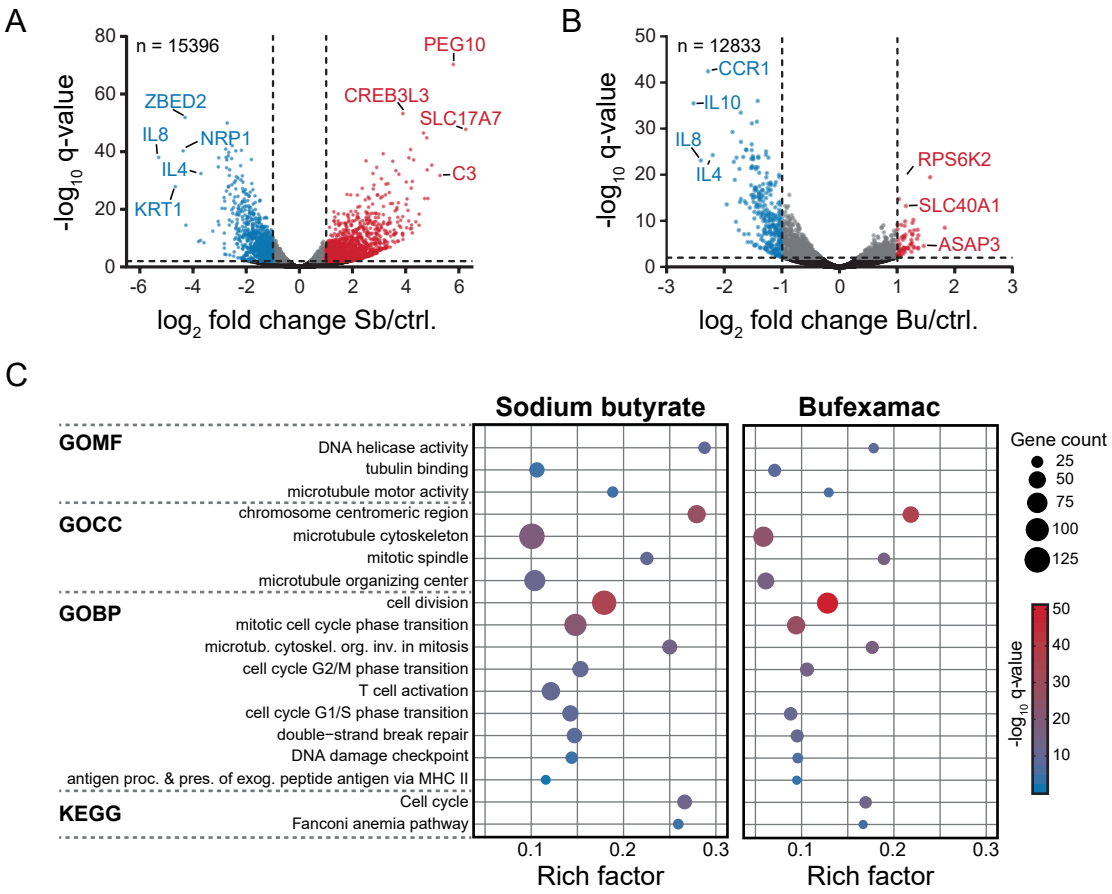

Figure 3.36. Transcriptome analysis of sodium butyrate (Sb) and bufexamac (Bu)-treated CD4$^+$ T-cells. **(A)** Volcano plot of identified transcripts showing changes in protein abundance between Sb-treated and control cells and the associated q-value for each transcript. Color code: Red dots represent significantly up-regulated transcripts (FDR$\leq$0.01 and $\log_2$ fold changes$\geq$1), blue dots represents significantly down-regulated transcripts (FDR$\leq$0.01 and $\log_2$ fold changes$\leq$-1), grey dots indicate significantly differential expressed genes (FDR$\leq$0.01), which are neither up- nor down-regulated. **(B)** Volcano plot for Bu-treated and control cells analogous to A. **(C)** GO-term and pathway enrichment analysis of significantly down-regulated genes in Sb- (left) and Bu-treated cells (right) based on the g:Profiler analysis tool. Representative terms are shown. The graphs display q-values and number of regulated genes for each indicated GO-term and KEGG pathway. Abbreviations: GO molecular function (GOMF), GO biological process (GOBP), GO cellular compartment (GOCC).

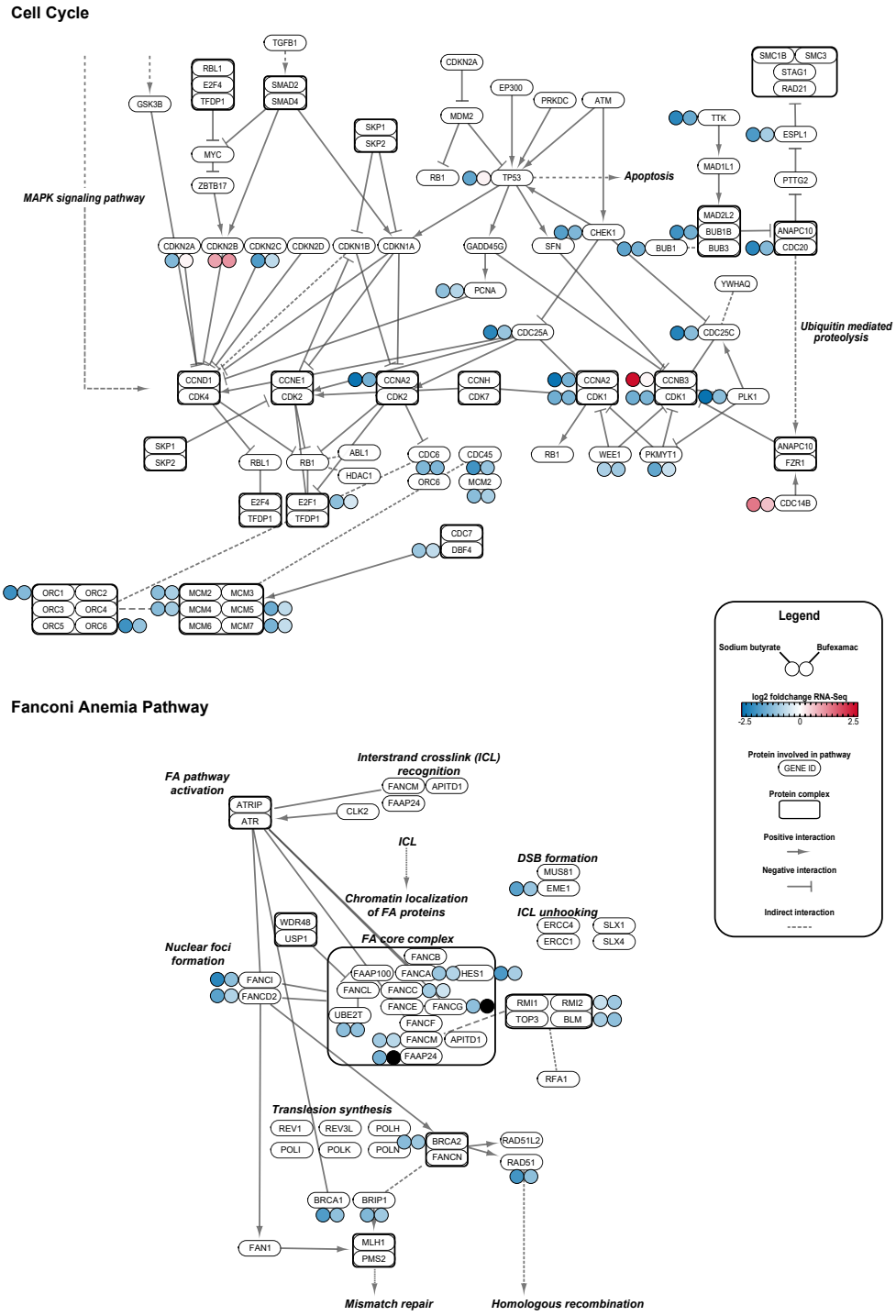

Figure 3.37. KEGG analysis of differentially regulated genes (DEGs) in sodium butyrate and bufexamac-treated CD4$^+$ T-cells. Schematic representation of the KEGG-terms "Cell cycle" (top) and "Fanconia anemia pathway" (bottom). Genes/proteins involved in the cellular pathway are illustrated as white nodes. Protein complexes are framed by black boxes. Pointy arrows show induction of expression/activation of target genes/proteins, negative/repressing (e.g. inhibition) interactions are indiciated by bar-headed arrows. Sb- or Bu-related changes in protein abundancies are shown as color coded small circles in the immediate vicinity of the respective gene symbol. Black filled circles indicate missing values in the respective condition.

Proteome analysis of sodium butyrate treated CD4$^+$ T-cells

The analysis of the transcriptome of Sb- and Bu-treated CD4$^+$ T-cells gave insights of ongoing intracellular changes. However, it has been shown, that changes at mRNA level does not necessarily correlate with changes on protein level [270] due to diverse regulatory elements at protein level such as PTMs affecting protein half-lives. Therefore, quantitative, TMT-based proteome analysis of treated CD4$^+$ T-cells was conducted. In this study, Sb as pan-HDAC inhibitor were investigated in the first place (fig. 3.38A). Here, 4082 proteins were identified, of which 92 proteins were found up-regulated ($\log_2$ fold changes$\geq$2xSD) and 92 proteins down-regulated ($\log_2$ fold changes$\leq$-2xSD) (fig. 3.38B). As expected, the correlation between mRNA and protein levels for single genes/proteins was rather low (R^2: 0.2, correlation not shown). However, GO and pathway enrichment analysis resulted in similar terms as for the transcriptome analysis, e.g. "cell cycle" (Reactome pathways, FDR: 0.0059) and "chromatin binding" (Sb, GOMF, FDR: 0.0138) were significantly enriched. In the set of differentially regulated proteins, several proteins have been previously associated with HIV-1 infection and replication according the NCBI HHID [36]. As examples, EP300, *Rac GTPase activating protein 1* (RACGAP1), *ubiquitin conjugating enzyme E2C* (UBE2C), *3-hydroxy-3-methylglutaryl-CoA synthase 1* (HMGCS1), *heterogeneous nuclear ribonucleoprotein U* (HNRNPU) or *dead box helicase 5* (DDX5) were down-regulated or *bromodomain containing 2* (BRD2) was up-regulated upon Sb-treatment (fig. 3.38C). Moreover, a large number of the differentially regulated proteins could be clustered in functional protein-protein networks using the STRING database [239].

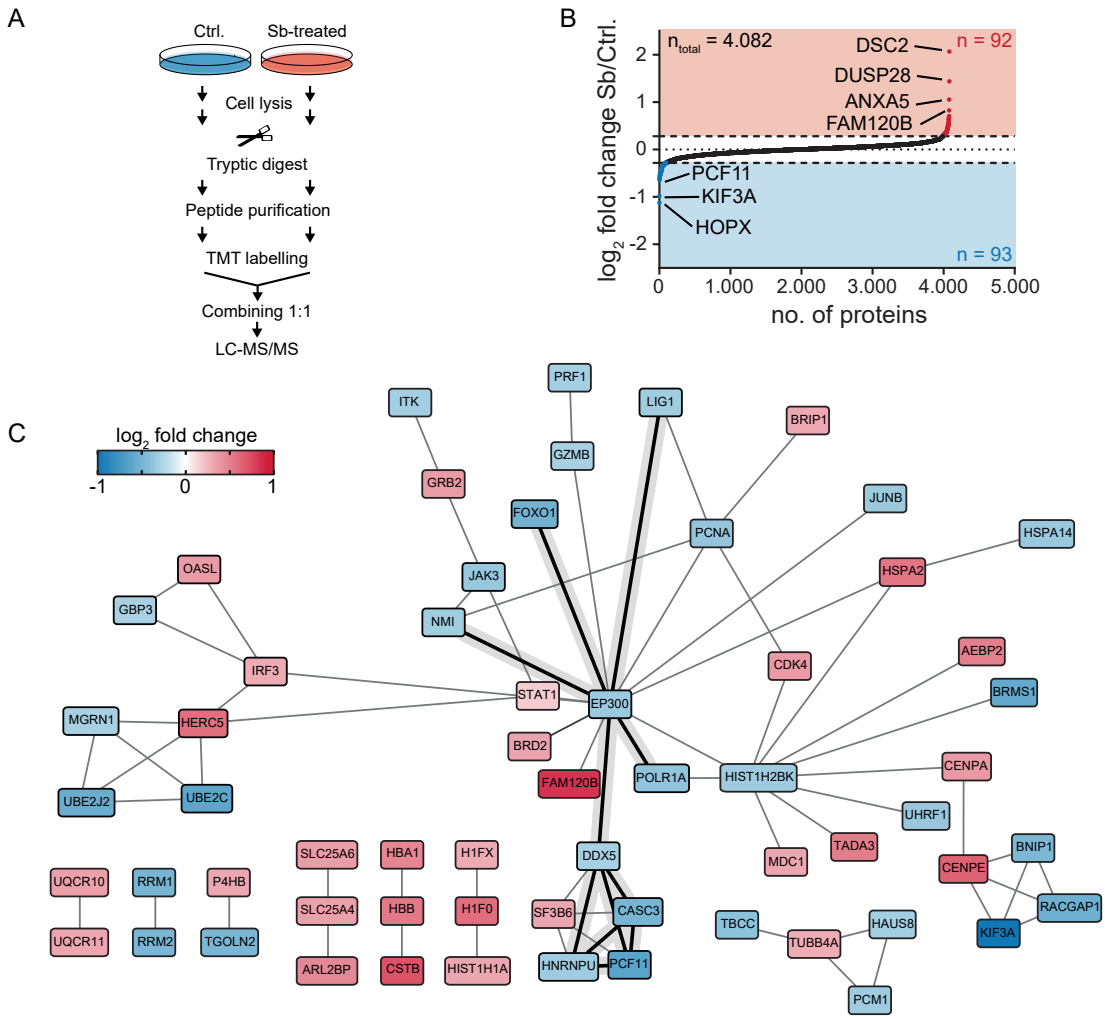

Figure 3.38. Proteomic analysis of sodium butyrate (Sb)-treated CD4$^+$ T-cells. (A) Schematic illustration of the preparation of Sb-treated cells for MS-based proteomic analysis. CD4$^+$ T-cells were treated with Sb for 48 h, lysed and, subsequently, proteins were subjected to trypic digest. Derived peptides from the treatment and control condition were purified, labeled with isobaric TMT-tags, mixed in an 1:1 ratio and analyzed by LC-MS/MS. **(B)** Dotplot of identified proteins and associated changes in protein abundance upon Sb-treatment in comparison to the control condition. Red area marks the cut-off for up-regulation (log_2 fold changes$\geq$2xSD), blue area mark the cut-off for down-regulation (log_2 fold changes$\leq$-2xSD). Numbers (n) of regulated proteins are indicated on the upper (up-regulated) and lower (down-regulated) right corner of the plot. Protein with large changes in abundance are indicated by the respective gene name. **(C)** Functional interaction network of differentially regulated proteins in Sb-treated cells. Network analysis was performed using the STRING database and network visualization was performed via Cytoscape [240]. The color code displays changes in protein abundance. Connected proteins, which were down-regulated at protein but not at mRNA level are highlighted with bold black edges.

4. Discussion

4.1. A novel database for PTM regulated HIV-1-host interactions

Successful HIV-1 replication is highly dependent on the host cellular machinery. Cellular proteins have to be exploited for the production of viral progeny and host factors with anti-HIV activity have to be overcome. HIV-1 encodes for a set of regulatory and accessory proteins to establish an viral replication favoring environment for its own replication and to enable immune escape. Multiple cellular pathways are modulated by HIV-1 during its replication cycle. Thereby, PTMs of viral and host proteins have gained growing attention in the regulation of any step of the viral replication process. To date, large data sets mainly from multi-omics screens reported 2910 HIV-1-host interactions [271] in total, summarized in public databases such as the NCBI HHID [36], VirHostNet [272] and Viruses.STRING [273]. However, a comprehensive overview of PTM-based HIV-1-host-interactions has been missing so far.

Consequently, a hand-curated database summarizing current knowledge of phosphorylation-, acetylation- and ubiquitination-regulated processes during HIV-1 infection was established. Notably, the constructed database involved also interactions described by system-wide mass spectrometry approaches [37, 274] and genome-wide screens [275, 276], that still require experimental confirmation.

Nevertheless, the newly generated database provides a comprehensive overview of PTM-based HIV-host interactions for the first time and thus will provide a solid basis for further research. The database facilitates cross-analysis, comparison with previous findings and studies of less explored areas such as the role of combinatorial PTMs known as "PTM crosstalk" [277] in regulation of protein function and disease progression. Therefore, it is expected, that the curated data sets will support scientists in HIV-1 research or other related fields. Due to the broad role of PTMs during HIV-1 replication, it is very likely, that further interactions will be discovered in future and the database has to be updated with new findings. Implementation of a public platform in the future, similar to Viruses.STRING [273], might be helpful to share the database for PTM regulated HIV-1-host interactions across the scientific community.

4.2. Time resolved analysis of the proteome in HIV-1-infected CD4$^+$ T-cell

4.2.1. Optimized HIV-1_{NL4-3} infection conditions for MS-based proteomic analysis

HIV-1 have to effectively re-program host cellular pathways to replicate and to escape immune defenses. However, studies disclosing quantified HIV-1-host interactions with temporal resolution are still lacking. To elucidate molecular mechanisms during acute HIV-1 infection using MS-based bottom up proteomic approaches, large quantities of HIV-1-infected cells were required to achieve sufficient proteome coverage. In particular for high PTMome coverage analysis, sufficient input material (cell lysate with ca. 7.5 mg protein) had to be ensured [278]. Assuming that 10 million T-cells are required to generate cell lysates containing 1 mg protein, ca. 75 million HIV-1-infected T-cells would be required. However, as determined in standard infection assays using HIV-1_{NL4-3} and HIV-$1_{NL4-3-IRES-GFP}$ in human primary activated CD4$^+$ T-cells (fig. 3.2B), cell lysate from <15% infected cells would be insufficient for high proteome/PTMome coverage analysis.

With this background, three parameters of infection assays were evaluated and optimized to generate large quantities of HIV-1-infected cells: The choice of (i) virus, (ii) inoculation mode and (iii) cell system. First, the full length, replication-competent HIV-1_{NL4-3} strain was preferred over GFP reporter HIV-1 to resemble more closely the "wild type" HIV infection scenario. Second, spin-infection was applied to induce actin activity in target cells resulting in up-regulation of CD4 and CXCR4 and, thereby, increasing likelihood of HIV-1 binding and entry [31]. The use of spin-infection improved infection efficiencies (48 h p.i.) remarkably in primary activated CD4$^+$ T-cells and in T-cell lines such as Jurkat-E6 or SupT1.CCR5 cells (fig. 3.3). Last but not least, in contrast to primary activated CD4$^+$ T-cells, infection of T-cell lines such as Jurkat-E6 cells did not suffer from donor variabilities and was more cost-efficient. Moreover, Jurkat-E6 cells maintained their viability despite spin-infection, in contrast to SupT1.CCR5 cells, in which spin-infection was not well-tolerated (fig. 3.3C and D). Using an optimized spin-infection system in Jurkat-E6 cells, 90-100% infection efficiency (assessed by p24 staining) was achieved after 48 h enabling time- and cost-efficient generation of HIV-1_{NL4-3}-infected input material for proteome/PTMome analysis.

After optimization of different parameters of the infection assays, the time (exposure of cells to virus) was considered. Classic HIV-1 infection assays based on GFP reporter genes or staining of HIV-1 capsid protein p24 were performed for at least 48 h. However, one complete HIV-1 replication cycle is described to take approximately 24 h [230]. For the monitoring of early infection stages below 24 h, a sensitive detection method had to be established. Earliest GFP expression in Jurkat-E6 cells spin-infected with reporter virus HIV-$1_{NL4-3-\Delta Nef-GFP}$ was detectable by flow cytometry from 12 h p.i. onwards (fig. 3.4D), however, earlier time points

could not be covered due to the dependence on GFP expression. In contrast, intracellular p24 staining and subsequent flow cytometry analysis enabled sensitive detection of infected primary cells or T-cell lines from 4 h p.i. onwards and progressing infection could be monitored by the increase in p24-positive cells (fig. 3.4A). The cell treatment with fusion inhibitor T-20 or anti-CD4 antibodies confirmed the specifity of p24 staining for the detection of successful CD4 receptor-dependent virus-cell-fusion events (fig. 3.4B, supplemental fig. S1). Moreover, trypsination of cells, which were shortly incubated with virus (4 h), corroborated the specific staining of intracellular p24 after successful virus entry (fig. 3.4C). However, in order to define infected cells, it was important to differentiate successful virus-cell-fusion events from productively infected cells (resulting in the replication of virus progeny). It is assumed, that, not all p24-positive cells indicate productive HIV-1 replication due to post-entry antiviral restriction mechanisms by the host cell, defects during reverse transcription leading to abortive infection or the establishment of latent infection [279]. This assumption was corroborated by the relatively slow increase of p24-positive cells measured by flow cytometry (fig. 3.4B) and viral proteins measured by LC-MS/MS (e.g. *env* and *gag*, fig. 3.5E) from 4 to 24 h p.i.. Therefore, it should be noted, that the input virus was very likely responsible for the strong increase p24-positive cells (fig. 3.4B) and *env*-/*gag*-encoded proteins observed at the 4 h time point.

Nevertheless, successful virus-fusion events could be detected by p24 staining and subsequent flow cytometric analysis enabled the monitoring of different HIV-1 infection stages. Even if not every positive virus-fusion event lead to productive HIV-1 infection, it was anticipated, that the presence of viral proteins in the cell alone is sufficient to trigger HIV-1-associated host responses as observed in the subsequent whole proteome study in HIV-1-infected CD4$^+$ T-cells (fig. 3.5).

4.2.2. Dynamics of HIV-1 proteins

In this whole proteome study, time courses of HIV-1 proteins encoded by *env*, *gag*, *pol* and *nef* (fig. 3.5E), as well as host proteins (fig. 3.5D and 3.7B), were acquired in a CD4$^+$ T-cell context infected by a full length, replication competent HIV-1 strain for 24 h. Viral time courses provided details about the HIV-1 protein dynamics (fig. 3.5E). Proteins encoded by *env* and *gag* showed steady increase peaking from 12 h p.i. onwards, indicating the entry of input virus (0-4 h, as discussed in section 4.2.1) and the start of virus production (12-24 h). Interestingly, the time course of *pol* showed early peaking at 4 h p.i. suggesting an early increased activity of RT and IN during reverse transcription and integration of viral transcripts. In contrast, Nef's time course was more fluctuating, suggesting early expression within 8 h p.i. and so far unknown mechanism of Nef degradation at 12 h. These HIV-1 proteome dynamics showed high correlation with several time resolved HIV-1 transcriptome studies [230, 280, 281] confirming the findings in this thesis.

4.2.3. Dynamics of the host proteome

The omics-approach allowed continuous surveillance of more than 4000 proteins during infection, whereby 987 HIV-1-dependent changes were identified in infected CD4$^+$ T-cells. While general trends of stable, increasing or decreasing abundancies of proteins could be detected, an overall drop of significant changes at 8 h p.i. was observed. This suggested a categorization of proteome changes in response to either early infection phases (4-8 h) from viral entry, reverse transcription to integration or late phases (12-24 h) linked to HIV-1 gene expression, assembly and release [230] (fig. 3.7B). Many changes occurred during the early stage (fig. 3.7B), demonstrating the ability of HIV-1 to rapidly exert broad-range remodeling of the host environment.

The analysis of time courses of single proteins provided new insight into the respective dynamics during HIV-1 infection. For example, VHL, part of the von Hippel-Lindau ubiquitination complex, was found to be down-regulated early (fig. 3.7B) and was associated with IN degradation, which has been described to be necessary for proper transition between integration and transcription of the viral genome [127]. Since VHL down-regulation and up-regulation of *pol*-encoded proteins (fig. 3.5E) occurred nearly at the same time, VHL down-regulation might be part of an anti-viral host mechanism, which is so far unknown, to decelerate virus replication. An example of late up-regulation was indicated by MIF (fig. 3.7B), which is a pro-inflammatory cytokine, that has been reported to be elevated in the plasma of HIV-1-infected patients and is considered to up-regulate HIV-1 replication [282]. Moreover, high MIF levels have been associated with severe bacterial sepsis, which is a major cause of mortality in HIV-1 patients [283, 284]. Therefore, elevated MIF levels might contribute to increased susceptibility of HIV-1-infected individuals to sepsis. Anti-MIF antibodies as well as ISO-1, a compound targeting the tautomerase activity of MIF, have been shown to protect from sepsis and their therapeutic implication might also be relevant in HIV-1-associated severe sepsis [285, 286]. Proteins with "peaking" dynamics, exemplified by NFIP1 and others (fig. 3.7B), suggested time-specific responses, which had to be further evaluated. In the case of NFIP1, it was conceivable that higher levels of NFIP1 might benefit HIV-replication during early phases by activating the NF-κB signaling pathway [287, 288] until down-regulation by negative feedback loops, which has to be further investigated for more details.

4.2.4. Dynamics of host phosphoproteome and acetylome

Targeting PTM regulated pathways is another mechanism, by which HIV-1 is able to change the host environment in favor of its own replication [40]. In this study, over 2800 phosphorylation sites and over 200 acetylation sites were quantified in a time resolved manner (fig. 3.5C). Most HIV-1-dependent changes in the phosphoproteome and in the acetylome were found at later stages of HIV-1 infection (12-24 h) propably in response to post-integration events (ca. 8 h p.i. [230]). In the case of the regulated phosphoproteome, measured changes

in response to HIV-1 infection were largely confirmed by a recent HIV-1-phosphoproteomic study by Johnson *et al.* [231] (fig. 3.6A and B), that was conducted with an Env-deficient, VSV-G pseudeotyped HIV-1 in Jurkat T-cells in a similar 24 h set-up. Most of the determined regulated PTM sites have not been linked to HIV-1 infection according to the NCBI HHID [36], making these findings to a valuable resources for further research. For example, phosphorylated EP300 at S2309 was found to be down-regulated (fig. 3.7C) during late stages. EP300 has been known to acetylate HIV-1 Tat, thereby, co-activating HIV-1 gene expression [151]. Phosphorylation of EP300 by CDK1 and ERK1/2 has been associated with its reduced stability during mitosis [289]. Therefore, the down-regulation of phosphorylated EP300 at S2309 might be linked with increased stability and co-activating activity, which has to be further evaluated. Another example is the increase in E3 ubiquitin ligase TRIM33 acetylated at K254 (fig. 3.7D). TRIM33 has been described as major determinant of HIV-1 IN stability and to block viral gene expression. However, further research is required to investigate the potential link between acetylated TRIM33 and IN degradation.

Findings with regard to HIV-1-dependent changes in the host phosphoproteome and acetylome were limited in this first study probably due to low PTMome coverage. It is likely, that high PTM coverage require much more input material than expected for the investigation of HIV-1-dependent changes. The use of spike-in SILAC standard prepared from Jurkat-E6 cells and HEK293T cells might also contribute to low PTMome coverage, since the increased sample complexity correlates with higher complexity of the MS spectra resulting in lower numbers of identified sites due to re-sequencing of peptides in the different SILAC states [290]. Moreover, incomplete time courses arose from missing matching peptide pairs (SILAC heavy-to-light ratios) in one of the five time points, resulting in reduction in the depth of analysis.

To address these issues, one could consider the use of VSV-G pseudotyped HIV-1 for infection to generate input material, while accepting VSV-G mediated viral entry through endocytosis, which is different from HIV-1 Env mediated entry [291]. Therefore, results based on an endocytotic entry model of HIV-1 would have to be interpreted with caution. Another option could also be the engineering T-cell lines with higher HIV-1 susceptibility e.g. by overexpression of HIV-1 co-receptors to generate input material of higher quality. In this case, finding the balance between increased HIV-1 susceptibility and tolerable cell loss/death due to accelerated infection progression [292] might be challenging. Optimizing large-scale methods for the specific enrichment of modified peptides, in particular acetylated peptides, would also increase PTMome coverage and depth of analysis. One could also consider TMT labeling for the quantification of PTM sites, since sample complexity would be reduced and the risk of missing matching peptide pairs is significantly lower as shown in this study (fig. 3.5C and D). However, quantification of acetylated peptides using the TMT labeling approach could be at the expenses at lower number of identified acetylation sites, since the amine-reactive chemistry of the isobaric tages requires free lysine residues for labeling. Nevertheless, it

has been shown, that acetylome profiling is compatible with TMT labeling [48] suggesting an alternative quantification approach to the SILAC spike-in approach as performed in this study.

4.2.5. Explorative analysis of HIV-1-dependent changes in cellular signaling pathways

To gain more time resolved insights of biological consequences of HIV-1-dependent changes, KEGG pathway enrichment analysis was performed, which revealed early remodeling of the host pathways associated with pathogen infection (fig. 3.8, 4 h). Interestingly, proteins of the RIG-I-like receptor signaling pathway (supplemental fig. S5) as well as several metabolism-associated pathways such as glycolysis (supplemental fig. S4), were found to be disregulated early. Early induced changes in the RIG-I-like receptor signaling pathway suggest rapid suppression of hyperresponse to viral RNA e.g. by overexpression of ATG12, a negative regulator of innate antiviral immune response [236], and down-regulation of TBK1, an activator of IRF3/IRF7-mediated interferon induction [237]. In the case of HIV-1-dependent changes in cell metabolism related pathways, up-regulation of key enzymes of the energy releasing phase of glycolysis (e.g. GAPDH, PGK, ENO3) (supplemental fig. S4) suggest rapid hijacking of the host energy supplies to fuel HIV-1 protein expression. Interestingly, enhanced aerobic glycolysis has been correlated with declining cognitive status in patients with persistent HIV-1 infection [293, 294], which is also in line with the HIV-1-dependent changes in mechanisms related to neuronal degeneration identified in this study (fig. 3.8). Based on these findings of enhanced aerobic glycolysis during HIV-1 infection, one could suggest the implication of carbohydrate-free or ketogenic diet complementing ART to mitigate HIV-associated neurocognitive disorder. Clearly, further research is required to address the impact of diet on HIV-associated neurocognitive disorders.

Changes in the metabolic control is also linked with changes during cell proliferation [295]. During late phases of HIV-1 infection, the KEGG pathway "cell cycle" was highly disregulated (fig. 3.8B and 3.9A). In particular, proteins assigned to G2 or M phase were found to be highly up-regulated. In the context of HIV-1-induced cell cycle disruption, HIV-1 Vpr has been shown to induce G2/M arrest and apoptosis, which is thought to benefit viral proliferation and enable immune escape [199]. This Vpr-mediated G2/M arrest has been described to be dependent on the activation of the ATR DNA damage response pathway [200]. Proteins downstream of the ATR DNA damage response pathway such as *serine/threonine-protein kinase Chk1* (Chk1), CDK1 and Wee were found to be strongly up-regulated through the entire HIV-1 time course (fig. 3.9A). In the process of G2/M arrest, phosphorylation of Chk1 induces Wee-mediated phosphorylation of CDK1, resulting in its inactivation [296]. Considering HIV-1-dependent changes in the phosphoproteome in the KEGG pathway "cell cycle" (fig. 3.9A), late decrease (12-24 h) in phosphorylated CDK1 (fig. 3.9B) was observed suggesting a potential counter

response to the early Vpr-induced G2/M arrest. This counter mechanism might involve *M-phase inducer phosphatase 1, 2* and *3* (CDC25A, CDC25B, CDC25C), which remove inhibitory phosphorylations of CDK1 [297–299]. Interestingly, Vpr-associated degradation of CDC25B and CDC25C have been described [199, 300] suggesting a time-dependent fine-regulation of G2/M arrest by Vpr. Clearly, further experiments are required to elucidate the detailed modes of action.

4.2.6. HIV-1-associated kinase-substrate relationships

The comprehensive analysis of HIV-1-dependent changes of cellular signaling pathways highlighted the importance of understanding HIV-1-associated kinase-substrate relationships. The phosphosite motif enrichment analysis (fig. 3.10A) suggested increased activity of casein kinase II (CK2), G protein-coupled receptor kinases and kinases with 14-3-3-domains during early HIV-1 infection stages. In the following, findings with regards to CK2, as an example, will be further expanded. CK2 has been reported to phosphorylate cellular proteins involved in HIV-1 transactivation [301] and stimulate HIV-1 PR and RT [302]. Differentially up-regulated and known CK2-targeted phosphorylation sites of two proteins, *uracil-DNA glycosylase* (UNG) and *DNA ligase 1* (LIG1) were identified in this study (fig.3.10B). Phosphorylated UNG has been associated with high levels of HIV-1 Vpr expression and UNG incorporation into virions has been reported to positively influence HIV-1 infectivity [303–306]. Therefore, the findings suggest a potential link between HIV-1 Vpr and CK2-mediated phosphorylation of UNG, which has to be further evaluated. LIG1 has not been linked to HIV-1 infection so far. However, its involvement in the repair of viral integration intermediates was conceivable [307] and LIG1 activity might be regulated by CK2-mediated phosphorylation since phosphomutants of LIG1 have been shown to have impaired functionality in DNA replication and repair [308].
The phosphosite motif enrichment analysis (fig. 3.10A) also showed increased activity of several other kinases, such as *cAMP-dependent protein kinase A* (PKA) and *calcium-dependent protein kinase C* during the late stages of HIV-1 infection. Interestingly, enzymatically active PKA was found to bind to phosphorylated HIV-1 capsid protein p24, to be packaged into HIV-1 virions and important for optimal reverse transcription [309,310], which indicates early HIV-1 infection events. One could hypothesize, that PKA was overexpressed in post-integration phases, resulting in increased phosphorylated substrates and incorporation into newly synthesized virions.With regard to PKC, compounds modulating PKC activity have been identified as latency reversing agents by activating the NF-κB pathway [311]. Therefore, further investigation of substrates might elucidate mechanisms related to PKC-mediated latency reversal.
Moreover, the study of HIV-1-associated kinase-substrate relationships identified confirmed substrates of six kinases, MAP3K3, PKMYT1, WNK2, SRPK1, CLK1 and CLK2, which have not been linked with HIV-1 infection themselves (fig.3.10B). MAP3K3, PKMYT1 and

WNK2 have been associated with cell cycle regulation or immune response [312–314], whereas SRPK1, CLK1 and CLK2, have been related to RNA splicing processes [315–317], suggesting these kinases as interesting subjects for further research on their impact on HIV-1 infection. Taken together, the time course analysis of HIV-1-dependent changes in the proteome, phosphoproteome and acetylome in this study provided a first draft of the dynamics in CD4$^+$ T-cells during HIV-1 infection. The data presented here facilitate the formulation of new hypotheses on modes of action, and the exemplified findings highlight the need for further time resolved investigations of PTM dynamics to understand critical signaling pathways during HIV-1 infection. The data resource provided in this study is anticipated to support the design of further validation experiments e.g. by immunoblotting, treatment with inhibitors or (conditional) knock-out/-down experiments in infected primary CD4$^+$ T-cells. For future time course analysis, quantification methods with increased level of sample multiplexing such as TMTpro 16plex (Thermo Fisher Scientific) might enable analysis of HIV-1-host interactions with higher temporal resolution. Details about the timing of certain host responses in combination with improved understanding of PTM-based mechanisms can support the optimization of anti-HIV-1 treatments and the identification of HIV-1 vulnerable nodes in order to develop novel treatment strategies.

4.2.7. Temporal proteomic analysis of HIV-1 infection using HIV-1-GFP reporter virus

In addition to the time course analysis in CD4$^+$ T-cells, that were infected with the full length, wildtype HIV-1 lab strain HIV-1$_{NL4\text{-}3}$, another time course analysis using the HIV-1 GFP reporter lab strain HIV-1$_{NL4\text{-}3\text{-}\Delta Nef\text{-}GFP}$ was performed. As discussed in section 4.2.1, ongoing HIV-1 replication was monitored first time by intracellular p24-staining of infected cells only. While this indicated successful fusion of viral particles with the host cell, no information could be determined about productive HIV-1 replication. Thus, a GFP reporter virus was used in a second experiment, which allowed the determination of 67% infected, GFP-positive cells with productive HIV-1 replication 48 h p.i. (fig.3.4D). However, the time frame needed to be extended to 48 h to yield sufficient GFP expression. As a consequence, host responses might be triggered also by a second round of infection with newly produced virus, which needed be considered for data interpretation. Overall, the data from the HIV-1$_{NL4\text{-}3}$- as well as the HIV-1$_{NL4\text{-}3\text{-}\Delta Nef\text{-}GFP}$-time course were comparable in terms of numbers of identified proteins 3.11A), temporal progression of HIV-1 proteins (fig. 3.11B) and tendencies of regulated host proteins as exemplified for the KEGG pathway "cell cycle" (fig. 3.12). However, the dynamic range in the HIV-1$_{NL4\text{-}3\text{-}\Delta Nef\text{-}GFP}$-time course was not as large as in the HIV-1$_{NL4\text{-}3}$-time course, which might be partly explained by the absence of the viral accessory protein Nef. Nef plays an important role in the establishment of full HIV-1 virulence *in vivo* [14, 15]. Nef-defective viruses have been reported to show reduced pathogenic potential when compared

with the wild-type strain [318–321]. Therefore, the host responses to HIV-$1_{NL4\text{-}3\text{-}\Delta Nef\text{-}GFP}$ might be more attenuated compared to the wild-type strain.
Overall, the use of HIV-$1_{NL4\text{-}3}$ for time course analysis provided several advantages compared to the use of HIV-$1_{NL4\text{-}3\text{-}\Delta Nef\text{-}GFP}$. Besides of the monitoring of ongoing HIV-1 infection within a single round of HIV-1 replication as discussed in section 4.2.1, the proteomic analysis of infected CD4$^+$ T-cells showed also a larger dynamic range in the host responses. Nevertheless, the additional time course with HIV-$1_{NL4\text{-}3\text{-}\Delta Nef\text{-}GFP}$ corroborated the findings in the HIV-$1_{NL4\text{-}3}$-time course experiment. Moreover, the comparison of the two time courses supports the role of the viral protein Nef in enhancing HIV-1 disease progression. Future time-dependent proteomic studies of Nef-dependent host responses with higher resolution will help to elucidate the mechanistic details of the effect of Nef on HIV-1 infectivity and intracellular replication.

4.3. MS data analysis workflow for visualization of quantified changes in signaling pathways

Recently, the amount of biological data has been ever-expanding and, therefore, computionally supported analysis has become an vital tool for exploratory data analysis. Different from confirmatory analysis, which is based on the testing of pre-formulated hypotheses, exploratory data analysis involves a broader investigation, focusing on finding the right questions rather on the right answers [322]. In combination with effective data visualization, exploratory data analysis is able to guide and shape scientific discovery to support formation of new ideas and design of experiments [323]. For the study of biology, pathway maps have become helpful tools for the analysis of biological data sets and understanding of underlying molecular processes. In comparison with single gene-based approaches, pathway-based approaches have been widely used in the analysis of omics high-throughput data sets [323, 324]. However, pathway-based data integration of proteome/PTMome dynamics or visualization of time courses requires complex algorithms for data processing and transformation and the implementation is still challenging for scientists with low bioinformatic background.

Here, an R-scripted data analysis workflow for MS quantitative data from label-free, TMT or SILAC experiments was established (see section 3.6). The scripted algorithm enables fast and reproducible downstream data processing/transformation of MaxQuant evidence tables into structured formats required to apply functions from (i) the Proteus package [221] for peptide/protein intensity aggregration and normalization, (ii) from the ClusterProfiler package [223] for GO term/KEGG enrichment and (iii) from the Pathview package [224] for data visualization and graphical rendering of signaling pathways (fig. 3.14). Examples of rendered pathway maps were shown in fig. 3.9, supplemental fig. S3, S4 and S5.

Since R is an open-source programming language, the scripted code is accessible and available for anyone with basic R skills - without the need for a license or a fee, independent from the platform (Windows, Linux, Mac). The workflow was coded in a modular and comprehensible manner, that on the one hand is easy to apply for users unexperienced in MS related bioinformatics, on the other hand can be still customized to the needs of more experienced MS data analysts. Functions for high quality plotting and graphing are also implemented within the workflow enabling fast visualization of changes in the proteomic landscape. In particular, the mapping of quantified changes with temporal resolution into KEGG pathways supports data interpretation in a biologically relevant context. Moreover, the workflow facilitates fast reports at any stage of the analysis, e.g. boxplots of peptide intensities in different conditions before/after normalization and interactive Shiny web apps, e.g. to identify strongly upregulated PTM peptides with Uniprot annotated function of the corresponding protein in Vulcano plots. The established algorithm is anticipated to help scientists to perform high-throughput data analysis of qualitative and quantitative MS data. It serves as an alternative or as complementation to Perseus, which is a commonly used

computational platform for MS data [214]. Apart from the application for proteomics data, the algorithm can be also easily adapted to process other types of omics data e.g. genomics and transcriptomics analysis.

Nevertheless, usage of the established workflow still requires experience in R programming, since R is a command line driven program. Moreover, data visualization with functions provided by Pathview are limited to collection of pathway maps of the KEGG database [242]. Hitherto unknown pathways or new molecular mechanisms are difficult to address by the KEGG pathway mapping function. Apart from the restriction to KEGG pathways in the mapping function, another issue emerged in the analysis at PTM level. Implementation of quantified PTM site information into KEGG pathways maps have been proven to be difficult, since multiple PTMs can occur on multiple sites within the same protein or even within the same peptide at different amino acid positions (PTM multiplicity). Despite of PTM multiplicity, a database providing cellular pathway maps, including known regulatory PTM sites of relevant proteins, does not exist so far. To handle cases of PTM multiplicity, the algorithm selects species of modified peptides of highest intensities or calculates the median intensity of all identified PTM sites for protein aggregation. However, selecting sites of highest intensity might neglect PTM sites resulted from transient/weak interactions with PTM enzymes or overestimate the effect of one regulated PTM site. The alternative option using the median intensity of all identified PTM sites for protein aggregation, in turn, might lead to underestimation the effect of biological relevant regulatory PTM sites. These are two aspects, users of the established algorithm have to be aware of during PTM analysis. In order to fulfill the full potential of this worfklow, PTM databases have to grow. For phosphorylation in human cells, PhosphoSitePlus [238] provides already an valuable knowledgebase. However, annotation of regulatory sites and site specific information are still lacking, in particular for acetylation targets. With increasing number of identified PTM sites and crosscorrelations of databases, the established data analysis workflow is anticipated to enable multi-omics approaches to provide an holistic view not only of molecular mechanisms during HIV-1 infection but also other severe diseases.

4.4. Changes in the host acetylome upon HIV-1 infection

A growing body of work has emphasized the importance of alterations in protein acetylation during infection with HIV-1 [75, 147, 148, 154, 243, 245, 246]. It has become clear, that both, cellular and viral proteins, are modified by lysine acetylations, and that these PTMs contribute to core host defense and virus replication processes [40]. Further investigation of the extent of protein acetylation events during HIV-1 infection can provide an important new perspective on the intricate mechanisms underlying the biology and pathogenesis.

In this study, the first draft of the quantified global acetylome in HIV-1 infected $CD4^+$ T-cells was provided (fig. 3.13). Among the observed changes in the host acetylome, lysine acetylation sites of histone proteins, e.g. H2B and H1, were found to be mainly down-regulated at 48 h p.i.. In the time resolved acetylome analysis (fig. 3.7D), down-regulation of acetylated H2B, that started already within 24 h p.i., was also reported. In general, acetylation of the core histone proteins, H2A, H2B, H3, and H4, have been described to result in destabilization of the DNA/histone interactions and increases accessibility of the local DNA [325, 326]. Consequently, the observed decrease of acetylated H2B or H1 proteins is associated with suppressed gene expression, which might be reflected also by the decelerated increase in GFP-positive cells at the 48 h time point in comparison to the 24 h time point (fig. 3.4D).The down-regulation of H2B acetylation at K6 might be linked with increased HDAC activity and HIV-1 latency establishment by reduced chromatin accessibility at the viral LTR promoter over time, that can be reverted by pharmacological perturbations using HDAC inhibitors as shown in several studies [75,175,176,178,183,327]. Interestingly, adjacent H2B acetylation at K5 has been associated with higher gene expression [326], which implied a similar relationship for H2B acetylation at K6. Clearly, this has to be experimentally confirmed, since histone deacetylation is correlated with gene silencing in general, however, studies of single deacetylated sites have also shown to enhance gene expression [328,329]. In the case of H1, H1 has been reported to be deposited onto unintegrated, extrachromosomal HIV-1 DNA early after infection, which has been linked with transcriptional silencing in the presence of the posttranslational histone modifications characteristic of inactive chromatin [330]. Loading of histones onto newly synthesized viral DNA might transcriptionally block the initiation of infection by invading viruses - a system, that has been already described to act against murine leukemia viruses (MLV) [331], herpes viruses [332] and adenoviruses [333]. Nevertheless, the role of H1 acetylation (as suggested at K21 in this study) in this mechanism needs further research.

Apart from from histone modifications, down-regulation of acetylation on non-histone proteins was observed. This is exemplified by key enzymes of the energy releasing phase of glycolysis such as *phosphoglycerate kinase 1* (PGK1) and *glyceraldehyde-3-phosphate dehydrogenase* (GAPDH) (fig. 3.13). Interestingly, acetylation of GAPDH and PGK1 by PCAF has been linked with increase glycolytic activity [334] and HIV-1 up-regulation of these enzymes was also observed in the time resolved proteome analysis in infected $CD4^+$ T-cells (supplemental

fig. S4). Therefore, the decrease in acetylated GAPDH and PGK at the 48 h time point might be explained as counter measure by the host cell to restrain the energy supply to fuel HIV-1 protein expression. Interestingly, a recent study has shown a relationship between host metabolic state and the likelihood for virus-cell fusion in $CD4^+$ T-cells, which were treated with glycolysis inhibitor 2-deoxyglucose and , as a result, become resistant to HIV-1 infection [335]. It is also conceivable, that a higher energy requirement due to HIV-1 infection caused a reduction in the pool of acetyl coenzyme A and, consequently, decreased non-enzymatic (unspecific) acetylation by acetyl coenzyme A.

The examples of proteins with changed acetylation profile demonstrated the relevance of studying the acetylation landscape in HIV-1-infected $CD4^+$ T-cells. The whole acetylome study complemented findings of the time course analysis of the proteome in HIV-1-infected $CD4^+$ T-cells and provided reference points for further research.

4.5. Functional analysis of acetyl-acceptor lysines in HIV-1 Tat

4.5.1. Impact of acetylation sites on HIV-1 Tat's LTR transactivation ability

The HIV-1 encoded Tat protein is an essential viral factor, regulating processive transcription from the HIV-1 LTR by controlling transcriptional elongation of viral transcripts by RNA polymerase II (RNAPII) [336]. Tat binds to the HIV-related RNA stem loop structure, encoded by the transactivation responsive region (TAR), and recruits the P-TEFb complex, consisting of CDK9 and CCNT1 [136]. CCNT1 improves the Tat-TAR RNA interaction and CDK9 phosphorylates RNAPII, thereby, increasing the rate of transcriptional elongation of viral transcripts [337–339]. Apart from kinases such as CDK9, Tat-associated lysine acetyltransferases (KATs) and deacetylases (KDACs or HDACs)/sirtuins also play multiple roles during HIV-1 gene expression. These Tat-regulated KATs and KDACs/sirtuins do not only remodel the chromatin organization at the site of the viral promotor [340], Tat itself has at least two acetyl-acceptor lysines [243], K28 and K50/51, that are targeted by KATs and KDACs. Acetylation related enzymes, that act on these sites, include KAT2B (also known as PCAF) [150, 152, 245], EP300 [150, 245, 246], KAT2A (also known as GCN5) [154] and HDAC6 [153] (fig. 3.15A). While many studies demonstrated, that Tat acetylation, regulated by the exemplified KATs and KDACs, plays an important role in HIV-1 gene expression in general, little is known about the impact of site specific acetylation on Tat's transactivation ability and the course of HIV-1 infection.

Therefore, Tat expressing constructs, mimicking either an permanently acetylated (K-to-Q subsititution) or deacetylated state (K-to-R substitution) at K28, K50, K51 and K50/51, were designed and used for different HIV-1 LTR transactivation studies (section 3.7.2, fig. 3.22). In concordance with other studies of Tat mutants [150, 246, 341, 342], the transactivation ability of K28R, K28Q, K50Q, K51Q and K50/51Q were drastically reduced in transfected or transduced TZM-bl cells, which contain a luciferase reporter under the control of an integrated HIV-1-LTR [250–254]. In parallel, the respective K-to-R mutants showed comparable or slightly increased transactivation capability with Tat wt (fig. 3.19 A). In the direct comparison of K28R with K28Q, K28R was still able to maintain 40-65% of the transactivation capability relative to Tat wt. In general, the levels of reduced transactivation in the K-to-Q mutants were comparable with the respective K-to-A mutations mimicking removed acetyl-acceptor lysine residues. These results confirmed, that differential Tat acetylations at residues K28, K50, K51 and K50/51 exert large impact on HIV-1 LTR transactivation. Since the K-to-Q mutations behaved like the K-to-A substitutions, it is conceivable, that Tat with a mimicked acetylated state reduced LTR transactivation either due to decreased TAR RNA binding or impaired interactions/recruitment with transcription initiation or elongation associated factors.

After different HIV-1 LTR transactivation abilities were associated to the Tat mutants mimicking different acetylation states, the influence of the mutants on *de novo* HIV-1 infection in Jurkat-E6 cells stably expressing Tat wt or mutants was evaluated using HIV-$1_{NL4\text{-}3\text{-}IRES\text{-}GFP}$. For this experiment, it was assumed, that the overexpression of Tat in the T-cell lines outcompetes the Tat encoded by the infecting virus and is able to boost the expression of the reporter virus. As proof of principle, infection in Tat wt expressing cells was enhanced two-fold compared to control cells 24 h p.i. (fig. 3.20A). Interestingly all acetylation or deacetylation mockups for K28, K50, K51 and K50/51 except for K28Q, K50/51A and K50/51Q were able to retain 1.4 to 1.8-fold enhancement of infection. K28Q, K50/51A and K50/51Q did not show enhanced infection remarkably confirming their impaired functionality as observed in the transactivation assays in TZM-bl and J-Lat cells. In contrast to the assays in TZM-bl and J-Lat cells, the single K-to-A and K-to-R mutations at K28, K50 and K51 did not result in severe reduction of the infection-boosting effect. Since TZM-bl and J-Lat cells express reporter genes controlled by an already integrated HIV-1 LTR [168], the effects exerted by the mutants during the transactivation assays in these systems might be more direct and, therefore, more pronounced compared to the *de novo* HIV-1 infection assay. This assumption was also supported by the evaluation of virion production by HEK293T cells transfected with the respective Tat expressing constructs and a full length HIV-1 HXB2 ΔTat. This system was dependent on the activation of non-integrated HIV-1 LTR by Tat (fig. 3.21). These observations were in line with similar findings of Bres *et al.* [342], describing severely reduced transactivating ability of Tat K28R, K28Q and K50Q on integrated LTR in comparison to unintegrated LTR.

Nevertheless, through all tested systems, K28Q, K50/51A and K50/51Q showed dysfunctional activation of the HIV-1 LTR (fig. 3.22) emphasizing the importance of the acetyl-acceptor lysines K28 and K50/51 of Tat during HIV-1 replication. K28Q and K28R mutations have been described to exert intact interaction with TAR RNA [342], which suggests impaired Tat-TAR complex formation as reason for the HIV-1 LTR transactivation deficiency as shown in fig. 3.19 less likely. This implied, that the reduction in HIV-1 LTR transactivation due to mutations in K28 might be based on disregulated interactions with other proteins required for transcriptional elongation. In contrast, a weak interaction with TAR RNA has been described previously at least for K50Q, implying, that reduced transactivation ability in the case of K50Q, K51Q and K50/51Q, were due to disrupted complex formation with TAR RNA [342]. Since K28Q and K50/51Q were related with decreased HIV-1 LTR activation in this study, while Tat acetylation has been described to be critical during HIV-1 transcription [150–152, 246, 343], the findings in this study support the concept of (de-)acetylation regulated "Tat recycling" for multiple rounds of efficient HIV-1 transcription elongation [155, 343, 344].

4.5.2. Acetylation-dependent changes in the HIV-1 Tat-associated interactome

The Tat mutants mimicking a permanently acetylated state by K-to-Q mutations at K28 and K50/51 demonstrated their malfunction to activate HIV-1 LTR (fig. 3.22). Considering more than 180 known human host proteins, that directly bind/interact with Tat [36], the Tat-associated interactome was assessed by Co-IP and mutant specific changes were analyzed for K28 and K50/51 by label-free quantification (LFQ) via LC-MS/MS.

In every Tat expressing condition, significant enrichment of subunits from known Tat-associated complexes such as the P-TEFb complex (fig. 3.23C) or interactors linked to HIV-1 infection were observed, while the number of enriched non-Tat-related proteins (ca. 2%) from the control lysates was very limited suggesting a low risk for false-positively identified Tat interactors due to the high specificity of the Co-IP. However, the sensitivity for transient, weak interactions or proteins of low abundance might be limited in the used system indicated by the identification of numerous highly abundant constituents of ribosomal complexes (fig. 3.23C, fig. 3.24 and fig. 3.25). It has been described, that HIV-1 Tat is able to affect rRNA maturation and to control ribosome biogenesis [345, 346], which was also observed in this study. However, further analysis was focused on non-ribosome constituents, that are less characterized so far.

Considering constituents of the P-TEFb complex or the superordinate SEC, CDK9, MLLT1 and MLLT3 were not affected by any of the K-to-R or K-to-Q mutations at K28 or K50/51 suggesting, that their interaction with Tat is independent of these acetylation sites. Interestingly, CCNT1 was found enriched in K28R mimicking non-acetylated Tat compared to K28Q mimicking acetylated Tat at K28 (TatK28Ac) (fig. 3.25A). While acetylation at K28 by KAT2B (PCAF) has been described to enhanced binding to CDK9 or P-TEFb complex in general [150], the interaction of TatK28Ac with CCNT1 is less elucidated. The findings in this study suggested, that a disrupted interaction of TatK28Ac with CCNT1 contributed to the deficient HIV-1 LTR transactivation (fig. 3.22, K28Q), since it has been shown, that binding of Tat to CCNT1 is required for efficient transactivation of the HIV-1 LTR and that K28R as well as K28Q do not affect interaction of Tat with TAR-RNA [342]. Apart from CCNT1 as part of Tat-associated P-TEFb complex, several other HIV-1 infection linked proteins with different abundancies in K28R and K28Q were identified, e.g. virus restriction factor TRIM21 [347], which was enriched in K28Q. Interestingly, TRIM21 has been recently discovered as substrate of HDAC6 [348] and HDAC6 has been shown to deacetylate Tat at K28 [153]. The increased levels of TRIM21 in K28Q suggest a triggered intracellular innate immunity in the presence of TatK28Ac via TRIM21-mediated degradation of intracellular virus-antibody-complexes [347], which might correspond to the observation of reduced virus production in K28Q transfected producer cells (fig. 3.21). Therefore, a TatK28Ac induced recruitment of TRIM21 and/via HDAC6 exerting anti-viral effects is presumed here, which

requires clearly further investigation.
Different from the R/Q mutations at K28, CDK9 and also CCNT1 protein abundancies were not affected neither by K50/51R nor by K50/51Q (fig. 3.24B) concluding, that the mutations did not lead to disruption of the interaction between Tat and the P-TEFb complex. In conclusion, the impaired transactivation capability by K50/51Q mimicking acetylated Tat at K50 and K51 (Tat50/51Ac) could be very likely explained by disabled complex formation with the TAR RNA since K50Q as well as K50 acetylation by KAT2B (PCAF) have been reported to compromise Tat's binding to TAR RNA [342, 349]. Based on these findings, TatK50/51Ac by KAT2B might regulate controlled dissociation of Tat from the TAR RNA to be recycled for further rounds of HIV-1 transcription elongation. Nevertheless, several identified K50/51R-associated interactors might provide additional information of cellular processes induced by recruiting of certain host factors by Tat during HIV-1 replication. As an example in the set of proteins only identified in K50/51R mimicking non-acetylated Tat at K50 and K51 (TatK50/51), RNA helicase DDX24 (fig. 3.25B) has been reported to increase HIV-1 RNA packaging [350] and to interact with EP300 leading to suppressed EP300-mediated acetylation of p53 and, subsequently, induced cell cycle arrest and senescence [351]. Another host protein enriched in K50/51Q and linked to HIV-1 infection is FTSJ3 (fig. 3.25B), which mediates methylation of the HIV-1 genome, allowing the virus to escape the innate immune system [352].
Overall, the performed HIV-1 Tat interactome analysis based on mutants mimicking different acetylation states of Tat at the two acetyl-acceptor lysine sites K28 and K50/51 provide new evidences for acetylation-based fine-tuning of HIV-1 Tat's transactivational activity. Moreover, the study revealed HIV-1-associated protein-protein interactions, which have not been related to HIV-1 Tat acetylation so far and emphasized the importance of understanding the HIV-1-host acetylome. However, further validation studies e.g. by immunoblotting or (conditional) knock-out/-in will be required. Given the importance of Tat acetylation, further research of the HIV-1-dependent changes in the acetylome would likely resolve ambiguities in regards of HIV-1 replication and latency establishment. Moreover, conditional knock-out/-down of Tat-associated KATs/HDACs and analysis of the resulting changes in the interactome will provide additional insights about the role of Tat acetylation during HIV-1 pathogenesis.

4.6. Comprehensive evaluation of the function of HIV-1 Tat exon 2

HIV-Tat is encoded by two exons. Exon 1 corresponds to the N-terminal 72 amino acids and harbors Tat's activation domain (position 1 to 48), nuclear localization signal and the TAR RNA binding site (both position 49 to 57) [353–357]. Deletion of exon 2 has demonstrated, that exon 1 is sufficient for Tat's transcriptional function [248]. So far, HIV-1 replication supporting functions such as NF-κB-activation [358], repression of transcription of major histocompatibility (MHC) class I genes [359] and containment of interferon-stimulated gene (ISG) expression in antigen presenting cells enabling immune escape [360] have been associated with Tat exon 2. However, the function of the second exon as well as its mode of action is largely unexplored.

Therefore, the function of Tat exon 2 was comprehensively investigated using a deletion mutant of exon 2. Based on the transactivation assays in TZM-bl and J-Lat cells (fig. 3.19 C), Δexon2 maintained at least 60% of the transactivation capability of full length Tat. Moreover, Δexon2 was able to increase *de novo* HIV-1 infection in a T-cell line (fig. 3.20) and induce production of viral particles (fig. 3.21) to a comparable extent as full length Tat. This findings confirmed the sufficiency of exon 1 to transactivate HIV-1 transcription. Together with findings of other studies [358–360], it is likely, that the function of the second exon is linked with interaction of host proteins. The comparison of the interactome of Δexon2 and full length Tat showed, that CCNT1, ELL, AFF1 and AFF4 were more enriched in full length Tat than in Δexon2 (fig. 3.24C and fig. 3.25C) suggesting an decreased affinity of Δexon2 for these subunits of the P-TEFb complex or SEC. Therefore, exon 2 of Tat might be responsible for the stabilization of Tat's interaction with P-TEFb or SEC, that jointly drive transcription elongation and, thereby, optimize the transactivation capability of Tat. Moreover, the analysis also highlighted the importance of Tat exon 2 coordinated interactions with AFF1 and AFF2, since knock-out experiments of AFF1 and AFF2 have been described to diminish Tat transactivation [361]. Interestingly, non-P-TEFb/SEC-related proteins such as *probable ATP-dependent RNA helicase DDX5* (DDX5) were found to be enriched in the Δexon2 mutant (fig. 3.25C). DDX5 has been reported as co-factor enhancing HIV-1 replication and to promote nuclear export of viral transcripts in concerted action with HIV-1 Rev [362]. The increased DDX5 abundance in Δexon2 suggests the possibility, that the second exon is able to control DDX5/Rev-mediated transcript export to suppress Tat induced immune surveillance. As a matter of course, the dependency of these interactions on Tat exon 2 needs to be validated. However, the interactome analysis provided evidences of so far unknown relationships between Tat exon 2 and host factors for efficient HIV-1 transcription elongation and suggested further research of Tat exon 2 regulated HIV-host interactions.

Based on the immunoblot analysis of Δexon2 transfected HEK293T (fig. 3.16B) and stable transduced Jurkat-E6 cells (fig. 3.17B), remarkably lower protein abundance of Tat Δexon2

was observed in comparison to full length Tat-independent of the used cell system. Flow cytometric analysis of the BFP-MFI in Jurkat-Tat(Δexon2)-HA-T2A-BFP in comparison with full length Tat (fig. 3.18B) disconfirmed the possibility of restrictions at transcription level, since BFP-MFI in Tat Δexon2 expressing cells was not lower than in full length Tat expressing systems. However, the treatment of stable (Δexon2) expressing Jurkat-E6 cells with proteasome inhibitor MG-132 (fig. 3.26A) showed no rescue of Δexon2 to levels comparable protein levels as full length Tat, thereby, ruling out that Tat Δexon2 was subjected to proteosomal degradation. Another hypothesis of secreted Tat Δexon2 into the extracellular space evaluated by anti-HA antibody based enrichment of Tat-HA molecules from supernatant (fig. 3.26B) could also not be confirmed. As a consequence, the reason for the low abundance of Tat Δexon2 in comparison to full length Tat and its consequences on Tat transactivation remained unclear. Possible explanations, which need to be experimentally evaluated included lysosomal protein degradation or possible protease cleavage sites that become exposed in the absence of exon 2 due to steric effects.

Taken together, the comprehensive investigation of the function of Tat exon 2 revealed novel aspects into the multifaceted role of HIV-1 Tat including regulating its own transactivation capability and modulation of the host immune response. Based on the findings here, it is assumed, that the second exon is associated with even more so far undiscovered regulatory functions.

4.7. Latency reversing agents for reactivation of latent HIV-1 uncovered by epigenetic compound screening

Current ART is highly effective in the reduction of HIV-1 loads to undetectable levels in plasma allowing an almost normal life of HIV-1-infected patients. However, HIV-1-infected individuals have to commit to lifelong treatment, since ART does not eliminate latent cellular HIV-1 reservoirs. In addition, studies have shown, that, despite effective ART, HIV-1 replication can remain persistent in lymphoid tissue reservoirs under conditions, in which drug concentrations are too low to completely block virus replication [255,256]. Therefore, several trials have been performed to develop drugs, that are more effectively delivered to the site of viral replication and, in the same time, erase latent HIV-1 reservoirs for complete viral clearance. In the last years, especially the cellular mechanisms, which maintain HIV-1 latency, are attempted to be disrupted by pharmaceutical interventions with the idea to reactivate latently infected cells and sensitize them for immune cells and common ART (known as "shock-and-kill" approach) [363]. However, trials have not been clinically successful so far. Consequently, there is still a strong demand to identify either latency maintaining cellular factors or novel agents specifically targeting latent HIV-1 reservoirs.

Based on recent findings in regards of the relevance of PTMs (such as protein acetylation) for HIV-1 replication and latency [40], the aim of this study was to screen a library of epigenetic compounds for novel LRAs. For this purpose, a stable Jurkat-E6 based reporter cell line was established as latent reporter HIV-1 provirus model, which enables sample handling under biosafety level 1 conditions allowing more cost efficient high-throughput screenings. The primary screen in this cell system comprised titrations and determination of cell toxicity of each test substance and resulted in six compounds (10% of tested in total), which are able to activate the HIV-1 LTR-promotor in a concentration-dependent manner. For validation and for comparison with common latency cell systems, identified lead compounds were tested in J-Lat cells under biosafety level 3** conditions. The secondary screen in J-Lat cells mainly confirmed the results from the primary screen. The six lead compounds, namely vorinostat (SAHA), CI-994 (Tacedinaline), SR-4370, HPOB, CPI-203 and bromosporine, showed strong reactivation ability with low cellular toxicity in both cell systems. The analysis of GFP expression by fluorescence microscopy confirmed the the reactivation properties of the six lead compounds. Notably, in comparison to most of the lead compounds, GFP expression of HPOB treated cells was lower in intensity but more evenly distributed (fig 3.28D). Therefore, HPOB may target a wider range of latently infected cells compared to common class I HDAC inhibitors.

All six lead compounds belong either to HDAC inhibitors or inhibitors of bromodomain containing proteins, emphasizing the importance of lysine acetylation in the context of HIV-1 latency. Earlier studies and clinical trials have described vorinostat and CI-994 as potent LRAs targeting mainly class I HDACs [256, 258], which regulate acetylation of histones and

transcription factors such as LSF and YY1 [147, 176, 177, 364]. In a similar way, one target of bromosporine and CPI-203 among others is *bromodomain-containing protein 4* (BRD4), which is a repressor of HIV transcription during latency by cooperating with the SWI/ SNF nucleosome [365]. In this context, both inhibitors of bromodomain containing proteins have shown latency reversing properties [257,259]. Different from vorinostat, CI-994, bromosporine and CPI-203, two new compounds, SR-4370 and HPOB, with latency reversing ability were identified in this study. In contrast to vorinostat and CI-994, the cytosolic deacetylase HDAC6 is also inhibited by SR-4370 and HPOB. In the HIV context, HDAC6 has been found to be involved in autophagic degradation of the HIV-1 Vif protein and, thereby, acts as antiviral factor [108]. HDAC6 has been also described to restrict α-tubulin- and HIV-1 Env-dependent cell fusion and infection [366]. Moreover, HDAC6 has been also shown to deacetylate HIV-1 Tat, thereby, resulting in the inhibition of Tat's transactivation activity [153].
Based on these HDAC6-associated mechanisms and the findings in this study, further studies should be conducted to elucidate the role of HDAC6 in HIV-1 latency. Overall, the clinical usability of SR-4370 and HPOB should be evaluated, since both are promising candidates for realizing the clinical success of the "shock-and-kill" approach.
In addition to the identification of new LRAs, general compatibility of the tested lead compounds with other immune cells such as cytotoxic T-cells and cells of the myeloid lineage was observed in this study, which was investigated in primary cells. All six identified lead compounds did not activate resting $CD4^+$ T-cells (fig. 3.32). This is a prerequisite for further clinical tests as T-cell activation might be associated with unfavorable cytotoxic cytokine release [260], which may increase the susceptibility of adjacent T-cells and the risk of HIV reservoir relocation. Moreover, all six identified lead compounds did not show detrimental impact on any leukocyte-associated cell type as the cell fractions of B-cells, NK and NK-like T-cells, $CD4^+$ and $CD8^+$ T-cells did not change upon treatment in comparison with untreated cells (fig. 3.33). Only the population of monocytes showed minor fluctuations, which might be associated with induced proliferation or differentiation of myeloid cells [367]. More importantly, all six lead compounds showed no increased overall cytotoxicity in the PBMC population, emphasizing the potential usability of these compounds. Further investigation of the compounds may include tests in $CD4^+$ T-cells isolated from ART-suppressed HIV-1 patients to provide additional pre-clinical evidences. If the new identified compounds pass further (pre-)clinical tests, they might help to eradicate latent viral reservoirs in HIV-1-infected patients and optimize common treatment strategies.

4.8. Effect of HDAC inhibitor treatment on HIV-1 *de novo* infection

HIV-1 reactivation in latently infected cells has been of high interest as a strategy to aim for removal of HIV-1 reservoirs in the context of the "shock-and-kill" approach. A high demand for compounds exists, that are able to reactivate HIV-1 gene expression from the integrated, latent provirus and, thereby, induce the "shock" phase. The "shock" phase is complemented by maintaining ART to allow effective reduction of viral loads from neosynthesized HIV-1 during the "kill" phase, in which latently infected cells die from viral cytopathic effects, host cytolytic effector mechanisms following viral reactivation or ART [363]. For this idea of combination antiretroviral treatment (cART), the use of HDAC inhibitors has come into focus since HDACs have been shown to induce chromatin condensation by deacetylation of histones and, thereby, prevent HIV-1 transcription in the silent state of HIV-1 latency [175, 176, 178, 183, 327]. However, the "shock-and-kill" strategy using HDAC inhibitors has not been clinically successful in the complete eradication of latent HIV-1 reservoirs in HIV-1-infected patients so far and infection of new cells by reactivated virus remains a clinical concern [261, 368]. In this context, the HDAC inhibitors, romidepsin and SAHA have demonstrated to reactivate HIV-1 efficiently but also may support HIV-1 infection in $CD4^+$ T-cell [261, 262]. Generally, only very limited information is available about how HDAC inhibitors affect *de novo* HIV-1 infections.

In this study, the impact of 15 inhibitors of HDACs/sirtuins on *de novo* HIV-1 infection in human primary activated $CD4^+$ T-cells was evaluated. The set of selected inhibitors with demonstrated latency reversing properties in the J-Lat cell-based latency system (fig. 3.34) covered the entire selectivity range for human HDACs/sirtuins. Interestingly, 13 inhibitors did not affect *de novo* HIV-1 infection except for sodium butyrate and bufexamac. These two compounds, which have been shown to inhibit different HDACs, i.e. class I HDACs [369] and HDAC6/10 [370], respectively, caused an unexpected, highly significant reduction of p24-positive cells suggesting an impairing effect on HIV-1 infection (fig. 3.35C). Similar findings were made for X4-tropic $HIV_{NL4\text{-}3}$ and R5-tropic HIV-1 transmitted founder (T/F) strain CH058 (fig. 3.35D) demonstrating, that decrease of HIV-1 infection levels was also observed for a molecular HIV-1 clone that closely resembles primary isolates. Moreover, reduction of HIV-1 infection levels was shown for X4- and R5-tropic viruses indicating, that it was independent of the co-receptor usage. In addition, the reduction did not correlate with the compounds target specificity, which is exemplified by the common selectivity of bufexamac, tubacin and LBH 589 for HDAC6, however, the latter two inhibitors did not negatively affect *de novo* HIV-1 infection in treated cells in this screen. Therefore, it is assumed, that the observed effect by sodium butyrate and bufexamac was compound-specific. In summary, these results disproved the potential risk of enhanced *de novo* infections at least in $CD4^+$ T-cells. Furthermore, this study highlights two HDAC inhibitors, namely

sodium butyrate and bufexamac, as potential novel drugs for the treatment of HIV-1-infected individuals.

To elucidate the underlying molecular mechanisms of the two compounds on a global level, transcriptome analysis was performed. The comparison of identified DEGs with the NCBI HHID [36] showed, that a substantial number of genes (Sb: ca. 25%, Bu: ca. 34% that are significantly affected upon treatment have been reported to be associated with HIV-1 infection. Hits which were found down-regulated for both compounds comprised several cytokines/interleukins such as CXCL8 (IL8) and IL4 (fig. 3.36A and B). IL8 is known to promote HIV-1 replication in human monocyte-derived macrophages [371] and IL4 has been reported as important regulator of HIV-1 expression via transcriptional activation mechanisms [372]. Therefore, interleukin regulated cell responses might contribute to the latency reversing ability of sodium butyrate and bufexamac. Furthermore, IL4 influences T-cell activation, differentiation, proliferation, and survival [373] and, thus, might affect the susceptibility of T-cells towards *de novo* HIV-1 infection. GO term and pathway analysis showed enriched gene sets for terms related to cell cycle (fig. 3.36C). A more detailed analysis at level of single genes/proteins showed strong down-regulation of factors regulating checkpoint-mediated cell cycle arrest and activation of DNA repair in response to the presence of DNA damage or unreplicated DNA, such as *serine/threonine-protein kinase Chk1* (CHEK1), *cyclin-dependent kinase 1* (CDK1) or *proliferating cell nuclear antigen* (PCNA) (fig. 3.37). These evidences suggest the ability of sodium butyrate or bufexamac to block cellular proliferation in treated $CD4^+$ T-cells. Earlier studies have demonstrated, that HIV-1 infection of quiescent lymphocytes does not result in efficient production of viral progeny and that the completion of reverse transcription and viral integration is highly dependent on the stage of cell cycle during acute HIV-1 infection [30, 374]. Furthermore, it has been also shown, that the majority of HIV-1-infected cells arise from cell proliferation in latently infected cell populations during ART [375, 376]. Thus, the anti-proliferative effect of sodium butyrate and bufexamac might contribute to their latency reactivating and *de novo* infection inhibiting properties. Besides the KEGG pathway "cell cycle", sodium butyrate and bufexamac treatment also resulted in down-regulation of genes of the KEGG "Fanconi anemia pathway" (fig. 3.37), a mechanism, which is responsible for the maintenance of genomic stability by repairing DNA interstrand crosslinks [377]. It is conceivable, that down-regulation of this pathway might impair mechanism favoring viral cDNA integration during *de novo* HIV-1 infection since the repair of HIV-1 integration-related DNA lesions is a critical process for efficient HIV-1 replication [378–380].

For sodium butyrate, quantitative proteomic analysis of treated $CD4^+$ T-cells was performed to gain additional insights, which are not covered by the transcriptome analysis. Among the proteins with changed protein abundance upon treatment, several proteins have been associated with HIV-1 infection according the NCBI HHID [36]. Down-regulated proteins linked to HIV-1 infection in this analysis included RACGAP1, UBE2C, HNRNPU and

HMGCS1, which have been described in genome-wide shRNA/siRNA screens to be required during HIV-1 replication in Jurkat cells [276, 381]. DDX5 has been also described as HIV-1 replication enhancing factor [362], which was also found down-regulated in this proteomic analysis. Interestingly, HIV-1 Tat's second exon has been also associated with decreased DDX5 levels (fig. 3.24C) as discussed in section 4.6 suggesting a potential link between sodium butyrate and Tat exon 2-dependent protein interactions. Another down-regulated protein in this data set was EP300, which interacts with HIV-1 Tat and functions as co-activator of HIV-1 gene expression [151]. In parallel to the exemplified down-regulated proteins associated with increased HIV-1 infection, up-regulation of factors with anti-viral effects were also found as exemplified by BRD2, which is described as suppressor of viral gene expression in a Tat-independent manner [382].
In summary, the HDAC inhibitor screen in this study identified in particular class I and class II HDACs as modulators during HIV-1 gene expression and latency. Moreover, clinical concerns about reseeding of HIV-1 reservoirs by HDAC inhibitors could not be confirmed in this screen. Furthermore, sodium butyrate and bufexamac were identified as compounds with latency reversing and *de novo* infection inhibiting properties. Global transcriptome and proteome analysis provided several evidences for the mode of action of these two compounds including blocking of of cell proliferation, inhibition of DNA repair mechanisms and restriction of viral transcription. Therefore, both HDAC inhibitors might be capable to improve existing cART strategies. Consequently, findings of this study suggest further clinical evaluation of the use of sodium butyrate and bufexamac for the treatment of HIV-1 infections.

In summary, this doctoral thesis examined various aspects of HIV-1 infection - from the investigations of virus-host interactions to the evaluation of potential new compounds for pharmaceutical intervention. The results provide a valuable resource as well as novel analysis tools, which are anticipated to be useful in the investigation of the underlying molecular mechanisms of productive and latent HIV-1 infection. Moreover, they will help to optimize current therapies or support the evaluation of new treatment strategies for HIV-1-infected individuals.

Bibliography

[1] K. B. Hymes, J. B. Greene, A. Marcus, D. C. William, T. Cheung, N. S. Prose, H. Ballard, and L. J. Laubenstein, "Kaposi's sarcoma in homosexual men. A report of eight cases," *Lancet*, vol. 318, no. 8247, pp. 598–600, 1981.

[2] Hiv.gov, "A Timeline of HIV/AIDS." https://www.hiv.gov/sites/default/files/aidsgov-timeline.pdf, date accessed: 03.06.2020.

[3] F. Barré-Sinoussi, J. C. Chermann, F. Rey, M. T. Nugeyre, S. Chamaret, J. Gruest, C. Dauguet, C. Axler-Blin, F. Vézinet-Brun, C. Rouzioux, W. Rozenbaum, and L. Montagnier, "Isolation of a T-lymphotropic retrovirus from a patient at risk for acquired immune deficiency syndrome (AIDS)," *Science*, vol. 220, no. 4599, pp. 868–871, 1983.

[4] WHO, "HIV/AIDS." https://www.who.int/news-room/fact-sheets/detail/hiv-aids, date accessed: 04.06.2020.

[5] S. G. Deeks, J. Overbaugh, A. Phillips, and S. Buchbinder, "HIV infection," *Nature Reviews Disease Primers*, p. 15035, 2015.

[6] T. W. Chun, L. Stuyver, S. B. Mizell, L. A. Ehler, J. A. M. Mican, M. Baseler, A. L. Lloyd, M. A. Nowak, and A. S. Fauci, "Presence of an inducible HIV-1 latent reservoir during highly active antiretroviral therapy," *Proceedings of the National Academy of Sciences of the United States of America*, vol. 94, no. 24, pp. 13193–13197, 1997.

[7] C. W. Peterson and H. P. Kiem, "Cell and Gene Therapy for HIV Cure," in *Current Topics in Microbiology and Immunology*, vol. 417, pp. 211–248, Curr Top Microbiol Immunol, 2018.

[8] Y. Nishimura and M. A. Martin, "Of Mice, Macaques, and Men: Broadly Neutralizing Antibody Immunotherapy for HIV-1," 2017.

[9] D. H. Barouch, F. L. Tomaka, F. Wegmann, D. J. Stieh, G. Alter, M. L. Robb, N. L. Michael, L. Peter, J. P. Nkolola, E. N. Borducchi, and A. Chandrashekar et al., "Evaluation of a mosaic HIV-1 vaccine in a multicentre, randomised, double-blind, placebo-controlled, phase 1/2a clinical trial (APPROACH) and in rhesus monkeys (NHP 13-19)," *The Lancet*, vol. 392, no. 10143, pp. 232–243, 2018.

[10] A. M. Spivak and V. Planelles, "Novel Latency Reversal Agents for HIV-1 Cure," jan 2018.

[11] C. Petropoulos, *Retroviral Taxonomy, Protein Structures, Sequences, and Genetic Maps*. New York: Cold Spring Harbor Laboratory Press, 1997.

[12] M. B. Feinberg and W. C. Greene, "Molecular insights into human immunodeficiency virus type 1 pathogenesis," *Current Opinion in Immunology*, vol. 4, no. 4, pp. 466–474, 1992.

[13] A. Engelman and P. Cherepanov, "The structural biology of HIV-1: Mechanistic and therapeutic insights," *Nature Reviews Microbiology*, vol. 10, no. 4, pp. 279–290, 2012.

[14] G. Li and E. De Clercq, "HIV Genome-Wide Protein Associations: a Review of 30 Years of Research.," *Microbiology and molecular biology reviews : MMBR*, vol. 80, no. 3, pp. 679–731, 2016.

[15] M. H. Malim and M. Emerman, "HIV-1 Accessory Proteins-Ensuring Viral Survival in a Hostile Environment," *Cell Host and Microbe*, vol. 3, no. 6, pp. 388–398, 2008.

[16] D. Klatzmann, F. Barré-Sinoussi, M. T. Nugeyre, C. Dauguet, E. Vilmer, C. Griscelli, F. Brun-Vezinet, C. Rouzioux, J. C. Gluckman, J. C. Chermann, and L. Montagnier, "Selective tropism of lymphadenopathy associated virus (LAV) for helper-inducer T lymphocytes," *Science*, vol. 225, pp. 59–63, jul 1984.

[17] H. Masur, F. P. Ognibene, R. Yarchoan, J. H. Shelhamer, B. F. Baird, W. Travis, A. F. Suffredini, L. Deyton, J. A. Kovacs, J. Falloon, R. Davey, M. Polis, J. Metcalf, M. Baseler, R. Wesley, V. J. Gill, A. S. Fauci, and H. C. Lane, "CD4 counts as predictors of opportunistic pneumonias in human immunodeficiency virus (HIV) infection," *Annals of Internal Medicine*, vol. 111, no. 3, pp. 223–231, 1989.

[18] A. G. Dalgleish, P. C. Beverley, P. R. Clapham, D. H. Crawford, M. F. Greaves, and R. A. Weiss, "The CD4 (T4) antigen is an essential component of the receptor for the AIDS retrovirus," *Nature*, vol. 312, no. 5996, pp. 763–767, 1984.

[19] K. M. Murphy, *Janeway's Immunobiology*. Garland Science, 8 ed., 2012.

[20] G. Gaud, R. Lesourne, and P. E. Love, "Regulatory mechanisms in T cell receptor signalling," *Nature Reviews Immunology*, vol. 18, no. 8, pp. 485–497, 2018.

[21] U.S. Department of Health and Human Services, "CD4 T Lymphocyte | Definition." https://aidsinfo.nih.gov/understanding-hiv-aids/glossary/113/cd4-t-lymphocyte, date accessed: 07.08.2020, 2019.

[22] J. A. Zack, S. J. Arrigo, S. R. Weitsman, A. S. Go, A. Haislip, and I. S. Chen, "HIV-1 entry into quiescent primary lymphocytes: Molecular analysis reveals a labile, latent viral structure," *Cell*, vol. 61, pp. 213–222, apr 1990.

[23] X. Pan, H. M. Baldauf, O. T. Keppler, and O. T. Fackler, "Restrictions to HIV-1 replication in resting CD4 + T lymphocytes," *Cell Research*, vol. 23, pp. 876–885, jul 2013.

[24] K. A. Jones, J. T. Kadonaga, P. A. Luciw, and R. Tjian, "Activation of the AIDS retrovirus promoter by the cellular transcription factor, Sp1," *Science*, vol. 232, no. 4751, pp. 755–759, 1986.

[25] S. Kinoshita, B. K. Chen, H. Kaneshima, and G. P. Nolan, "Host control of HIV-1 parasitism in T cells by the nuclear factor of activated T cells," *Cell*, vol. 95, pp. 595–604, nov 1998.

[26] J. Liu, N. D. Perkins, R. M. Schmid, and G. J. Nabel, "Specific NF-kappa B subunits act in concert with Tat to stimulate human immunodeficiency virus type 1 transcription.," *Journal of Virology*, vol. 66, no. 6, pp. 3883–3887, 1992.

[27] J. Karn and U. Mbonye, "Control of HIV Latency by Epigenetic and Non-Epigenetic Mechanisms," *Current HIV Research*, vol. 9, pp. 554–567, jan 2012.

[28] R. Weil and A. Israël, "Deciphering the pathway from the TCR to NF-κB," *Cell Death and Differentiation*, vol. 13, pp. 826–833, may 2006.

[29] Y. Wu and J. W. Marsh, "Selective transcription and modulation of resting T cell activity by preintegrated HIV DNA," *Science*, vol. 293, pp. 1503–1506, aug 2001.

[30] M. Stevenson, T. L. Stanwick, M. P. Dempsey, and C. A. Lamonica, "HIV-1 replication is controlled at the level of T cell activation and proviral integration," *EMBO Journal*, vol. 9, pp. 1551–1560, may 1990.

[31] J. Guo, W. Wang, D. Yu, and Y. Wu, "Spinoculation Triggers Dynamic Actin and Cofilin Activity That Facilitates HIV-1 Infection of Transformed and Resting CD4 T Cells," *Journal of Virology*, vol. 85, no. 19, pp. 9824–9833, 2011.

[32] H. M. Baldauf, X. Pan, E. Erikson, S. Schmidt, W. Daddacha, M. Burggraf, K. Schenkova, I. Ambiel, G. Wabnitz, T. Gramberg, S. Panitz, E. Flory, N. R. Landau, S. Sertel, F. Rutsch, F. Lasitschka, B. Kim, R. König, O. T. Fackler, and O. T. Keppler, "SAMHD1 restricts HIV-1 infection in resting CD4 + T cells," *Nature Medicine*, vol. 18, pp. 1682–1687, nov 2012.

[33] M. Stevenson, "HIV-1 pathogenesis," *Nature Medicine*, vol. 9, pp. 853–860, jul 2003.

[34] J. M. McCune, "The dynamics of CD4+ T-cell depletion in HIV disease," *Nature*, vol. 410, pp. 974–979, apr 2001.

[35] NIAID, "HIV Replication Cycle | NIH: National Institute of Allergy and Infectious Diseases." https://www.niaid.nih.gov/diseases-conditions/hiv-replication-cycle, date accessed: 23.07.2020.

[36] D. Ako-Adjei, W. Fu, C. Wallin, K. S. Katz, G. Song, D. Darji, J. R. Brister, R. G. Ptak, and K. D. Pruitt, "HIV-1, Human Interaction database: Current status and new features," *Nucleic Acids Research*, vol. 43, no. D1, pp. D566–D570, 2015.

[37] S. Jäger, P. Cimermancic, N. Gulbahce, J. R. Johnson, K. E. McGovern, S. C. Clarke, M. Shales, G. Mercenne, and L. Pache et al., "Global landscape of HIV–human protein complexes," *Nature*, vol. 481, 2011.

[38] D. Virág, B. Dalmadi-Kiss, K. Vékey, L. Drahos, I. Klebovich, I. Antal, and K. Ludányi, "Current Trends in the Analysis of Post-translational Modifications," 2020.

[39] M. Mann and O. N. Jensen, "Proteomic analysis of post-translational modifications," *Nature Biotechnology*, vol. 21, no. 3, pp. 255–261, 2003.

[40] L. Chen, O. T. Keppler, and C. Schölz, "Post-translational modification-based regulation of HIV replication," *Frontiers in Microbiology*, vol. 9, no. 9, p. 2131, 2018.

[41] E. H. Fischer and E. G. Krebs, "Conversion of phosphorylase b to phosphorylase a in muscle extracts.," *The Journal of Biological Chemistry*, vol. 216, no. 1, pp. 121–132, 1955.

[42] G. Manning, G. D. Plowman, T. Hunter, and S. Sudarsanam, "Evolution of protein kinase signaling from yeast to man," *Trends in Biochemical Sciences*, vol. 27, no. 10, pp. 514–520, 2002.

[43] X. Yue, A. Schunter, and A. B. Hummon, "Comparing Multistep Immobilized Metal Affinity Chromatography and Multistep TiO2 Methods for Phosphopeptide Enrichment," *Analytical Chemistry*, vol. 87, no. 17, pp. 8837–8844, 2015.

[44] T. E. Thingholm and M. R. Larsen, "Phosphopeptide Enrichment by Immobilized Metal Affinity Chromatography," in *Phospho-Proteomics*, pp. 123–133, Springer, New York, NY, 2016.

[45] T. Kouzarides, "Acetylation: a regulatory modification to rival phosphorylation?," *The EMBO journal*, vol. 19, no. 6, pp. 1176–1179, 2000.

[46] C. Choudhary, C. Kumar, F. Gnad, M. L. Nielsen, M. Rehman, T. C. Walther, J. V. Olsen, and M. Mann, "Lysine acetylation targets protein complexes and co-regulates major cellular functions.," *Science*, vol. 325, no. 5942, pp. 834–40, 2009.

[47] G.-W. Kim, X.-J. Yang, and T. Kouzarides et al., "Comprehensive lysine acetylomes emerging from bacteria to humans.," *Trends in biochemical sciences*, vol. 36, pp. 211–20, apr 2011.

[48] T. Svinkina, H. Gu, J. C. Silva, P. Mertins, J. Qiao, S. Fereshetian, J. D. Jaffe, E. Kuhn, N. D. Udeshi, and S. A. Carr, "Deep, quantitative coverage of the lysine acetylome using novel anti-acetyl-lysine antibodies and an optimized proteomic workflow.," *Molecular & cellular proteomics : MCP*, vol. 14, no. 9, pp. 2429–40, 2015.

[49] M. R. Shakespear, M. A. Halili, K. M. Irvine, D. P. Fairlie, and M. J. Sweet, "Histone deacetylases as regulators of inflammation and immunity," *Trends in Immunology*, vol. 32, no. 7, pp. 335–343, 2011.

[50] S. Spange, T. Wagner, T. Heinzel, and O. H. Krämer, "Acetylation of non-histone proteins modulates cellular signalling at multiple levels," *International Journal of Biochemistry and Cell Biology*, vol. 41, no. 1, pp. 185–198, 2009.

[51] P. Filippakopoulos, S. Picaud, M. Mangos, T. Keates, J. P. Lambert, D. Barsyte-Lovejoy, I. Felletar, R. Volkmer, S. Müller, T. Pawson, A. C. Gingras, C. H. Arrowsmith, and S. Knapp, "Histone recognition and large-scale structural analysis of the human bromodomain family," *Cell*, vol. 149, no. 1, pp. 214–231, 2012.

[52] T. Fujisawa and P. Filippakopoulos, "Functions of bromodomain-containing proteins and their roles in homeostasis and cancer," *Nature Reviews Molecular Cell Biology*, vol. 18, no. 4, pp. 246–262, 2017.

[53] C. Choudhary, B. T. Weinert, Y. Nishida, E. Verdin, and M. Mann, "The growing landscape of lysine acetylation links metabolism and cell signalling.," *Nature reviews. Molecular cell biology*, vol. 15, no. 8, pp. 536–50, 2014.

[54] I. L. Goldknopf, M. F. French, R. Musso, and H. Busch, "Presence of protein A24 in rat liver nucleosomes.," *Proceedings of the National Academy of Sciences of the United States of America*, vol. 74, no. 12, pp. 5492–5495, 1977.

[55] C. M. Pickart, "Mechanisms underlying ubiquitination," *Annual Review of Biochemistry*, vol. 70, pp. 503–533, jun 2001.

[56] B. A. Schulman and J. Wade Harper, "Ubiquitin-like protein activation by E1 enzymes: The apex for downstream signalling pathways," *Nature Reviews Molecular Cell Biology*, vol. 10, pp. 319–331, may 2009.

[57] Y. Ye and M. Rape, "Building ubiquitin chains: E2 enzymes at work," *Nature Reviews Molecular Cell Biology*, vol. 10, pp. 755–764, nov 2009.

[58] R. J. Deshaies and C. A. Joazeiro, "RING domain E3 ubiquitin ligases," *Annual Review of Biochemistry*, vol. 78, pp. 399–434, 2009.

[59] J. J. Smit and T. K. Sixma, "RBR E3-ligases at work," *EMBO Reports*, vol. 15, no. 2, pp. 142–154, 2014.

[60] D. Rotin and S. Kumar, "Physiological functions of the HECT family of ubiquitin ligases," *Nature Reviews Molecular Cell Biology*, vol. 10, pp. 398–409, jun 2009.

[61] K. Husnjak and I. Dikic, "Ubiquitin-binding proteins: Decoders of ubiquitin-mediated cellular functions," *Annual Review of Biochemistry*, vol. 81, pp. 291–322, jul 2012.

[62] D. Komander, M. J. Clague, and S. Urbé, "Breaking the chains: Structure and function of the deubiquitinases," *Nature Reviews Molecular Cell Biology*, vol. 10, pp. 550–563, aug 2009.

[63] M. J. Clague, I. Barsukov, J. M. Coulson, H. Liu, D. J. Rigden, and S. Urbé, "Deubiquitylases from genes to organism," *Physiological Reviews*, vol. 93, pp. 1289–1315, jul 2013.

[64] M. J. Emanuele, A. E. Elia, Q. Xu, C. R. Thoma, L. Izhar, Y. Leng, A. Guo, Y. N. Chen, J. Rush, P. W. C. Hsu, H. C. S. Yen, and S. J. Elledge, "Global identification of modular cullin-RING ligase substrates," *Cell*, vol. 147, pp. 459–474, oct 2011.

[65] W. Kim, E. J. Bennett, E. L. Huttlin, A. Guo, J. Li, A. Possemato, M. E. Sowa, R. Rad, J. Rush, M. J. Comb, J. W. Harper, and S. P. Gygi, "Systematic and quantitative assessment of the ubiquitin-modified proteome," *Molecular Cell*, vol. 44, pp. 325–340, oct 2011.

[66] D. Komander and M. Rape, "The ubiquitin code," *Annual Review of Biochemistry*, vol. 81, pp. 203–229, 2012.

[67] M. H. Glickman and A. Ciechanover, "The ubiquitin-proteasome proteolytic pathway: Destruction for the sake of construction," *Physiological Reviews*, vol. 82, no. 2, pp. 373–428, 2002.

[68] J. Terrell, S. Shih, R. Dunn, and L. Hicke, "A function for monoubiquitination in the internalization of a G protein-coupled receptor," *Molecular Cell*, vol. 1, no. 2, pp. 193–202, 1998.

[69] D. Mukhopadhyay and H. Riezman, "Proteasome-independent functions of ubiquitin in endocytosis and signaling," *Science*, vol. 315, pp. 201–205, jan 2007.

[70] J. Peng, D. Schwartz, J. E. Elias, C. C. Thoreen, D. Cheng, G. Marsischky, J. Roelofs, D. Finley, and S. P. Gygi, "A proteomics approach to understanding protein ubiquitination," *Nature Biotechnology*, vol. 21, pp. 921–926, aug 2003.

[71] V. Ravikumar, C. Jers, and I. Mijakovic, "Elucidating host-pathogen interactions based on post-translational modifications using proteomics approaches," 2015.

[72] D. Salomon and K. Orth, "What Pathogens Have Taught Us about Posttranslational Modifications," *Cell Host and Microbe*, vol. 14, pp. 269–279, sep 2013.

[73] P. M. Jean Beltran, J. D. Federspiel, X. Sheng, and I. M. Cristea, "Proteomics and integrative omic approaches for understanding host–pathogen interactions and infectious diseases," *Molecular Systems Biology*, vol. 13, p. 922, mar 2017.

[74] S. D. McCarthy, D. Sakac, A. Neschadim, and D. R. Branch, "C-SRC protein tyrosine kinase regulates early HIV-1 infection post-entry," *AIDS*, vol. 30, no. 6, pp. 849–857, 2016.

[75] K. Shirakawa, L. Chavez, S. Hakre, V. Calvanese, and E. Verdin, "Reactivation of latent HIV by histone deacetylase inhibitors," *Trends in Microbiology*, vol. 21, no. 6, pp. 277–285, 2013.

[76] P. J. Maddon, A. G. Dalgleish, J. S. McDougal, P. R. Clapham, R. A. Weiss, and R. Axel, "The T4 gene encodes the AIDS virus receptor and is expressed in the immune system and the brain," *Cell*, vol. 47, no. 3, pp. 333–348, 1986.

[77] J. S. McDougal, J. K. Nicholson, G. D. Cross, S. P. Cort, M. S. Kennedy, and A. C. Mawle, "Binding of the human retrovirus HTLV-III/LAV/ARV/HIV to the CD4 (T4) molecule: conformation dependence, epitope mapping, antibody inhibition, and potential for idiotypic mimicry.," *Journal of immunology (Baltimore, Md. : 1950)*, vol. 137, no. 9, pp. 2937–44, 1986.

[78] Y. Wu and A. Yoder, "Chemokine coreceptor signaling in HIV-1 infection and pathogenesis," *PLoS Pathogens*, vol. 5, p. e1000520, dec 2009.

[79] W. Abbas and G. Herbein, "Plasma membrane signaling in HIV-1 infection," *Biochimica et Biophysica Acta (BBA) - Biomembranes*, vol. 1838, pp. 1132–1142, apr 2014.

[80] M. Viard, I. Parolini, S. S. Rawat, K. Fecchi, M. Sargiacomo, A. Puri, and R. Blumenthal, "The role of glycosphingolipids in HIV signaling, entry and pathogenesis," *Glycoconjugate Journal*, vol. 20, no. 3, pp. 213–222, 2003.

[81] E. Flory, C. K. Weber, P. Chen, A. Hoffmeyer, C. Jassoy, and U. R. Rapp, "Plasma membrane-targeted Raf kinase activates NF-kappaB and human immunodeficiency virus type 1 replication in T lymphocytes.," *Journal of virology*, vol. 72, no. 4, pp. 2788–94, 1998.

[82] C. Cicala, J. Arthos, N. Censoplano, C. Cruz, E. Chung, E. Martinelli, R. A. Lempicki, V. Natarajan, D. VanRyk, M. Daucher, and A. S. Fauci, "HIV-1 gp120 induces NFAT nuclear translocation in resting CD4+ T-cells," *Virology*, vol. 345, no. 1, pp. 105–114, 2006.

[83] E. M. Campbell and T. J. Hope, "HIV-1 capsid: the multifaceted key player in HIV-1 infection," *Nature Reviews Microbiology*, vol. 13, no. 8, pp. 471–483, 2015.

[84] M. D. Miller, C. M. Farnet, and F. D. Bushman, "Human immunodeficiency virus type 1 preintegration complexes: studies of organization and composition.," *Journal of virology*, vol. 71, no. 7, pp. 5382–90, 1997.

[85] A. Fassati and S. P. Goff, "Characterization of intracellular reverse transcription complexes of human immunodeficiency virus type 1.," *Journal of virology*, vol. 75, no. 8, pp. 3626–35, 2001.

[86] A. E. Hulme, O. Perez, and T. J. Hope, "Complementary assays reveal a relationship between HIV-1 uncoating and reverse transcription," *Proceedings of the National Academy of Sciences of the United States of America*, vol. 108, no. 24, pp. 9975–9980, 2011.

[87] H. Xu, T. Franks, G. Gibson, K. Huber, N. Rahm, C. S. De Castillia, J. Luban, C. Aiken, S. Watkins, N. Sluis-Cremer, and Z. Ambrose, "Evidence for biphasic uncoating during HIV-1 infection from a novel imaging assay," *Retrovirology*, vol. 10, no. 1, p. 70, 2013.

[88] X. Lahaye, T. Satoh, M. Gentili, S. Cerboni, C. Conrad, I. Hurbain, A. ElMarjou, C. Lacabaratz, J. D. Lelièvre, and N. Manel, "The Capsids of HIV-1 and HIV-2 Determine Immune Detection of the Viral cDNA by the Innate Sensor cGAS in Dendritic Cells," *Immunity*, vol. 39, no. 6, pp. 1132–1142, 2013.

[89] J. Rasaiyaah, C. P. Tan, A. J. Fletcher, A. J. Price, C. Blondeau, L. Hilditch, D. A. Jacques, D. L. Selwood, L. C. James, M. Noursadeghi, and G. J. Towers, "HIV-1 evades innate immune recognition through specific cofactor recruitment," *Nature*, vol. 503, no. 7476, pp. 402–405, 2013.

[90] D. A. Jacques, W. A. McEwan, L. Hilditch, A. J. Price, G. J. Towers, and L. C. James, "HIV-1 uses dynamic capsid pores to import nucleotides and fuel encapsidated DNA synthesis," *Nature*, vol. 536, pp. 349–353, aug 2016.

[91] C. Cartier, P. Sivard, C. Tranchat, D. Decimo, C. Desgranges, and V. Boyer, "Identification of three major phosphorylation sites within HIV-1 capsid. Role of phosphorylation during the early steps of infection," *Journal of Biological Chemistry*, vol. 274, pp. 19434–19440, jul 1999.

[92] H. Takeuchi, H. Saito, T. Noda, T. Miyamoto, T. Yoshinaga, K. Terahara, H. Ishii, Y. Tsunetsugu-Yokota, and S. Yamaoka, "Phosphorylation of the HIV-1 capsid by MELK triggers uncoating to promote viral cDNA synthesis," *PLoS Pathogens*, vol. 13, no. 7, p. e1006441, 2017.

[93] S. Misumi, M. Inoue, T. Dochi, N. Kishimoto, N. Hasegawa, N. Takamune, and S. Shoji, "Uncoating of human immunodeficiency virus type 1 requires prolyl isomerase Pin1," *Journal of Biological Chemistry*, vol. 285, no. 33, pp. 25185–25195, 2010.

[94] T. Dochi, T. Nakano, M. Inoue, N. Takamune, S. Shoji, K. Sano, and S. Misumi, "Phosphorylation of human immunodeficiency virus type 1 capsid protein at serine 16, required for peptidyl-prolyl isomerase-dependent uncoating, is mediated by virion-incorporated extracellular signal-regulated kinase 2," *Journal of General Virology*, vol. 95, pp. 1156–1166, may 2014.

[95] C. Mettling, C. Desmetz, A.-L. Fiser, B. Réant, P. Corbeau, and Y.-L. Lin, "Galphai protein-dependant extracellular signal-regulated kinase-1/2 activation is required for HIV-1 reverse transcription.," *AIDS (London, England)*, vol. 22, pp. 1569–76, aug 2008.

[96] J. Leng, H. P. Ho, M. J. Buzon, F. Pereyra, B. D. Walker, X. G. Yu, E. J. Chang, and M. Lichterfeld, "A cell-intrinsic inhibitor of HIV-1 reverse transcription in CD4 + T cells from elite controllers," *Cell Host and Microbe*, vol. 15, no. 6, pp. 717–728, 2014.

[97] A. Sáez-Cirión, C. Hamimi, A. Bergamaschi, A. David, P. Versmisse, A. Mélard, F. Boufassa, F. Barré-Sinoussi, O. Lambotte, C. Rouzioux, and G. Pancino, "Restriction of HIV-1 replication in macrophages and CD4+ T cells from HIV controllers," *Blood*, vol. 118, no. 4, pp. 955–964, 2011.

[98] J. F. Okulicz, V. C. Marconi, M. L. Landrum, S. Wegner, A. Weintrob, A. Ganesan, B. Hale, N. Crum-Cianflone, J. Delmar, V. Barthel, G. Quinnan, B. K. Agan, and M. J. Dolan, "Clinical outcomes of elite controllers, viremic controllers, and long-term nonprogressors in the US department of defense HIV natural history study," *Journal of Infectious Diseases*, vol. 200, no. 11, pp. 1714–1723, 2009.

[99] A. Cribier, B. Descours, A. L. C. Valadão, N. Laguette, and M. Benkirane, "Phosphorylation of SAMHD1 by Cyclin A2/CDK1 Regulates Its Restriction Activity toward HIV-1," *Cell Reports*, vol. 3, no. 4, pp. 1036–1043, 2013.

[100] H. Lahouassa, W. Daddacha, H. Hofmann, D. Ayinde, E. C. Logue, L. Dragin, N. Bloch, C. Maudet, M. Bertrand, T. Gramberg, G. Pancino, S. Priet, B. Canard, N. Laguette, M. Benkirane, C. Transy, N. R. Landau, B. Kim, and F. Margottin-Goguet, "SAMHD1 restricts the replication of human immunodeficiency virus type 1 by depleting the intracellular pool of deoxynucleoside triphosphates," *Nature Immunology*, vol. 13, no. 3, pp. 223–228, 2012.

[101] M. Coiras, M. Bermejo, B. Descours, E. Mateos, J. García-Pérez, M. R. López-Huertas, M. M. Lederman, M. Benkirane, and J. Alcamí, "IL-7 Induces SAMHD1 Phosphorylation in CD4+ T Lymphocytes, Improving Early Steps of HIV-1 Life Cycle," *Cell Reports*, vol. 14, no. 9, pp. 2100–2107, 2016.

[102] H. Zhang, B. Yang, R. J. Pomerantz, C. Zhang, S. C. Arunachalam, and L. Gao, "The cytidine deaminase CEM15 induces hypermutation in newly synthesized HIV-1 DNA," *Nature*, vol. 424, no. 6944, pp. 94–98, 2003.

[103] A. E. Armitage, K. Deforche, C. hao Chang, E. Wee, B. Kramer, J. J. Welch, J. Gerstoft, L. Fugger, A. McMichael, A. Rambaut, and A. K. Iversen, "APOBEC3G-induced hypermutation of human immunodeficiency

virus type-1 is typically a discrete "all or nothing" phenomenon," *PLoS Genetics*, vol. 8, no. 3, p. e1002550, 2012.

[104] Y. Iwatani, D. S. Chan, F. Wang, K. S. Maynard, W. Sugiura, A. M. Gronenborn, I. Rouzina, M. C. Williams, K. Musier-Forsyth, and J. G. Levin, "Deaminase-independent inhibition of HIV-1 reverse transcription by APOBEC3G," *Nucleic Acids Research*, vol. 35, no. 21, pp. 7096–7108, 2007.

[105] X. Yu, Y. Yu, B. Liu, K. Luo, W. Kong, P. Mao, and X. F. Yu, "Induction of APOBEC3G Ubiquitination and Degradation by an HIV-1 Vif-Cul5-SCF Complex," *Science*, vol. 302, pp. 1056–1060, nov 2003.

[106] J. Goncalves and M. Santa-Marta, "HIV-1 Vif and APOBEC3G: multiple roads to one goal.," *Retrovirology*, vol. 1, p. 28, sep 2004.

[107] T. Izumi, A. Takaori-Kondo, K. Shirakawa, H. Higashitsuji, K. Itoh, K. Io, M. Matsui, K. Iwai, H. Kondoh, T. Sato, M. Tomonaga, S. Ikeda, H. Akari, Y. Koyanagi, J. Fujita, and T. Uchiyama, "MDM2 is a novel E3 ligase for HIV-1 Vif," *Retrovirology*, vol. 6, p. 1, jan 2009.

[108] M.-S. Valera, L. de Armas-Rillo, J. Barroso-González, S. Ziglio, J. Batisse, N. Dubois, S. Marrero-Hernández, S. Borel, L. García-Expósito, M. Biard-Piechaczyk, J.-C. Paillart, and A. Valenzuela-Fernández, "The HDAC6/APOBEC3G complex regulates HIV-1 infectiveness by inducing Vif autophagic degradation," *Retrovirology*, vol. 12, no. 1, p. 53, 2015.

[109] M. Sorin, J. Cano, S. Das, S. Mathew, X. Wu, K. P. Davies, X. Shi, S.-W. W. Cheng, D. Ott, and G. V. Kalpana, "Recruitment of a SAP18-HDAC1 complex into HIV-1 virions and its requirement for viral replication," *PLoS Pathogens*, vol. 5, no. 6, p. e1000463, 2009.

[110] C.-W. Lin and A. Engelman, "The Barrier-to-Autointegration Factor Is a Component of Functional Human Immunodeficiency Virus Type 1 Preintegration Complexes," *Journal of Virology*, vol. 77, no. 8, pp. 5030–5036, 2003.

[111] M. Llano, M. Vanegas, O. Fregoso, D. Saenz, S. Chung, M. Peretz, and E. M. Poeschla, "LEDGF/p75 Determines Cellular Trafficking of Diverse Lentiviral but Not Murine Oncoretroviral Integrase Proteins and Is a Component of Functional Lentiviral Preintegration Complexes," *Journal of Virology*, vol. 78, no. 17, pp. 9524–9537, 2004.

[112] S. Iordanskiy, R. Berro, M. Altieri, F. Kashanchi, and M. Bukrinsky, "Intracytoplasmic maturation of the human immunodeficiency virus type 1 reverse transcription complexes determines their capacity to integrate into chromatin," *Retrovirology*, vol. 3, p. 4, 2006.

[113] N. K. Raghavendra, N. Shkriabai, R. L. Graham, S. Hess, M. Kvaratskhelia, and L. Wu, "Identification of host proteins associated with HIV-1 preintegration complexes isolated from infected CD4+cells," *Retrovirology*, vol. 7, p. 66, aug 2010.

[114] K. A. Matreyek and A. Engelman, "Viral and cellular requirements for the nuclear entry of retroviral preintegration nucleoprotein complexes," *Viruses*, vol. 5, no. 10, pp. 2483–2511, 2013.

[115] V. Malikov, E. S. Da Silva, V. Jovasevic, G. Bennett, D. A. De Souza Aranha Vieira, B. Schulte, F. Diaz-Griffero, D. Walsh, and M. H. Naghavi, "HIV-1 capsids bind and exploit the kinesin-1 adaptor FEZ1 for inward movement to the nucleus," *Nature Communications*, vol. 6, p. 6660, 2015.

[116] V. Malikov and M. H. Naghavi, "Localized Phosphorylation of a Kinesin-1 Adaptor by a Capsid-Associated Kinase Regulates HIV-1 Motility and Uncoating," *Cell Reports*, vol. 20, no. 12, pp. 2792–2799, 2017.

[117] A. Jaspart, C. Calmels, O. Cosnefroy, P. Bellecave, P. Pinson, S. Claverol, V. Guyonnet-Dupérat, B. Dartigues, M. S. Benleulmi, E. Mauro, P. A. Gretteau, V. Parissi, M. Métifiot, and M. L. Andreola, "GCN2 phosphorylates HIV-1 integrase and decreases HIV-1 replication by limiting viral integration," *Scientific Reports*, vol. 7, p. 2283, may 2017.

[118] J. del Pino, J. L. Jiménez, I. Ventoso, A. Castelló, M. Á. Muñoz-Fernández, C. de Haro, and J. J. Berlanga, "GCN2 Has Inhibitory Effect on Human Immunodeficiency Virus-1 Protein Synthesis and Is Cleaved upon Viral Infection," *PLoS ONE*, vol. 7, no. 10, 2012.

[119] O. Cosnefroy, A. Jaspart, C. Calmels, V. Parissi, H. Fleury, M. Ventura, S. Reigadas, and M. L. Andréola, "Activation of GCN2 upon HIV-1 infection and inhibition of translation," *Cellular and Molecular Life Sciences*, vol. 70, no. 13, pp. 2411–2421, 2013.

[120] A. Cereseto, L. Manganaro, M. I. Gutierrez, M. Terreni, A. Fittipaldi, M. Lusic, A. Marcello, and M. Giacca, "Acetylation of HIV-1 integrase by p300 regulates viral integration.," *The EMBO journal*, vol. 24, pp. 3070–81, sep 2005.

[121] M. Terreni, P. Valentini, V. Liverani, M. I. Gutierrez, C. Di Primio, A. Di Fenza, V. Tozzini, A. Allouch, A. Albanese, M. Giacca, and A. Cereseto, "GCN5-dependent acetylation of HIV-1 integrase enhances viral integration," *Retrovirology*, vol. 7, p. 18, 2010.

[122] M. Topper, Y. Luo, M. Zhadina, K. Mohammed, L. Smith, and M. A. Muesing, "Posttranslational Acetylation of the Human Immunodeficiency Virus Type 1 Integrase Carboxyl-Terminal Domain Is Dispensable for Viral Replication," *Journal of Virology*, vol. 81, no. 6, pp. 3012–3017, 2007.

[123] A. Allouch, C. Di Primio, E. Alpi, M. Lusic, D. Arosio, M. Giacca, and A. Cereseto, "The TRIM family protein KAP1 inhibits HIV-1 integration," *Cell Host and Microbe*, vol. 9, no. 6, pp. 484–495, 2011.

[124] J. A. Smith, J. Yeung, G. D. Kao, and R. Daniel, "A role for the histone deacetylase HDAC4 in the life-cycle of HIV-1-based vectors," *Virology Journal*, vol. 7, p. 237, 2010.

[125] J. A. Smith and R. Daniel, "Following the path of the virus: the exploitation of host DNA repair mechanisms by retroviruses.," *ACS chemical biology*, vol. 1, no. 4, pp. 217–226, 2006.

[126] L. C. Mulder and M. A. Muesing, "Degradation of HIV-1 integrase by the N-end rule pathway," *Journal of Biological Chemistry*, vol. 275, pp. 29749–29753, sep 2000.

[127] A. Mousnier, N. Kubat, A. Massias-Simon, E. Ségéral, J. C. Rain, R. Benarous, S. Emiliani, and C. Dargemont, "Von Hippel-Lindau binding protein 1-mediated degradation of integrase affects HIV-1 gene expression at a postintegration step," *Proceedings of the National Academy of Sciences of the United States of America*, vol. 104, pp. 13615–13620, aug 2007.

[128] P. Cherepanov, G. Maertens, P. Proost, B. Devreese, J. Van Beeumen, Y. Engelborghs, E. De Clercq, and Z. Debyser, "HIV-1 integrase forms stable tetramers and associates with LEDGF/p75 protein in human cells," *Journal of Biological Chemistry*, vol. 278, pp. 372–381, jan 2003.

[129] L. C. Mulder, L. A. Chakrabarti, and M. A. Muesing, "Interaction of HIV-1 integrase with DNA repair protein hRad18," *Journal of Biological Chemistry*, vol. 277, pp. 27489–27493, jul 2002.

[130] Y. Zheng, Z. Ao, B. Wang, K. D. Jayappa, and X. Yao, "Host protein Ku70 binds and protects HIV-1 integrase from proteasomal degradation and is required for HIV replication," *Journal of Biological Chemistry*, vol. 286, pp. 17722–17735, may 2011.

[131] K. E. Ocwieja, S. Sherrill-Mix, R. Mukherjee, R. Custers-Allen, P. David, M. Brown, S. Wang, D. R. Link, J. Olson, K. Travers, E. Schadt, and F. D. Bushman, "Dynamic regulation of HIV-1 mRNA populations analyzed by single-molecule enrichment and long-read sequencing," *Nucleic Acids Research*, vol. 40, no. 20, pp. 10345–10355, 2012.

[132] A. Shukla, N. G. P. Ramirez, and I. D'Orso, "HIV-1 proviral transcription and latency in the new era," *Viruses*, vol. 12, may 2020.

[133] G. Nabel and D. Baltimore, "An inducible transcription factor activates expression of human immunodeficiency virus in T cells," *Nature*, vol. 326, no. 6114, pp. 711–713, 1987.

[134] J. T. Kadonaga and R. Tjian, "Affinity purification of sequence-specific DNA binding proteins," *Proceedings of the National Academy of Sciences of the United States of America*, vol. 83, no. 16, pp. 5889–5893, 1986.

[135] R. A. Marciniak and P. A. Sharp, "HIV-1 Tat protein promotes formation of more-processive elongation complexes," *EMBO Journal*, vol. 10, no. 13, pp. 4189–4196, 1991.

[136] C. Dingwall, I. Ernberg, M. J. Gait, S. M. Green, S. Heaphy, J. Karn, A. D. Lowe, M. Singh, and M. A. Skinner, "HIV-1 tat protein stimulates transcription by binding to a U-rich bulge in the stem of the TAR RNA structure.," *The EMBO Journal*, vol. 9, no. 12, pp. 4145–4153, 1990.

[137] Y. H. Ping and T. M. Rana, "DSIF and NELF Interact with RNA Polymerase II Elongation Complex and HIV-1 Tat Stimulates P-TEFb-mediated Phosphorylation of RNA Polymerase II and DSIF during Transcription Elongation," *Journal of Biological Chemistry*, vol. 276, no. 16, pp. 12951–12958, 2001.

[138] M. E. Garber, P. Wei, and K. A. Jones, "HIV-1 Tat interacts with cyclin T1 to direct the P-TEFb CTD kinase complex to TAR RNA," in *Cold Spring Harbor Symposia on Quantitative Biology*, vol. 63, pp. 371–380, 1998.

[139] Y. K. Kim, C. F. Bourgeois, C. Isel, M. J. Churcher, and J. Karn, "Phosphorylation of the RNA Polymerase II Carboxyl-Terminal Domain by CDK9 Is Directly Responsible for Human Immunodeficiency Virus Type 1 Tat-Activated Transcriptional Elongation," *Molecular and Cellular Biology*, vol. 22, no. 13, pp. 4622–4637, 2002.

[140] M. Zhou, M. A. Halanski, M. F. Radonovich, F. Kashanchi, J. Peng, D. H. Price, and J. N. Brady, "Tat Modifies the Activity of CDK9 To Phosphorylate Serine 5 of the RNA Polymerase II Carboxyl-Terminal Domain during Human Immunodeficiency Virus Type 1 Transcription," *Molecular and Cellular Biology*, vol. 20, no. 14, pp. 5077–5086, 2000.

[141] T. P. Cujec, H. Okamoto, K. Fujinaga, J. Meyer, H. Chamberlin, D. O. Morgan, and B. M. Peterlin, "The HIV transactivator TAT binds to the CDK-activating kinase and activates the phosphorylation of the carboxy-terminal domain of RNA polymerase II," *Genes and Development*, vol. 11, no. 20, pp. 2645–2657, 1997.

[142] T. Yamada, Y. Yamaguchi, N. Inukai, S. Okamoto, T. Mura, and H. Handa, "P-TEFb-mediated phosphorylation of hSpt5 C-terminal repeats is critical for processive transcription elongation," *Molecular Cell*, vol. 21, no. 2, pp. 227–237, 2006.

[143] Y. Yamaguchi, T. Takagi, T. Wada, K. Yano, A. Furuya, S. Sugimoto, J. Hasegawa, and H. Handa, "NELF, a multisubunit complex containing RD, cooperates with DSIF to repress RNA polymerase II elongation," *Cell*, vol. 97, no. 1, pp. 41–51, 1999.

[144] T. Ammosova, K. Washington, Z. Debebe, J. Brady, and S. Nekhai, "Dephosphorylation of CDK9 by protein phosphatase 2A and protein phosphatase-1 in Tat-activated HIV-1 transcription.," *Retrovirology*, vol. 2, p. 47, 2005.

[145] M. Tyagi, S. Iordanskiy, T. Ammosova, N. Kumari, K. Smith, D. Breuer, A. V. Ilatovskiy, Y. S. Kont, A. Ivanov, A. Üren, D. Kovalskyy, M. Petukhov, F. Kashanchi, and S. Nekhai, "Reactivation of latent HIV-1 provirus via targeting protein phosphatase-1," *Retrovirology*, vol. 12, pp. 1–17, dec 2015.

[146] V. W. Gautier, L. Gu, N. O'Donoghue, S. Pennington, N. Sheehy, and W. W. Hall, "In vitro nuclear interactome of the HIV-1 Tat protein," *Retrovirology*, vol. 6, p. 47, 2009.

[147] M. Lusic, A. Marcello, A. Cereseto, and M. Giacca, "Regulation of HIV-1 gene expression by histone acetylation and factor recruitment at the LTR promoter," *EMBO Journal*, vol. 22, no. 24, pp. 6550–6561, 2003.

[148] D. Boehm, R. J. Conrad, and M. Ott, "Bromodomain proteins in HIV Infection," *Viruses*, vol. 5, no. 6, pp. 1571–1586, 2013.

[149] B. Furia, L. Deng, K. Wu, S. Baylor, K. Kehn, H. Li, R. Donnelly, T. Coleman, and F. Kashanchi, "Enhancement of nuclear factor-κB acetylation by coactivator p300 and HIV-1 Tat proteins," *Journal of Biological Chemistry*, vol. 277, no. 7, pp. 4973–4980, 2002.

[150] R. E. Kiernan, C. Vanhulle, L. Schiltz, E. Adam, H. Xiao, F. Maudoux, C. Calomme, A. Burny, Y. Nakatani, K. T. Jeang, M. Benkirane, and C. Van Lint, "HIV-1 Tat transcriptional activity is regulated by acetylation," *EMBO Journal*, vol. 18, no. 21, pp. 6106–6118, 1999.

[151] L. Deng, C. De la Fuente, P. Fu, L. Wang, R. Donnelly, J. D. Wade, P. Lambert, H. Li, C. G. Lee, and F. Kashanchi, "Acetylation of HIV-1 Tat by CBP/P300 increases transcription of integrated HIV-1 genome and enhances binding to core histones," *Virology*, vol. 277, pp. 278–295, nov 2000.

[152] I. D'Orso and A. D. Frankel, "Tat acetylation modulates assembly of a viral-host RNA-protein transcription complex.," *Proceedings of the National Academy of Sciences of the United States of America*, vol. 106, no. 9, pp. 3101–6, 2009.

[153] L. Huo, D. Li, X. Sun, X. Shi, P. Karna, W. Yang, M. Liu, W. Qiao, R. Aneja, and J. Zhou, "Regulation of Tat acetylation and transactivation activity by the microtubule-associated deacetylase HDAC6," *Journal of Biological Chemistry*, vol. 286, pp. 9280–9286, mar 2011.

[154] E. Col, C. Caron, D. Seigneurin-Berny, J. Gracia, A. Favier, and S. Khochbin, "The Histone Acetyltransferase, hGCN5, Interacts with and Acetylates the HIV Transactivator, Tat," *Journal of Biological Chemistry*, vol. 276, no. 30, pp. 28179–28184, 2001.

[155] S. Pagans, A. Pedal, B. J. North, K. Kaehlcke, B. L. Marshall, A. Dorr, C. Hetzer-Egger, P. Henklein, R. Frye, M. W. McBurney, H. Hruby, M. Jung, E. Verdin, and M. Ott, "SIRT1 regulates HIV transcription via Tat deacetylation," *PLoS Biology*, vol. 3, pp. 0210–0220, feb 2005.

[156] R. Harrod, J. Nacsa, C. Van Lint, J. Hansen, T. Karpova, J. McNally, and G. Franchini, "Human immunodeficiency virus type-1 Tat/co-activator acetyltransferase interactions inhibit p53Lys-320 acetylation and p53-responsive transcription," *Journal of Biological Chemistry*, vol. 278, pp. 12310–12318, apr 2003.

[157] E. Col, C. Caron, C. Chable-Bessia, G. Legube, S. Gazzeri, Y. Komatsu, M. Yoshida, M. Benkirane, D. Trouche, and S. Khochbin, "HIV-1 Tat targets Tip60 to impair the apoptotic cell response to genotoxic stresses.," *The EMBO journal*, vol. 24, no. 14, pp. 2634–45, 2005.

[158] V. Sapountzi, I. R. Logan, and C. N. Robson, "Cellular functions of TIP60," *International Journal of Biochemistry and Cell Biology*, vol. 38, no. 9, pp. 1496–1509, 2006.

[159] M. Creaven, F. Hans, V. Mutskov, E. Col, C. Caron, S. Dimitrov, and S. Khochbin, "Control of the histone-acetyltransferase activity of Tip60 by the HIV-1 transactivator protein, Tat," *Biochemistry*, vol. 38, no. 27, pp. 8826–8830, 1999.

[160] L. Zhang, J. Qin, Y. Li, J. Wang, Q. He, J. Zhou, M. Liu, and D. Li, "Modulation of the stability and activities of HIV-1 Tat by its ubiquitination and carboxyl-terminal region," *Cell and Bioscience*, vol. 4, no. 1, 2014.

[161] V. Brès, R. E. Kiernan, L. K. Linares, C. Chable-Bessia, O. Plechakova, C. Tréand, S. Emiliani, J.-M. Peloponese, K.-T. Jeang, O. Coux, M. Scheffner, and M. Benkirane, "A non-proteolytic role for ubiquitin in Tat-mediated transactivation of the HIV-1 promoter.," *Nature cell biology*, vol. 5, no. 8, pp. 754–761, 2003.

[162] T. B. Faust, Y. Li, G. M. Jang, J. R. Johnson, S. Yang, A. Weiss, N. J. Krogan, and A. D. Frankel, "PJA2 ubiquitinates the HIV-1 Tat protein with atypical chain linkages to activate viral transcription," *Scientific Reports*, vol. 7, p. 45394, mar 2017.

[163] T. D. Zaikos and K. L. Collins, "Long-lived reservoirs of HIV-1," *Trends in Microbiology*, vol. 22, no. 4, pp. 173–175, 2014.

[164] G. Q. Lee and M. Lichterfeld, "Diversity of HIV-1 reservoirs in CD4+ T-cell subpopulations," *Current Opinion in HIV and AIDS*, vol. 11, no. 4, pp. 383–387, 2016.

[165] D. J. Colby, L. Trautmann, S. Pinyakorn, L. Leyre, and A. Pagliuzza et al., "Rapid HIV RNA rebound after antiretroviral treatment interruption in persons durably suppressed in Fiebig I acute HIV infection brief-communication," *Nature Medicine*, vol. 24, no. 7, pp. 923–926, 2018.

[166] T. W. Chun, D. Engel, M. M. Berrey, T. Shea, L. Corey, and A. S. Fauci, "Early establishment of a pool of latently infected, resting CD4+ T cells during primary HIV-1 infection," *Proceedings of the National Academy of Sciences of the United States of America*, vol. 95, no. 15, pp. 8869–8873, 1998.

[167] S. Eriksson, E. H. Graf, V. Dahl, M. C. Strain, S. A. Yukl, E. S. Lysenko, R. J. Bosch, J. Lai, S. Chioma, F. Emad, M. Abdel-Mohsen, R. Hoh, F. Hecht, P. Hunt, M. Somsouk, J. Wong, R. Johnston, R. F. Siliciano, D. D. Richman, U. O'Doherty, S. Palmer, S. G. Deeks, and J. D. Siliciano, "Comparative Analysis of Measures of Viral Reservoirs in HIV-1 Eradication Studies," *PLoS Pathogens*, vol. 9, no. 2, 2013.

[168] A. Jordan, D. Bisgrove, and E. Verdin, "HIV reproducibly establishes a latent infection after acute infection of T cells in vitro," *EMBO Journal*, vol. 22, no. 8, pp. 1868–1877, 2003.

[169] T. Folks, D. M. Powell, M. M. Lightfoote, S. Benn, M. A. Martin, and A. S. Fauci, "Induction of HTLV-III/LAV from a nonvirus-producing T-cell line: Implications for latency," *Science*, vol. 231, no. 4738, pp. 600–602, 1986.

[170] L. Chavez, V. Calvanese, and E. Verdin, "HIV Latency Is Established Directly and Early in Both Resting and Activated Primary CD4 T Cells," *PLoS Pathogens*, vol. 11, no. 6, 2015.

[171] L. M. Agosto and A. J. Henderson, "CD4+ T Cell Subsets and Pathways to HIV Latency," *AIDS Research and Human Retroviruses*, vol. 34, no. 9, pp. 780–789, 2018.

[172] B. Lindqvist, S. S. Akusjärvi, A. Sönnerborg, M. Dimitriou, and J. P. Svensson, "Chromatin maturation of the HIV-1 provirus in primary resting CD4+ T cells," *PLoS Pathogens*, vol. 16, no. 1, p. e1008264, 2020.

[173] M. K. Lewinski, D. Bisgrove, P. Shinn, H. Chen, C. Hoffmann, S. Hannenhalli, E. Verdin, C. C. Berry, J. R. Ecker, and F. D. Bushman, "Genome-Wide Analysis of Chromosomal Features Repressing Human Immunodeficiency Virus Transcription," *Journal of Virology*, vol. 79, no. 11, pp. 6610–6619, 2005.

[174] C. Van Lint and V. Quivy, "Diversity of acetylation targets and roles in transcriptional regulation: the human immunodeficiency virus type 1 promoter as a model system.," *Biochemical pharmacology*, vol. 64, no. 5-6, pp. 925–34, 2002.

[175] C. Van Lint, S. Emiliani, M. Ott, and E. Verdin, "Transcriptional activation and chromatin remodeling of the HIV-1 promoter in response to histone acetylation," *EMBO Journal*, vol. 15, no. 5, pp. 1112–1120, 1996.

[176] J. J. Coull, F. Romerio, J.-M. Sun, J. L. Volker, K. M. Galvin, J. R. Davie, Y. Shi, U. Hansen, and D. M. Margolis, "The Human Factors YY1 and LSF Repress the Human Immunodeficiency Virus Type 1 Long Terminal Repeat via Recruitment of Histone Deacetylase 1," *Journal of Virology*, vol. 74, no. 15, pp. 6790–6799, 2000.

[177] W. Bernhard, K. Barreto, S. Raithatha, and I. Sadowski, "An Upstream YY1 Binding Site on the HIV-1 LTR Contributes to Latent Infection," *PLoS ONE*, vol. 8, no. 10, p. e77052, 2013.

[178] S. A. Williams, L. F. Chen, H. Kwon, C. M. Ruiz-Jarabo, E. Verdin, and W. C. Greene, "NF-κB p50 promotes HIV latency through HDAC recruitment and repression of transcriptional initiation," *EMBO Journal*, vol. 25, no. 1, pp. 139–149, 2006.

[179] J. K. Chan and W. C. Greene, "NF-κB/Rel: Agonist and antagonist roles in HIV-1 latency," *Current Opinion in HIV and AIDS*, vol. 6, no. 1, pp. 12–18, 2011.

[180] M. Tyagi and J. Karn, "CBF-1 promotes transcriptional silencing during the establishment of HIV-1 latency," *EMBO Journal*, vol. 26, no. 24, pp. 4985–4995, 2007.

[181] C. Marban, L. Redel, S. Suzanne, C. Van Lint, D. Lecestre, S. Chasserot-Golaz, M. Leid, D. Aunis, E. Schaeffer, and O. Rohr, "COUP-TF interacting protein 2 represses the initial phase of HIV-1 gene transcription in human microglial cells," *Nucleic Acids Research*, vol. 33, no. 7, pp. 2318–2331, 2005.

[182] K. Imai and T. Okamoto, "Transcriptional repression of human immunodeficiency virus type 1 by AP-4," *Journal of Biological Chemistry*, vol. 281, no. 18, pp. 12495–12505, 2006.

[183] G. Jiang, A. Espeseth, D. J. Hazuda, and D. M. Margolis, "c-Myc and Sp1 Contribute to Proviral Latency by Recruiting Histone Deacetylase 1 to the Human Immunodeficiency Virus Type 1 Promoter," *Journal of Virology*, vol. 81, no. 20, pp. 10914–10923, 2007.

[184] K. S. Keedy, N. M. Archin, A. T. Gates, A. Espeseth, D. J. Hazuda, and D. M. Margolis, "A Limited Group of Class I Histone Deacetylases Acts To Repress Human Immunodeficiency Virus Type 1 Expression," *Journal of Virology*, vol. 83, no. 10, pp. 4749–4756, 2009.

[185] N. M. Archin, A. Espeseth, D. Parker, M. Cheema, D. Hazuda, and D. M. Margolis, "Expression of latent HIV induced by the potent HDAC inhibitor suberoylanilide hydroxamic acid.," *AIDS research and human retroviruses*, vol. 25, pp. 207–12, feb 2009.

[186] A. Sabò, M. Lusic, A. Cereseto, and M. Giacca, "Acetylation of Conserved Lysines in the Catalytic Core of Cyclin-Dependent Kinase 9 Inhibits Kinase Activity and Regulates Transcription," *Molecular and Cellular Biology*, vol. 28, no. 7, pp. 2201–2212, 2008.

[187] A. P. Rice, "P-TEFb as a target to reactivate latent HIV: Two Brds are now in hand," *Cell Cycle*, vol. 12, no. 3, pp. 392–393, 2013.

[188] M. Taura, E. Kudo, R. Kariya, H. Goto, K. Matsuda, S. Hattori, K. Vaeteewoottacharn, F. McDonald, M. A. Suico, T. Shuto, H. Kai, and S. Okada, "COMMD1/Murr1 Reinforces HIV-1 Latent Infection through IκB-α Stabilization," *Journal of Virology*, vol. 89, pp. 2643–2658, mar 2015.

[189] N. He, M. Liu, J. Hsu, Y. Xue, S. Chou, A. Burlingame, N. J. Krogan, T. Alber, and Q. Zhou, "HIV-1 Tat and Host AFF4 Recruit Two Transcription Elongation Factors into a Bifunctional Complex for Coordinated Activation of HIV-1 Transcription," *Molecular Cell*, vol. 38, pp. 428–438, may 2010.

[190] M. Liu, J. Hsu, C. Chan, Z. Li, and Q. Zhou, "The Ubiquitin Ligase Siah1 Controls ELL2 Stability and Formation of Super Elongation Complexes to Modulate Gene Transcription," *Molecular Cell*, vol. 46, pp. 325–334, may 2012.

[191] A. Kudoh, S. Takahama, T. Sawasaki, H. Ode, M. Yokoyama, A. Okayama, A. Ishikawa, K. Miyakawa, S. Matsunaga, H. Kimura, W. Sugiura, H. Sato, H. Hirano, S. Ohno, N. Yamamoto, and A. Ryo, "The phosphorylation of HIV-1 Gag by atypical protein kinase C facilitates viral infectivity by promoting Vpr incorporation into virions," *Retrovirology*, vol. 11, p. 9, jan 2014.

[192] B. Hemonnot, C. Cartier, B. Gay, S. Rebuffat, M. Bardy, C. Devaux, V. Boyer, and L. Briant, "The host cell MAP kinase ERK-2 regulates viral assembly and release by phosphorylating the p6gag protein of HIV-1," *Journal of Biological Chemistry*, vol. 279, no. 31, pp. 32426–32434, 2004.

[193] J. M. Jacqué, A. Mann, H. Enslen, N. Sharova, B. Brichacek, R. J. Davis, and M. Stevenson, "Modulation of HIV-1 infectivity by MAPK, a virion-associated kinase," *EMBO Journal*, vol. 17, no. 9, pp. 2607–2618, 1998.

[194] X. Ye, N. Ong, H. An, and Y. Zheng, "The Emerging Roles of NDR1/2 in Infection and Inflammation," *Frontiers in Immunology*, vol. 11, p. 534, 2020.

[195] G. Clerzius, E. Shaw, A. Daher, S. Burugu, J.-F. Gélinas, T. Ear, L. Sinck, J.-P. Routy, A. J. Mouland, R. C. Patel, and A. Gatignol, "The PKR activator, PACT, becomes a PKR inhibitor during HIV-1 replication," *Retrovirology*, vol. 10, p. 96, sep 2013.

[196] S. Burugu, A. Daher, E. F. Meurs, and A. Gatignol, "HIV-1 translation and its regulation by cellular factors PKR and PACT," *Virus Research*, vol. 193, pp. 65–77, nov 2014.

[197] E. Chukwurah, I. Handy, and R. C. Patel, "ADAR1 and PACT contribute to efficient translation of transcripts containing HIV-1 trans-activating response (TAR) element," *Biochemical Journal*, vol. 474, pp. 1241–1257, mar 2017.

[198] K. Hrecka, M. Gierszewska, S. Srivastava, L. Kozaczkiewicz, S. K. Swanson, L. Florens, M. P. Washburn, and J. Skowronski, "Lentiviral Vpr usurps Cul4-DDB1[VprBP] E3 ubiquitin ligase to modulate cell cycle," *Proceedings of the National Academy of Sciences of the United States of America*, vol. 104, pp. 11778–11783, jul 2007.

[199] G. Li, H. U. Park, D. Liang, and R. Y. Zhao, "Cell cycle G2/M arrest through an S phase-dependent mechanism by HIV-1 viral protein R," *Retrovirology*, vol. 7, p. 59, jul 2010.

[200] M. Roshal, B. Kim, Y. Zhu, P. Nghiem, and V. Planelles, "Activation of the ATR-mediated DNA damage response by the HIV-1 viral protein R," *Journal of Biological Chemistry*, vol. 278, pp. 25879–25886, jul 2003.

[201] I. Alroy, S. Tuvia, and T. Greener et al., "The trans-Golgi network-associated human ubiquitin-protein ligase POSH is essential for HIV type 1 production.," *Proceedings of the National Academy of Sciences of the United States of America*, vol. 102, pp. 1478–83, feb 2005.

[202] J. Votteler, E. Iavnilovitch, O. Fingrut, V. Shemesh, D. Taglicht, O. Erez, S. Sörgel, T. Walther, N. Bannert, U. Schubert, and Y. Reiss, "Exploring the functional interaction between POSH and ALIX and the relevance to HIV-1 release," *BMC Biochemistry*, vol. 10, no. 1, p. 12, 2009.

[203] I. Amit, L. Yakir, M. Katz, Y. Zwang, and M. D. Marmor et al., "Tal, a Tsg101-specific E3 ubiquitin ligase, regulates receptor endocytosis and retrovirus budding," *Genes and Development*, vol. 18, pp. 1737–1752, jul 2004.

[204] C. Setz, M. Friedrich, P. Rauch, K. Fraedrich, A. Matthaei, M. Traxdorf, and U. Schubert, "Inhibitors of deubiquitinating enzymes block HIV-1 replication and augment the presentation of gag-derived MHC-I epitopes," *Viruses*, vol. 9, p. 222, aug 2017.

[205] T. Tada, Y. Zhang, T. Koyama, M. Tobiume, Y. Tsunetsugu-Yokota, S. Yamaoka, H. Fujita, and K. Tokunaga, "March8 inhibits HIV-1 infection by reducing virion incorporation of envelope glycoproteins," dec 2015.

[206] S. K. Choudhary and D. M. Margolis, "Curing HIV: Pharmacologic approaches to target HIV-1 Latency," *Annual Review of Pharmacology and Toxicology*, vol. 51, pp. 397–418, feb 2011.

[207] T. Geiger, J. R. Wisniewski, J. Cox, S. Zanivan, M. Kruger, Y. Ishihama, M. Mann, and S. Zanivan, "Use of stable isotope labeling by amino acids in cell culture as a spike-in standard in quantitative proteomics," *Nature Protocols*, vol. 6, no. 2, pp. 147–157, 2011.

[208] O. Boussif, F. LezoualC'H, M. A. Zanta, M. D. Mergny, D. Scherman, B. Demeneix, and J. P. Behr, "A versatile vector for gene and oligonucleotide transfer into cells in culture and in vivo: Polyethylenimine," *Proceedings of the National Academy of Sciences of the United States of America*, vol. 92, no. 16, pp. 7297–7301, 1995.

[209] P. A. Longo, J. M. Kavran, M. S. Kim, and D. J. Leahy, "Transient mammalian cell transfection with polyethylenimine (PEI)," in *Methods in Enzymology*, vol. 529, pp. 227–240, NIH Public Access, 2013.

[210] W.-Z. Ho, R. Cherukuri, S.-D. Ge, J. R. Cutilli, L. Song, S. Whitko, and S. D. Douglas, "Centrifugal enhancement of human immunodeficiency virus type 1 infection and human cytomegalovirus gene expression in human primary monocyte/macrophages in vitro," *Journal of Leukocyte Biology*, vol. 53, pp. 208–212, feb 1993.

[211] D. M. Knipe, *Fields' virology*. New York, NY: Wolters Kluwer Health, 6 ed., 2013.

[212] R. W. Figliozzi, F. Chen, A. Chi, and S. C. V. Hsia, "Using the inverse Poisson distribution to calculate multiplicity of infection and viral replication by a high-throughput fluorescent imaging system," *Virologica Sinica*, vol. 31, no. 2, pp. 180–183, 2016.

[213] D. C. Montefiori, "Measuring HIV neutralization in a luciferase reporter gene assay," *Methods in Molecular Biology*, vol. 485, pp. 395–405, 2009.

[214] S. Tyanova, T. Temu, P. Sinitcyn, A. Carlson, M. Y. Hein, T. Geiger, M. Mann, and J. Cox, "The Perseus computational platform for comprehensive analysis of (prote)omics data," *Nature Methods*, vol. 13, no. 9, pp. 731–740, 2016.

[215] S. Tyanova and J. Cox, "Perseus: A bioinformatics platform for integrative analysis of proteomics data in cancer research," in *Methods in Molecular Biology*, vol. 1711, pp. 133–148, Humana Press Inc., 2018.

[216] R. C. T. (2018), "R: A Language and Environment for Statistical Computing." https://www.gbif.org/tool/81287/r-a-language-and-environment-for-statistical-computing, date accessed: 01.09.2020, 2008.

[217] U. Raudvere, L. Kolberg, I. Kuzmin, T. Arak, P. Adler, H. Peterson, and J. Vilo, "G:Profiler: A web server for functional enrichment analysis and conversions of gene lists (2019 update)," *Nucleic Acids Research*, vol. 47, pp. W191–W198, jul 2019.

[218] A. Thompson, J. Schäfer, K. Kuhn, S. Kienle, J. Schwarz, G. Schmidt, T. Neumann, and C. Hamon, "Tandem mass tags: A novel quantification strategy for comparative analysis of complex protein mixtures by MS/MS," *Analytical Chemistry*, vol. 75, pp. 1895–1904, apr 2003.

[219] S. Tyanova, T. Temu, and J. Cox, "The MaxQuant computational platform for mass spectrometry-based shotgun proteomics," *Nature Protocols*, vol. 11, no. 12, pp. 2301–2319, 2016.

[220] J. E. Elias and S. P. Gygi, "Target-decoy search strategy for increased confidence in large-scale protein identifications by mass spectrometry," *Nature Methods*, vol. 4, no. 3, pp. 207–214, 2007.

[221] M. Gierlinski, F. Gastaldello, C. Cole, and G. J. Barton, "Proteus: an R package for downstream analysis of MaxQuant output," *bioRxiv*, p. 416511, 2018.

[222] M. Ashburner, C. A. Ball, J. A. Blake, D. Botstein, H. Butler, J. M. Cherry, A. P. Davis, K. Dolinski, S. S. Dwight, J. T. Eppig, M. A. Harris, D. P. Hill, L. Issel-Tarver, A. Kasarskis, S. Lewis, J. C. Matese, J. E. Richardson, M. Ringwald, G. M. Rubin, and G. Sherlock, "Gene ontology: Tool for the unification of biology," 2000.

[223] G. Yu, L. G. Wang, Y. Han, and Q. Y. He, "ClusterProfiler: An R package for comparing biological themes among gene clusters," *OMICS A Journal of Integrative Biology*, vol. 16, no. 5, pp. 284–287, 2012.

[224] W. Luo and C. Brouwer, "Pathview: An R/Bioconductor package for pathway-based data integration and visualization," *Bioinformatics*, vol. 29, no. 14, pp. 1830–1831, 2013.

[225] HGNC, "HUGO Gene Nomenclature Commitee (HGNC)." https://www.genenames.org, date accessed: 08.08.2018.

[226] B. Medvar, V. Raghuram, T. Pisitkun, A. Sarkar, and M. A. Knepper, "Comprehensive database of human E3 ubiquitin ligases: Application to aquaporin-2 regulation," *Physiological Genomics*, vol. 48, pp. 502–512, jul 2016.

[227] T. Gao, Z. Liu, Y. Wang, H. Cheng, Q. Yang, A. Guo, J. Ren, and Y. Xue, "UUCD: A family-based database of ubiquitin and ubiquitin-like conjugation," *Nucleic Acids Research*, vol. 41, no. D1, 2013.

[228] G. Manning, D. Whyte, and R. Martinez et al., "The protein kinase complement of the human genome.," *Science (New York, N.Y.)*, vol. 298, no. 5600, pp. 1912–34, 2002.

[229] G. Duan, X. Li, and M. Köhn, "The human DEPhOsphorylation database DEPOD: A 2015 update," *Nucleic Acids Research*, vol. 43, no. D1, pp. D531–D535, 2015.

[230] P. Mohammadi, S. Desfarges, I. Bartha, B. Joos, N. Zangger, M. Muñoz, H. F. Günthard, N. Beerenwinkel, A. Telenti, and A. Ciuffi, "24 Hours in the Life of HIV-1 in a T Cell Line," *PLoS Pathogens*, vol. 9, no. 1, p. 1003161, 2013.

[231] J. Johnson, D. Crosby, J. Hultquist, D. Li, J. Marlett, J. Swann, R. Hüttenhain, E. Verschueren, T. Johnson, B. Newton, M. Shales, P. Beltrao, A. Frankel, A. Marson, O. Fregoso, J. Young, and N. Krogan, "Global post-translational modification profiling of HIV-1-infected cells reveals mechanisms of host cellular pathway remodeling," *bioRxiv*, p. 2020.01.06.896365, jan 2020.

[232] A. Foli, M. A. Maiocchi, J. Lisziewicz, and F. Lori, "A checkpoint in the cell cycle progression as a therapeutic target to inhibit HIV replication," *Journal of Infectious Diseases*, vol. 196, no. 9, pp. 1409–1415, 2007.

[233] D. J. Salamango, T. Ikeda, S. A. Moghadasi, J. Wang, J. L. McCann, A. A. Serebrenik, D. Ebrahimi, M. C. Jarvis, W. L. Brown, and R. S. Harris, "HIV-1 Vif Triggers Cell Cycle Arrest by Degrading Cellular PPP2R5 Phospho-regulators," *Cell Reports*, vol. 29, no. 5, pp. 1057–1065.e4, 2019.

[234] R. Y. Zhao and R. T. Elder, "Viral infections and cell cycle G2/M regulation," *Cell Research*, vol. 15, no. 3, pp. 143–149, 2005.

[235] Y. M. Loo and M. Gale, "Immune Signaling by RIG-I-like Receptors," *Immunity*, vol. 34, pp. 680–692, may 2011.

[236] N. Jounai, F. Takeshita, K. Kobiyama, A. Sawano, A. Miyawaki, K. Q. Xin, K. J. Ishii, T. Kawai, S. Akira, K. Suzuki, and K. Okuda, "The Atg5-Atg12 conjugate associates with innate antiviral immune responses," *Proceedings of the National Academy of Sciences of the United States of America*, vol. 104, pp. 14050–14055, aug 2007.

[237] S. Liu, X. Cai, J. Wu, Q. Cong, X. Chen, T. Li, F. Du, J. Ren, Y. T. Wu, N. V. Grishin, and Z. J. Chen, "Phosphorylation of innate immune adaptor proteins MAVS, STING, and TRIF induces IRF3 activation," *Science*, vol. 347, pp. aaa2630–aaa2630, mar 2015.

[238] P. V. Hornbeck, B. Zhang, B. Murray, J. M. Kornhauser, V. Latham, and E. Skrzypek, "PhosphoSitePlus, 2014: Mutations, PTMs and recalibrations," *Nucleic Acids Research*, vol. 43, no. D1, pp. D512–D520, 2015.

[239] D. Szklarczyk, A. L. Gable, D. Lyon, A. Junge, S. Wyder, J. Huerta-Cepas, M. Simonovic, N. T. Doncheva, J. H. Morris, P. Bork, L. J. Jensen, and C. Von Mering, "STRING v11: Protein-protein association networks with increased coverage, supporting functional discovery in genome-wide experimental datasets," *Nucleic Acids Research*, vol. 47, pp. D607–D613, jan 2019.

[240] P. Shannon, A. Markiel, O. Ozier, N. S. Baliga, J. T. Wang, D. Ramage, N. Amin, B. Schwikowski, and T. Ideker, "Cytoscape: A software Environment for integrated models of biomolecular interaction networks," *Genome Research*, vol. 13, no. 11, pp. 2498–2504, 2003.

[241] S. Carbon, E. Douglass, N. Dunn, B. Good, and N. L. Harris et al., "The Gene Ontology Resource: 20 years and still GOing strong," *Nucleic Acids Research*, vol. 47, no. D1, pp. D330–D338, 2019.

[242] M. Kanehisa, M. Furumichi, M. Tanabe, Y. Sato, and K. Morishima, "KEGG: New perspectives on genomes, pathways, diseases and drugs," *Nucleic Acids Research*, vol. 45, no. D1, pp. D353–D361, 2017.

[243] M. Y. Jeng, I. Ali, and M. Ott, "Manipulation of the host protein acetylation network by human immunodeficiency virus type 1.," *Critical reviews in biochemistry and molecular biology*, vol. 50, no. 4, pp. 314–325, 2015.

[244] M. He, L. Zhang, X. Wang, L. Huo, L. Sun, C. Feng, X. Jing, D. Du, H. Liang, M. Liu, Z. Hong, and J. Zhou, "Systematic Analysis of the Functions of Lysine Acetylation in the Regulation of Tat Activity," *PLoS ONE*, vol. 8, no. 6, p. e67186, 2013.

[245] K. Wong, A. Sharma, S. Awasthi, E. F. Matlock, L. Rogers, C. Van Lint, D. J. Skiest, D. K. Burns, and R. Harrod, "HIV-1 tat interactions with p300 and PCAF transcriptional coactivators inhibit histone acetylation and neurotrophin signaling through CREB," *Journal of Biological Chemistry*, vol. 280, no. 10, pp. 9390–9399, 2005.

[246] M. Ott, M. Schnölzer, J. Garnica, W. Fischle, S. Emiliani, H. R. Rackwitz, and E. Verdin, "Acetylation of the HIV-1 tat protein by p300 is important for its transcriptional activity," *Current Biology*, vol. 9, no. 24, pp. 1489–1493, 1999.

[247] K. Kamieniarz and R. Schneider, "Tools to Tackle Protein Acetylation," *Chemistry and Biology*, vol. 16, no. 10, pp. 1027–1029, 2009.

[248] K. Verhoef, M. Bauer, A. Meyerhans, and B. Berkhout, "On the role of the second coding exon of the HIV-1 tat protein in virus replication and MHC class I downregulation," *AIDS Research and Human Retroviruses*, vol. 14, pp. 1553–1559, nov 1998.

[249] M. Giurgiu, J. Reinhard, B. Brauner, I. Dunger-Kaltenbach, G. Fobo, G. Frishman, C. Montrone, and A. Ruepp, "CORUM: The comprehensive resource of mammalian protein complexes - 2019," *Nucleic Acids Research*, vol. 47, pp. D559–D563, jan 2019.

[250] E. J. Platt, K. Wehrly, S. E. Kuhmann, B. Chesebro, and D. Kabat, "Effects of CCR5 and CD4 Cell Surface Concentrations on Infections by Macrophagetropic Isolates of Human Immunodeficiency Virus Type 1," *Journal of Virology*, vol. 72, pp. 2855–2864, apr 1998.

[251] C. A. Derdeyn, J. M. Decker, J. N. Sfakianos, X. Wu, W. A. O'Brien, L. Ratner, J. C. Kappes, G. M. Shaw, and E. Hunter, "Sensitivity of Human Immunodeficiency Virus Type 1 to the Fusion Inhibitor T-20 Is Modulated by Coreceptor Specificity Defined by the V3 Loop of gp120," *Journal of Virology*, vol. 74, pp. 8358–8367, sep 2000.

[252] Y. Takeuchi, M. O. McClure, and M. Pizzato, "Identification of Gammaretroviruses Constitutively Released from Cell Lines Used for Human Immunodeficiency Virus Research," *Journal of Virology*, vol. 82, pp. 12585–12588, dec 2008.

[253] E. J. Platt, M. Bilska, S. L. Kozak, D. Kabat, and D. C. Montefiori, "Evidence that Ecotropic Murine Leukemia Virus Contamination in TZM-bl Cells Does Not Affect the Outcome of Neutralizing Antibody Assays with Human Immunodeficiency Virus Type 1," *Journal of Virology*, vol. 83, pp. 8289–8292, aug 2009.

[254] X. Wei, J. M. Decker, H. Liu, Z. Zhang, R. B. Arani, J. M. Kilby, M. S. Saag, X. Wu, G. M. Shaw, and J. C. Kappes, "Emergence of resistant human immunodeficiency virus type 1 in patients receiving fusion inhibitor (T-20) monotherapy," *Antimicrobial Agents and Chemotherapy*, vol. 46, no. 6, pp. 1896–1905, 2002.

[255] R. Lorenzo-Redondo, H. R. Fryer, T. Bedford, E. Y. Kim, J. Archer, S. L. Kosakovsky Pond, Y. S. Chung, S. Penugonda, J. G. Chipman, C. V. Fletcher, T. W. Schacker, M. H. Malim, A. Rambaut, A. T. Haase, A. R. McLean, and S. M. Wolinsky, "Persistent HIV-1 replication maintains the tissue reservoir during therapy," *Nature*, vol. 530, no. 7588, pp. 51–56, 2016.

[256] T. D. Zaikos, M. M. Painter, N. T. Sebastian, V. H. Terry, and K. L. Collins, "Class 1-selective histone deacetylase inhibitors enhance HIV latency reversal while preserving the activity of HDAC isoforms necessary for maximal HIV gene expression," *Journal of Virology*, vol. 92, no. 6, pp. JVI.02110–17, 2018.

[257] T. Liang, X. Zhang, F. Lai, J. Lin, C. Zhou, X. Xu, X. Tan, S. Liu, and L. Li, "A novel bromodomain inhibitor, CPI-203, serves as an HIV-1 latency-reversing agent by activating positive transcription elongation factor b," *Biochemical Pharmacology*, vol. 164, pp. 237–251, 2019.

[258] X. Contreras, M. Schweneker, C. S. Chen, J. M. McCune, S. G. Deeks, J. Martin, and B. M. Peterlin, "Suberoylanilide hydroxamic acid reactivates HIV from latently infected cells," *Journal of Biological Chemistry*, vol. 284, no. 11, pp. 6782–6789, 2009.

[259] H. Pan, P. Lu, Y. Shen, Y. Wang, Z. Jiang, X. Yang, Y. Zhong, H. Yang, I. U. Khan, M. Zhou, B. Li, Z. Zhang, J. Xu, H. Lu, and H. Zhu, "The bromodomain and extraterminal domain inhibitor bromosporine synergistically reactivates latent HIV-1 in latently infected cells," *Oncotarget*, vol. 8, no. 55, pp. 94104–94116, 2017.

[260] M. A. Moro-García, J. C. Mayo, R. M. Sainz, and R. Alonso-Arias, "Influence of inflammation in the process of T lymphocyte differentiation: Proliferative, metabolic, and oxidative changes," *Frontiers in Immunology*, vol. 9, p. 1, mar 2018.

[261] M. B. Lucera, C. A. Tilton, H. Mao, C. Dobrowolski, C. O. Tabler, A. A. Haqqani, J. Karn, and J. C. Tilton, "The Histone Deacetylase Inhibitor Vorinostat (SAHA) Increases the Susceptibility of Uninfected CD4+ T Cells

to HIV by Increasing the Kinetics and Efficiency of Postentry Viral Events," *Journal of Virology*, vol. 88, no. 18, pp. 10803–10812, 2014.

[262] O. Sogaard, M. E. Graversen, S. Leth, C. R. Brinkmann, A. S. Kjaer, R. Olesen, P. W. Denton, S. K. Nissen, M. Sommerfelt, and T. A. Rasmussen, "The HDAC inhibitor romidepsin is safe and effectively reverses HIV-1 latency in vivo as measured by standard clinical assays," *20th Int AIDS Conf*, 2014.

[263] D. G. Wei, V. Chiang, E. Fyne, M. Balakrishnan, T. Barnes, M. Graupe, J. Hesselgesser, A. Irrinki, J. P. Murry, G. Stepan, K. M. Stray, A. Tsai, H. Yu, J. Spindler, M. Kearney, C. A. Spina, D. McMahon, J. Lalezari, D. Sloan, J. Mellors, R. Geleziunas, and T. Cihlar, "Histone Deacetylase Inhibitor Romidepsin Induces HIV Expression in CD4 T Cells from Patients on Suppressive Antiretroviral Therapy at Concentrations Achieved by Clinical Dosing," *PLoS Pathogens*, vol. 10, no. 4, 2014.

[264] T. A. Rasmussen, M. Tolstrup, C. R. Brinkmann, R. Olesen, C. Erikstrup, A. Solomon, A. Winckelmann, S. Palmer, C. Dinarello, M. Buzon, M. Lichterfeld, S. R. Lewin, L. Ostergaard, and O. S. Søgaard, "Panobinostat, a histone deacetylase inhibitor, for latent virus reactivation in HIV-infected patients on suppressive antiretroviral therapy: A phase 1/2, single group, clinical trial," *The Lancet HIV*, vol. 1, no. 1, pp. e13–e21, 2014.

[265] D. R. Liston and M. Davis, "Clinically relevant concentrations of anticancer drugs: A guide for nonclinical studies," *Clinical Cancer Research*, vol. 23, pp. 3489–3498, jul 2017.

[266] M. Loprevite, M. Tiseo, F. Grossi, T. Scolaro, C. Semino, A. Pandolfi, R. Favoni, and A. Ardizzoni, "In vitro study of CI-994, a histone deacetylase inhibitor, in non-small cell lung cancer cell lines," *Oncology Research*, vol. 15, no. 1, pp. 39–48, 2005.

[267] J. Sauer, K. K. Richter, and B. L. Pool-Zobel, "Physiological concentrations of butyrate favorably modulate genes of oxidative and metabolic stress in primary human colon cells," *Journal of Nutritional Biochemistry*, vol. 18, no. 11, pp. 736–745, 2007.

[268] A. R. Cillo, M. D. Sobolewski, R. J. Bosch, E. Fyne, M. Piatak, J. M. Coffin, and J. W. Mellors, "Quantification of HIV-1 latency reversal in resting CD4+ T cells from patients on suppressive antiretroviral therapy," *Proceedings of the National Academy of Sciences of the United States of America*, vol. 111, no. 19, pp. 7078–7083, 2014.

[269] C. Ochsenbauer, T. G. Edmonds, H. Ding, B. F. Keele, J. Decker, M. G. Salazar, J. F. Salazar-Gonzalez, R. Shattock, B. F. Haynes, G. M. Shaw, B. H. Hahn, and J. C. Kappes, "Generation of Transmitted/Founder HIV-1 Infectious Molecular Clones and Characterization of Their Replication Capacity in CD4 T Lymphocytes and Monocyte-Derived Macrophages," *Journal of Virology*, vol. 86, no. 5, pp. 2715–2728, 2012.

[270] D. Wang, B. Eraslan, T. Wieland, B. Hallström, T. Hopf, D. P. Zolg, J. Zecha, A. Asplund, L. Li, C. Meng, M. Frejno, T. Schmidt, K. Schnatbaum, M. Wilhelm, F. Ponten, M. Uhlen, J. Gagneur, H. Hahne, and B. Kuster, "A deep proteome and transcriptome abundance atlas of 29 healthy human tissues," *Molecular Systems Biology*, vol. 15, feb 2019.

[271] S. Ivanov, A. Lagunin, D. Filimonov, and O. Tarasova, "Network-Based Analysis of OMICs Data to Understand the HIV–Host Interaction," *Frontiers in Microbiology*, vol. 11, jun 2020.

[272] T. Guirimand, S. Delmotte, and V. Navratil, "VirHostNet 2.0: Surfing on the web of virus/host molecular interactions data," *Nucleic Acids Research*, vol. 43, pp. D583–D587, jan 2015.

[273] H. V. Cook, N. T. Doncheva, D. Szklarczyk, C. von Mering, and L. J. Jensen, "Viruses.STRING: A virus-host protein-protein interaction database," *Viruses*, vol. 10, oct 2018.

[274] Y. Luo, E. Y. Jacobs, T. M. Greco, K. D. Mohammed, T. Tong, S. Keegan, J. M. Binley, I. M. Cristea, D. Fenyö, M. P. Rout, B. T. Chait, and M. A. Muesing, "HIV–host interactome revealed directly from infected cells," *Nature Microbiology*, vol. 1, no. 7, p. 16068, 2016.

[275] R. J. Park, T. Wang, D. Koundakjian, J. F. Hultquist, P. Lamothe-Molina, B. Monel, K. Schumann, H. Yu, K. M. Krupzcak, W. Garcia-Beltran, A. Piechocka-Trocha, N. J. Krogan, A. Marson, D. M. Sabatini, E. S. Lander, N. Hacohen, and B. D. Walker, "A genome-wide CRISPR screen identifies a restricted set of HIV host dependency factors," *Nature Genetics*, vol. 49, pp. 193–203, jan 2017.

[276] H. Zhou, M. Xu, Q. Huang, A. T. Gates, X. D. Zhang, J. C. Castle, E. Stec, M. Ferrer, B. Strulovici, D. J. Hazuda, and A. S. Espeseth, "Genome-Scale RNAi Screen for Host Factors Required for HIV Replication," *Cell Host and Microbe*, vol. 4, pp. 495–504, nov 2008.

[277] A. S. Venne, L. Kollipara, and R. P. Zahedi, "The next level of complexity: Crosstalk of posttranslational modifications," *Proteomics*, vol. 14, no. 4-5, pp. 513–524, 2014.

[278] P. Mertins, J. W. Qiao, J. Patel, N. D. Udeshi, K. R. Clauser, D. R. Mani, M. W. Burgess, M. A. Gillette, J. D. Jaffe, and S. A. Carr, "Integrated proteomic analysis of post-translational modifications by serial enrichment," *Nature Methods*, vol. 10, pp. 634–637, jul 2013.

[279] P. J. Klasse, "Molecular determinants of the ratio of inert to infectious virus particles," in *Progress in Molecular Biology and Translational Science*, vol. 129, pp. 285–326, Elsevier B.V., 2015.

[280] Y. Wu and J. W. Marsh, "Early Transcription from Nonintegrated DNA in Human Immunodeficiency Virus Infection," *Journal of Virology*, vol. 77, pp. 10376–10382, oct 2003.

[281] M. Golumbeanu, S. Desfarges, C. Hernandez, M. Quadroni, S. Rato, P. Mohammadi, A. Telenti, N. Beerenwinkel, and A. Ciuffi, "Proteo-Transcriptomic Dynamics of Cellular Response to HIV-1 Infection," *Scientific Reports*, vol. 9, p. 213, dec 2019.

[282] E. G. Regis, V. Barreto-de Souza, M. G. Morgado, M. T. Bozza, L. Leng, R. Bucala, and D. C. Bou-Habib, "Elevated levels of macrophage migration inhibitory factor (MIF) in the plasma of HIV-1-infected patients and in HIV-1-infected cell cultures: A relevant role on viral replication," *Virology*, vol. 399, pp. 31–38, mar 2010.

[283] M. A. Huson, M. P. Grobusch, and T. van der Poll, "The effect of HIV infection on the host response to bacterial sepsis," *The Lancet Infectious Diseases*, vol. 15, pp. 95–108, jan 2015.

[284] T. Calandra, B. Echtenacher, D. Le Roy, J. Pugin, C. N. Metz, L. Hültner, D. Heumann, D. Männel, R. Bucala, and M. P. Glauser, "Protection from septic shock by neutralization of macrophage migration inhibitory factor," *Nature Medicine*, vol. 6, pp. 164–170, feb 2000.

[285] Y. Al-Abed, D. Dabideen, B. Aljabari, A. Valster, D. Messmer, M. Ochani, M. Tanovic, K. Ochani, M. Bacher, F. Nicoletti, C. Metz, V. A. Pavlov, E. J. Miller, and K. J. Tracey, "ISO-1 binding to the tautomerase active site of MIF inhibits its pro-inflammatory activity and increases survival in severe sepsis," *Journal of Biological Chemistry*, vol. 280, no. 44, pp. 36541–36544, 2005.

[286] A. Sparkes, P. De Baetselier, L. Brys, I. Cabrito, Y. G. Sterckx, S. Schoonooghe, S. Muyldermans, G. Raes, R. Bucala, P. Vanlandschoot, J. A. Van Ginderachte, and B. Stijlemans, "Novel half-life extended anti-MIF nanobodies protect against endotoxic shock," *FASEB Journal*, vol. 32, pp. 3411–3422, jun 2018.

[287] R. König, Y. Zhou, D. Elleder, T. L. Diamond, G. M. Bonamy, J. T. Irelan, C. yuan Chiang, B. P. Tu, P. D. De Jesus, C. E. Lilley, S. Seidel, A. M. Opaluch, J. S. Caldwell, M. D. Weitzman, K. L. Kuhen, S. Bandyopadhyay, T. Ideker, A. P. Orth, L. J. Miraglia, F. D. Bushman, J. A. Young, and S. K. Chanda, "Global Analysis of Host-Pathogen Interactions that Regulate Early-Stage HIV-1 Replication," *Cell*, vol. 135, pp. 49–60, oct 2008.

[288] A. Matsuda, Y. Suzuki, G. Honda, S. Muramatsu, O. Matsuzaki, Y. Nagano, T. Doi, K. Shimotohno, T. Harada, E. Nishida, H. Hayashi, and S. Sugano, "Large-scale identification and characterization of human genes that activate NF-κB and MAPK signaling pathways," *Oncogene*, vol. 22, pp. 3307–3318, may 2003.

[289] S. A. Wang, C. Y. Hung, J. Y. Chuang, W. C. Chang, T. I. Hsu, and J. J. Hung, "Phosphorylation of p300 increases its protein degradation to enhance the lung cancer progression," *Biochimica et Biophysica Acta - Molecular Cell Research*, vol. 1843, no. 6, pp. 1135–1149, 2014.

[290] X. Wang, Y. He, Y. Ye, X. Zhao, S. Deng, G. He, H. Zhu, N. Xu, and S. Liang, "SILAC-based quantitative MS approach for real-time recording protein-mediated cell-cell interactions," *Scientific Reports*, vol. 8, pp. 1–9, dec 2018.

[291] D. Yu, W. Wang, A. Yoder, M. Spear, and Y. Wu, "The HIV envelope but not VSV glycoprotein is capable of mediating HIV latent infection of resting CD4 T cells," *PLoS Pathogens*, vol. 5, oct 2009.

[292] J. Lama and V. Planelles, "Host factors influencing susceptibility to HIV infection and AIDS progression," *Retrovirology*, vol. 4, p. 52, jul 2007.

[293] A. M. Dickens, D. C. Anthony, R. Deutsch, M. M. Mielke, T. D. Claridge, I. Grant, D. Franklin, D. Rosario, T. Marcotte, S. Letendre, J. C. McArthur, and N. J. Haughey, "Cerebrospinal fluid metabolomics implicate bioenergetic adaptation as a neural mechanism regulating shifts in cognitive states of HIV-infected patients," *AIDS*, vol. 29, pp. 559–569, mar 2015.

[294] B. Cotto, K. Natarajanseenivasan, and D. Langford, "HIV-1 infection alters energy metabolism in the brain: Contributions to HIV-associated neurocognitive disorders," *Progress in Neurobiology*, vol. 181, p. 101616, oct 2019.

[295] J. Kalucka, R. Missiaen, M. Georgiadou, S. Schoors, C. Lange, K. De Bock, M. Dewerchin, and P. Carmeliet, "Metabolic control of the cell cycle," *Cell Cycle*, vol. 14, no. 21, pp. 3379–3388, 2015.

[296] B. B. S. Zhou and S. J. Elledge, "The DNA damage response: Putting checkpoints in perspective," *Nature*, vol. 408, pp. 433–439, nov 2000.

[297] O. Timofeev, O. Cizmecioglu, F. Settele, T. Kempf, and I. Hoffmann, "Cdc25 phosphatases are required for timely assembly of CDK1-cyclin B at the G2/M transition," *Journal of Biological Chemistry*, vol. 285, pp. 16978–16990, may 2010.

[298] N. B. Trunnell, A. C. Poon, S. Y. Kim, and J. E. Ferrell, "Ultrasensitivity in the Regulation of Cdc25C by Cdk1," *Molecular Cell*, vol. 41, pp. 263–274, feb 2011.

[299] D. O. Morgan, *The Cell Cycle, Principles of Control*. New Science Press, 15 ed., 2007.

[300] W. C. Goh, N. Manel, and M. Emerman, "The human immunodeficiency virus Vpr protein binds Cdc25C: Implications for G2 arrest," *Virology*, vol. 318, pp. 337–349, jan 2004.

[301] J. W. Critchfield, J. E. Coligan, T. M. Folks, and S. T. Butera, "Casein kinase II is a selective target of HIV-1 transcriptional inhibitors," *Proceedings of the National Academy of Sciences of the United States of America*, vol. 94, pp. 6110–6115, jun 1997.

[302] E. Haneda, T. Furuya, S. Asai, Y. Morikawa, and K. Ohtsuki, "Biochemical characterization of casein kinase II as a protein kinase responsible for stimulation of HIV-1 protease in vitro," *Biochemical and Biophysical Research Communications*, vol. 275, pp. 434–439, aug 2000.

[303] C. A. Guenzel, C. Herate, E. Le Rouzic, P. Maidou-Peindara, H. A. Sadler, M.-C. Rouyez, L. M. Mansky, and S. Benichou, "Recruitment of the Nuclear Form of Uracil DNA Glycosylase into Virus Particles Participates in the Full Infectivity of HIV-1," *Journal of Virology*, vol. 86, pp. 2533–2544, mar 2012.

[304] S. Priet, N. Gros, J. M. Navarro, J. Boretto, B. Canard, G. Quérat, and J. Sire, "HIV-1-associated uracil DNA glycosylase activity controls dUTP misincorporation in viral DNA and is essential to the HIV-1 life cycle," *Molecular Cell*, vol. 17, pp. 479–490, feb 2005.

[305] X. Wen, L. Klockow, M. Nekorchuk, H. J. Sharifi, and C. M. de Noronha, "The HIV1 protein Vpr acts to enhance constitutive DCAF1-dependent UNG2 turnover," *PLoS ONE*, vol. 7, jan 2012.

[306] K. E. Willetts, F. Rey, I. Agostini, J.-M. Navarro, Y. Baudat, R. Vigne, and J. Sire, "DNA Repair Enzyme Uracil DNA Glycosylase Is Specifically Incorporated into Human Immunodeficiency Virus Type 1 Viral Particles through a Vpr-Independent Mechanism," *Journal of Virology*, vol. 73, pp. 1682–1688, feb 1999.

[307] K. E. Yoder and F. D. Bushman, "Repair of Gaps in Retroviral DNA Integration Intermediates," *Journal of Virology*, vol. 74, pp. 11191–11200, dec 2000.

[308] S. Vijayakumar, B. Dziegielewska, D. S. Levin, W. Song, J. Yin, A. Yang, Y. Matsumoto, V. P. Bermudez, J. Hurwitz, and A. E. Tomkinson, "Phosphorylation of Human DNA Ligase I Regulates Its Interaction with Replication Factor C and Its Participation in DNA Replication and DNA Repair," *Molecular and Cellular Biology*, vol. 29, pp. 2042–2052, apr 2009.

[309] C. Cartier, B. Hemonnot, B. Gay, M. Bardy, C. Sanchiz, C. Devaux, and L. Briant, "Active cAMP-dependent protein kinase incorporated within highly purified HIV-1 particles is required for viral infectivity and interacts with viral capsid protein," *Journal of Biological Chemistry*, vol. 278, pp. 35211–35219, sep 2003.

[310] C. Giroud, N. Chazal, B. Gay, P. Eldin, S. Brun, and L. Briant, "HIV-1-associated PKA acts as a cofactor for genome reverse transcription," *Retrovirology*, vol. 10, p. 157, dec 2013.

[311] J. L. Sloane, N. L. Benner, K. N. Keenan, X. Zang, M. S. Soliman, X. Wu, M. Dimapasoc, T. W. Chun, M. D. Marsden, J. A. Zack, and P. A. Wender, "Prodrugs of PKC modulators show enhanced HIV latency reversal and an expanded therapeutic window," *Proceedings of the National Academy of Sciences of the United States of America*, vol. 117, pp. 10688–10698, may 2020.

[312] Y. He, L. Wang, W. Liu, J. Zhong, S. Bai, Z. Wang, D. G. Thomas, J. Lin, R. M. Reddy, N. Ramnath, P. W. Carrott, W. R. Lynch, M. B. Orringer, A. C. Chang, D. G. Beer, and G. Chen, "MAP3K3 expression in tumor cells and tumor-infiltrating lymphocytes is correlated with favorable patient survival in lung cancer," *Scientific Reports*, vol. 5, jun 2015.

[313] F. Liu, C. Rothblum-Oviatt, C. E. Ryan, and H. Piwnica-Worms, "Overproduction of Human Myt1 Kinase Induces a G2 Cell Cycle Delay by Interfering with the Intracellular Trafficking of Cdc2-Cyclin B1 Complexes," *Molecular and Cellular Biology*, vol. 19, pp. 5113–5123, jul 1999.

[314] S. Moniz, F. Veríssimo, P. Matos, R. Brazão, E. Silva, L. Kotevelets, E. Chastre, C. Gespach, and P. Jordan, "Protein kinase WNK2 inhibits cell proliferation by negatively modulating the activation of MEK1/ERK1/2," *Oncogene*, vol. 26, pp. 6071–6081, sep 2007.

[315] J. F. Gui, W. S. Lane, and X. D. Fu, "A serine kinase regulates intracellular localization of splicing factors in the cell cycle," *Nature*, vol. 369, no. 6482, pp. 678–682, 1994.

[316] A. Eisenreich, V. Y. Bogdanov, A. Zakrzewicz, A. Pries, S. Antoniak, W. Poller, H. P. Schultheiss, and U. Rauch, "Cdc2-like kinases and DNA topoisomerase I regulate alternative splicing of tissue factor in human endothelial cells," *Circulation Research*, vol. 104, pp. 589–599, mar 2009.

[317] P. I. Duncan, D. F. Stojdl, R. M. Marius, K. H. Scheit, and J. C. Bell, "The Clk2 and Clk3 dual-specificity protein kinases regulate the intranuclear distribution of SR proteins and influence pre-mRNA splicing," *Experimental Cell Research*, vol. 241, pp. 300–308, jun 1998.

[318] D. I. Rhodes, L. Ashton, A. Solomon, A. Carr, D. Cooper, J. Kaldor, and N. Deacon, "Characterization of Three nef-Defective Human Immunodeficiency Virus Type 1 Strains Associated with Long-Term Nonprogression," *Journal of Virology*, vol. 74, pp. 10581–10588, nov 2000.

[319] F. Kirchhoff, R. C. Desrosiers, T. C. Greenough, J. L. Sullivan, and D. B. Brettler, "Absence of intact nef sequences in a long-term survivor with nonprogressive hiv-1 infection," *New England Journal of Medicine*, vol. 332, pp. 228–232, jan 1995.

[320] R. Salvi, A. R. Garbuglia, A. Di Caro, S. Pulciani, F. Montella, and A. Benedetto, "Grossly Defective nef Gene Sequences in a Human Immunodeficiency Virus Type 1-Seropositive Long-Term Nonprogressor," *Journal of Virology*, vol. 72, pp. 3646–3657, may 1998.

[321] M. Y. Chowers, C. A. Spina, T. J. Kwoh, N. J. Fitch, D. D. Richman, and J. C. Guatelli, "Optimal infectivity in vitro of human immunodeficiency virus type 1 requires an intact nef gene.," *Journal of Virology*, vol. 68, no. 5, pp. 2906–2914, 1994.

[322] J. W. Tukey, "Exploratory data analysis," in *Exploratory Data Analysis*, p. 688, Addison-Wesley Publishing Company, 2 ed., 1977.

[323] T. Kelder, B. R. Conklin, C. T. Evelo, and A. R. Pico, "Finding the right questions: Exploratory pathway analysis to enhance biological discovery in large datasets," *PLoS Biology*, vol. 8, no. 8, pp. 11–12, 2010.

[324] F. Emmert-Streib and G. V. Glazko, "Pathway analysis of expression data: Deciphering functional building blocks of complex diseases," *PLoS Computational Biology*, vol. 7, may 2011.

[325] L. Mariño-Ramírez, M. G. Kann, B. A. Shoemaker, and D. Landsman, "Histone structure and nucleosome stability," *Expert Review of Proteomics*, vol. 2, pp. 719–729, oct 2005.

[326] Z. Wang, C. Zang, J. A. Rosenfeld, D. E. Schones, A. Barski, S. Cuddapah, K. Cui, T. Y. Roh, W. Peng, M. Q. Zhang, and K. Zhao, "Combinatorial patterns of histone acetylations and methylations in the human genome," *Nature Genetics*, vol. 40, pp. 897–903, jul 2008.

[327] T. A. Rasmussen, M. Tolstrup, A. Winckelmann, L. Østergaard, and O. S. Søgaard, "Eliminating the latent HIV reservoir by reactivation strategies: Advancing to clinical trials," *Human Vaccines and Immunotherapeutics*, vol. 9, no. 4, pp. 790–799, 2013.

[328] S. M. Dehm, T. L. Hilton, E. H. Wang, and K. Bonham, "SRC Proximal and Core Promoter Elements Dictate TAF1 Dependence and Transcriptional Repression by Histone Deacetylase Inhibitors," *Molecular and Cellular Biology*, vol. 24, pp. 2296–2307, mar 2004.

[329] I. Nusinzon and C. M. Horvath, "Histone deacetylases as transcriptional activators? Role reversal in inducible gene regulation.," *Science's STKE : signal transduction knowledge environment*, vol. 2005, pp. re11–re11, aug 2005.

[330] F. K. Geis and S. P. Goff, "Unintegrated HIV-1 DNAs are loaded with core and linker histones and transcriptionally silenced," *Proceedings of the National Academy of Sciences of the United States of America*, vol. 116, pp. 23735–23742, nov 2019.

[331] Y. Zhu, G. Z. Wang, O. Cingöz, and S. P. Goff, "NP220 mediates silencing of unintegrated retroviral DNA," *Nature*, vol. 564, pp. 278–282, dec 2018.

[332] J. H. Arbuckle and T. M. Kristie, "Epigenetic repression of herpes simplex virus infection by the nucleosome remodeler CHD3," *mBio*, vol. 5, jan 2014.

[333] S. Schreiner, C. Bürck, M. Glass, P. Groitl, P. Wimmer, S. Kinkley, A. Mund, R. D. Everett, and T. Dobner, "Control of human adenovirus type 5 gene expression by cellular Daxx/ATRX chromatin-associated complexes," *Nucleic Acids Research*, vol. 41, pp. 3532–3550, apr 2013.

[334] J. Li, T. Wang, J. Xia, W. Yao, and F. Huang, "Enzymatic and nonenzymatic protein acetylations control glycolysis process in liver diseases," nov 2019.

[335] C. A. Coomer, I. Carlon-Andres, M. Iliopoulou, M. L. Dustin, E. B. Compeer, A. A. Compton, and S. Padilla-Parra, "Single-cell glycolytic activity regulates membrane tension and HIV-1 fusion," *PLoS Pathogens*, vol. 16, p. e1008359, feb 2020.

[336] H. Okamoto, C. T. Sheline, J. L. Corden, K. A. Jones, and B. M. Peterlin, "Trans-activation by human immunodeficiency virus Tat protein requires the C-terminal domain of RNA polymerase II," *Proceedings of the National Academy of Sciences of the United States of America*, vol. 93, pp. 11575–11579, oct 1996.

[337] K. Fujinaga, T. P. Cujec, J. Peng, J. Garriga, D. H. Price, X. Graña, and B. M. Peterlin, "The Ability of Positive Transcription Elongation Factor b To Transactivate Human Immunodeficiency Virus Transcription Depends on a Functional Kinase Domain, Cyclin T1, and Tat," *Journal of Virology*, vol. 72, pp. 7154–7159, sep 1998.

[338] P. D. Bieniasz, T. A. Grdina, H. P. Bogerd, and B. R. Cullen, "Recruitment of cyclin T1/P-TEFb to an HIV type 1 long terminal repeat promoter proximal RNA target is both necessary and sufficient for full activation of transcription," *Proceedings of the National Academy of Sciences of the United States of America*, vol. 96, pp. 7791–7796, jul 1999.

[339] D. Ivanov, Y. T. Kwak, E. Nee, J. Guo, L. F. García-Martínez, and R. B. Gaynor, "Cyclin T1 domains involved in complex formation with Tat and TAR RNA are critical for tat-activation," *Journal of Molecular Biology*, vol. 288, pp. 41–56, apr 1999.

[340] G. Marzio, M. Tyagi, M. I. Gutierrez, and M. Giacca, "HIV-1 Tat transactivator recruits p300 and CREB-binding protein histone acetyltransferases to the viral promoter," *Proceedings of the National Academy of Sciences of the United States of America*, vol. 95, pp. 13519–13524, nov 1998.

[341] V. Brès, H. Tagami, J. M. Péloponèse, E. Loret, K. T. Jeang, Y. Nakatani, S. Emiliani, M. Benkirane, and R. E. Kiernan, "Differential acetylation of Tat coordinates its interaction with the co-activators cyclin T1 and PCAF," *EMBO Journal*, vol. 21, pp. 6811–6819, dec 2002.

[342] V. Brès, R. Kiernan, S. Emiliani, and M. Benkirane, "Tat acetyl-acceptor lysines are important for human immunodeficiency virus type-1 replication," *Journal of Biological Chemistry*, vol. 277, no. 25, pp. 22215–22221, 2002.

[343] M. Ott, A. Dorr, C. Hetzer-Egger, K. Kaehlcke, M. Schnolzer, P. Henklein, P. Cole, M. M. Zhou, E. Verdin, Allis, and Khochbin, "Tat acetylation: A regulatory switch between early and late phases in HIV transcription elongation," *Novartis Foundation Symposium*, vol. 259, pp. 182–196, oct 2004.

[344] K. Kaehlcke, A. Dorr, C. Hetzer-Egger, V. Kiermer, P. Henklein, M. Schnoelzer, E. Loret, P. A. Cole, E. Verdin, and M. Ott, "Acetylation of Tat defines a CyclinT1-independent step in HIV transactivation," *Molecular Cell*, vol. 12, pp. 167–176, jul 2003.

[345] D. Ponti, M. Troiano, G. Bellenchi, P. A. Battaglia, and F. Gigliani, "The HIV Tat protein affects processing of ribosomal RNA precursor," *BMC Cell Biology*, vol. 9, p. 32, jun 2008.

[346] M. A. Jarboui, C. Bidoia, E. Woods, B. Roe, K. Wynne, G. Elia, W. W. Hall, and V. W. Gautier, "Nucleolar Protein Trafficking in Response to HIV-1 Tat: Rewiring the Nucleolus," *PLoS ONE*, vol. 7, p. e48702, nov 2012.

[347] D. L. Mallery, W. A. McEwan, S. R. Bidgood, G. J. Towers, C. M. Johnson, and L. C. James, "Antibodies mediate intracellular immunity through tripartite motif-containing 21 (TRIM21)," *Proceedings of the National Academy of Sciences of the United States of America*, vol. 107, pp. 19985–19990, nov 2010.

[348] S. Xie, L. Zhang, D. Dong, R. Ge, Q. He, C. Fan, W. Xie, J. Zhou, D. Li, and M. Liu, "HDAC6 regulates antibody-dependent intracellular neutralization of viruses via deacetylation of TRIM21," *Journal of Biological Chemistry*, p. jbc.RA119.011006, aug 2020.

[349] S. Mujtaba, Y. He, L. Zeng, A. Farooq, J. E. Carlson, M. Ott, E. Verdin, and M. M. Zhou, "Structural basis of lysine-acetylated HIV-1 Tat recognition by PCAF bromodomain," *Molecular Cell*, vol. 9, no. 3, pp. 575–586, 2002.

[350] J. Ma, L. Rong, Y. Zhou, B. B. Roy, J. Lu, L. Abrahamyan, A. J. Mouland, Q. Pan, and C. Liang, "The requirement of the DEAD-box protein DDX24 for the packaging of human immunodeficiency virus type 1 RNA," *Virology*, vol. 375, pp. 253–264, may 2008.

[351] D. Shi, C. Dai, J. Qin, and W. Gu, "Negative regulation of the p300-p53 interplay by DDX24," *Oncogene*, vol. 35, pp. 528–536, jan 2016.

[352] M. Ringeard, V. Marchand, E. Decroly, Y. Motorin, and Y. Bennasser, "FTSJ3 is an RNA 2-O-methyltransferase recruited by HIV to avoid innate immune sensing," *Nature*, vol. 565, pp. 500–504, jan 2019.

[353] M. Kuppuswamy, T. Subramanian, A. Srinivasan, and G. Chinnadurai, "Multiple functional domains of Tat, the trans-activator of HIV-1, defined by mutational analysis," *Nucleic Acids Research*, vol. 17, pp. 3551–3561, may 1989.

[354] A. U. Metzger, T. Schindler, D. Willbold, M. Kraft, C. Steegborn, A. Volkmann, R. W. Frank, and P. Rösch, "Structural rearrangements on HIV-1 Tat (32-72) TAR complex formation," *FEBS Letters*, vol. 384, no. 3, pp. 255–259, 1996.

[355] B. J. Calnan, S. Biancalana, D. Hudson, and A. D. Frankel, "Analysis of arginine-rich peptides from the HIV Tat protein reveals unusual features of RNA-protein recognition," *Genes and Development*, vol. 5, no. 2, pp. 201–210, 1991.

[356] L. S. Tiley, P. H. Brown, and B. R. Cullen, "Does the human immunodeficiency virus tat trans-activator contain a discrete activation domain?," *Virology*, vol. 178, no. 2, pp. 560–567, 1990.

[357] J. A. Garcia, D. Harrich, L. Pearson, R. Mitsuyasu, and R. B. Gaynor, "Functional domains required for tat-induced transcriptional activation of the HIV-1 long terminal repeat.," *The EMBO journal*, vol. 7, no. 10, pp. 3143–3147, 1988.

[358] U. Mahlknecht, I. Dichamp, A. Varin, C. Van Lint, and G. Herbein, "NF-κB-dependent control of HIV-1 transcription by the second coding exon of Tat in T cells," *Journal of Leukocyte Biology*, vol. 83, pp. 718–727, mar 2008.

[359] J. D. Weissman, J. A. Brown, T. K. Howcroft, J. Hwang, A. Chawla, P. A. Roche, L. Schiltz, Y. Nakatani, and D. S. Singer, "HIV-1 Tat binds TAFII250 and represses TAFII250-dependent transcription of major histocompatibility class I genes," *Proceedings of the National Academy of Sciences of the United States of America*, vol. 95, pp. 11601–11606, sep 1998.

[360] S. Kukkonen, M. D. P. Martinez-Viedma, N. Kim, M. Manrique, and A. Aldovini, "HIV-1 Tat second exon limits the extent of Tat-mediated modulation of interferon-stimulated genes in antigen presenting cells," *Retrovirology*, vol. 11, p. 30, apr 2014.

[361] A. Kuzmina, S. Krasnopolsky, and R. Taube, "Super elongation complex promotes early HIV transcription and its function is modulated by P-TEFb," *Transcription*, vol. 8, pp. 133–149, may 2017.

[362] X. Zhou, J. Luo, L. Mills, S. Wu, T. Pan, G. Geng, J. Zhang, H. Luo, C. Liu, and H. Zhang, "DDX5 Facilitates HIV-1 Replication as a Cellular Co-Factor of Rev," *PLoS ONE*, vol. 8, may 2013.

[363] A. Ait-Ammar, A. Kula, G. Darcis, R. Verdikt, S. De Wit, V. Gautier, P. W. Mallon, A. Marcello, O. Rohr, and C. Van Lint, "Current Status of Latency Reversing Agents Facing the Heterogeneity of HIV-1 Cellular and Tissue Reservoirs," *Frontiers in Microbiology*, vol. 10, p. 3060, 2020.

[364] G. He and D. M. Margolis, "Counterregulation of chromatin deacetylation and histone deacetylase occupancy at the integrated promoter of human immunodeficiency virus type 1 (HIV-1) by the HIV-1 repressor YY1 and HIV-1 activator Tat.," *Molecular and cellular biology*, vol. 22, pp. 2965–73, may 2002.

[365] R. J. Conrad, P. Fozouni, S. Thomas, H. Sy, Q. Zhang, M. M. Zhou, and M. Ott, "The Short Isoform of BRD4 Promotes HIV-1 Latency by Engaging Repressive SWI/SNF Chromatin-Remodeling Complexes," *Molecular Cell*, vol. 67, no. 6, pp. 1001–1012.e6, 2017.

[366] A. Valenzuela-Fernández, S. Alvarez, M. Gordon-Alonso, M. Barrero, A. Ursa, J. R. Cabrero, G. Fernández, S. Naranjo-Suárez, M. Yáñez-Mo, J. M. Serrador, M. A. Muñoz-Fernández, and F. Sánchez-Madrid, "Histone deacetylase 6 regulates human immunodeficiency virus type 1 infection.," *Molecular biology of the cell*, vol. 16, pp. 5445–54, nov 2005.

[367] K. Das Gupta, M. R. Shakespear, A. Iyer, D. P. Fairlie, and M. J. Sweet, "Histone deacetylases in monocyte/macrophage development, activation and metabolism: refining HDAC targets for inflammatory and infectious diseases," *Clinical and Translational Immunology*, vol. 5, p. e62, jan 2016.

[368] O. S. Søgaard, M. E. Graversen, S. Leth, R. Olesen, C. R. Brinkmann, S. K. Nissen, A. S. Kjaer, M. H. Schleimann, P. W. Denton, W. J. Hey-Cunningham, K. K. Koelsch, G. Pantaleo, K. Krogsgaard, M. Sommerfelt, R. Fromentin, N. Chomont, T. A. Rasmussen, L. Østergaard, and M. Tolstrup, "The Depsipeptide Romidepsin Reverses HIV-1 Latency In Vivo," *PLoS Pathogens*, vol. 11, no. 9, p. e1005142, 2015.

[369] I. C. Boffa, G. Vidali, R. S. Mann, and V. G. Allfrey, "Suppression of histone deacetylation in vivo and in vitro by sodium butyrate," *Journal of Biological Chemistry*, vol. 253, no. 10, pp. 3364–3366, 1978.

[370] M. Bantscheff, C. Hopf, M. M. Savitski, A. Dittmann, P. Grandi, A. M. Michon, J. Schlegl, Y. Abraham, I. Becher, G. Bergamini, M. Boesche, M. Delling, B. Dümpelfeld, D. Eberhard, C. Huthmacher, T. Mathieson, D. Poeckel, V. Reader, K. Strunk, G. Sweetman, U. Kruse, G. Neubauer, N. G. Ramsden, and G. Drewes, "Chemoproteomics profiling of HDAC inhibitors reveals selective targeting of HDAC complexes," *Nature Biotechnology*, vol. 29, pp. 255–268, mar 2011.

[371] M. K. Mamik and A. Ghorpade, "Chemokine CXCL8 promotes HIV-1 replication in human monocyte-derived macrophages and primary microglia via nuclear factor-κB pathway," *PLoS ONE*, vol. 9, mar 2014.

[372] A. Valentin, W. Lu, M. Rosati, R. Schneider, J. Albert, A. Karlsson, and G. N. Pavlakis, "Dual effect of interleukin 4 on HIV-1 expression: Implications for viral phenotypic switch and disease progression," *Proceedings of the National Academy of Sciences of the United States of America*, vol. 95, pp. 8886–8891, jul 1998.

[373] J. L. Silva-Filho, C. Caruso-Neves, and A. A. Pinheiro, "IL-4: An important cytokine in determining the fate of T cells," *Biophysical Reviews*, vol. 6, pp. 111–118, mar 2014.

[374] J. A. Zack, "The role of the cell cycle in HIV-1 infection," *Advances in Experimental Medicine and Biology*, vol. 374, pp. 27–31, 1995.

[375] D. B. Reeves, E. R. Duke, S. M. Hughes, M. Prlic, F. Hladik, and J. T. Schiffer, "Anti-proliferative therapy for HIV cure: A compound interest approach," *Scientific Reports*, vol. 7, pp. 1–10, dec 2017.

[376] D. B. Reeves, E. R. Duke, T. A. Wagner, S. E. Palmer, A. M. Spivak, and J. T. Schiffer, "A majority of HIV persistence during antiretroviral therapy is due to infected cell proliferation," *Nature communications*, vol. 9, p. 4811, dec 2018.

[377] R. Ceccaldi, P. Sarangi, and A. D. D'Andrea, "The Fanconi anaemia pathway: New players and new functions," *Nature Reviews Molecular Cell Biology*, vol. 17, pp. 337–349, jun 2016.

[378] A. M. Skalka and R. A. Katz, "Retroviral DNA integration and the DNA damage response," *Cell Death and Differentiation*, vol. 12, pp. 971–978, mar 2005.

[379] A. N. Anisenko and M. B. Gottikh, "Role of Cellular DNA Repair Systems in HIV-1 Replication," *Molecular Biology*, vol. 53, pp. 313–322, may 2019.

[380] L. Li, J. M. Olvera, K. E. Yoder, R. S. Mitchell, S. L. Butler, M. Lieber, S. L. Martin, and F. D. Bushman, "Role of the non-homologous DNA end joining pathway in the early steps of retroviral infection," *EMBO Journal*, vol. 20, pp. 3272–3281, jun 2001.

[381] M. L. Yeung, L. Houzet, V. S. Yedavalli, and K. T. Jeang, "A genome-wide short hairpin RNA screening of Jurkat T-cells for human proteins contributing to productive HIV-1 replication," *Journal of Biological Chemistry*, vol. 284, pp. 19463–19473, jul 2009.

[382] D. Boehm, V. Calvanese, R. D. Dar, S. Xing, S. Schroeder, L. Martins, K. Aull, P. C. Li, V. Planelles, J. E. Bradner, M. M. Zhou, R. F. Siliciano, L. Weinberger, E. Verdin, and M. Ott, "BET bromodomain-targeting compounds reactivate HIV from latency via a Tat-independent mechanism," *Cell Cycle*, vol. 12, pp. 452–462, feb 2013.

List of Abbreviations

ACN	acetonitrile
APC	allophycocyanin
BFP	blue fluorescent protein
BSA	bovine serum albumine
ddH_2O	doubly distilled water
DMSO	dimethysulfoxide
DTT	dithiothreitol
EDTA	ethylendiaminetetraacetic acid
EFN	efavirenz
ESI	electrospray ionization
EtOH	ethanol
FA	formic acid
FCS	fetal calf serum
FDA	food and drug administration
FDR	false discovery rate
FITC	fluorescein isothiocyanate
GFP	green fluorescent protein
HA	hemagglutinin
HIV	human deficiency virus
IL-2	interleukin 2
LB	lysogeny broth
LC	liquid chromatography
LDS	lithium dodecylsulfate
MeOH	methanol
MFI	mean fluorescent intensity
MOI	multiplicity of infection
MS	mass spectrometry
MS/MS or MS^2	tandem mass spectrometry
PAGE	polyacrylamide gel electrophoresis
PBS	phosphoate-buffered saline
PCR	polymerase chain reaction
PEI	polyethylenimine
PFA	paraformaldehyde
PHA-P	phytohemagglutinin-P
PSM	peptide spectrum match
PTM	post-translational modification
SD	standard deviation
SILAC	stable isotope labeling with amino acids in cell culture
TAE	Tris base, acetic acid and EDTA
TAT	transactivator of transcription
TB	terrific broth
TFA	trifluoracetic acid
TMT	tandem mass tag

Appendix

A. Supplemental figures

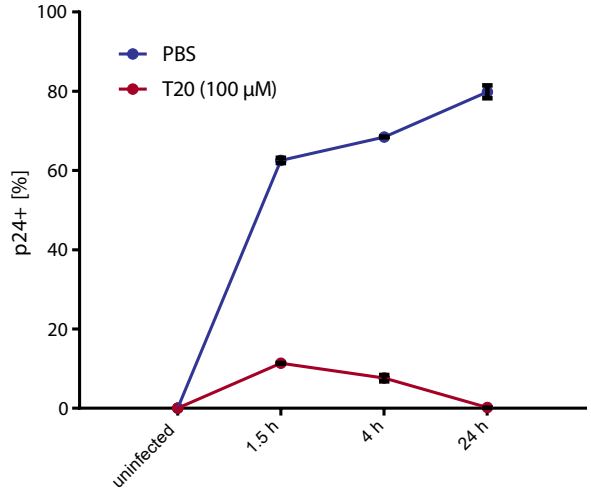

Figure S1. HIV-1 fusion inhibition in Jurkat-E6 cells. Jurkat-E6 cells were treated with fusion inhibitor T-20 and subsequently spin-infected with HIV-1_{NL4-3}. Cells were harvested after different time points, stained for viral p24 and analyzed by flow cytometry. Treatment with PBS served as control. Error bars show standard deviations.

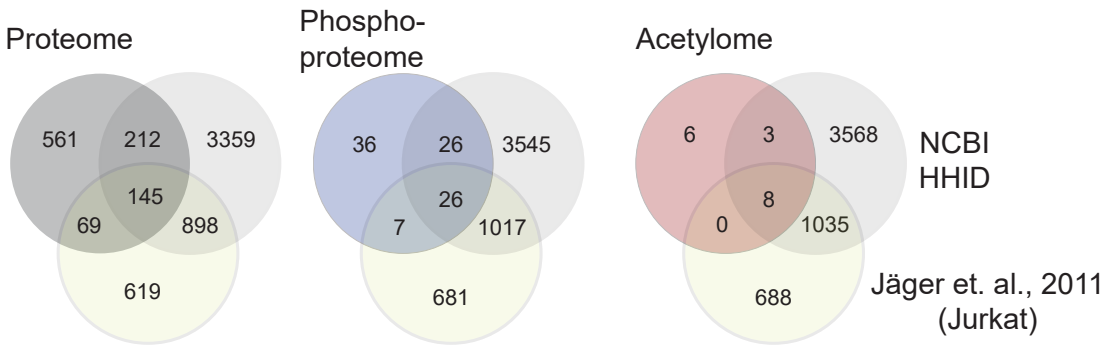

Figure S2.Confirmed HIV-1 regulated (phosphorylated or acetylated) proteins (24 h p.i.). Overlap of regulated proteins with the NCBI HIV-1 Human Interaction Database or hits identified by affinity tagging and purification mass spectrometry (Jäger et. al., 2011) [37].

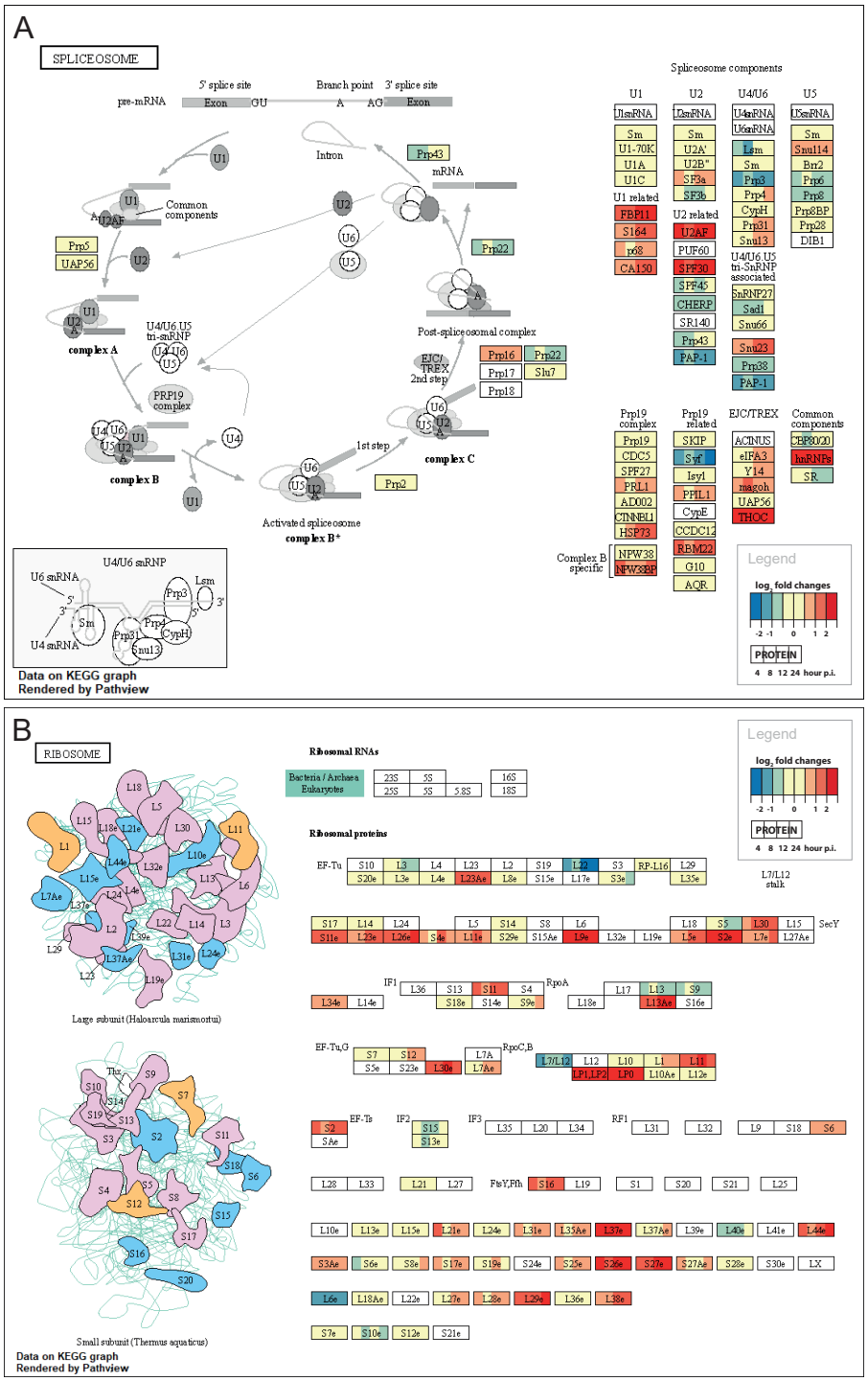

Figure S3. Mapping of quantified protein abundancies in HIV-1-infected Jurkats into the KEGG pathways spliceosome and ribosome. Proteins of pathway are depicted as squared time bars ranging from 4 to 24 h color-coded according to the protein abundance relative to control as $\log_2$ fold change. **(A)** Spliceosome (KEGG id: hsa03040, coverage: 85.7 %). **(B)** Ribosome (KEGG id: hsa03010, coverage 64.5 %).

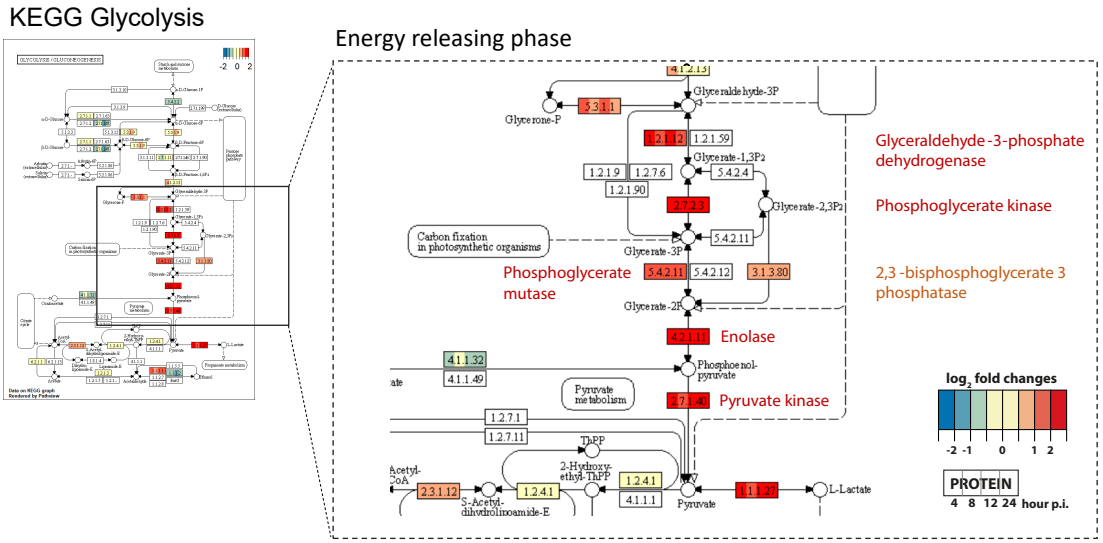

Figure S4. Mapping of quantified protein abundancies in HIV-1-infected Jurkats into the KEGG pathway glycolysis. Proteins of pathway are depicted as squared time bars ranging from 4 to 24 h color-coded according to the protein abundance relative to control as $\log_2$ fold change.

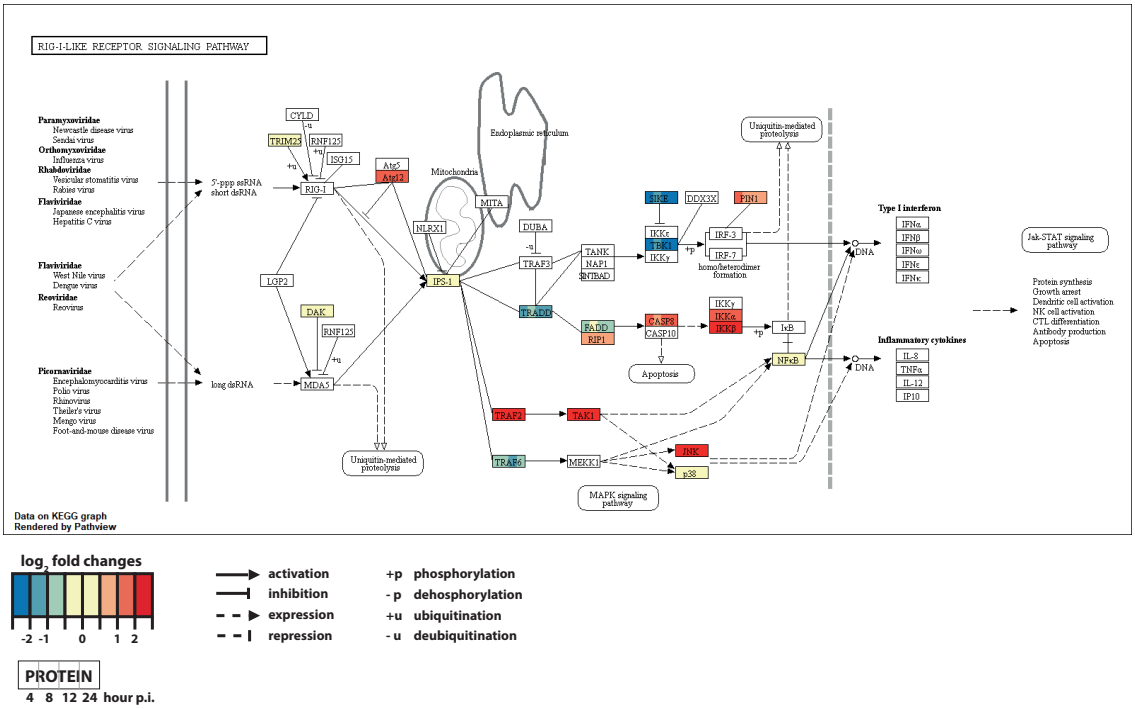

Figure S5. Mapping of quantified protein abundancies in HIV-1-infected Jurkats into the KEGG pathway Rig-I-like signaling. Proteins of pathway are depicted as squared time bars ranging from 4 to 24 h color-coded according to the protein abundance relative to control as $\log_2$ fold change.

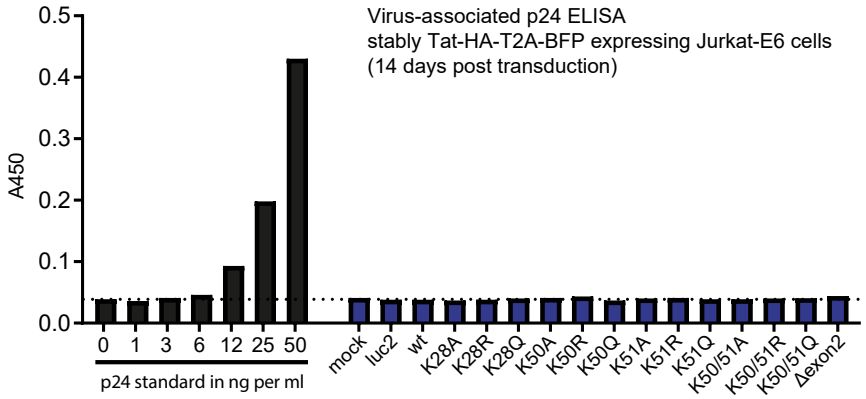

Figure S6. Clearance measurement of stably Tat-HA-T2A-BFP expressing Jurkat-E6 cells. Virus-associated p24 ELISA was performed to test for residual lentiviral particles 14 d post transduction.

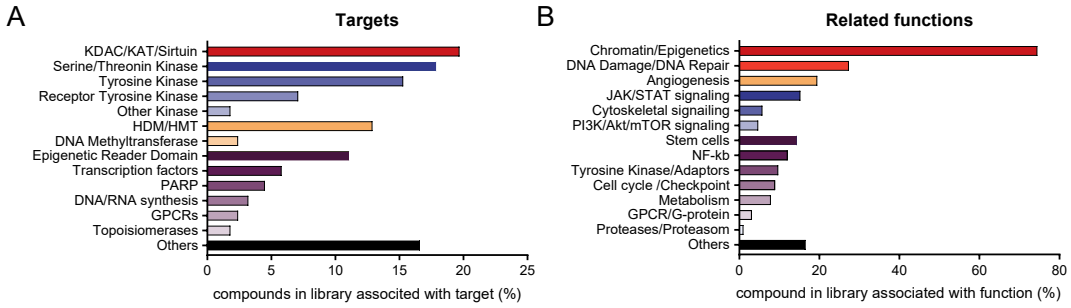

Figure S7. Composition of the epigenetic compound library (Targetmol). (A) Barchart displaying percentage of compounds targeting a specific group of proteins/protein family. **(B)** Diagram showing percentage of substances being associated with a certain cellular function.

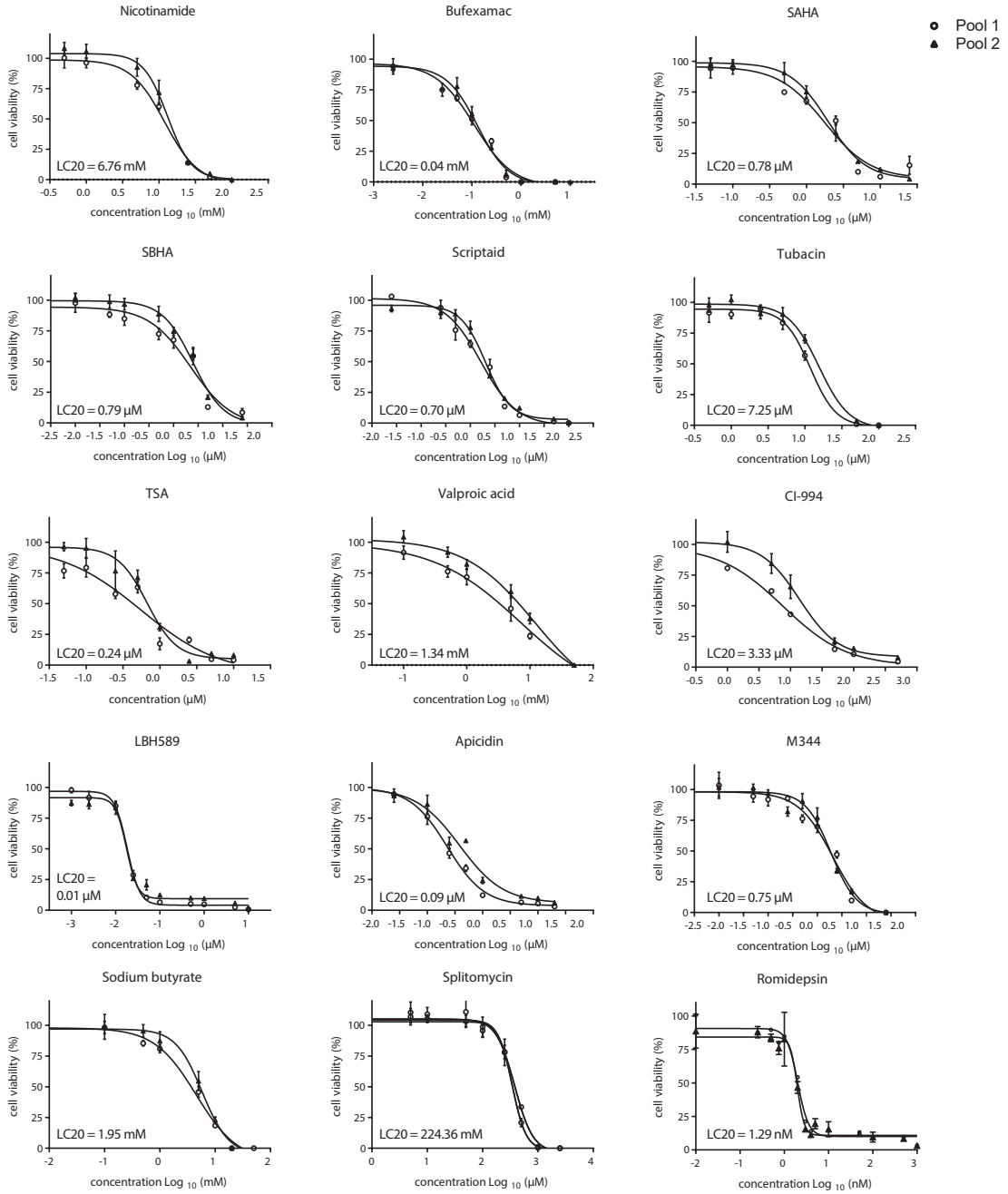

Figure S8. Toxicity/cell viability screen of HDAC inhibitors on human primary, activated CD4$^+$ T-cells. Human primary, activated CD4$^+$ T-cells were cultivated in the presence of different concentrations of the respective HDAC inhibitors for 72h. Afterwards, viability of cells was determined using a luminescence-based viability assay. Data were derived from three independent experiments each with two independent four-donor-pools of cells. Curve fitting and lethal concentration (LC20 are indicated. Error bars show standard deviation (SD).

List of Figures

List of Tables

Conference contributions and publications

Conferences

2020	<interact>, Munich	Proteomic profiling of human $CD4^+$ T-cells within the first 24 hours of HIV-1 infection (2^{nd} place winner in category "Best talks")
2018	MaxQuant Summer School, Barcelona	Deciphering post-translational modifications of the HIV-1 Tat protein (poster)

Publications

A. Zutz[§], **L. Chen**[§], F. Sippl and C. Schölz, "Epigenetic compound screening uncovers small molecules for reactivation of latent HIV-1", Antimicrobial Agents and Chemotherapy, vol. 65:e01815-20., 2021
doi:10.1128/AAC.01815-20

L. Chen[§], A. Zutz[§], J. Phillippou-Massier, T. Liebner, O. T. Keppler, C. Choudhary, H. Blum and C. Schölz, "Histone deacetylase inhibitors butyrate and bufexamac inhibit de novo HIV-1 infection in CD4 T-cells" bioRxiv, 2020
doi:10.1101/2020.04.29.067884

L. Chen, O. T. Keppler and C. Schölz, "Post-translational modification-based regulation of HIV replication," Frontiers in Microbiology, vol. 9, no. 9, p. 2131, 2018
doi: 10.3389/fmicb.2018.02131

([§] contributed equally)